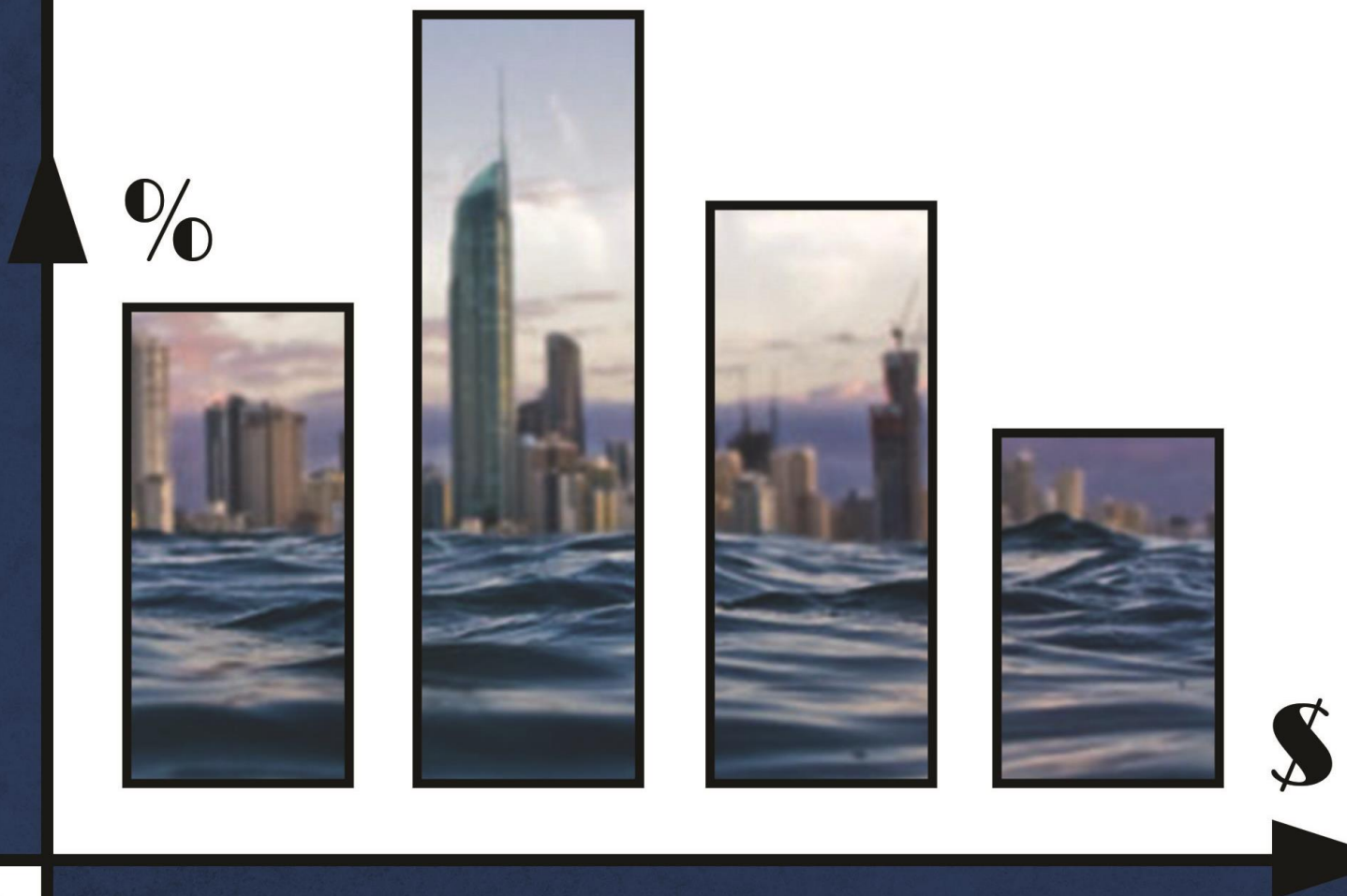


Impact Modelling of Hurricane Sandy on the Rockaways

Relating high-resolution storm characteristics to observed impact with use of Bayesian Belief Networks



MSc Thesis

Huub C.W. van Verseveld

Report type

MSc thesis TU Delft

Title

Impact Modelling of Hurricane Sandy on the Rockaways

Subtitle

Relating high-resolution storm characteristics to observed impact with use of Bayesian Belief Networks

Date

7 September 2014

Author

name: Huub C.W. van Verseveld
student no: 1365010
Programme/track: Hydraulic Engineering, Master of Science Civil Engineering
Specialisation: Coastal Engineering

Examination Committee

Chairman Prof. Dr. Ir. M.J.F. Stive, *Coastal Engineering (TU Delft)*
First Supervisor Dr. Ir. A.R. van Dongeren, *Coastal Morphology (Deltares)*
Supervisor Dr. N.G. Plant, *Center for Coastal & Watershed Studies (USGS)*
Supervisor MSc. Ir. W.S. Jäger, *Applied Mathematics (TU Delft)*
Supervisor Dr. Ir. C. den Heijer, *Coastal Engineering (TU Delft)*

In collaboration with

Deltares



U.S. Geological Survey

**Short summary**

Hurricane Sandy (2012), which made landfall in New Jersey on October 29th, made devastating impact on the East Coast of the USA and struck major parts of New York City, including the economic centre of Manhattan. The total damage (in the USA and Caribbean) is in excess of 100 billion US\$ with estimates ranging between 78 and 97 billion US\$ for direct damage and over 10 to 16 billion US\$ for indirect damage due to business interruption (M. Kunz et al., 2013).

Modelling impact (e.g. damage, fatalities) in the coastal zone due to hazardous storm events is a hardly explored practice. It is difficult to predict damage correctly where damage observations are scarce and the physical processes causing the damage are complex, diverse and can differ from site to site and event to event. Moreover, an increasing interest exists in getting insights in the uncertainty of prediction.

This report explores on the possibilities in coupling physics-based hydraulic and morphodynamic modelling to the practice of impact mapping by using Bayesian Belief Networks (BBN's). Using BBN's enables to look at the impact in a probabilistic context, which fits well to the highly unpredictable and rare nature of hurricanes. The morphodynamic storm impact model XBeach (Roelvink et al., 2009) is proposed as one of the process-based models, since Hurricane Sandy pointed out that morphodynamic aspects can be of great importance for the amount of damage. Part of the Rockaway Peninsula, NY, which has been severely damaged by Hurricane Sandy's surges, is used as case study. Only damage to residential buildings is considered in present study, in which delivering a proof of concept for the presented approach is the main goal. In general it can be concluded that the approach succeeded.

Acknowledgements

I am most grateful to my committee, consisting of Marcel Stive, Ap van Dongeren, Nathaniel Plant, Wiebke Jäger and Kees den Heijer, for helping me performing this thesis. Their knowledge, interests, insights, comments, criticism and optimism definitely made the results better and helped me in keeping track. Special thanks to Ap (Deltares) and Nathaniel (USGS), who gave me the opportunity and means to go on an adventurous and educational trip to Florida and New York. I really appreciated the hospitality and felt always valued, both at Deltares and USGS. In that perspective I also like to thank Cheryl Hapke, Soupy Dalyander, Dave Thompson and Joe Long, who helped me in finding my way in the States, facilitated in data, contacts and knowledge on computational modelling.

Special thanks also go to Wiebke, Kees, and (in the beginning) Jaap van Thiel de Vries, who supported me during all phases of the process. Thanks, Wiebke, for the company in Saint Petersburg and all the interesting conversations and discussions; these were really helpful in structuring my thoughts.

Furthermore, I'd really like to thank Joost den Bieman, who was always available and willing to answer my questions and Mohd Shahrizal Ab Razak from UNESCO-IHE, who helped me tremendously in finishing the last and largest XBeach run. Next to the above mentioned people, I had the privilege to speak to a lot of experts on varying matters; they were always interested and willing to help. To these people from amongst others Deltares, TU delft, VU Amsterdam, USGS, Office of the Mayor of NYC and FEMA I would like to say: thank you for your attribution.

Abstract

Hurricane Sandy (2012), which made landfall in New Jersey on October 29th, made devastating impact on the East Coast of USA and struck major parts of New York City, including the economic centre of Manhattan. The total damage (in the USA and Caribbean) is in excess of 100 billion US\$ with estimates ranging between 78 and 97 billion US\$ for direct damage and over 10 to 16 billion US\$ for indirect damage due to business interruption (M. Kunz et al., 2013).

Modelling impact (e.g. damage, fatalities) due to hazardous storm events is a hardly explored practice; especially in the coastal zones where predominantly wind induced hazards from sea (e.g. inundation, wave attack) cause the damage. It is difficult to predict damage correctly where damage observations are scarce and the physical processes causing the damage are complex, diverse and can differ for different sites and events. Moreover, an increasing interest exists in getting insights in the uncertainty of prediction. This report explores on the possibilities in coupling physics-based hydraulic and morphodynamic modelling to the practice of impact mapping by using Bayesian Belief Networks (BBN's). Using BBN's enables to look at the impact in a probabilistic context, which fits well to the highly unpredictable and rare nature of hurricanes. Part of the Rockaway Peninsula, NY, which has been severely damaged by Hurricane Sandy's surges, is used as case study. Only damage to residential buildings is considered in present study, in which delivering a proof of concept is the main goal.

The morphodynamic storm impact model XBeach (Roelvink et al., 2009) is proposed as one of the process-based models, since Hurricane Sandy pointed out that morphodynamic aspects can be of great importance to the amount of damage, especially for the barrier islands in front of the US coastlines. The hazards, predominantly coming from sea in the case of Hurricane Sandy, are propagated from large scale (100-1000 km) to the building level (1-10 m) with a nested routine which includes XBeach on the lowest scale level. With the use of extraction methods local hazard indicators are generated for every single residential building, which have been successfully used in combination with building type indicators to predict damage. 5300 observations of a qualitative damage assessment were enough to train a Bayesian Belief Network that is capable of reproducing the spatial pattern of the damage. Multiple analysis tools are available to analyse the quality of prediction and uncertainty quantification and it is possible with ease to visualize that in space with the use of an SQL database coupled to GIS software. In general it can be concluded that the presented approach succeeded.

XBeach is capable of providing multiple local hazard indicators on the building level, which proved to having predictive capacity. The indicators "inundation depth", "wave attack", "flow velocity" and (to a lesser extend) "scour depth" give together much better predictions than they do alone. The implementation of XBeach therefore fits perfectly in the multi-hazard approach that Bayesian Belief Networks make possible. On the contrary, it must be said that setting up an XBeach model for high resolution simulations and relatively large areas (order of 10 km wide) is a time consuming job. The results of the XBeach model used for present study show a structural overestimation of storm conditions, which can be addressed to a poor calibration. This assumedly limits the predictive skill of the statistical BBN model. There is still a large scope for improvement.

Some aspects of the approach have been studied in more detail; roughly, these aspects do either influence the predictive qualities of the individual indicators or have to do with the configuration of the statistical model, the Bayesian Belief Network. Considering the first category, it appeared that model resolution is not as important as expected. Indicator values based on model runs with grid cell sizes of 3x3 m² in the urban areas give hardly better predictions than runs with grid cell sizes of 9x9 m² where computational expenses are 25 times higher. Next to this aspect, the extraction method, in which hazard indicators are generated out of the XBeach output data, appeared to be very important for the predictive capacity of these indicators. The usage of (polygons of the) building perimeter outlines to determine buffer zones around these buildings works fine. Moreover, it can

be concluded that the extraction formulations and the size of extraction buffer zones around the buildings can make a substantial difference for the predictive skill of the local hazard indicators. A coarser grid asks for a larger buffer zone in order to prevent that the buildings are predicted to be non-flooded where they in reality have been flooded.

Considering the statistical model part, using Bayesian Belief Networks gives the opportunity to relate the damage to multiple aspects instead of only one, which has great advantages over the market standard approaches (in which the majority only considers the depth-damage relation). Comparing the spatial distribution of the means of the conditional Probability Mass Functions (PMF's) to the observed damage, it can be concluded that the established BBN's are good in capturing the spatial variability in risk (given the event) per building. Higher risks are predicted for the more severely damaged buildings. The BBN's perform not so well in predicting extremes where the most probable outcome of prediction for the most severely damaged buildings almost always concerns an underestimation of the damage.

Next to indicators that indicate the local severity of the hazards, the added value of implementing other indicators has been studied as well. Adding nodes to the BBN indicating differences between buildings increases the Log-likelihood ratio test scores of the hindcast, which implies an increase of the predictive skill of the model. The "tax base" indicator appears to be most skilful, followed by "Building Class", "Roof Height", "Shape Area" and "Residential Units per building" in that specific order. It is said that one has to be really careful with adding too much nodes. The consequences of the latter are demonstrated in present report: the predictions become worse if too much complexity is added to the BBN (when the amount of data is said to be over-fitted). This also becomes the case when more bins per node and mutual relations between the nodes are added.

Also the quantification of uncertainty depends strongly on the number of nodes, bins and relations within the BBN. More complexity in the network needs to be compensated by more training data in order to avoid poorly substantiated PMF's and retain the same quality of prediction. Quantities indicating uncertainty, such as standard deviation of these conditional PMF's, can be easily visualized in space and support statements about the confidence of the predictions. However, quantitatively the PMF's do not cover all sources of uncertainty in the approach as it is proposed right now. Mainly uncertainties concerning structural over- or underestimations (for instance due to too high XBeach boundary conditions) are not represented in the distributions of predictions. This is a direct cause of the training of the BBN's, which is based on the results of only one XBeach run.

Aggregation of the damage predictions to higher spatial scale levels, such as a neighbourhood or a complete city, is not straightforward within the present approach. Aggregation of risk given the event (mean of the PMF's) is a matter of summation. On the contrary, since (spatial) correlation between the predictions is at stake, predictions made in a certain area cannot be seen as independent. This, in combination with the fact that not all uncertainty is incorporated in the PMF's, makes aggregation of uncertainty difficult. Future research is necessary in order to find ways to overcome those aggregation issues.

Contents

Acknowledgements	5
Abstract	7
Contents	9
1. Introduction	13
1.1. Motivation.....	13
1.1.1. Hurricane Sandy	13
1.2. Problem Definition	18
1.2.1. Background.....	18
1.2.2. Quantifying Uncertainty of Predictions.....	24
1.2.3. Morphological Processes during the Storm	27
1.2.4. Spatial Scale and Applicability issues.....	28
1.3. Delineation	29
1.4. Research Questions.....	29
1.4.1. Main Question	29
1.4.2. Sub Questions.....	29
1.5. Research Approach	29
1.5.1. Approach	29
1.5.2. Objectives and Deliverables	30
2. Study Site	31
2.1. Rockaway Peninsula	31
2.1.1. Geographical analysis	31
2.1.1. Socio-economic analysis.....	35
2.2. Sandy’s Hazard Pathways and Impacts	37
2.2.1. Hazard Sources and Pathways.....	37
2.2.1. Impacts	42
2.3. Data	46
3. Methods.....	49
3.1. Concept	49
3.1.1. Physical Process Description	49
3.1.2. Statistical Opportunities.....	52
3.1.3. Bayesian Belief Networks	57
3.2. Implementation	60
3.2.1. Overall model structure	60
3.2.2. Describing the elements.....	62

3.3.	Scenarios	69
3.3.1.	XBeach Runs	69
3.3.2.	Local Hazard indicators-Damage Relations	70
3.3.3.	Indicators for building type and value at risk	71
4.	Results.....	73
4.1.	XBeach.....	73
4.1.1.	Hydrodynamics.....	73
4.1.2.	Morphodynamics	78
4.1.3.	Local hazard indicators.....	81
4.1.4.	Grid resolution.....	85
4.2.	Damage Dependencies.....	88
4.3.	Bayesian Belief Network	94
4.3.1.	Coupling Storm Conditions to Damage	94
4.3.2.	Building Type Indicators	103
5.	Discussion and Recommendations	109
5.1.	Achievements.....	109
5.1.1.	Overall Model Structure	109
5.1.2.	Physical Processes and Hazard Propagation	109
5.1.3.	Determining local hazard indicators.....	110
5.1.4.	Predicting Damage	111
5.1.5.	Quantifying Uncertainty	112
5.1.6.	Spatial Aggregation	113
5.2.	Applicability of the Concept	114
5.3.	Recommendations	115
6.	Conclusions	117

Appendices

A.	Merging Data based on Geospatial Information.....	120
B.	Multi-variate flood damage assessment – abbreviation description	121
C.	XBeach model formulations.....	122
C.1.	Short wave equations	122
C.2.	Roller energy balance.....	122
C.3.	Shallow water equations.....	123
C.4.	Sediment transport	123
C.5.	Bed updating	124
C.6.	Avalanching module.....	124
C.7.	Morphological acceleration factor	125
D.	XBeach model set-up	126
D.1.	Bathymetrical/topographical data	126
D.2.	Final bathymetrical input	129
D.2.1.	Building Perimeter Outlines	131
D.2.2.	Non-Erodible Layer	132
D.3.	Grid properties.....	133
D.3.1.	Domain	133
D.3.2.	Grid density	135
D.4.	Surge	136
D.5.	Waves.....	137
D.6.	Input parameters	140
E.	Delft3D and D-Flow FM model set-up	143
E.1.	Delft3D - US East Coast model	143
E.2.	Delft3D – New York Bight model.....	144
E.3.	D-Flow FM – New York Bight model	145
F.	Delft3D and D-Flow FM model results.....	146
F.1.	Storm Tide Propagation	146
F.2.	Storm Tide– Observed versus Simulated	147
F.3.	Wave Propagation.....	149
F.4.	Waves– Observed versus Simulated	150
F.4.1.	Significant Wave Height	150
F.4.2.	Peak Wave Period.....	151
G.	XBeach model results – multiple runs	152
H.	Reference studies - Bayesian Belief Networks.....	158

I.	Tools of Analysis.....	160
I.1.	Sensitivity Analysis	160
I.2.	(Log-)Likelihood Ratio Test.....	160
J.	FEMA Damage Classification description.....	162
K.	PLUTO - Data Description	163
K.1.	Tax Base Value	163
K.2.	Residential Units per Building	163
K.3.	Building Class.....	163
	Figures	165
	Tables.....	169
	Bibliography.....	171

1. Introduction

1.1. Motivation

In the night of October 29th to October 30th of 2012 Hurricane Sandy made landfall near Brigantine, New Jersey. Not even a category 3 storm on the Saffir -Simpson Hurricane Wind Scale (Schott et al. 2012) during landfall, Sandy affected 24 states and devastated larger parts of New Jersey and New York. With more than 286 (indirect) fatalities and over \$68 billion US\$ of damages, Hurricane Sandy became the second-costliest hurricane in the United States history, ranked after Katrina (2005) (Kunz et al. 2013).

Even though records over the past 50 years may suggest that a hurricane like Sandy is highly exceptional and not to be expected in New Jersey and New York, long term statistics tend to show different, see paragraph 1.1.1.2. Not the storm on itself was exceptional but in hybridity with other factors, such as a high tide and geographical features, it led to a tremendous disaster. The willingness to prevent similar disasters from happening in the future together with the strong politic and economic powers centred in the heart of New York City give a unique momentum to several new initiatives. New York is determined to make a change (PlaNYC 2013) to become more resilient.

Hurricanes (in more general: Tropical Cyclones) can be found in several parts of the world, where warm ocean waters near the equator cause low pressure areas which are traded towards the coastal zones and increase in strength during their traveling above the warm water. Tropical Cyclones can cause massive natural hazards, which may have huge impact on nature and human being. In low lying coastal areas surging water can induce enormous floods, which has proven to be more destructive than the accompanying winds in some cases. In the case of Sandy storm surges were far more troublesome than winds. This all should be put in a broader perspective by looking at future developments worldwide: on the one hand we have to deal with a non-beneficial climate change; on the other hand usage and economic value of coastal zones will increase further. Both are expected to increase risks in these areas significantly.

This has led to a common awareness of and willingness to control these risks, in order to minimize them in the future. On the one hand data are gathered indicating the damages and giving input to the understanding of the corresponding failure mechanisms. On the other hand we are more and more capable of simulating storm events and corresponding hydrodynamic and morphodynamic characteristics. Bringing these two aspects together is one of the challenges we are facing today in obtaining insight in the risks we are exposed to. This master thesis is a first attempt to couple the hydrodynamics and morphodynamics of a storm to its impacts by using Bayesian Belief Networks (BBN's), in order to demonstrate the statistical relationships. The result is a concept proving impact model, applied to hurricane Sandy and a study site at the Rockaway Peninsula, NY.

The significance of a fully statistical impact model can be found in several applications. It can provide for instance a very powerful tool for decision makers in order to determine whether or not to implement defence measures. It would be very useful to have information like "A 1/100year storm will probably cause that amount of damage/fatalities at that location if that measure is applied". Play the what-if game and you will quantitatively know how well a measure performs. Moreover this would give the opportunity to investigate the impact of future developments like climate change.

1.1.1. Hurricane Sandy

It is clear that wind induced storm surges, either caused by a tropical storm or other type of wind storm can cause large disasters in coastal areas. The next two paragraphs will give some background information about some characteristics of Hurricane Sandy (track, intensity) and its impact.

1.1.1.1.Characteristics

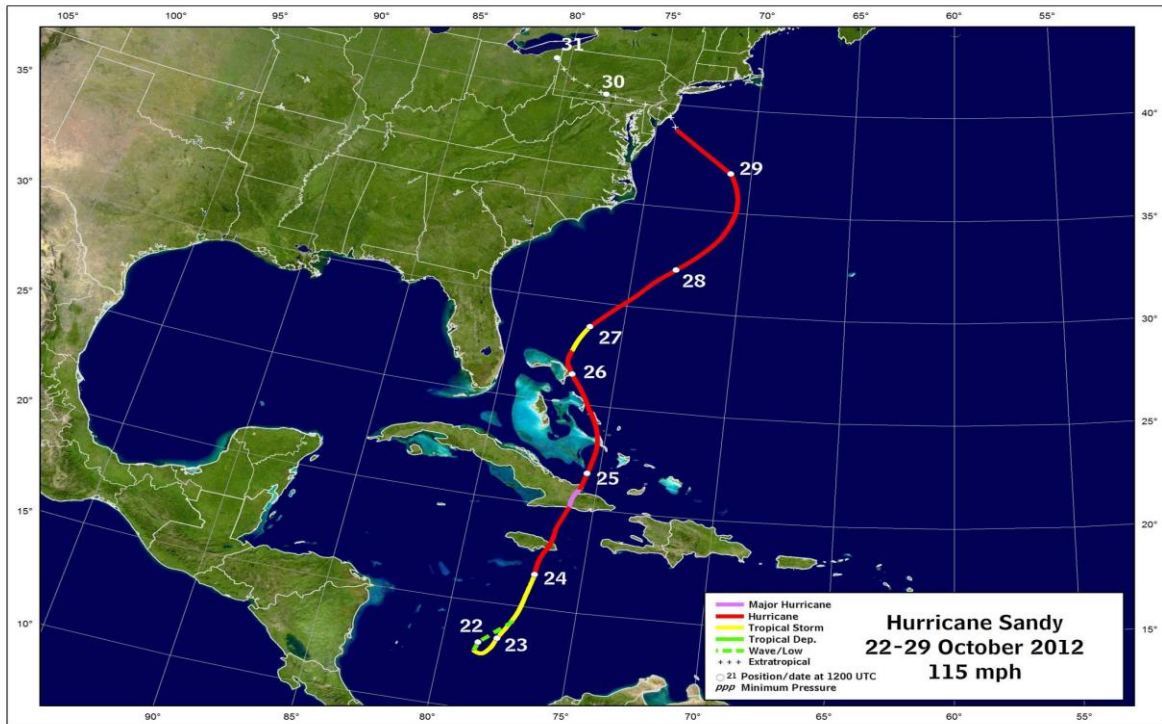


Figure 1-1 - Intensity and track of Hurricane Sandy (2012) from NOAA website

The track and intensity of Hurricane Sandy are shown in Figure 1-1. Generated in the Caribbean Sea on October 22nd, Sandy moved towards the Atlantic Ocean. Just before hitting Jamaica it became a Tropical Cyclone (Category 3 or higher). After some weakening due to shear over the south-eastern and central Bahamas, it interacted with an upper-level trough and surface front near the north-western Bahamas and underwent a partial extra tropical transition (E. Blake 2013). At this point the weather forecast models of NOAA’s National Hurricane Center (NHC)¹ were not in agreement with each other; most hurricanes at this point turn east towards the Atlantic Ocean. However, Sandy turned on a rare track northwest due to a high pressure area in the north and another low pressure area in the east, see Figure 1-2.

During its propagation towards the US East Coast (towards New Jersey and New York) Sandy retrained its strength and made landfall as a category 2 hurricane. After landfall Sandy turned northward and finally dissipated near Lake Erie (point 31 in Figure 1-1) after causing heavy rainfall in Pennsylvania, Maryland, New Jersey, Delaware and Virginia (100 to 200 mm). Additionally, Sandy caused severe snow storms especially in the southern and central Appalachian with snow amounts up to 1m (Kunz et al. 2013).

Hurricane Sandy caused measured wind speeds of 185 km/h during landfall, which is pretty severe but not uncommon for Atlantic tropical storms. What Hurricane Sandy made unique were not the meteorological characteristics on its own, but a combination of multiple

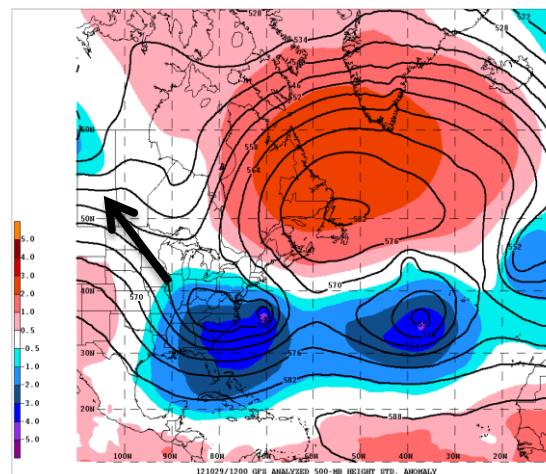


Figure 1-2 - High pressure areas (red) and Low pressure areas (blue) made Sandy turn northwest. Picture by NHC (2012)

¹ <http://www.nhc.noaa.gov/>

factors. It was the hybridity that made it unique:

- A very rare track. The severest hurricanes from the past 150 years in north-eastern US all approached the mainland more parallel to the coast. Sandy made landfall almost perpendicular to the coast (E. S. Blake et al. 2013);
- A forward speed of 20 knots, which is relatively fast²;
- An abnormally large wind spanning diameter of about 1700 km, covering almost the complete East Coast and caused by the extra tropical transition;
- An extremely low air pressure of 945 mb in the eye, which is the lowest ever recorded for north-eastern US;
- Sandy made landfall during high annual tide in combination with a full moon.

One could argue that Sandy's timing couldn't have been worse. The interaction between winds (direction and velocities), air pressure and the topographic configuration of the coast caused very large surge levels, especially northeast of the hurricane's eye in the York Bight. This was even increased by an astronomical high tide, leading to inundation of large areas along the coast and major parts of New York City (see Figure 1-4). At the Battery in Lower Manhattan water levels were measured of 14.6 ft (4.3 m) referenced to Mean Lower Low Water (MLLW), which exceeded the previous record set by Hurricane Dona (1960). Moreover, the sea state with waves over 10 m was the severest since the mid-1970's, with wave heights over 30 ft (+/- 10m), exceeding the conditions of Irene (2011) and the Nor'easter of 1992 (*Guy Carpenter 2013*). According to Hall and Sobel³ who performed probability analyses on model simulations of a synthetically generated track set, Sandy's surge can be considered to be a 700-year event. Other sources state that because of future developments like climate change a 500-year surge could happen every 25 to 240 years by the end of the century (Lin et al. 2012).



Figure 1-4 - Sandy inundation map by FEMA (Source: NOAA)

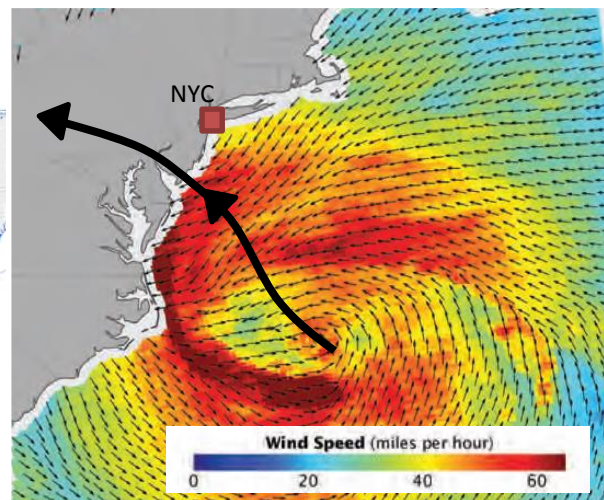


Figure 1-3 - Sandy before landfall - Wind speed and schematization of track by NASA

1.1.1.2. Impacts

Hurricane Sandy caused damage in many states, of which New York and New Jersey were affected the most. She impacted an area that is good for approximately 10% of the US economic output (*GuyCarpenter 2013*). Moreover, it made it in the top three of deadliest hurricanes in the US with a total of 113 fatalities nationwide (*Mühr et al. 2012*); see Table 1-1 for a historic overview of fatalities in New York City only.

² This is not necessarily a bad thing; hurricanes with high forward speeds show higher storm surge peaks while lower inland volumes of flood (*Rego and Li 2009*)

³ 'On the impact angle of Hurricane Sandy's New Jersey landfall' (*Hall and Sobel 2013*)

Table 1-1 - Most lethal hurricanes for New York ⁴

Hurricane	Year	Fatalities
New England	1938	60
Sandy	2012	48
Edna	1945	29
Norfolk	1821	17
Five	1894	10

The actual causes of these fatalities differ from falling down during repair (or preparation) work at building roofs to drowning in the flood. In 'CEDIM FDA-Report on Hurricane Sandy 22-30 October 2012' (Mühr et al. 2012), which hereafter is referred to as the CEDIM report, it is stated that a lot of people stayed home during Sandy while evacuation was recommended, because they expected Sandy to be less severe than predictions broadcasted in the media. This experience was probably based on the experience with Hurricane Irene, which struck the area one year before and was indeed less severe than predicted.

Besides fatalities, Hurricane Sandy affected over 305,000 houses only in New York state (Kunz et al. 2013). In some areas more than 1/5th of the houses have been completely destroyed, of which Breezy Point and Rockaway Beach, both located on the Rockaway Peninsula (Queens County), are good examples (PlaNYC 2013). According to the NHESS report (Kunz et al. 2013), energy systems are amongst the most important critical infrastructure due to their essential role in sustaining socioeconomic systems. More than 8.7 million households (21.3 million people) were victim of power outages during the storm on 29 and 30 October, of which 3.37 million were still waiting for electric supply after one week. This is a record for the US for power outages caused by hurricanes, leaving Irene (6 million households) and Isabel (4.3 million) behind. Power outages during the storm also have their effect on loss of life. First of all they limit the self-help capacity of humans (Mühr et al. 2012); secondly, they can cause electrical fires, which for instance happened in Breezy Point (Rockaway Peninsula) where at least 100 houses burned down to the ground. The strong winds accompanying the storm make fast spreading of the fires possible.

Other types of infrastructure have been affected as well. Metro services in New York City were disrupted for months because of flooded tunnels and some stations have not yet been fully repaired at the time of writing this report. Moreover, some areas were extremely hard to reach the days after the storm; At Rockaway Peninsula inundation caused large piles of debris in the streets, consisting of sand from the eroded dunes, inundation wood, insulation and household items. The 5 km long boardwalk in Rockaway Beach, which was situated at the beach front, was at some places completely destroyed or tilted from its foundation and flushed away inland. Similar to the damaged electrical system the sewing system and gas and fresh water supply systems were severely damaged. This implied disruption of normal life for months, even to those whom houses and businesses were spared during the storm.

The economic losses for New York State can be divided in direct and indirect losses:

- **Direct losses:** damage to housing, transit, road and bridges, business impact etc. See Figure 1-5 for a breakdown of direct losses (total of 32.8 billion US\$ for New York State).
- **Indirect losses:** failure of physical or economic linkages causing cascading effects (e.g. manufacture sector out of power for days). Business interruption losses have been estimated between 10.8 and 15.5 billion US\$.

For the direct losses an estimated breakdown is made by Cuomo in 2012 (Kunz et al. 2013), which is shown in the diagram of Figure 1-5. It can be seen that damage to infrastructure attributes pretty much the same to

⁴ source: CEDIM FDA-Report on Hurricane Sandy (Mühr et al. 2012)

total direct losses as damage to housing. However, it should be noted that damage to housing affects the individual citizen more.

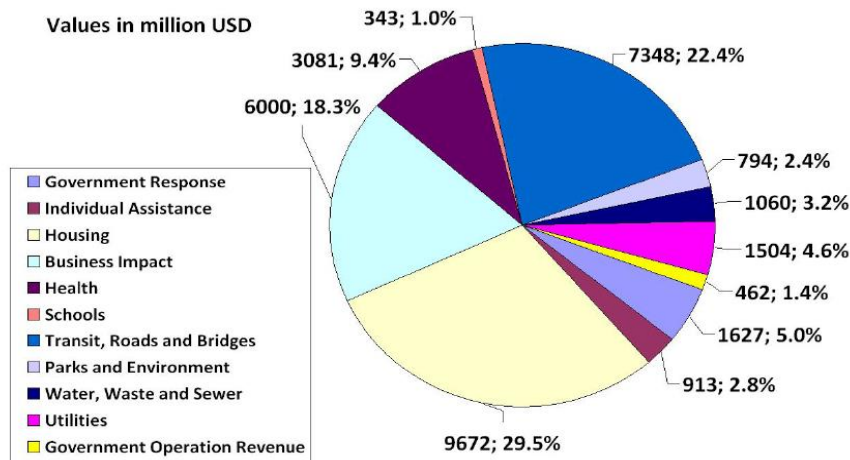


Figure 1-5 - A breakdown of direct losses in New York State (in million US\$ and %) reported Cuomo (2012) and graphed by Kunz et al. (2013)

The total economic losses in the US due to hurricane Sandy's direct damages is estimated to be 97 billion US dollars, (Kunz et al. 2013), of which an approximated 32.8 billion US dollars can be assigned to New York (according to Governor Andrew Cuomo). This makes Sandy the second costliest hurricane in US history after Hurricane Katrina (2005). However, this should be put in perspective by normalizing total costs of historical events to the cost base of 2005. This has been done for the hurricanes within the period of 1900 till 2005 (Pielke Jr et al. 2008) and is later updated till 2012. The outcome is graphed in Figure 1-6.

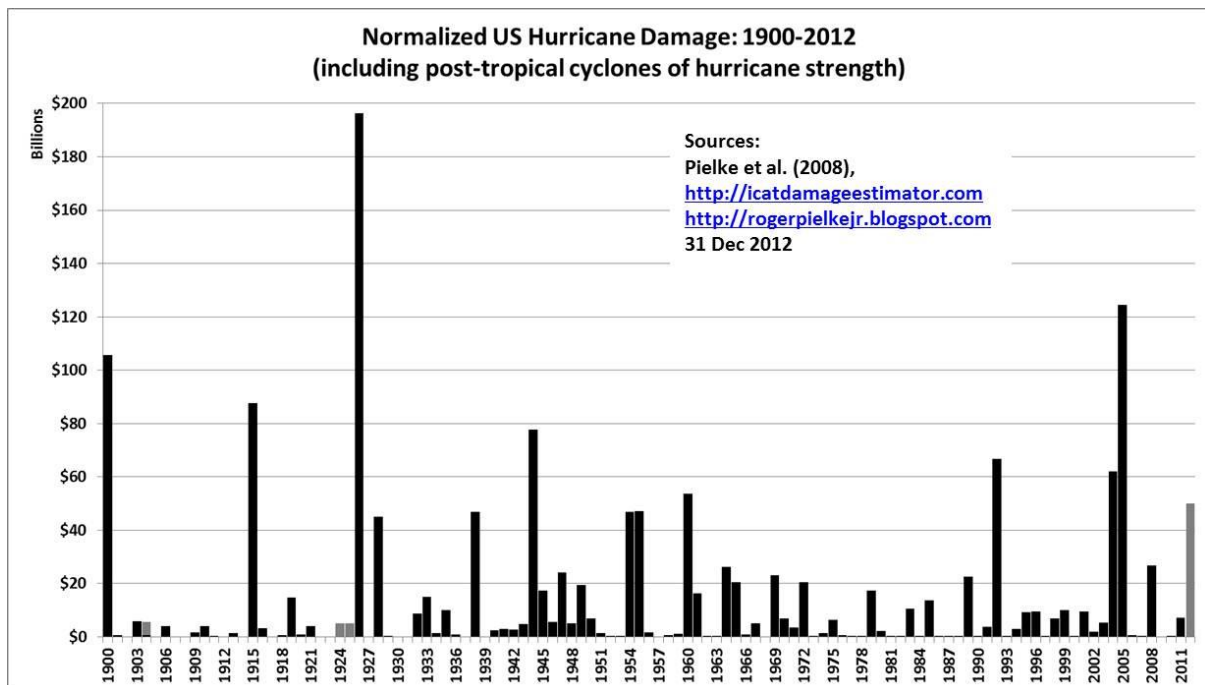


Figure 1-6 - Normalized US Hurricane Damage (source: Pielke et al.)

It can be concluded that hazardous events like Sandy and Katrina are not just events from the past decade, but did happen on a regular basis over the past 100 years and probably will happen the coming decades as well.

1.2. Problem Definition

From section 1.1 it can be learned that hazardous storms like Hurricane Sandy are very complex events. The processes steering the storm propagation are mostly at play on a global and regional spatial scale, but the related impacts do highly depend on local properties like geographic configuration of the coast, socio-economic aspects and the vulnerability of buildings and infrastructure. This section copes with these difficulties and the problems in modelling impacts are addressed.

1.2.1. Background

1.2.1.1. Hazard Modelling

The dictionary states about hazard *“A possible source of danger: a thing likely to cause injury”*.⁵ A more technical definition is given by the UNISDR: *“The combination of the probability of an event and its negative consequences”*.⁶ In the case of hurricanes, it can be learned from Sandy (but also from other examples like hurricane Katrina) that the danger in low lying coastal areas mainly comes from sea. In the field of hydraulic engineering, modelling of wind induces surge and sea states is certainly not new. A broad range of 1D, 2D and 3D physics-based numerical model software packages can be made use of, which can and have been used to simulate storm events like Hurricane Sandy. Amongst these physics-based models (sometimes referred to as deterministic, comprehensive or process-based models) are noticeable: Delft3D, D-Flow FM, SWAN and XBeach from TU Delft, Deltares and partners⁷; the MIKE software packages from DHI⁸; and ADCIRC from the University of North Carolina⁹.

Fluid dynamics, the study of fluids in motion, lies at the heart of most of the equations these numerical models solve. Water bodies are constantly affected by external and internal forces concerning gravity, inertia, air-water interactions, water-bed interactions, internal friction, earth rotation and density variations in for instance temperature and salinity. All these processes influence the hydraulic properties (e.g. water levels and wave heights) in time and space. For centuries scientist try to understand these physical processes and, since the invention of computers, describing them in numerical computer models.

The physical processes are translated into (fundamental) equations, of which the most are based on the conservation of mass, momentum and energy. Important contributions in the field of hydraulic engineering can be found in the Boussinesq approximation, Navier-Stokes equations and Stokes theorem. In numerical models external forces are parameterized and initial states (temporal boundary conditions) have to be determined, together with domain boundary states (spatial boundary conditions). Space and time are discretised to make computations finite and with use of time and space stepping the propagation of disturbances (relative to an equilibrium state) are computed. In this way water levels, wave heights, flow velocity and many other properties can be simulated for meteorological storm events.

With the continuously increasing processing speed of computers, more and more complexity can be added to these physics-based numerical models while keeping computation expenses within limits. On the other hand research provides more and more understanding of the physical processes. These two aspects together attributed to the fact that physics-based modelling has become extremely important in the field of hydraulic engineering.

For the simulation of wind induces surges and waves at deep water (>20 m water depth) different forces and processes are dominant than for instance the water propagation during floods in urban areas. In sandy coastal

⁵ The American Heritage® Dictionary of the English Language, Fourth Edition

⁶ <http://www.unisdr.org/we/inform/terminology>

⁷ <http://www.deltares.nl/nl/software>

⁸ <http://www.mikebydhi.com>

⁹ <http://www.adcirc.org>

zones, found in most parts of the US East Coast, the morphological changes due to storms can have significant impacts on the coastal appearances. Some software packages, like XBeach, are specifically made for modelling these morphological impacts and show fairly good results, which for instance can be seen in the study ‘Modelling storm impacts on beaches, dunes and barrier islands’ (Roelvink et al. 2009). It should be noted that all software packages have their own range of applicability and limitations at the same time.

1.2.1.2. Impact Modelling

Living on planet earth is just dangerous; no matter where you are, there are always risks. As long as human kind exists, people in general and politicians in specific try to minimize these risks for the benefits of themselves and the community. Understanding of possible social and economic impacts of hazardous events is therefore a key element, together with the accompanying probability of occurrence. Not only hurricanes cause hazards, but one can think of natural hazards in general (caused by earthquakes, landslides, tornados, volcanos and epidemics) and human caused hazards like terroristic attacks and burgling.

Risk, damage and impact have different meanings in different contexts to different kind of people. For coastal engineers the notion of hurricane impact usually refers to morphological impacts to the coast. This is completely different though for people with other expertise, of which insurers and politicians should be specifically named here. In general impact refers to the effect/consequence of a force, which is not necessarily damage. Where this thesis is about the destructiveness of hurricanes, impact refers here to damage in the forms of social and economic disruption in general and loss of life, physical damage and monetary losses specifically. Damage on itself can be split up as well and in this thesis the distinction between direct and indirect, tangible and intangible damage have been made, of which examples can be found in Table 1-2. For risk many definitions exist. Most of them seem to include the two dimensions consequence and probability. For this research the definition of Helm is used: “Risk = Probability of a Hazard x Consequences” (Helm 1996), where consequence is actually a synonym for impact and consists of both aspects exposure and vulnerability (Klijn et al. 2004). The consequences of present study are the concerned damages. The risk in monetary perspective for instance can be expressed in dollars/year.

Traditionally, (semi-)public research institutes and universities are charged with the task of quantifying these risks as indispensable first step for the purpose of minimizing them. An example can be found in the “Prediction of seasonal climate-induced variations in global food production” (Iizumi, Toshichika Hirofumi Sakuma, Yokozawa et al. 2012), where statistical crop failure prediction models were linked to ensemble seasonal climatic forecasts. It can be used in order to predict food shortages, which is especially interesting in developing countries.

One way to lessen the (indirect) impacts of hazardous events is to insure property and goods. The (re)insurance market can be both public and private. (Re)-insurers are interested in the economic losses of hazards in order to determine insurance premiums, which are profitable in the long run. Several financial service providers are active on the market, providing risk modelling services to reinsurers, insurance companies, large investment companies and governmental bodies. Since the 1980’s these services

Table 1-2 - Categorization of damage (source: Jonkman et al., 2008)

Table 1 – Different dimensions of flood damages		
	Tangible and priced	Intangible and unpriced
Direct	<ul style="list-style-type: none"> • Residences • Capital assets and inventory • Business interruption (inside the flooded area) • Vehicles • Agricultural land and cattle • Roads, utility and communication infrastructure • Evacuation and rescue operations • Reconstruction of flood defences • Clean up costs 	<ul style="list-style-type: none"> • Fatalities • Injuries • Inconvenience and moral damages • Utilities and communication • Historical and cultural losses • Environmental losses
Indirect	<ul style="list-style-type: none"> • Damage for companies outside the flooded area • Adjustments in production and consumption patterns outside the flooded area • Temporary housing of evacuees 	<ul style="list-style-type: none"> • Societal disruption • Psychological traumas • Undermined trust in public authorities

have become more and more advanced and the models are known as ‘Catastrophe Models’, or shorter ‘Cat Models’ (Grossi and TeHennepe 2008). Most of these models were empirical and have a statistical background. Since consequences of large natural hazardous events are immense and probability is often low, it is difficult to use statistical analysis tools in order to improve probabilistic approaches. Major events – including catastrophes in 2011 and 2012 such as earthquakes in New Zealand, Japan Earthquake and Tsunami and Hurricane Sandy– continue to demonstrate the levels of uncertainty that can exist in model results (Lloyd’s 2013).

Hydraulic engineers tend to start from a physical point of view, understanding the physics of the hazard, where the risk managers start from the impact side of the story, trying to distinguish different kinds of impact and break down costs. As is explained above, determining risk requires quantification of an event’s impact and the related probability. The latter can be determined fairly easy for some types of hazards. Car theft for instance happens on regular basis and with statistical tools one can determine the probability of occurrence. However, for rare events like hurricanes this cannot easily be done. The insurance branch is therefore integrating more and more physics into their models in order to bring the driving forces in their models back to a level for which using statistics is possible again, for instance on water levels and wave heights or meteorological characteristics of a hurricane. This is where both worlds come together.

General Approaches

A wide variety of impact models can be found in the industry and the model approaches show large mutual differences. In “Comparative flood damage model assessment: towards a European approach” (Jongman et al. 2012) seven different damage models for river floods from different countries are compared. Because the analogy with wind induced sea flooding is large, the methodologies are comparable. Jongman states that amongst others differences can be found in:

- Scale of application: local, regional or national;
- Units of analysis: Surface area (e.g. urban area) or individual objects (e.g. house);
- Hydrological characteristics: depth, inundation duration, velocity, debris;
- Data method: empirical, synthetic;
- Cost base: replacement value, depreciated value;
- Predicted damage: direct versus indirect and tangible versus intangible.

It is concluded that different applications ask for different approaches. However, one thing all methods have in common is that they consist of several modules representing the necessary modelling steps. A graphical representation of the Florida Hurricane Model 2013a methodology from EQECAT is shown in Figure 1-7. It should be noted that the figure distinguishes between damage and loss. First, the direct tangible damages are determined in a physical context. Subsequently, in the ‘Estimation of Loss’-module the monetary consequences of these damages are calculated; not only for the direct but also for the indirect and secondary damages, which for instance includes business interruption and inflation.

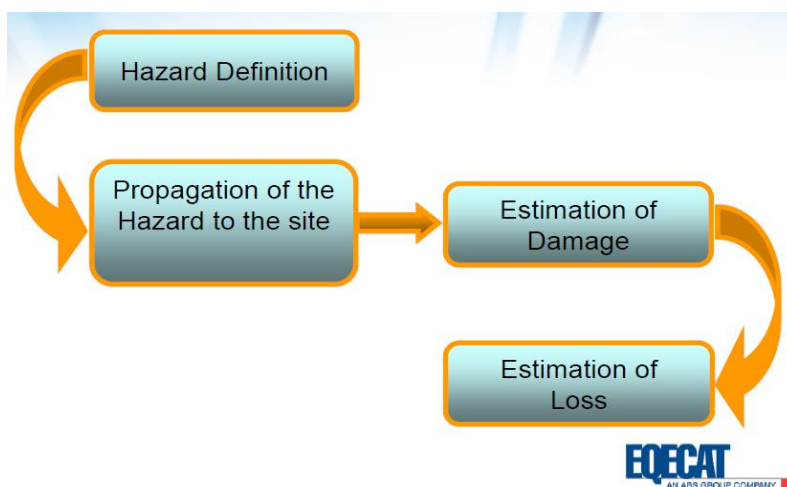


Figure 1-7 - Methodology of the Florida Hurricane Model 2013a
(source: EQECAT)

To make this more concrete and tangible another representation can be found in Figure 1-8, including spatial scales and some characteristics of the different information levels. Based on historical data a synthetic dataset of possible hurricanes is constructed, of which the track and intensity are calculated with meteorological forecast models. The hydraulic effects of these meteorological characteristics are propagated towards the areas of interest (in front of the coast) and corresponding large scale storm conditions (order of 1-10km) are calculated, of which wind speed and inundation depth are the most important ones. In order to determine local inundation depth (information level 3), the differences between large scale storm tide levels (information level 2) and local ground elevation levels are approximated. The last step is referred to as the ‘bathtub’ concept, where the water surface onshore is assumed to be as flat as a mirror. With use of vulnerability curves (also known as damage curves) the impacts are calculated; see information level 4. The last step comprises a financial module, which estimated the losses per storm event or aggregates the losses over a synthetic set of events in order to gain overall risk (information level 5).

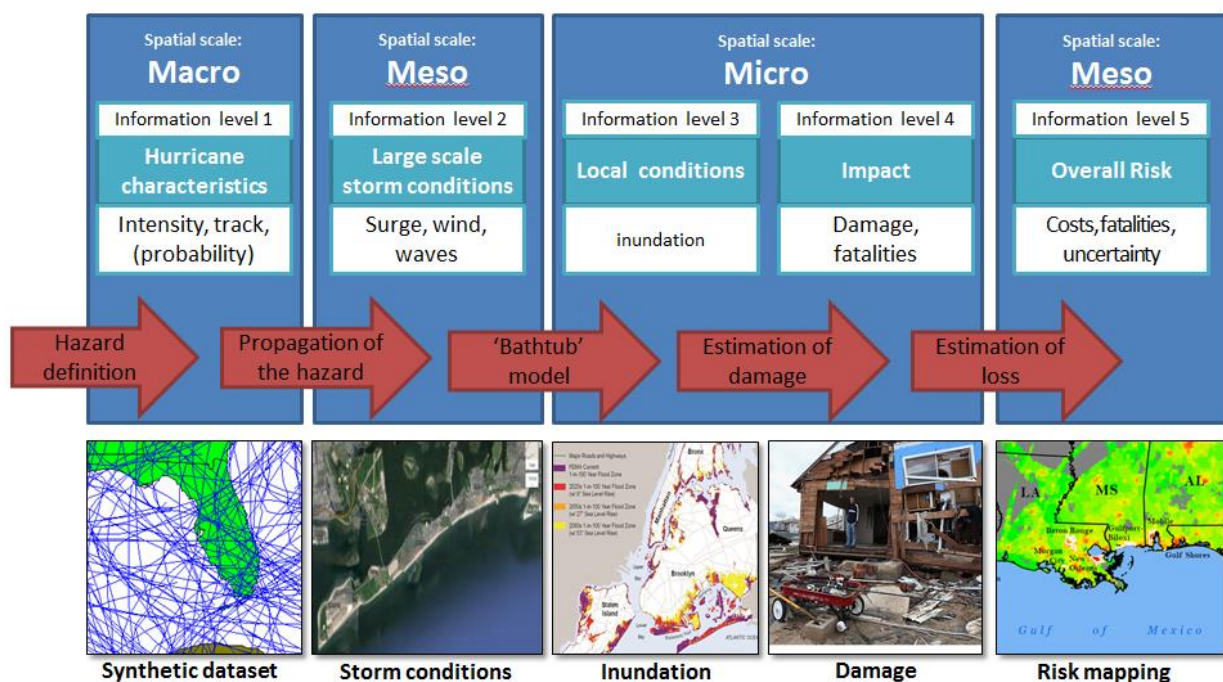


Figure 1-8 - Overall Model Methodology with spatial scales and properties of different information levels

1.2.1.3. Surge and Wave Induced Damage Estimations

In step 4 in Figure 1-8 the link is made between forcing (storm characteristics) and response (damage to objects at risk). To do so, more information is necessary on land use, vulnerability and sometimes socio-economic features. A presentation of the HIS-SSM¹⁰ methodology on damage estimation is given in Figure 1-9. This can be seen as the general procedure for the estimation of direct physical damages, consisting of three main elements: (1) determination of flood characteristics; (2) assembling information on land use data and maximum damage amounts; (3) application of stage-damage functions that relate the extent of economic damage to the flood characteristics (Pistrika and Jonkman 2009).

¹⁰ Impact Model of The Dutch Department of Waterways and Public Works (Dutch: Rijkswaterstaat)

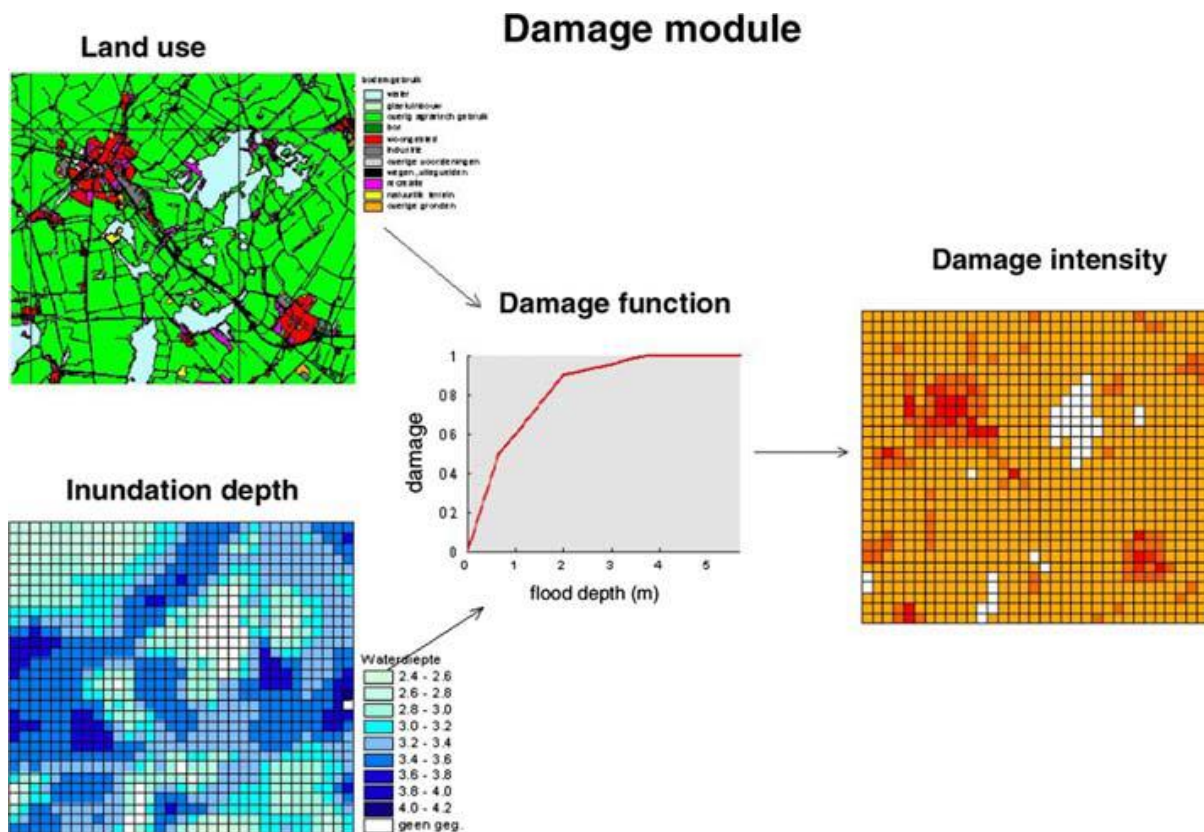


Figure 1-9 - Schematization of the HIS-SSM model methodology (source: Rijkswaterstaat)

In section 1.1.1 it is already mentioned that in low lying coastal zones the largest threats come from the sea and not from hurricane winds. Therefore, the storm characteristics for most of the impact models reduces to hydraulic properties (and no meteorological properties anymore), knowing inundation depth (surge level relative to the ground level) and sometimes wave height and/or flow velocity. In general the coupling is done with use of damage functions, of which an example is shown in Figure 1-9. Relative damage curves relate the forcing (in this case inundation depth) to a damage ratio between 0 and 1. The damage ratio indicates which percentage of the (value of the) exposed asset will be damaged/lost by the force. The total loss can be derived by:

$$\text{Loss} = \text{damage ratio} \times \text{value}$$

When the value is monetary, loss becomes cost, of which the meaning varies. In 'Damage to residential buildings due to flooding of New Orleans after hurricane Katrina' by Pistrika and Jonkman (2009) the damage ratio (or percentage damage value) relates the financial total loss of a building (value) to the cost of repairs (loss), which implies that the damage ratio can be more than 1 if the cost of repair is more than the financial total loss of a building. However, it is most common to use damage fractions, which are always between 0 and 1 and have also been used in HIS-SSM. On the contrary, absolute damage curves relate the forcing directly to costs. The categorization of the assets at risk differ per model, but for every asset category (e.g. single family building, flat building, high way, bridge) a damage curve has to be made. The number of assets categories used and thus damage curves varies from several curves to hundreds and depends on the scale of analysis and how easily damage curves can be established. Roughly they are established in three different ways:

1. By observation data regression;
2. By expert judgement;
3. By implementing knowledge from researches on the physical resistance.

Data regression is generally preferred since real observations do not tell lies, but this is only feasible when a sufficient amount of data is available. Pistrika and Jonkman (2009) analysed the direct damages of Hurricane Katrina to residential buildings in New Orleans. They found that there is no clear one-on-one relationship between flood characteristics and the exact value of observed damage percentages. The derived damage curves vary for different areas within the domain (spatial variations). Moreover, the spatial level of detail of the analysis appeared to be very important for the relative strength of the depth-damage relationships.

Expert judgement and research on the resistance of assets are mainly used when a sufficient amount of damage observations is absent. ‘What if’-analyses can be used to establish the damage curves. For the example of residential buildings, one can imagine what happens when the water rises and which parts of a representative house will be flooded and which parts of the contents will or won’t be spared. With logic a damage curve can be constructed. The effect of structural damage can be added with the use of knowledge from structural resistance studies; for instance ‘Wood Frame Building Response to Rapid-Onset Flooding’ (Becker et al. 2011). The HAZUS-MH methodology¹¹, as an example, is using a combination of data and what-if reasoning to determine their depth-damage relations (*Hazus –MH 2.1 Hurricane Model - User Manual* n.d.). It must be said that this method is far from ideal since important aspects may be forgotten or the corresponding effects underestimated; a few centimetres of salt water in a house for instance, can already severely damage wall isolation and drywalls, which involves high accompanying costs.

It should be noted that differences in establishing methods and the (spatial) variety of the data can give large differences in damage curves for different models but similar assets. Figure 1-10 shows damage curves for seven different river flood damage models for the same asset category. The large mutual differences illustrate the amount of uncertainty that is at play.

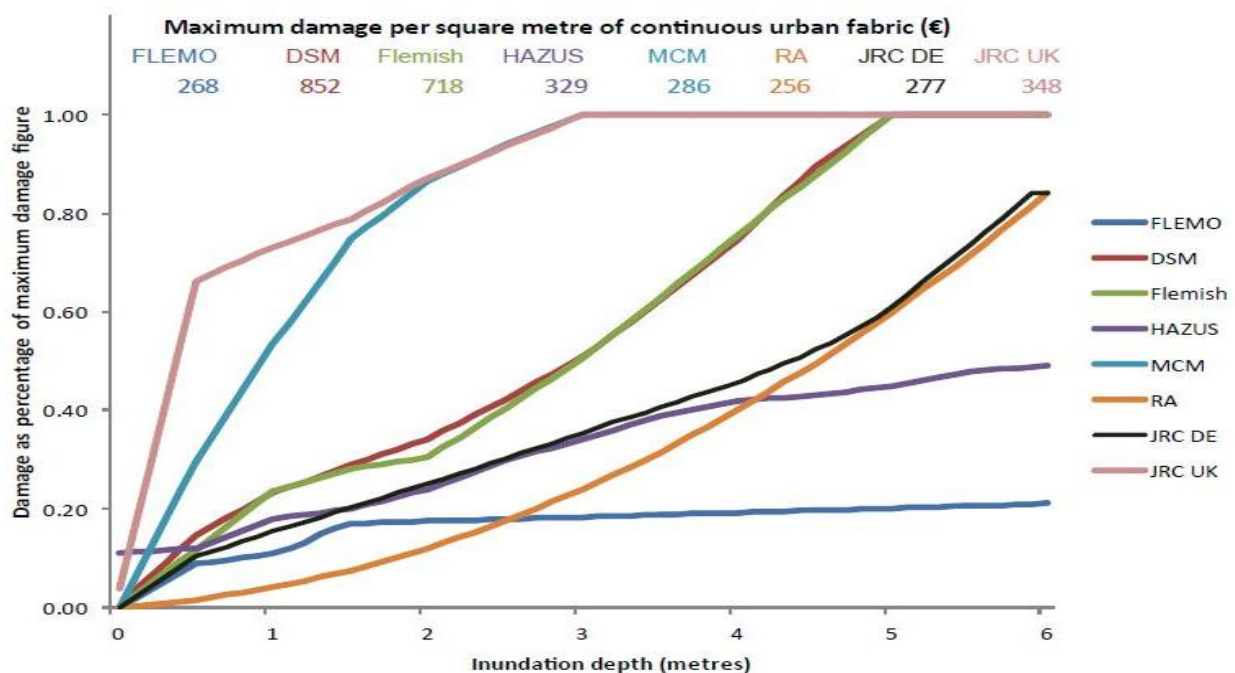


Figure 1-10 – Depth – damage functions and corresponding maximum damage figures for the CORINE land use class “continuous urban fabric”. The functions of each damage model are based on a manual selection of available damage classes, except for the JRC Model. (source: Jongman et al. 2012)

¹¹ <http://www.fema.gov/hazus>

1.2.2. Quantifying Uncertainty of Predictions

The meaning of risk can be very abstract, but it is not difficult to make it quantitative (see paragraph 1.2.1.2). It is tangible and can be expressed in units, for instance dollars/year or number of fatalities per event. Uncertainty (or certainty) is on the contrary more abstract and says something about the quality of prediction. The dictionary states about uncertainty *“not clearly or precisely determined; indefinite; unknown”*¹². This is very vague of course, but there are ways to make it more tangible and quantitative as well. This is where statistics comes into play, which provides multiple tools to do so. One of these tools is probabilistic logic, which combines the capacity of probability theory with the capacity of deductive reasoning. To understand how much uncertainty is at play it is important to know how probable the predicted most-probable event is and equally important: to know how probable other possible predicted (or non-predicted) events are. Indicators for uncertainty are for instance standard deviation and percentiles. In general, Indicators that say something about the shape and distribution of the outcome’s Probability Function (PF) say something about the uncertainty.

This can easily be demonstrated by throwing a dice, of which the amount of eyes afterwards is called the outcome. A set of outcomes is called the event and all possible outcomes the sample space. In the case of a dice the number “1” is one of the outcomes and throwing “1” is an event. In order to figure out for instance what the most probable outcome, average, standard deviation etc. is, one needs to know two things:

- 1) The full set of possible events;
- 2) The chance/probability of occurrence of every single event.

To gain that information one can use logic (exact formulations), real observations or synthetic observations. For the outcome of throwing a dice it is easy to get real observations: if one throws a few hundred times and applies a statistical analysis, one comes pretty close to the theoretical answer. The latter can be obtained by logic and the use of statistical formulas (which is on itself also based on logic): six possible events; all equally probable; an average of 3.5 and; a standard deviation of 1.709. It is said that for (a perfect) dice an exact answer can easily be determined, but for more complicated cases this becomes quickly impossible. As a combination of the first two methods, it would also be possible to synthesize observations by ‘throwing’ dice with a computer. By deriving variables, determining their variability and the mutual (physical) relations from the observations are generated, which again can be statistically analysed. This wouldn’t be very thrilling for the example of one dice, since there is only one variable influencing the outcome, knowing the number of eyes thrown with the dice.

But what if the outcome would depend on more variables, which is most of the time the case in reality? Let’s take for instance the sum of three dice, for which the probability of occurrence is not equal for all events anymore. For instance, the event ‘total nr of eyes = 11’ is more likely than ‘total nr of eyes = 18’. A prediction that uses that knowledge would therefore be better than choosing randomly. With a computerized random function the throwing of one dice can easily be simulated and with the use of relations (in this case: outcome sum of three independent dice) a set of observations can be created. By analysing these observations the Joint Probability Density Functions (PDF’s or discretized form: Joint Probability Mass Functions or PMF’s) of the variables can be derived. These Joint PDF’s or PMF’s are used in statistical models to establish not only marginal PDF’s (without prior knowledge), but also conditional PDF’s of PMF’s (based on known conditions). Conditional PMF’s written in table form are also known as Conditional Probability Tables (CPT’s). If one would, for example, know what the number of eyes is for one of the dice (for instance ‘total nr of eyes on dice 1 = 6), the situation is conditioned and the corresponding conditional PMF’s of the outcome (sum of dice) as well. The prediction of the outcome can now be better; see Figure 1-11. This is because the PMF of the sum of the dice is dependent on each of the three dice and will change if more is known about these dice. The conditional probability function will be narrower than the marginal PDF and the narrower the smaller uncertainty is

¹² <http://www.thefreedictionary.com/uncertain>

relatively. This is in analogy with the explanation of the dictionary: uncertainty = unknowing; and vice versa, certainty = knowing.

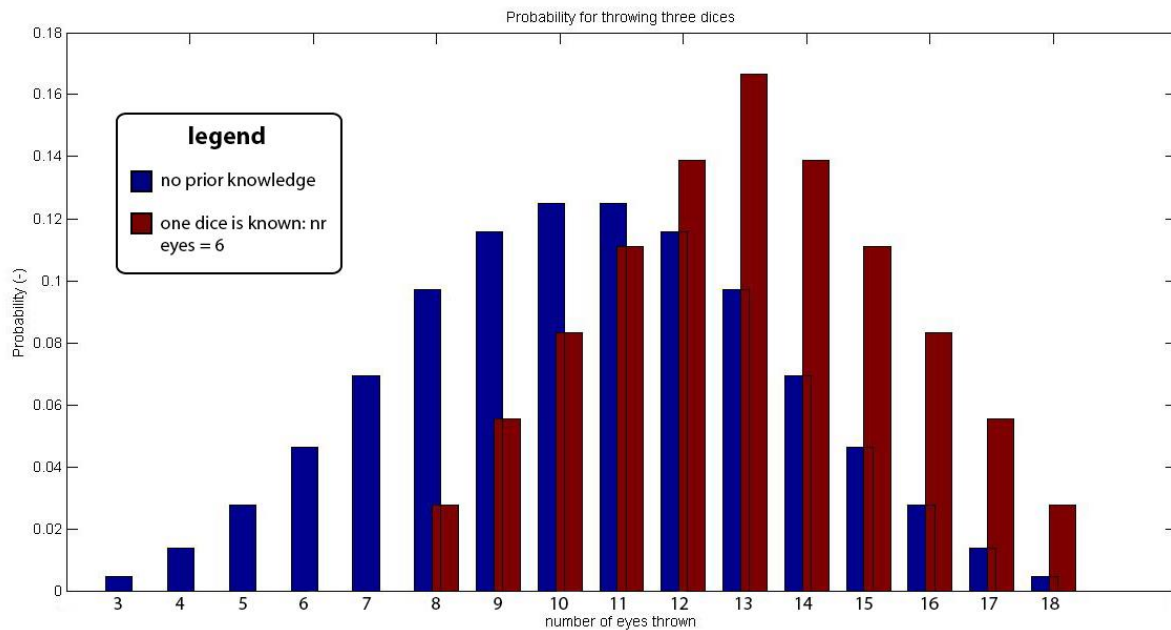


Figure 1-11 - Probability Mass Functions of the sum of three dice

It should be noted that the PMF's of Figure 1-11 are created with statistical formulations, which makes the obtained PMF's exact (assuming perfect dice), or in other words: the PMF's do not contain errors. If one wants to approach the PMF's of Figure 1-11 based on real or synthesized data, one needs a certain minimum amount of observations in order to minimize errors in the marginal and conditional PMF's. For the example of three dice more observations are necessary than for the example with only one dice to obtain equally certain probability functions. This is because there are more variables, implying a larger set of unique combinations (paths) and possible events. Conditional PF's are based on a smaller fraction of the data than that is used for the marginal PF. That fraction of data should always be numerous enough to obtain joint PDF's or PMF's with certain confidence in order to be able to derive good conditional PF's or CPT's. The other way around this counts as well: to which extend one can condition on (or isolate parts of) the data is limited given a finite number of data. Conditioning can give narrower conditional PDF's¹³ and thus better (more certain) predictions, but will at some point also exhaust the data resulting in poorly substantiated PDF's or PMF's; the data is said to being over-fitted.

In the example of the three dice not all (physical) processes of influence are known and fully understood. One could for instance try to include the angle of the hand and speed while throwing in a computer model in an attempt to improve the prediction by reducing the uncertainty. Even if you would know these things, other equally important physical properties like irregularities in the table are still unknown, meaning that uncertainty will not decrease. The associated uncertainty is known as aleatoric uncertainty or statistical uncertainty, which is uncertainty we simply cannot (or do not want to) reduce. In a computer model this uncertainty can be added by using random functions. The counterpart of aleatoric uncertainty is epistemic uncertainty, associated with processes that are unknown or not fully understood but could be known and are of influence on the probability of the outcome; for instance the asymmetry of an asymmetric dice. Not adding the asymmetry to the model will give simulated PDF's that differ from PDF's established with real observations. The difference is

¹³ The opposite can be the case as well: by conditioning it might be very well possible to isolate the data/observations that contain more uncertainty than the whole dataset on average. In that case the Conditional PDF is wider than the Marginal PDF.

associated with the epistemic uncertainty of that specific unknown physical process. Real observations are therefore not only of importance for the validation of model predictions, but also for the validation of uncertainty quantification.

It can be concluded that if in statistical models the PF's can be constructed based on observations from reality, than this is more valuable than constructing them based on model observations. This is especially true if not all processes are fully understood. However, this is not always as easy as in the previous example. For modelling of hurricane impact, three main problems can be addressed:

- 1) Not enough real observations;
- 2) Not all (physical) processes are known;
- 3) The more complexity is added to the model, the more observations are necessary.

Hurricanes do not happen often and it is simply not possible to repeat the event multiple times under the full range of conditions. The number of observations is thus limited. So this is where physics-based modelling can be brought into play as a secret weapon, in order to substitute the real observations with observations from simulations. These models are a reflection of reality and based on hindcasts against past observations. This entails a second problem. Without enough observations, it is hard to say if all processes of influence are (well) represented in the model and therefore hard to determine if all possible outcomes can be covered with model simulations. Moreover, the uncertainties associated with these unknown processes, either epistemic or aleatoric, are hard to quantify since validation possibilities are limited. You could say that there are blind spots. The attribution of these blind spots to the total amount of uncertainty is often hard to determine. The burning down of a complete block of houses (see 'Secondary Direct Damage' in paragraph 2.2.1.2), caused by power short circuits, can be seen as an example of this. Some processes will not be known before it happens and change the beforehand assumed hazard pathways.

Third, it should be noted that adding more complexity to a model, in order to better present processes of influence and therefore lower uncertainty, comes with a price. The more processes and variables are added to predict the outcome, the more observations are necessary to construct the CPT's in statistical models. The number of variables, relations and bins (for the discretisation) included in the model drive the required minimum amount of data to get qualitatively good predictions. This is in analogy with the example of throwing three dice instead of one.

1.2.2.1. Damage Curves

As has been described in paragraph 1.2.1.2 damage curves are used to couple local storm conditions to local damage, for instance to a house. Unfortunately, they do not cope with uncertainty. The damage (ratio) is always the same for 1m of water, whether it is building A or building B, which makes them deterministic. In reality however, this is certainly not true, see the spreading in Figure 1-12.

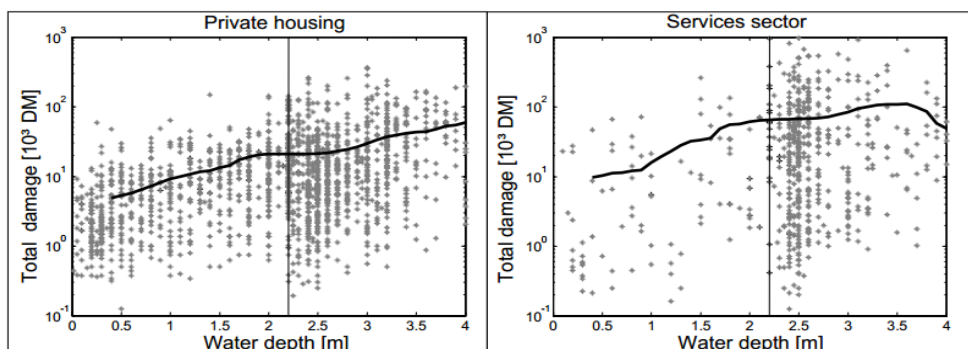


Figure 1-12 - Depth - Damage scatter plot with the corresponding damage curve (Merz et al. 2004)

It should be noted that deterministic damage curves are definitely a shortcoming in reaching the goal of quantifying all uncertainties at play. However, they proved to be useful in the quantification of risk on a large spatial scale level. This is because some uncertainty of the prediction on building level becomes relatively small when you aggregate to larger spatial scale levels; one could say that that the errors average out. The standard-deviation/mean ratio for the average damage of a number of comparable houses is relatively smaller than the damage for one single house. This phenomenon can be best explained by considering the hypothetical case of a stochastic random variable (eligibly damage to a building) for which counts¹⁴:

For one random variable X (damage to one house):

$$E[X] = \mu \quad std[X] = \sigma \quad \frac{std[X]}{E[X]} = \frac{\sigma}{\mu}$$

For n independent but equal random variables (damage to n houses):

$$E[\bar{X}] = \mu \quad std[\bar{X}] = \frac{\sigma}{\sqrt{n}} \quad \frac{std[\bar{X}]}{E[\bar{X}]} = \frac{\sigma}{\mu} \cdot \frac{1}{\sqrt{n}}$$

And

$$E[X_1 + \dots + X_n] = \mu \cdot n \quad std[X_1 + \dots + X_n] = \sigma \cdot \sqrt{n} \quad \frac{std[X_1 + \dots + X_n]}{E[X_1 + \dots + X_n]} = \frac{\sigma}{\mu} \cdot \frac{1}{\sqrt{n}}$$

The assumption of independent samples does unfortunately not hold for the kind of damage predictions in present thesis since (spatial) correlation is at play; two houses that lay close to each other are likely to have a correlated error ($E[X] - X$). This is for instance because of similarities in geospatial properties; more about this can be found in chapter 0 and 0. Moreover, not every damage prediction has the same distribution and thus the same standard deviation. However, this phenomenon (drop in standard deviation after aggregation) can to a certain extend be observed in practice and is for example described in ‘Damage to residential buildings due to flooding of New Orleans after hurricane Katrina’ (Pistrika and Jonkman 2009).

1.2.3. Morphological Processes during the Storm

Most of the earlier mentioned impact models assume that the dominant forces, causing the damage to assets at risk, can be first of all found in inundation depth, followed by wave attack and flow velocity; see paragraph 1.2.1.2. Where all three hazards are hydraulic properties, only the hydrodynamics are taken into account within the models; the morphodynamics during the storm are neglected, which makes computations less complex and cheaper. The price you have to pay for this simplification highly depends on local properties like coastal configuration, soil properties and human protection measures. For some coasts, of which the Long Island coastline is part of, it can have large consequences for the outcome of prediction.

In paragraph 1.2.1.1 it is stated that hurricanes have the ability to change the appearance of sandy coasts drastically. Natural or human made barriers (e.g. dunes, dikes, mangrove areas) can breach locally or get flushed away completely during the storm and change the initial situation in such a way that the local hydraulic characteristics (inundation depth, wave heights) inland can increase significantly. This can be compared with changing the rules during a game; neglecting the morphodynamics is like denying that the rules have been changed and within that analogy this means that the chance of winning –or making good predictions - decreases.

It must be noted that the morphodynamics have a strong two-dimensional character. A dune breach may occur at one spot, but the effects can reach much further than the specific transect when the water is spreading in all directions. Moreover, some areas show threshold problems: damage only occurs when some threshold is reached. This is for instance the case with dike systems: when a given storm may or may not be

¹⁴ From “The research manual: Design and statistics for applied linguistics” (Hatch and Lazaraton 1991)

able to cause a breach (threshold storm), a large uncertainty in the damage prediction can be expected. Especially for early warning systems this can be a big issue, where for risk quantification purposes these uncertainties will even out over the full set of events.

1.2.4. Spatial Scale and Applicability issues

In paragraph 1.2.1.2 it is stated that the more observations are made the better predictions can be made since more complexity can be added to the statistical model. More observations can come from real world observations to a certain extend and thereafter only from more (physics-based) model simulations. As a consequence the computational expenses will rise. Computational expenses on its turn are always bounded and therefore there is an inversely proportional relationship between the amount of complexity added to the statistical model and the process of quantifying uncertainties.

Next to the increase of computational expenses due to adding of complexity to the statistical model, there is also an increase of expenses when one increases the amount of processes and thus complexity in the physics-

based models. Adding morphodynamics in particular will raise the prediction skill of local storm conditions and thus indirectly the precision of damage predictions. However, computational time will increase as well. Less model simulations will solve this problem, but has its negative impacts on the amount of observations again. In this way the complexity of both statistical and physics-based models are bounded.

Moreover, the smaller the spatial scale level of analysis is, the more detail the physics-based models should contain. This has, again, its impact on computational time. Another disadvantage of more detail is

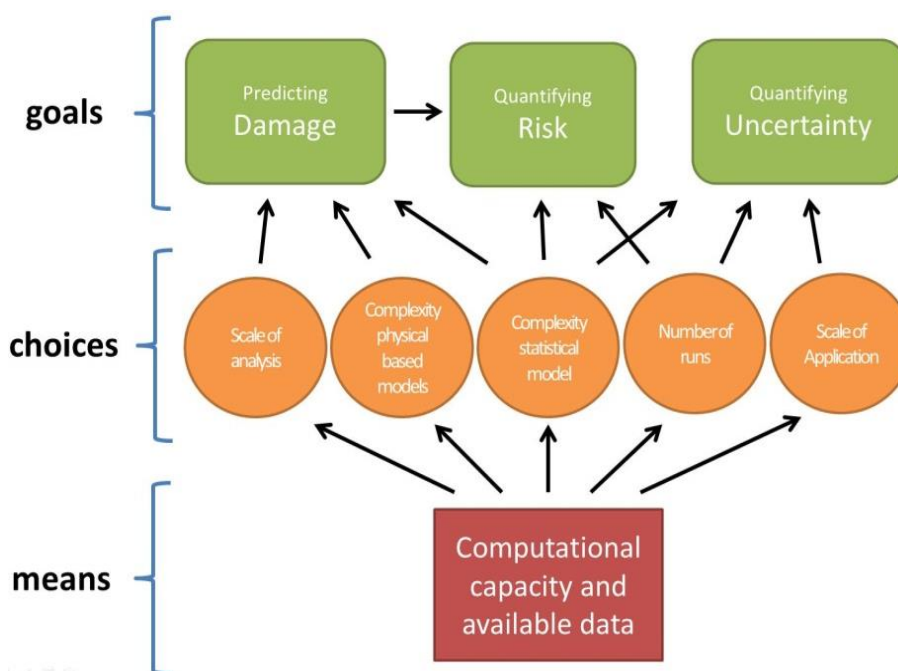


Figure 1-13 - A representation of the axis of freedom

that relatively large amounts of data should be gathered if one is still interested in a large area. The latter also can be of important to the statistical model. This is because damage observations are scarce; the larger the area, the more damage observations.

The above mentioned dilemmas are well known in the numerical modelling industry. In general, the way to cope with them is to: 1) find out which goals are important for the application; 2) pick the right scale level of analysis and application; 3) add as much complexity until the means become insufficient. The latter is easier said than done. Where to add complexity and where not (physics-based models versus statistical model) should be extensively analysed. A representation of the axis of freedom, means and goals is given in Figure 1-13.

1.3. Delineation

Considering Figure 1-13 again, most of the discussed model methodologies from paragraph 1.2.1.2 did not include the quantification of uncertainty in their main goals, but focused only on damage predictions and/or risk quantification. Developing a model concept including all three aspects is too large a topic for a time limited study like this. Therefore, this thesis focuses only on the prediction of damage and quantification of the corresponding uncertainties, leaving the risks out. This makes some decisions easier but limits the applicability, of which the impacts are elaborated in the discussion part (Chapter 0).

Some other simplifications have been made as well. First of all, the coupling is only researched on the object level, the lowest spatial scale level. Reasoning for this can be found in the idea that if the concept works on the lowest spatial scale, it will probably work as well on aggregated levels. Secondly, not at all types of damage are considered, but only direct tangible damage to residential buildings. A lot of data is available for that type of asset and it attributed the most to the total direct damage caused by Hurricane Sandy: almost 60% of the total losses (see paragraph 1.1.1.2). Third, this research is limited to the application of Bayesian Belief Networks as a statistical modelling tool and XBeach as part of the physics-based modelling train for the propagation of hazards. Both are choices and have their own limitations, which are in more detail elaborated in chapter 0. In this limited context probabilistic relations between vulnerability indicators, local storm exposure characteristics and corresponding damage are established and analysed.

1.4. Research Questions

1.4.1. Main Question

Based on the insights from the background, the defined problems and delineation the following main question is derived:

What are the steps needed to connect hazard modelling to impact modelling in order to predict damage in a probabilistic way?

1.4.2. Sub Questions

1. What model approach and structure can be used best and which aspects are important?
2. What are the effects of model resolution and inclusion of morphodynamic processes on prediction skill?
3. Which aspects are of influence on the quantification of uncertainty and what is the sensitivity of choices (number of variables, connections and bins)?
4. How can vulnerability and socio-economic data be integrated and what are the corresponding effects on prediction skill and the quantification of uncertainty?

1.5. Research Approach

1.5.1. Approach

To answer the questions posited in section 1.4 the following steps are taken. First of all a new modelling concept has been developed, which is introduced and extensively substantiated in chapter 0. To give a proof of concept the Rockaway Peninsula has been chosen as a case study. The study site is analysed and in chapter 2 geographical properties, socio-economic aspects and vulnerability to storms are elaborated, followed by an analysis on Sandy's impact and summary of the available data for the area. The implementation of the model concept is described in section 3.2.

The results, both from the physics-based modelling part and the statistical model, are given in chapter 0. This is also where the sensitivity of variables and impact of choices to damage prediction skill and uncertainty quantification are presented. The results are discussed in chapter 0 and based on the obtained insights recommendations are given for future research.

1.5.2. Objectives and Deliverables

The following objectives and deliverables are derived:

1. Results of Hurricane Sandy simulations executed with the physics-based models and straightforward description of output;
2. A proof of the proposed model concept;
3. Recommendations for future research;
4. Conclusions – answers to the main and sub questions.

2. Study Site

This chapter elaborates geographical and socio-economic properties of the Rockaway Peninsula, both before and after Hurricane Sandy struck the area. The specific pathways of the hazards are described in section 2.2 and the data that has been used for the implementation of the concepts of Chapter 3 are summarized together with the corresponding sources in Section 2.3.

2.1. Rockaway Peninsula

2.1.1. Geographical analysis

2.1.1.1. Coastal Configuration

Most parts of the US East Coast can be considered as barrier coasts, showing sandy coastlines with wide beaches, dunes, typical barrier islands in front of the coast and behind it estuaries or lagoons. The Long Island coastline, of which the Rockaway Peninsula is part of, forms no exception. In the top panel of Figure 2-1 typical configurations of barrier coasts can be seen and in the lower panel a top view of the South-Western part of Long Island is presented. The peninsula is thus a typical barrier spit.

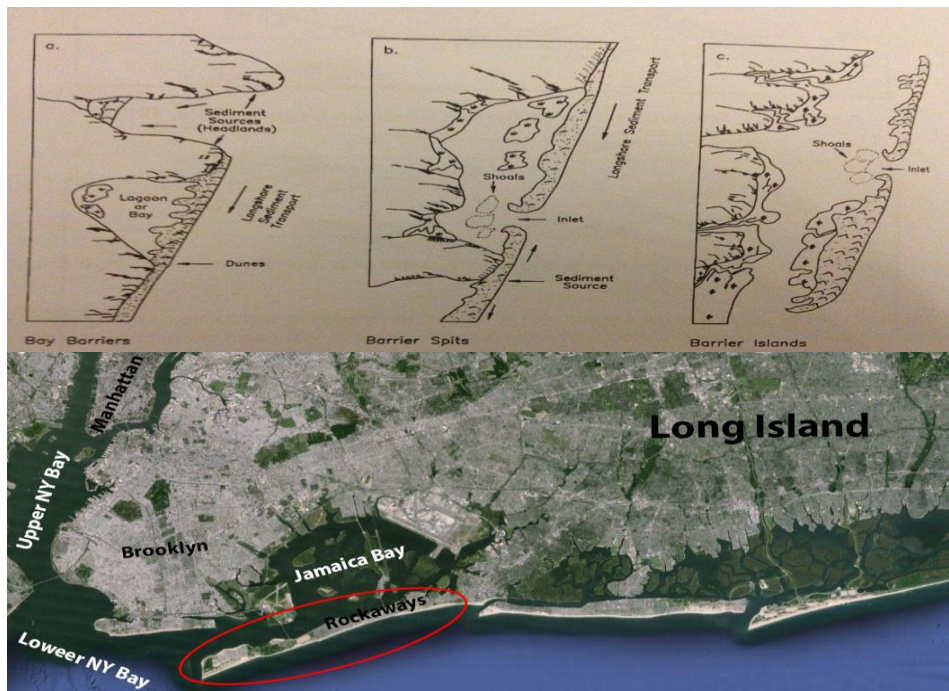


Figure 2-1 - Top panel: typical configurations of barrier coasts (source: Royal HaskoningDHV); lower panel: top view of the South-Western part of Long Island (source: Google Earth)

It can be seen that the Rockaway Peninsula (encircled in red) is part of a lagoon system consisting of: 1) the Jamaica Bay with the typical shoals; 2) the Rockaway inlet, which connects the Jamaica Bay to the Lower New York Bay in the west and; 3) the barrier split, which is the Rockaway Peninsula itself. Barrier coasts are wave dominated and exposed to mixed-energy sea states. It should be noted that these coastal systems are typically very dynamic: large storms can easily change the configuration of the coast. Since barrier islands, either attached to the mainland (spits) or isolated by inlets, are sandy low lying areas they can breach or move hundreds of meters land inwards when overwash or inundation occurs during high storm surges. Historical maps show that this has also been the case for the Jamaica Bay area during the past centuries; see Figure 2-2.

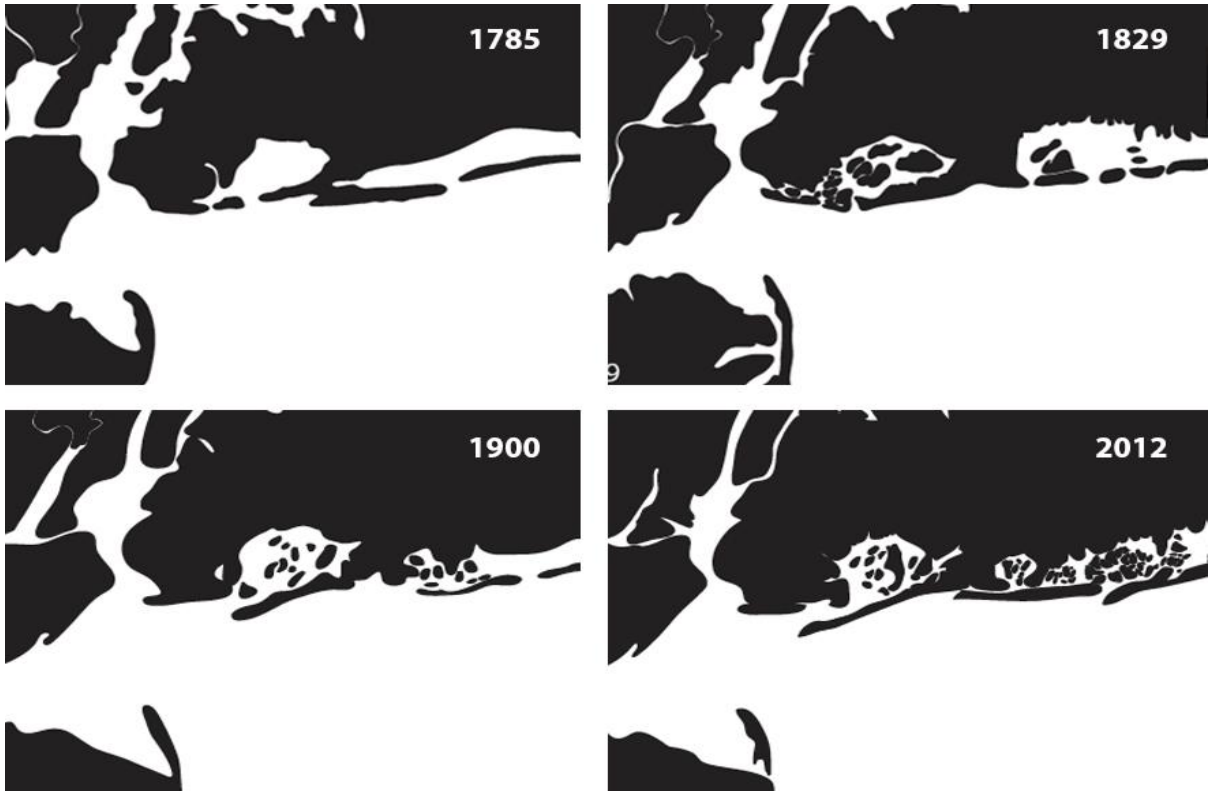


Figure 2-2 – Schematic evolution of the Jamaica Bay (source: Royal HaskoningDHV)

Looking at the cross shore profile of a typical barrier island (Figure 2-3), one can distinguish the following elements: 1) a nearshore surf zone with migrating submerged sand bars; 2) sandy beaches consisting of the steeper intertidal zone and a higher situated berm; 3) a fore dune at the ocean side and a back dune at the bay side with a sheltered area in between (inter dune); 4) a back-barrier bay (lagoon or creek) with tidal marshes and shoals. The bay, sheltered from waves, traps a lot of fine muddy sediments and has the ability to give home to rich and diverse ecosystems.

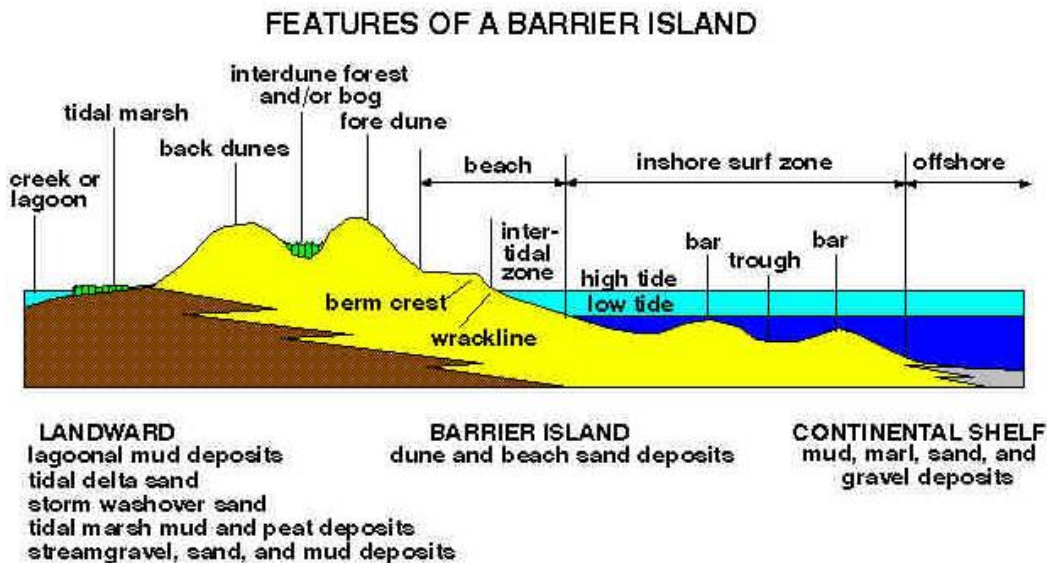


Figure 2-3 - Features of a Barrier Island (source: CUNY¹⁵)

¹⁵ <http://www.geo.hunter.cuny.edu/bight/beach.html>

The Rockaway-Jamaica Bay system consists roughly out of the same features as in Figure 2-3, but human intervention changed the natural configuration radically. Larger parts of the back dune and inter dune areas are cultivated and turned into urban areas. The beaches are maintained by the US Army Corps of Engineers (USACE) and on top of a fore dune (better described as a human made berm) a 5 mile long board walk is constructed. At the bay side of the peninsula the transition from island to lagoon is fixed by a local access road, named Beach Channel Drive. These human interventions changed the natural dynamics of the system, which is elaborated extensively in the next section.

The orientation of the peninsula is East-West, which is in agreement with the direction of net alongshore sediment transport. The latter is caused by a dominant incoming sea swell coming from the South-East, approaching the coastline under an angle. Some other geographical characteristics of the area are given here:

- The berm crest reaches on average to a height of 8.9 ft. or 2.7 m above North American Vertical Datum of 1988 coordinate system (NAVD88), where Mean Sea Level (MSL) is at 0 m NAVD88 with a tidal range of 1.8 m (NOAA 2013).
- The ground levels of the residential areas are on average 2.23 m high (referenced to NAVD88). The buildings in the first block from the ocean side are located on higher grounds (+/- 3.5 m) and the blocks behind on lower grounds (+/- 1.5 m). See Figure 2-4 in which the ground elevations per building are shown spatially;
- Jamaica Bay is in general shallow with bed levels within the tidal range or a little bit below, but the main channels are deeper (-10 m below MSL) and are located directly behind the Rockaway Peninsula; see also Figure 3-16.



Figure 2-4 - Ground Elevations per building in meters ref. to NAVD88 (source: NYC buildings dataset)

2.1.1.2. Morphodynamics

Different physical processes drive morphological changes of barrier coasts in general and the Rockaway Peninsula specifically. In Figure 2-5 the forces and corresponding morphological effects of these processes are schematically shown. In the case of long-term equilibrium, morphological impacts caused by the dominant processes (e.g. high waves and surge) during a storm are 'restored' by a much slower recovering process (mainly wind and low waves). For this research only the physical processes during storms are of importance

and therefore explanation is restricted to these only. However, it is good to realize that for the general appearance and configuration of the barrier coast the long term processes (e.g. dune formation by wind and vegetation, the alongshore drifts, net onshore directed transport during low-energy sea states) are equally important.

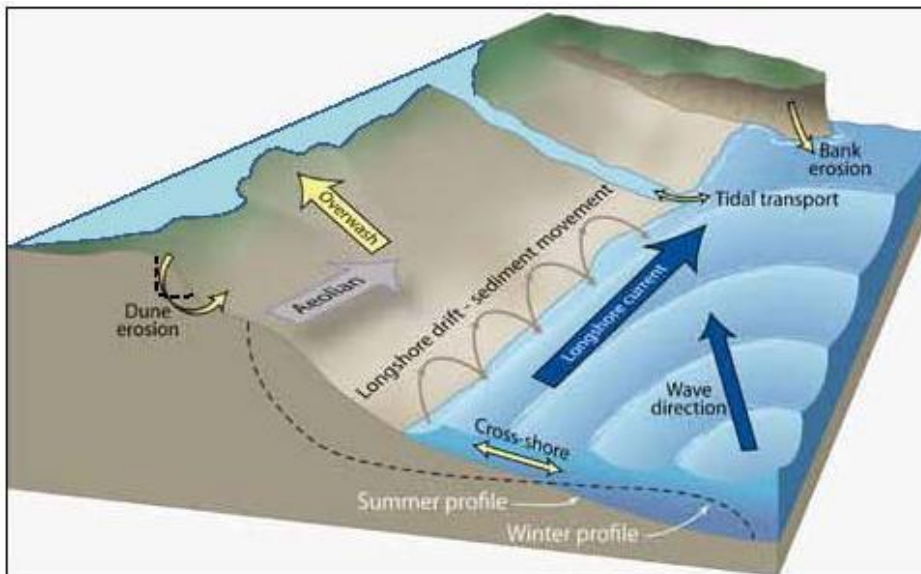


Figure 2-5 - Nearshore Dynamics (source: Royal HaskoningDHV)

The Long Island coastline is exposed to Nor'easters during the winter months and rare hurricanes during the hurricane season, which normally starts in June and ends in the month of November. Although this means that threats are present almost the whole year round, sea states are in the winter on average rougher than in summer, causing a difference in winter and summer profile; see the differences between the two profiles in Figure 2-5. This is because during high-energy sea states the onshore directed sediment transport processes are dominated by the offshore directed transport processes. During hurricanes and Nor'easters this dominance is huge and since large amounts of sediments are transported offshore the waterfront retreats inland. The first stage, which is always reached during these storms, is schematically shown in Figure 2-6 and is referred to as the swash regime.

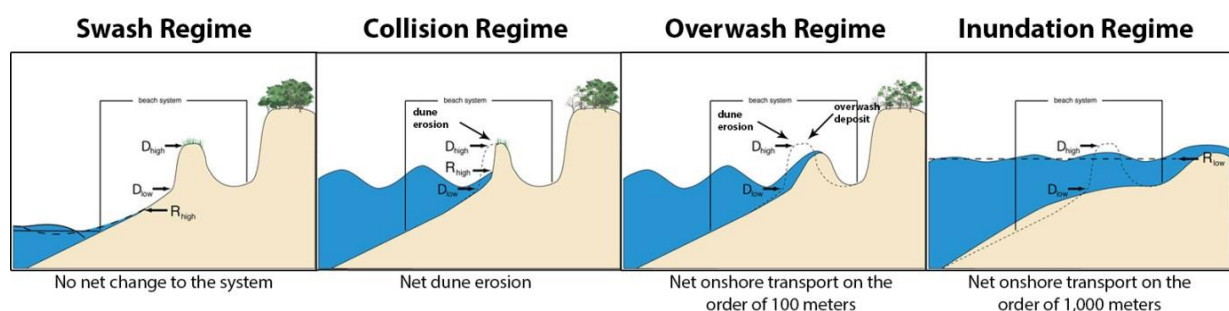


Figure 2-6 - Different regimes during a storm (source: USGS¹⁶)

The other three stages can happen subsequently when water levels rise. If the water levels are high enough the dunes are attacked by the waves and will episodically erode away. This step is referred to as the collision regime. During the overwash regime the water levels and waves are so high that waves are overtopping the partly eroded dune crest. The last stage is known as the inundation regime when the water level is higher than the (remaining) dune crest height and when sediment is transported from the beaches and fore dune to the

¹⁶ <http://coastal.er.usgs.gov/hurricanes/impact-scale/inundation.php>

hinterland (inundation regime). It should be noted that next to these cross shore processes, alongshore processes can be of great importance as well. Spatial differences in alongshore erosion rates and weak spots in the fore dunes can cause local breaching. Moreover, during high surges the water levels in the Jamaica Bay will rise as well, which can cause flooding of the Rockaway Peninsula from the bay side; this is known as back-barrier flooding, which happened during Hurricane Sandy as well.

2.1.1. Socio-economic analysis

Nowadays, the Rockaway Peninsula is primarily a residential area. However, this was completely different in the turn of the 20th century, when the New Yorkers vacationed in brand-new hotels and bungalows enjoying the Rockaway beaches. With the advent of automobiles in the 1920's this started to change, since that made driving to more distant beaches at Long Island possible (Chan et al. 2013). Because of this drop in tourism, a lack of economic opportunities due to geographical isolation and exposure to erosion and weather, the area pauperized rapidly. In the 1940's and 1950's politicians decided to use the Rockaways to accommodate the growing need for affordable housing and relocated New York residents who had to be displaced for large city's renewal projects to the Rockaways. Today, the heritage of these choices can still be seen. Of the 80 public housing communities of whole Queens County, 21 are located on the Rockaways, exposing a vulnerable group of residents, of which a lot are in need of social services and assistance, to hazardous storm surges (Chan et al. 2013).



Figure 2-7 - Map showing neighbourhoods (Source: Project Jamaica Bay)

As of 2010, the Rockaway Peninsula is home to approximately 112,518 residents (Chan et al. 2013) who live in the communities of Breezy Point, Roxbury, Fort Tilden, Jacob Riis Park, Belle Harbor, Hammels, Arverne, Bayswater, Neponsit, Seaside, Rockaway Beach, Somerville, Rockaway Park and in the east Far Rockaways. Of them 40% are African American, 34% white, 21% Hispanic and the residual 5% Asian or of other race. According to the American Community Survey (ACS), the average household incomes show huge spatial variability, ranging from 120,000 dollars per year in the western part to less than 20,000 dollars per year in one of the communities, see Figure 2-8.



Figure 2-8 - Median Income in the Rockaways (source: Averno East Study)

The Rockaways incorporate 44,325 housing units in 2011 according to the American Census Bureau. 87% of these units are occupied of which 62% (a majority) are renter-occupied and 5% are vacant properties, predominantly for own use. 18% of the buildings contain more than 20 housing units, which reflect the high concentration of public housing properties. The construction material of most single-family houses (majority of buildings) is wood with concrete foundations and basement with brick cladding, where larger buildings are generally completely made of concrete (Guy Carpenter 2013). The fact that both rich and poor have experienced the impacts of Hurricane Sandy and the high density and variability of residential buildings makes the Rockaway very interesting for present study.



Figure 2-9 - Predominant land use class per tax lot, obtained from the PLUTO dataset

Next to residential purposes the Land use of the Rockaway Peninsula mainly consists of open space, outdoor recreation and vacant land; hardly any commercial or industrial activity can be found in the area. Land use can be spatially observed from Figure 2-9, which comes from the PLUTO dataset from the NYC Department of City Planning.

2.2. Sandy's Hazard Pathways and Impacts

Sandy's overall propagation and impacts are already discussed in section 1.1.1.2. This section will elaborate on the specific hazard sources and pathways at the Rockaways, together with the corresponding impacts. How the super storm interacted with the existing geographical components of the system and what the corresponding impacts were is discussed. Sandy's eye made landfall near Brigantine, New Jersey, which is as the crow flies over 120km away from the Rockaway Peninsula. Nevertheless, the Rockaways got the full load where wind speeds were maximal on the North-West side of the eye, which in combination with the geographical features appeared to be unfavourable for New York and surroundings.

2.2.1. Hazard Sources and Pathways

2.2.1.1. Surge and Inundation

The notion of storm tide, storm surge, water level and inundation level can differ. In this thesis storm tide refers to the water level including the abnormal rise of sea level caused by the cyclone (storm surge) in combination with the astronomical tide, which is in agreement with the terminology of NOAA¹⁷. Water levels in general can refer to storm tide, but in this thesis it will include short and long waves as well. All are referenced to a level (e.g. Mean Lower Low Water (MLLW) or NAVD88, which is more or less equal Mean Sea Level). Inundation depth though is often not very clear defined. In this thesis inundation depth is defined as the difference between the water level excluding short waves but including storm surge, tide, setup and long waves; and the topographic level (of the ground elevation).

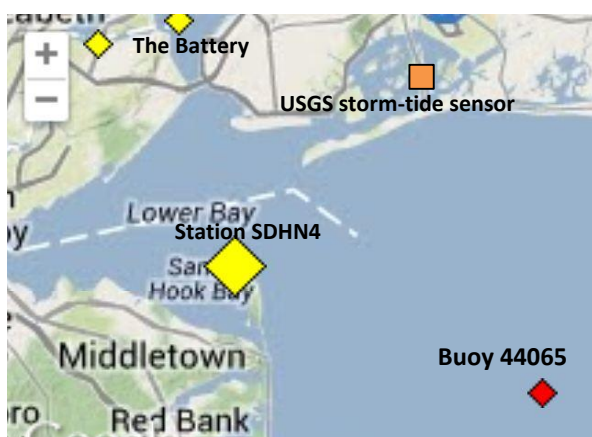


Figure 2-10 - Gauging Stations and USGS's temporary storm-tide sensor (based on a figure of NOAA)

In Paragraph 1.1.1.1 it is stated that storm tides of 4.4 m (ref. to MLLW) have been observed near the Battery (station NOAA), exceeding the previous record of Hurricane Dona (1960). Where the Battery is located in the New York Upper Bay area, The Rockaway Peninsula is located outside the Bay and more exposed to open sea. Unfortunately, no water level recording gauges are situated directly offshore of the Rockaway Peninsula, which makes it hard to make a comparison to the battery. The closest station is SDHN4¹⁸ near Sandy Hooke, NJ, located on the ocean side of the Lower Bay, which recorded a storm tide of 13.2 ft. or 4.03 m above MLLW and equivalently: 3.175 m above NAVD88. Hereby it is noted that the sensor stopped recording just before

the expected time of the peak and it is likely that the storm tide peak would be pretty much equal to the storm tide at the Battery (NOAA 2013). It is therefore assumed that storm tides in front of the Rockaway Peninsula were a little bit higher than the last recorded levels. Moreover, it is assumed that storm tide in the Jamaica Bay was in the same order as well, which is in agreement with a temporary storm tide sensor from USGS¹⁹ (installed a day before landfall) at the water side of Broad Channel, showing a storm tide of 10.38 ft. or 3.16 m above NAVD88; see Figure 2-11.

¹⁷ <http://www.nhc.noaa.gov/surge/>

¹⁸ Station SDHN4 - 8531680 - http://www.ndbc.noaa.gov/station_page.php?station=sdhn4

¹⁹ SSS-NY-QUE-005WL - Jamaica Bay at Broad Channel at Queens, NY - Storm-Tide Sensor

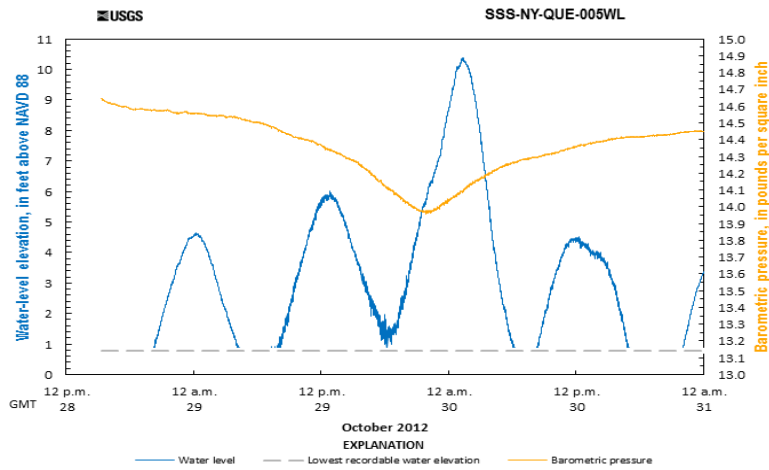
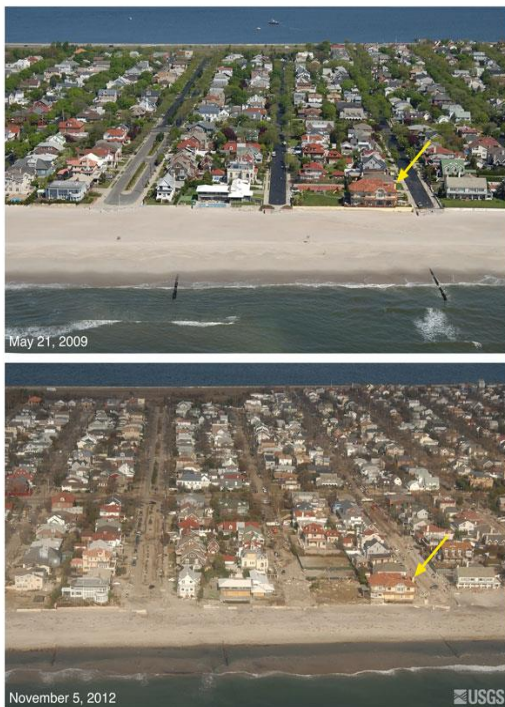


Figure 2-11 - water level records in time by USGS's temporary storm-tide sensor (source: USGS)



Comparing the bay side storm tides to the ground elevations of the peninsula, it can be concluded that back-barrier flooding was indeed inevitable and corresponding local inundations depths in the order of 1 to 2 meter are explainable (E. Blake 2013; PlaNYC 2013). According to the Army Corps (USACE 2013) Sandy's storm tide at the berm (the small maintained fore dune with boardwalk) was 11.6 ft. or 3.53 m above NAVD88, which is higher than the offshore storm tide approximation, possibly as a result of wind and wave set up. This means that the depth over berm was 2.7 ft. or 0.82 m; overwash and inundation were thus both at play. The Army Corps state that at some areas the beaches were heavily eroded and at these places the boardwalk was completely destroyed, mainly because of the wave impact; see Figure 2-13.

Figure 2-12 - Oblique aerial photographs of Neponsit, NY (source: USGS). The view is looking northwest across Rockaway Peninsula. Sand was washed from the beach into the streets, and towards the bayside of the island, and several rows of ocean-facing houses were destroyed or damaged. The yellow arrow in each image points to the same feature.



Figure 2-13 - Destroyed boardwalk (photographer: Nathan Kensinger)

Especially the area between 90th and 149th street was heavily affected and overwash deposited piles of sediment from the pre-storm berm and beach land inwards; see Figure 2-12. In other areas, where the pre-storm beaches were wider (which were also the areas with groins), the boardwalk suffered less damage and the full inundation regime was never reached. In Figure 2-14 the coastline has been divided in stretches with

more or less similar damage properties, which are described in Table 2-1.



Figure 2-14 - Overview of damage to the beaches and Boardwalk; based on aerial pictures taken directly after the storm.

Table 2-1- Description of the situation and observed damaged for the locations of Figure 2-14.

Stretch	From	To	Situation	Damage
A	Beach 149 th St	Beach 126 th St	No Boardwalk, narrow beach	wash-over till end of first block
B	Beach 126 th St	Beach 110 th St	Beach Walk Promenade, narrow beach	Promenade swept away, wash-over
C	Beach 110 th St	Beach 90 th St	Boardwalk, narrow beach	Boardwalk swept away, wash-over
D	Beach 90 th St	Beach 74 th St	Boardwalk, wider beach, groynes	Boardwalk survived, heavy erosion of beach
E	Beach 74 th St	Beach 61 th St	Boardwalk, narrow beach, groynes	Boardwalk mostly broken, wash-over
F	Beach 61 th St	Beach 40 th St	Boardwalk, wider beach, few groynes	Boardwalk survived, erosion and wash-over
G	Beach 40 th St	Beach 35 th St	Boardwalk, narrow beach, few groynes	Boardwalk mostly broken, wash-over

Next to the temporary storm-tide sensor at Broad Channel, the USGS collected multiple high water marks (McCallum et al. 2013). The locations of these marks within the area of interest are shown in Figure 2-15 and the corresponding elevations (ref. to NAVD88) and approximations for inundation depth are given in Table 2-2.

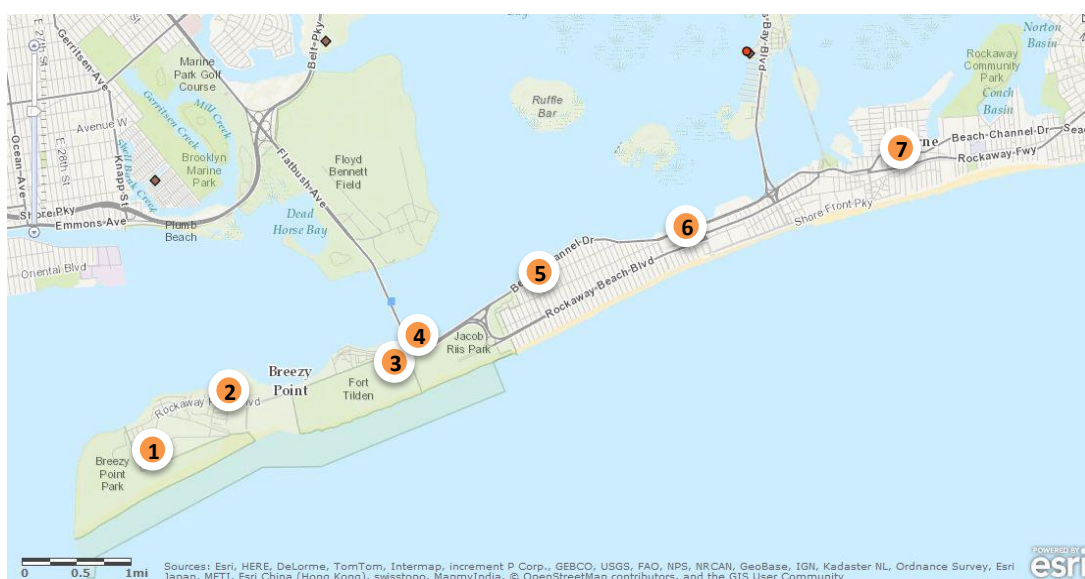


Figure 2-15 - Location of the USGS high water marks

The locations of the high water marks are both interior and exterior, stating something about the maximum water levels with and without short waves. The differences are small, so it is assumed that at these locations waves are small compared to the surge and it can therefore be concluded that the high water marks give good approximations for the onshore storm tide.

Table 2-2- USGS High water marks for the Rockaways

#	Name	Elevation (NAVD88)		Inundation Depth		Description
		Feet	Meters	Feet	Meters	
1	HWM-NY-QUE-729	12.7	3.87	5.4	1.65	wash line on side of house
2	HWM-NY-QUE-728	10.7	3.26	3.6	1.10	wash line on wall inside building
3	HWM-NY-QUE-727	10.8	3.29	0	0	debris line in parking lot
4	HWM-NY-QUE-726	10.5	3.20	0	0	debris line
5	HWM-NY-QUE-730	11.2	3.41	5.4	1.65	wash line in front of building
6	HWM-NY-QUE-731	10.3	3.14	0	0	wash line on wall
7	HWM-NY-QUE-007	10.7	3.26	4.5	1.37	debris line on fence

2.2.1.2. Wind and Waves

Wind and waves are in contrast to storm surge peak levels not measured within the study area. However, they are recorded by buoys offshore, of which buoy 44065²⁰ from NOAA's National Data Buoy Center is the closest and most interesting one. This buoy lies right in front of the Rockaway Peninsula, some 25 km out of the coast where the average water depth is about 50 m. In Figure 2-17 the hourly maximal wind gust speed (red dots) and sustained wind speeds (blue) are given in the upper panel. The significant wave height (H_s) is given in the lower panel. Both wind and wave graphs seem to be pretty much in phase with peaks around midnight, which is more or less the same as for the storm tide peak from Figure 2-11.



Figure 2-16 - buoy 44065 (source: NOAA)

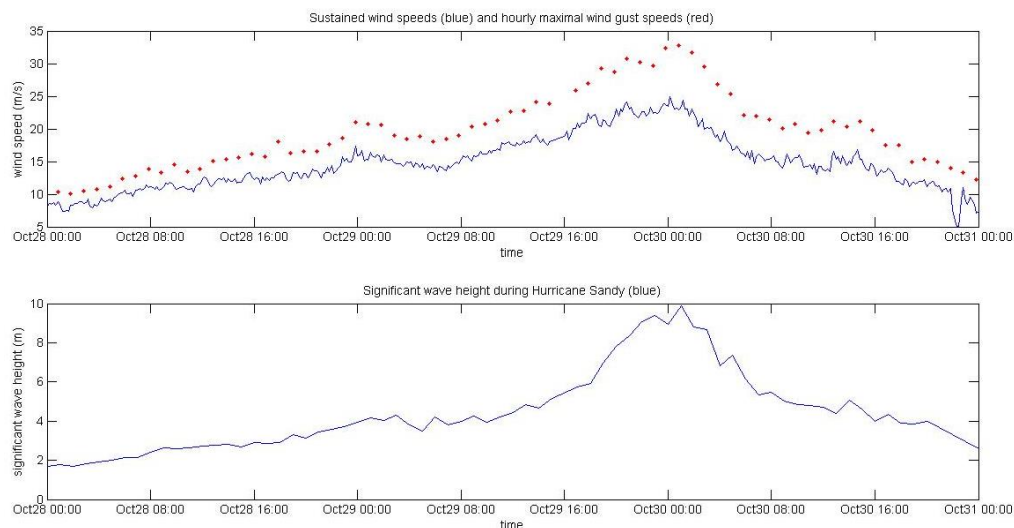


Figure 2-17 - Wind speed and significant wave heights during Hurricane Sandy - recorded by buoy 44065

Maximum wind gust speeds of 35 m/s (126 km/h) on the open water are high, but not uncommon for storms in the region. Sandy was technically not a hurricane anymore at the time of landfall, so this is also to be

²⁰ (LLNR 725) - New York Harbor Entrance - 15 NM SE of Breezy Point , NY
http://www.ndbc.noaa.gov/station_page.php?station=44065

expected. On the contrary, significant wave heights of almost 10 m are extreme. They exceed the previous record of 7.95 m recorded at Buoy 44065 (during Hurricane Irene in 2011) and 9.30 m observed at the same buoy during the Nor-Easter of December 1992 (Sopkin et al. 2014). No return periods have been found for these records.

Wind predictions from the North American Meso-scale Forecast System (NAM) model simulations from the National Centre for Environmental Prediction (NCEP) give a clear idea of the spatial and temporal propagation of wind direction. The black arrows in Figure 2-18 represent these wind directions for three different moments in time: before, during and after the peak of the storm. The yellow dot is the location of buoy 44065 and the red arrow shows the direction of the corresponding recorded half hourly mean wind direction. It can be seen that the wind is turning from almost parallel to perpendicular to the coast. Moreover, the wind direction simulations are in agreement with the observations.

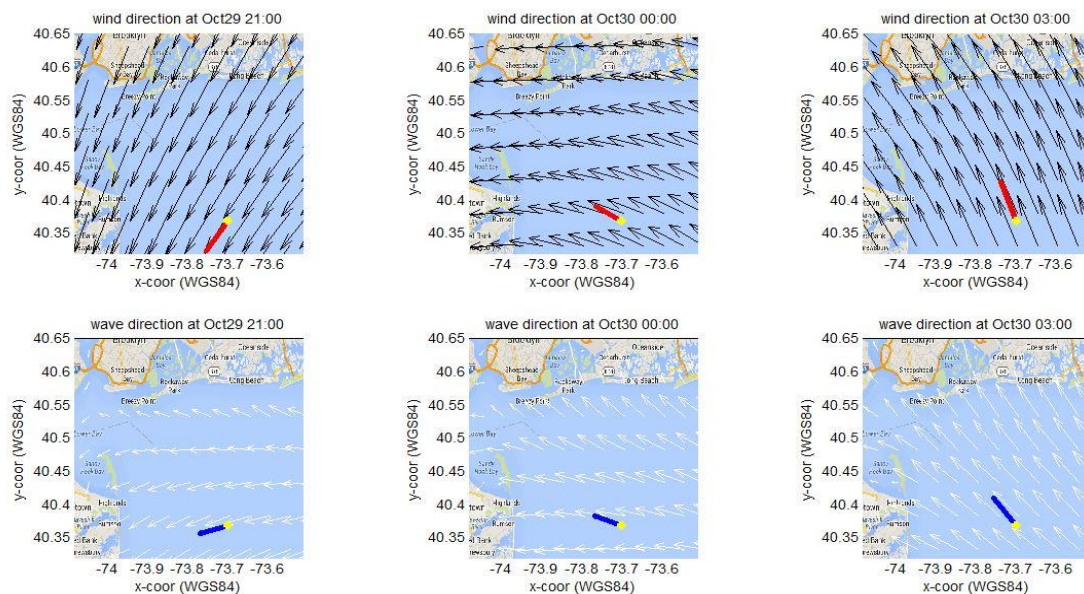


Figure 2-18 - Upper panels: wind directions observed (red) and simulated (black) with the North American Meso-scale Forecast System (NAM) model; lower panels: wave directions observed (blue) and simulated (white) with SWAN

The white arrows in the three lower panels in Figure 2-18 show the wave directions at the same three moments. These wave directions are generated with a SWAN model of the New York Bight and Long Island, which is elaborated in more detail in section 3.2. Again, the observed records of buoy 44065 (blue arrows) are added as well. It can be concluded that the SWAN model, which uses the wind simulation of NAM as input, is in agreement with the observations and that the mean wave direction rotates towards the coast during the storm as well.

Near the coast the wave heights decrease because of the wave breaking in limited water depths. However, larger waves easily overtopped the fore dunes and at the location of the breaches waves penetrated into the residential areas. How far these waves penetrate into the area is not really clear, but it is noticed that the elevation of the high water marks is not much higher than the maximum recorded storm tide of the temporary USGS storm-tide sensor in the Jamaica Bay. Therefore it is assumed that at the locations of the high water marks, the wave heights of both long and short waves are relatively small. Since all high water marks are at the bay-side of the area, this information can't be used as an indication for wave heights on the ocean side of the Peninsula. However, post-sandy pictures of destroyed houses close to the beach give proof of severe wave attack; see Figure 2-20.

2.2.1. Impacts

2.2.1.1. Morphological Impacts

The USACE has conducted multiple LIDAR surveys in order to obtain high-resolution topographical datasets covering most parts of the Long Island coastline, including the Rockaway Peninsula. The LIDAR datasets are also elaborated in section 3.2 and in detail described in Appendix D. In addition to their normal survey campaign, for which they survey every 5-7 years, the USACE conducted a post-sandy survey. The differences between pre- and post-Sandy LIDAR data show the erosion and sedimentation caused by the storm, indicating the morphological impact. A visualisation of the topographical changes is shown in Figure 2-19.

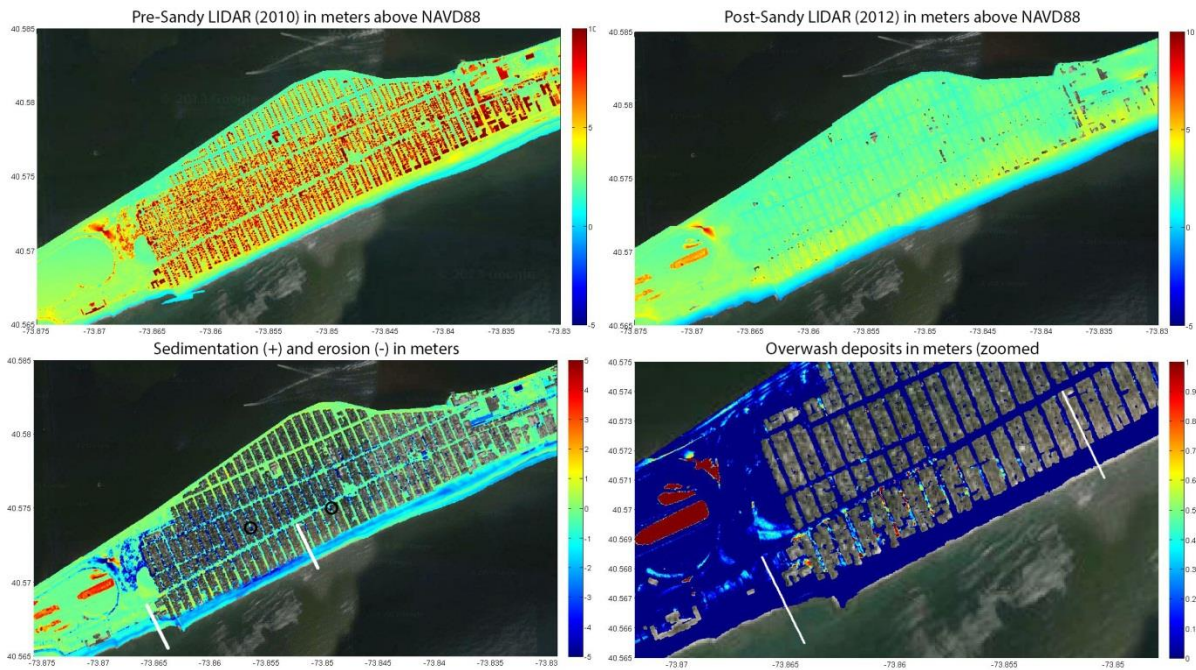


Figure 2-19 - Bed level changes due to Sandy. Left upper panel: pre-Sandy LIDAR, right upper panel: post-Sandy LIDAR, panels below: differences between post- and pre-Sandy LIDAR

In the upper panels pre- and post-Sandy LIDAR data are plotted and the differences (sedimentation is positive and erosion negative) are plotted in the lower panels. The post-processing techniques differ: buildings, trees and other objects have been filtered out in the post-Sandy LIDAR (bare earth) and not in the pre-Sandy LIDAR. This is why the buildings have been removed in the sedimentation-erosion subplots; see Appendix A for more details on this. Moreover, some blue spots can be noticed in the sedimentation/erosion subplots, especially in the middle part of the peninsula. These spots can be ignored, since they are not caused by actual erosion but correspond to objects like trees and cars. Unfortunately, a good bare earth extraction of the LIDAR was not available.

From Figure 2-19 it becomes clear that the overwash regime has been reached during the storm. The beaches and berm have been eroded heavily and due to the overwash large amounts of sand have been deposited behind the berm in the residential areas. In the lower right plot the sedimentation between 0 and 1 m ref. to NAVD88 is given, which shows the inland overwash deposits more clearly. Especially between the white stripes in the blocks directly behind the sand berm, deposits can be observed. Figure 2-12, which shows the overwash in the areas directly behind the berm, is taken between these two white stripes.

2.2.1.2. Direct Damage

According to 'Post-Sandy: Damage Survey' (Guy Carpenter, 2013) both eastern and western part of the Rockaway Peninsula are considered two of the eleven most affected areas in the US, where they make

distinction between the Breezy Point community (west) and Rockaway community (east). This paragraph elaborates the direct damage to different kinds of assets, but focusses on damage to individual property (residential buildings and belongings) as a direct result of the overwash and inundation. Normal water damage (deterioration of assets because of getting wet) and structural failure related damage due to hydraulic forcing are both considered as primary damage, together with wind damage. Secondary damage, which is additional damage caused by the primary damage, can have many elements and depends strongly on the pre-storm situation. Fire damage caused by electrical short circuit burnings is an example of secondary damage²¹.

Primary Direct Damage

The surveyors of Guy Carpenter found a few roof tops missing some shingles and only one boarded upper-story window, indicating that wind induced damage was minimal. On the contrary, water induced damage was significant. In the Breezy Point area most houses had interior flood damage. Large debris piles out front of the buildings consisting of inundated wood, insulation and household items confirm the interior flooding. Roads were therefore impassable and the fact that traffic lights were broken worsened the situation. The water and gas supply networks were damaged too. About the Rockaway area they state that every property was severely inundated. Although most properties looked undamaged from the exterior, large piles of debris in front of the houses showed different. Sand residues were found well inland from the foot of 116th street up to Rockaway Beach Boulevard, which corresponds to the area with narrower beaches and fully eroded berm (see paragraph 2.2.1.1). In the same area more aggressive wave battering effects were clearly visible as well. Figure 2-20 gives a selection of pictures taken from the post-sandy situation.



Figure 2-20 - The oceanfront of The Rockaways has been almost completely demolished by wave battering (photos by Nathan Kensinger)

The task of short term disaster assistance and guidance of the rebuilding process is assigned to the federal organisation FEMA. The weeks after Sandy FEMA performed surveys in major parts of the Sandy affected area in order to assess the damages. The Hurricane Sandy Imagery Based Preliminary Damage Assessments (IPDA) is one of these assessments. Imagery collected by the Civil Air Patrol (CAP) and NOAA was then processed by analysts at ImageCat in order to use the results to expedite housing assistance for disaster survivors (FEMA 2013). Based on the aerial pictures buildings were divided into 4 categories: Affected, Minor, Major and Destroyed, of which a more detailed description can be found in Section 2.3. A visualisation of the spatial distribution of the damage from the ImageCat dataset (ImageCat Imagery Based PDA²²) is shown in Figure 2-21.

²¹ Notice the difference between secondary and indirect damage, where secondary damage has a physical relation to the storm and indirect damage a relation to the disrupted socio-economic situation.

²² <http://fema.maps.arcgis.com/home/webmap/viewer.html?webmap=307dd522499d4a44a33d7296a5da5ea0>



Figure 2-21 - Spatial representation of the ImageCat damage Analysis

From Figure 2-21 the following conclusions can be drawn:

- The most severely damaged buildings (destroyed or major damage) are almost all located in the ocean fronting rows;
- The rest of the buildings within the first block from the beach are not too much damaged, which is assumed having a relation with the higher ground elevation levels within that area, see Figure 2-4;
- Some hotspots can be designated, for instance in the middle of the eastside of the area, which can be seen in the zoomed view on the right side.

Additional to the aerial survey, FEMA has sent thousands of surveyors into the field²³, as part of their Housing Assistance Program. The goal was to find out which households qualify for temporary housing and/or financial assistance for repair and replacements costs, in addition to the contribution of insurance companies. The corresponding reports and data are not public and it appeared to be impossible to get it from FEMA in the form needed for present study; namely coupled to geospatial information.

Secondary Direct Damage

Not directly related to the forcing of the water or wind, secondary direct damage can still be related directly to the storm. Besides short circuit burns, not much is documented about Sandy's secondary direct damage at the Rockaways. However, the fires had an immense impact on some communities. As is already mentioned in section 1.1.1.2, 111 houses completely burned down to the ground at Breezy Point. The results can be seen in Figure 2-22. Also in Belle Harbor six residential buildings burned down at Beach 130th Street and at Rockaway Beach Boulevard a broken power line fell on a three-story building and caused a fire, burning down 19 of the surrounding buildings. This hazard on its own took care of more than 125 of the in total 195 completely devastated buildings in the Rockaway Peninsula area.

²³ Found on FEMA's timeline of Hurricane Sandy: <http://www.fema.gov/hurricane-sandy-timeline>



Figure 2-22 - Short-circuit fires burned down complete neighbourhood at Breezy Point and some other places in the area (Photographs by USACE and Nathan Kensinger amongst others)

It is questionable whether this number of burned down houses is representative or rather exceptional. The answer is not easy to find, but it is for sure not exceptional, given that an internet search for electrical fires caused by Sandy results in multiple stories about other cases in several states, of which the boardwalk fire in Seaside Park, NJ, is most noticeable. Moreover, New York Daily News states that the New York Police Department (NYPD) has concluded that 68 of the 94 separately originated fires during Sandy started due to electrical causes²⁴.

2.2.1.3. Monetary Losses

As has been mentioned before, data on monetary damage have been surveyed by FEMA, but these data were not available for present study. Nonetheless, to some extent the data is public, which is shortly summarized here in order to give an idea of what is out there. FEMA only published their observations of the survivors that got the maximum grant of \$31,900 that was rewarded from the FEMA Individual Assistance Program per postcode. With it come the unmet needs²⁵, the gross income per year of the household and the number of members of the household; see Figure 2-23. However, an address or anything else that could have been helped to trace back the geospatial identity is not given; unfortunately, because this is of great importance for present study.

Obviously, much more people got a grant from FEMA lower than the maximum amount, which are not published in the list. FEMA was willing to give an indication of the spread of the grants: in New York City, of the

²⁴ <http://www.nydailynews.com/new-york/sea-water-surge-behind-serious-sandy-fires-fdny-article-1.1226891>

²⁵ Adding this up to the maximum grant a total damage to the property of that specific victim can be determined.

152,766 total FEMA registrants, the average grant for homeowners and renters were \$11,612 and \$5,333 respectively, which adds up to a total of about 1 billion dollars.

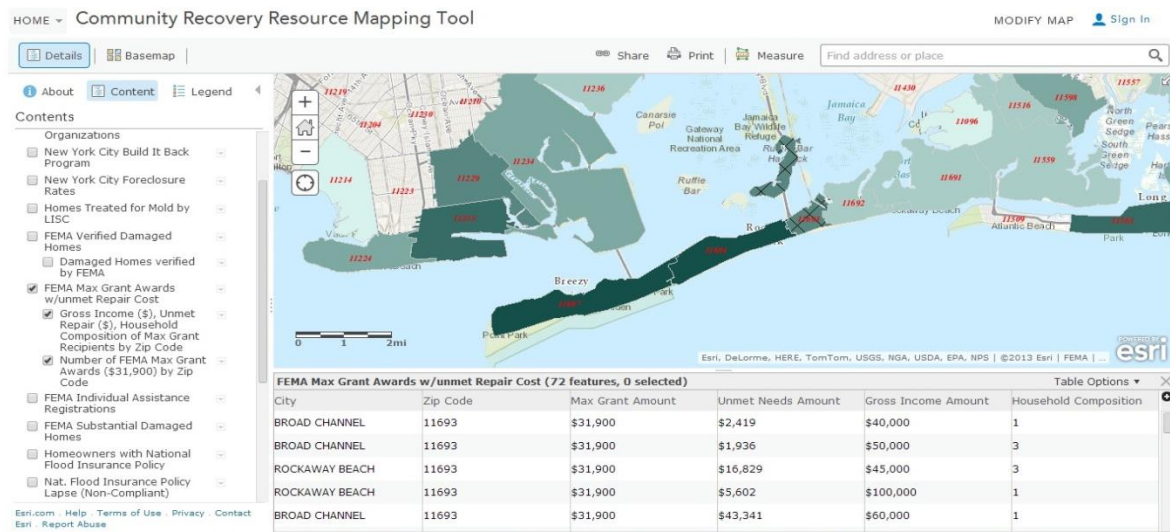


Figure 2-23 - impression of the available data on monetary damage. Source: FEMA’s Community Recovery Resource Mapping Tool²⁶.

2.3. Data

Most of the sources and datasets have already been discussed in the previous sections of this chapter. Three of them are elaborated in more detail here, knowing the ImageCat dataset, the buildings dataset from the NYC Department of Information Technology and Telecommunications and the PLUTO dataset from NYC Department of City Planning. All consist of geospatial identities of the object to which properties are attached. For the ImageCat dataset the geospatial information consists of points, for the PLUTO dataset of tax lots (with polygons corresponding to the perimeter outlines of the lots) and for the buildings dataset these are buildings (with building polygons). A spatial representation of the three datasets is given in Figure 2-24.



Figure 2-24 - Spatial representation of the ImageCat, Buildings and PLUTO datasets

²⁶ <http://fema.maps.arcgis.com/home/webmap/viewer.html?webmap=c8e880eb4e7f4996ac26947884205da0>

Based on geospatial querying the properties data from the ImageCat and PLUTO datasets have been assigned to the building polygons and therefore combined with the properties data of the buildings dataset (see Appendix A for more detail on the coupling process). In this way all properties can be used as damage indicators on the same spatial scale level (scale of analysis), which is on the building level. An example of this can be found in section 2.2, where Figure 2-21 shows the property ‘physical damage’ from the ImageCat dataset (originally dots) assigned to the corresponding building polygons.

The ImageCat dataset consists of qualitative descriptions of the damage; see Appendix J. Based on aerial pictures the structural and exterior damage has been observed and mapped. Based on this in combination with inundation depth (established based on water levels from storm simulations) the buildings have been classified as “Affected”, “Minor damaged”, “Major Damaged” or “Destroyed”. Where all urban areas were flooded, all buildings are assumed to be at least affected by the inundation. The consequence is that there are no non-damaged buildings within the area. Probably this is not 100% true, but that is not a big problem for delivering a proof of concept within this thesis. Considering the other two datasets, Table 2-3 and Table 2-4 show the relevant properties of the Buildings and PLUTO datasets and a brief description.

Table 2-3 - Properties of the Buildings dataset

Buildings	
Property	Description
Height roof	Height of the roof referenced to local ground level
Building type	Residential, garage or commercial
Ground elevation	The elevation of the ground referenced to NAVD88
Shape surface area	The ground floor area of the building

Table 2-4 - Properties of the PLUTO dataset

PLUTO	
Property	Description
Number of buildings on lot	The number of buildings on the tax lot
Number of floors	In the primary building on the tax lot, the number of full and partial stories starting from the ground floor
Building class	A code describing the major use of structures on the tax lot
Lot area	Total area of the tax lot
Floor area of total building	The total gross area of all buildings
Residential units	The sum of residential units in all buildings on the tax lot
Tax base - assessed value	The tax lot’s estimated full market value multiplied by a uniform percentage for the property’s tax class

It should be noted that studying the added value of including an indicator like construction material would be very interesting. However, data on the construction type of buildings are not included in the PLUTO or the buildings dataset. That information is available (though not publically) and forms part of the Mass Appraisal System (MAS) dataset from NYC Department of Buildings. Unfortunately MAS is not easy to work with²⁷, which is why it is not used for present study. Moreover, for the villages Breezy Point and Roxbury PLUTO data are only available on aggregated level. For both villages PLUTO contains only one big lot (whole village) in the dataset, which can also be seen in Figure 2-9.

²⁷ Strongly recommended by the NYC City Hall

3. Methods

This chapter describes the concept, implementation and considered scenarios. In section 3.1 the general concept is elaborated. Section 3.2 is about implementation of this concept on the case study and section 3.3 is about the scenarios which are considered in analysing different aspects of the approach.

3.1. Concept

3.1.1. Physical Process Description

As has been described in paragraph 1.2.1.1 modelling storm propagation has already extensively been done and documented within the field of hydraulic engineering, either for coastal purposes or rivers. In general all approaches for simulating the physical aspects of storms follow a fairly similar pattern: start with a large and coarse model, covering the complete area of influence of the storm, and zoom in to the scale of analysis by using more detailed but smaller nested models. When the amount of detail is sufficient, enough information on that spatial scale can be extracted from the models and can be used as indicators for the severity of the hazards locally. This general approach is also used for present study.

The actual implementation of the storm propagation differs per impact model and mainly depends on the choices the modellers had to make to achieve their goals: predicting damage; quantifying risk; or quantifying uncertainty. This is elaborated in subsection 1.2.4. To reach the goals of present study, which are predicting damage and quantifying uncertainties, the following choices/requirements have been made:

- The scale of analysis is on the object level, where the objects are residential buildings;
- The model grid resolution (micro spatial scale level) must therefore be in the order of 1-10m;
- At least the storm characteristics inundation depth, wave height, stream velocity and scour depth should be able to extract from the simulations on that spatial scale;
- The scale of application should be in the order of kilometres in order to include a sufficient amount of observations.

The scale of application determines the dimensions of the area of interest for which the damage predictions have to be made. This is for instance the scale of the Rockaway peninsula for present study. In order to gain the required amount of detail in the area of application the storm characteristics have to be propagated from a much larger macro scale level to the scale of analysis. In theory it would be possible to cover all spatial scales in one single model. However, to properly simulate the storm on the largest spatial scale level the domain should be taken fairly large (in the order of 100-1000 km in both x and y direction) to cover the whole area that is significantly influenced by and influences the storm. Combining a large domain with the requirement of a high model resolution (1-10m) is computationally and economically infeasible. It should be noted that this disadvantage can be overcome by using unstructured grid models (with the use of non-equidistant and/or meshed grid configurations, such as in D-Flow FM). However, in such a setup it is cumbersome to rerun the model. Moreover, with a nested model one could for instance turn on morphology only in the nested model on the lowest scale level. This is why the nested approach is considered to be the best for the present study.

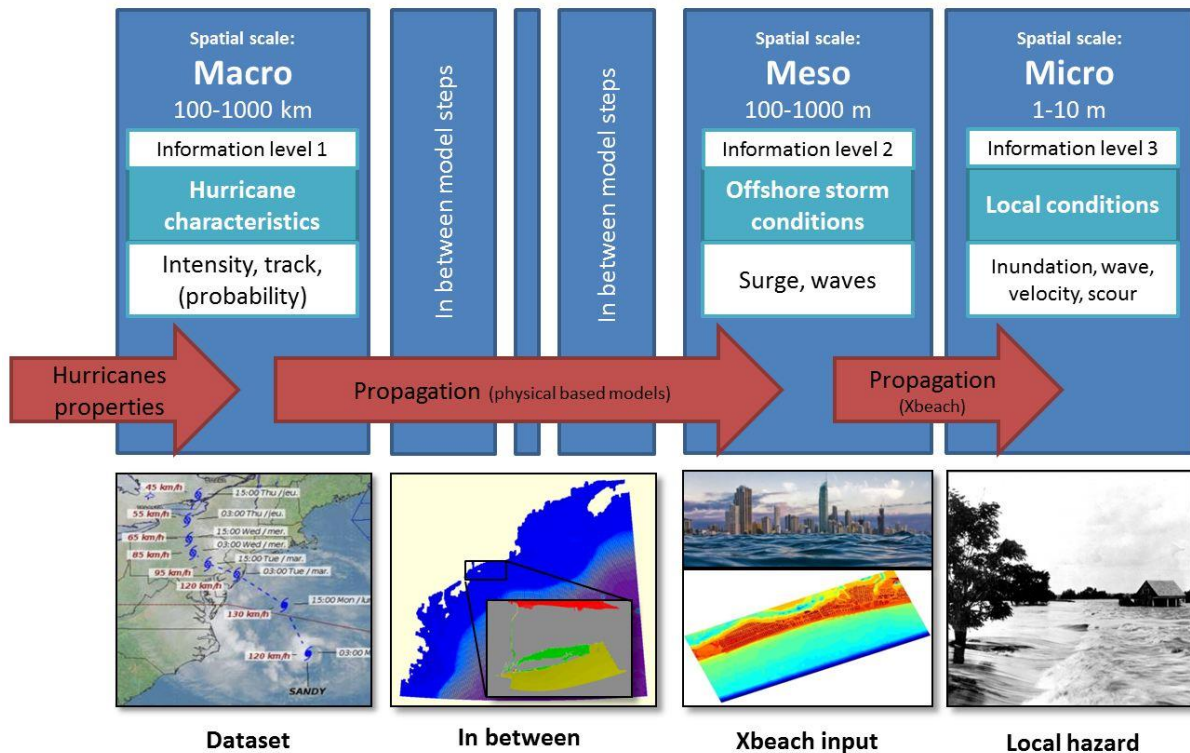


Figure 3-1 - Schematic representation of the proposed approach

In the next paragraph 3.1.1.1 the choice of implementing XBeach is explained, which is a key element for the approach of present study. XBeach is capable of propagating storm characteristics just offshore (meso scale level information with a resolution of 100-1000m) to the desired micro scale level onshore. How many steps and models are necessary for the propagation from macro to meso scale depends on the study site, what information is available and whether other operational models are available or not. The proposed approach is schematically shown in Figure 3-1.

In analogy with physical approaches, this approach has a causal order: large storm characteristics cause smaller storm scale characteristics, causing on its turn damages. The larger and most dominant forces (astronomical and meteorological forces) are coped with on the largest spatial scale, whereas for instance wave attack and the vulnerability of a house are included on the lowest spatial scale. Moreover, in the nesting approach it is assumed these processes on the smaller spatial scale have no effect on the processes on the larger scale.

3.1.1.1. Morphodynamic influences

Subsection 1.2.3 showed that neglecting of morphodynamics is definitely a shortcoming for a lot of (coastal) sites for which the Rockaway Peninsula serves proof. This is one of the main problems addressed in Chapter 1.

In order to solve this problem, inclusion of the morphodynamics is essential. To do so, one can make use of a handful of numerical models (e.g. Delft3D, Mike, XBeach). Differences between these models can be found in the type of numerical schemes, type of formulas solved (both in hydraulics and morphodynamics) and some other aspects such as the 'avalanching' module, the wave group module and infragravity waves module in XBeach (Deltares 2010). Since this research is not about developing a fully proved operational impact model, but about giving proof of concept, a thorough comparison -weighting pros and cons- has not been made. However, there are reasons for choosing XBeach. One of the main reasons can be found in the fact that it has shown good performances in modelling morphodynamics of barrier islands exposed to hurricanes (McCall et al. 2010). In Figure 2-6 the schematisation of the four different storm surge regimes can be seen for which XBeach

has been designed for the case of Santa Rosa Island, FL, under Hurricane Ivan conditions, as has been defined by Abby Sallenger (2000)²⁸.

The processes described in XBeach are the long waves, travelling with the wave groups and released in the surf zone, and together with the storm surge level and short waves cause dune erosion during storms. The long waves are solved separately from short waves, which are assumed to be important for sediment transport processes only. The physical processes are solved in a specific order: first the hydrodynamics are considered; secondly, instabilities in the dune face are predicted, causing local avalanches of sand (see Figure 3-2). The subsequent sediment transport, directed offshore (collision regime) or onshore (overwash and inundation regime), is a function of flow velocity and stirring effects of short waves. The corresponding local transport rates are used to update the bed levels, which on its turn affects the hydraulics. With this constant feedback loop in time XBeach is capable of coping with breaching and large sediment depositions during the storm. In this way the storm propagation can be simulated in better agreement with reality. The formulations XBeach solves are summarized in Appendix C; more detailed information can be found in the XBeach manual.

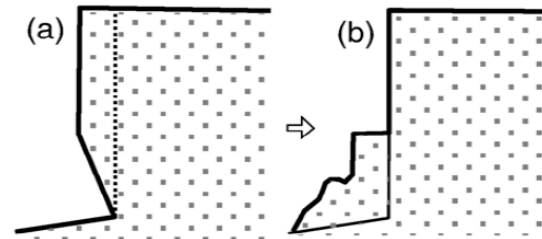


Figure 3-2 - Instabilities cause episodic sliding down of land slumps. This is simulated by the avalanching-module

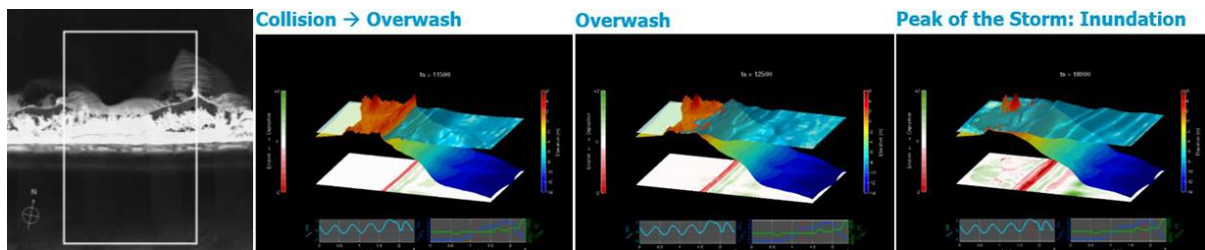


Figure 3-3 - Regimes during Hurricane Ivan (2004) at Beasley Park, FL (source: Dave Thompson, USGS)

A representation of XBeach simulating the collision, overwash and inundation regime for Hurricane Ivan (2004) hitting Beasley Park, FL, is given in Figure 3-3. From McCall et al.²⁹ it can be concluded that XBeach is doing a fairly good job in predicting the morphological changes to barrier islands. The differences in predicted and observed bed levels after Hurricane Ivan are fairly small, as can be seen in Figure 3-4.

²⁸ 'Storm Impact Scale for Barrier Island' (Sallenger 2000)

²⁹ 'Two-dimensional time dependent hurricane overwash and erosion modelling at Santa Rosa Island' (McCall et al. 2010)

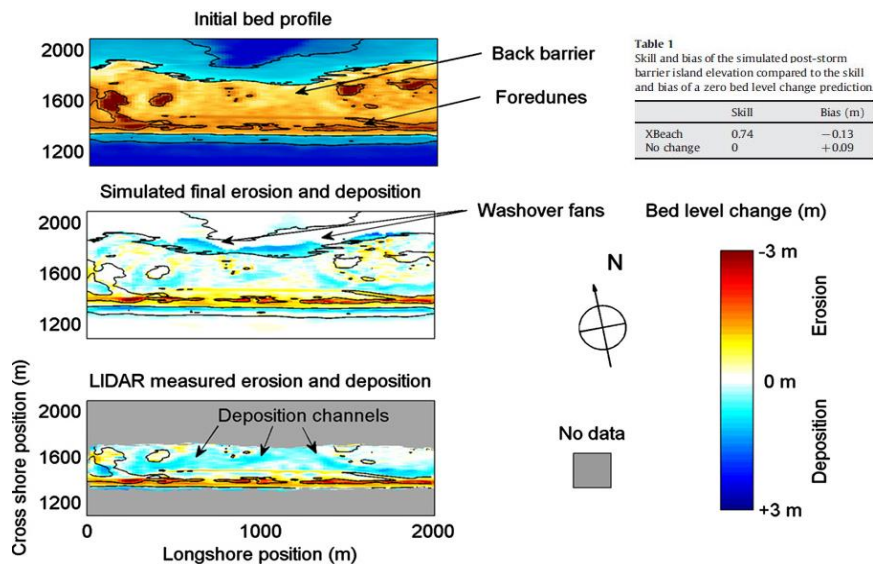


Figure 3-4 - Observed and predicted bed level changes are in agreement. XBeach shows skill for predicting hurricane impacts at barrier islands.

Where XBeach is designed for storm impacts to sandy coasts, it is assumed to perform adequately for other sites than Santa Rosa as well, including the Rockaway Peninsula. There are differences though; The Rockaways have been subject to extensive urbanisation where this was not the case for Santa Rosa Island. For sites with other geographical configurations and soil compositions it might be interesting to compare the performances of different numerical models as well.

It should be noted that XBeach is designed for fairly high resolution purposes and it is far from ideal to use for storm simulations on larger spatial scales due to high accompanying computational expenses. XBeach should therefore always be used in combination with and nested into another numerical model, in which detailed processes such as morphodynamics and long wave are turned off. As has been mentioned before, a summary of the formulations XBeach uses can be found in Appendix C.

3.1.2. Statistical Opportunities

This section is about the opportunities in approaching the physics-based modelling from a probabilistic perspective. First, the uncertainty that comes with the physics-based modelling is described in more detail. Secondly, the approach to quantify these uncertainties is explained in general and in more detail for the coupling of local hazard characteristics to damage.

3.1.2.1. Uncertainty in Physics-based Modelling

Paragraph 1.2.1.1 elaborates storm simulations and the storm propagation in time, space and spatial scale, based on simplified physical relations. The way these physics-based models work is deterministic; every unique combination of input (initial conditions, boundary conditions and parameters) produces only one possible outcome, the prediction. This prediction is based on a simplified world and how it matches reality is not exactly known. As has been extensively elaborated in paragraph 1.2.1.2 the ability of quantifying uncertainty (or certainty) of these predictions is of great importance in modelling risks. Subsection 0 addressed the problems in quantifying uncertainties in hurricane impact modelling. For physics-based modelling in general the following aspects attribute to the uncertainty of outcome:

- 1) Simplification of complex reality;
- 2) Uncertainty in model input;
- 3) Numerical (in)accuracy

Since it is simply impossible to cover full complexity of reality in models, the predicted future state will always partly be wrong and therefore unknown. It is said to be an approximation. Moreover, the output is as good as the input. However, it could be worse: if the involved processes are unstable, irregularities (uncertainties) can grow exponentially. The same holds for numerical schemes, which are used to solve the physical relations: uncertainties or irregularities can grow to infinity (explode) or decay when there is numerical stability.

If we now combine the insight of these uncertainties with the model train proposed in subsection 3.1.1, it can be concluded that every additional step is adding uncertainty to the final outcome. This is schematically shown in Figure 3-5. The part of the uncertainty that is epistemic gives opportunities, since that part of the uncertainty can be reduced. The aleatoric part of the uncertainty cannot be reduced, but can still be quantified.

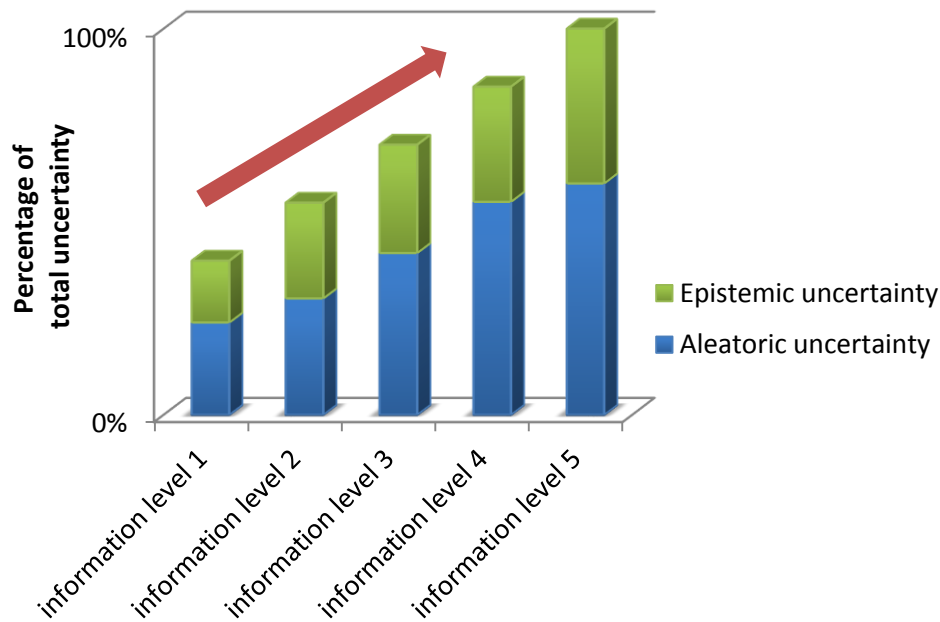


Figure 3-5 - Schematic representation of the growing uncertainty within the model train (not based on real data)

3.1.2.2. The Probabilistic Approach

Exactly the same principles as has been described in subsection 0 can be used in order to quantify uncertainties in the model train: real and synthetic data can be used to feed a statistical model with prediction skill. By coupling the right variables in the right order (from large spatial scale towards final impacts) it is theoretically possible to quantify uncertainty for every step in the process. This is schematically shown in Figure 3-6. Comparably information levels as in Figure 1-8 and Figure 3-1 are shown again. If the most important variables on every level are interlinked in a network and dependency relations trained with a sufficient amount of data (real observations and partly generated by the physics-based modelling train) a statistical model can be created with the potential of predicting overall impact or risk. Based on information from the highest spatial scale level (boundary conditions on level 1) predictions for the lowest spatial scale level can be made in a fully probabilistic way.

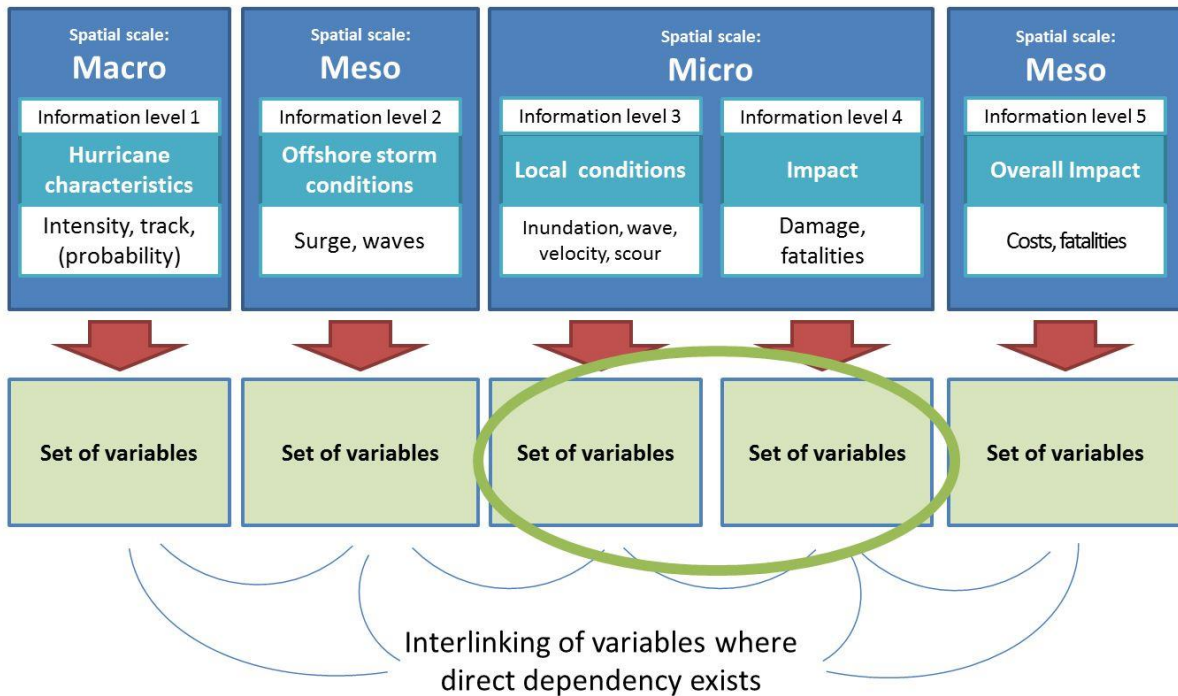


Figure 3-6 - Information on all levels can be coupled with the use of a statistical model

In subsection 1.2.4 the problems are addressed that are involved in this process. Overcoming all of these problems for every step in the model train can easily embody multiple theses. As is explained in section 1.3 this thesis will only focus on the step in which local storm conditions are coupled to actual damage. The sets of variables encircled in green are therefore the relevant ones for the present study. One thing that becomes clear from section 0 is that the more observations are available the better; this is in general true for all statistical approaches. Although storms like Hurricane Sandy are exceptional, one storm can provide multiple observations on the smallest spatial scale level. This can best be explained on the basis of Figure 3-7.



Figure 3-7 - Two comparable houses are subject to different (maximal) hazard intensities during the same storm

In the left part of the figure a house is shown during a storm, situated at location A. A comparable house, situated at location B, is shown in the right part during the same storm. The local storm conditions for the

same storm differ due to geographical and geospatial variations in the impacted area. This is not only the case for these two houses, but for every building in the area. For a densely populated area as New York City, and the Rockaway Peninsula as part of it, this can give thousands of damage observations. The good part is that the damage caused by Sandy has been surveyed really thoroughly and for almost every house in the area a damage observation is available, both physical and monetary, although the latter was not available for present study; see Chapter 2. If it would be possible to couple this information with local storm conditions from hurricane Sandy model simulations, a direct relationship can be established between (simulated) storm and (observed) damage. With this method not only inundation depth can be coupled to the corresponding damages; the dependency of damage to indicators like wave attack, flow velocity and scour depth can be established as well. In analogy to the example with dice: the more one knows the more certain a prediction becomes. By just establishing the relationships and analysing them, the added value of specific indicators can be examined. Moreover, not only indicators indicating the severity of the hazards can be used as predictor. Additionally, other variables, indicating the vulnerability of buildings and the amount of value at risk, can be added as well.

The flow chart in Figure 3-8 is an example of a potential structure. The overall configuration is based on knowledge of what happens during a storm and the damaging factors. Considering the physical damage, the forcing (destructive power of the hazards) and resistance (strength of the properties at risk) determine what the structural damage to a building is. Considering monetary damage, the physical damage to the structure is obviously important; whether a building collapses or not makes for instance a big difference. However, even without large structural damage, monetary damage to walls and contents due to inundation can still be substantial. Therefore a direct link with the local hazard characteristics is added as well. Additionally, the value of the property at risk becomes important too when the monetary consequences of a hazardous event are of interest.

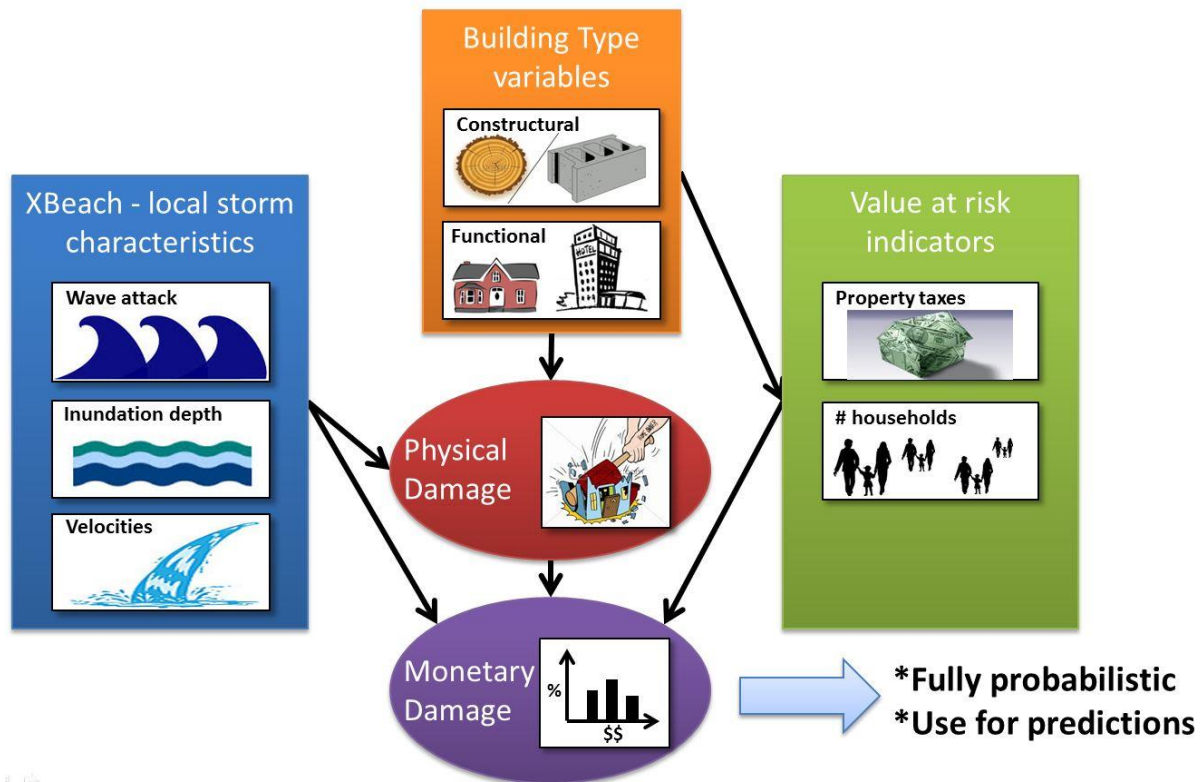


Figure 3-8 - Schematic representation of some damage indicators with potential and how they relate to each other; Note: this is an example and can differ from site to site

3.1.2.3. Indicating Damage

Which indicators should be added depends on the data that are available for the study site. Information about the construction type for instance can be useful; a house built of masonry is probably stronger than a house built of wood. A flat building containing multiple households can probably withstand more severe storms than a single-family house. This kind of information can be used to make a better prediction for physical or structural damage. Again, the added value can be examined. For value at risk indicators other data might be interesting. A flooded building containing high value contents will have larger corresponding damages than an empty building. Information like household income, functionality of the building and ground floor surface might be useful indicators. Hereby it should be noted that indicators like household income are often sensitive to privacy issues and are therefore not always available. The same holds for data on monetary damage.

In the Multi-variate flood damage assessment of Merz et al. (2013) a correlation analysis has been carried out for a dataset of more than 1000 records of direct damage to residential buildings in Germany, mostly caused by river floods. The Pearson correlation coefficients between 28 potential predictors (damage indicators) and the loss ratio (rloss) have been established and are shown in Figure 3-9, where blue dots stand for a significant correlation.

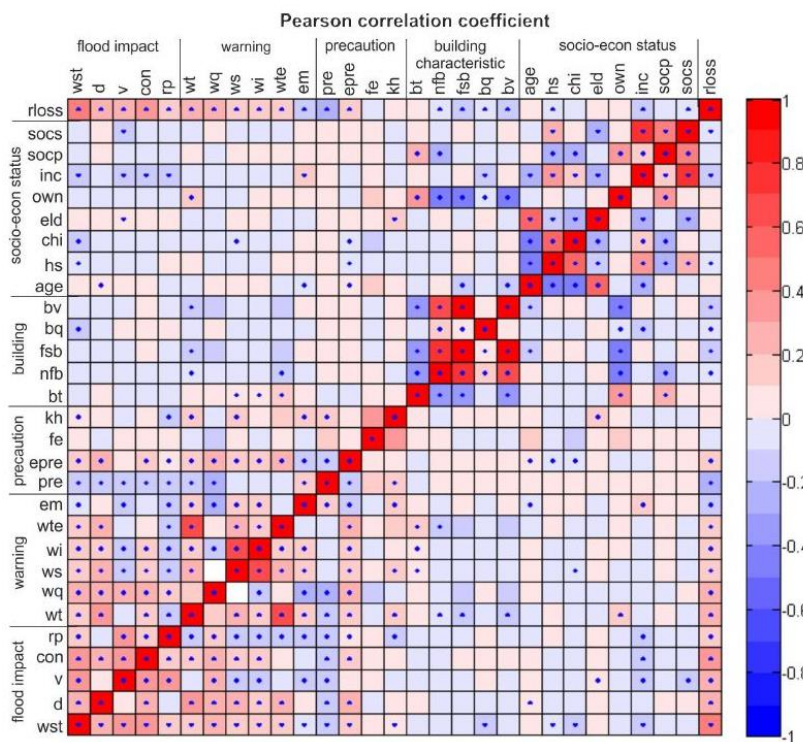


Figure 3-9 - Pearson correlation of the 29 variables (28 candidate damage predictors and loss ratio); significant correlation (1% significance level) is marked by a dot (source: (Merz, Kreibich, and Lall 2013))

A description of the abbreviations can be found in Appendix B. Some conclusions are stated here, which can be used as a starting point:

- The loss ratio (rloss) mainly depends on flood impact predictors where first the water depth (wst) and secondly contamination indicator (con) appear to be the most important ones;
- Early warning/emergency measures appear to be important together with building characteristics, where correlations with the loss ratio are high as well;
- Within the socio-economic status predictors, income and household size show a high correlation with the loss ratio;

- Mutual dependencies between the flood impact predictions (hydraulic and hydrologic aspects) are high.

The number of variables that can be added (more complexity) depends on the number of observations and how the variables mutually relate. This is more extensively elaborated in the next section. Moreover, it should be noted that predictions can only be made within the range of the data that is used for training the model. If a different storm causes much larger local storm conditions near a different type of house than has been used to establish the relationships, a good prediction will not be possible to make³⁰. To overcome this problem it is recommended to use data from different areas and different storms for the establishments of the relationships. This has been done in the multi-variate flood damage assessment of Merz et al., but not for the proof of concept in this master thesis. Only observations of the Rockaway-Sandy case study are used for the training, which limits the range of applicability but still provides a solid base for demonstrating the concept.

3.1.3. Bayesian Belief Networks

From subsection 3.1.2 it becomes clear that with the use of statistical tools it is possible to look at the model train of subsection 3.1.1 from a probabilistic perspective. Especially for the coupling of local storm characteristics with damage -for which a nice set of observations can be created relatively easy- there are opportunities, but how to do this? Creating joint PDF's or PMF's for two dependant variables is not difficult, but what if more variables are involved in a network comparable to the flow chart of Figure 3-8?

To establish the dependency relationships between the variables one can make use of several types of statistical models. For this thesis Bayesian Belief Networks (BBN's) are used, but it is not proven that other methods, like Neural Networks, would do worse or better. Bayesian Belief Network (BBN or short: Bayesian net), forming part of the directed acyclic graphical model family, is a probabilistic model, which represents a set of random variables and the mutual conditional dependencies based on data via directed acyclic graphs. The principle is based on the Bayes' rule, which relates the odds of an observant event, here called O_j , to a to be predicted event F_i (from Forecast). The odds of event F_i can be expresses, both before (prior to) and after (posterior to) conditioning on event O_j or another (set of) observation(s). For events O_j and F_i the Bayes rule formulation is gives as follows:

$$p(F_i|O_j) = p(O_j|F_i)p(F_i)/p(O_j)$$

Where $p(F_i|O_j)$ is the updated conditional probability of a forecast, F_i , given a set of observation (prior knowledge), O_j . A number of good examples can be found on the internet³¹ and in textbooks³², which explain and demonstrate the principles in more detail. A brief introduction to the principle is given below.

For this thesis, the Netica software package from Norsys³³ is used to construct and work with the BBN's. Constructing a BBN model consists roughly of two phases:

- 1) Determining the network structure;
- 2) Training of the network.

The first phase implies determining relevant variables, which are involved in a certain process, and connecting these variables with arrows, indicating the mutual conditional dependencies. To make this more tangible the

³⁰ It must be said that within Netica the prediction goes to complete uncertainty if the entry is out the range of applicability, which is a good feature. This is in more detail elaborated in paragraph 4.3.1.3.

³¹ For instance: <http://people.cs.pitt.edu/~milos/courses/cs2001/cs2001-2.pdf> and http://artint.info/html/ArtInt_148.html

³² For instance: *'The Theory that would not Die'* by Sharon Bertsch McGrayne and *'Bayesian Networks and Decision Graphs'* by Finn V. Jensen and Thomas D. Nielsen

³³ <https://www.norsys.com/netica.html>

example of the three dice is used again. The number of eyes thrown for each dice are variables (in Netica variables are called nodes) and the sum of the three dice is another one, see Figure 3-10.

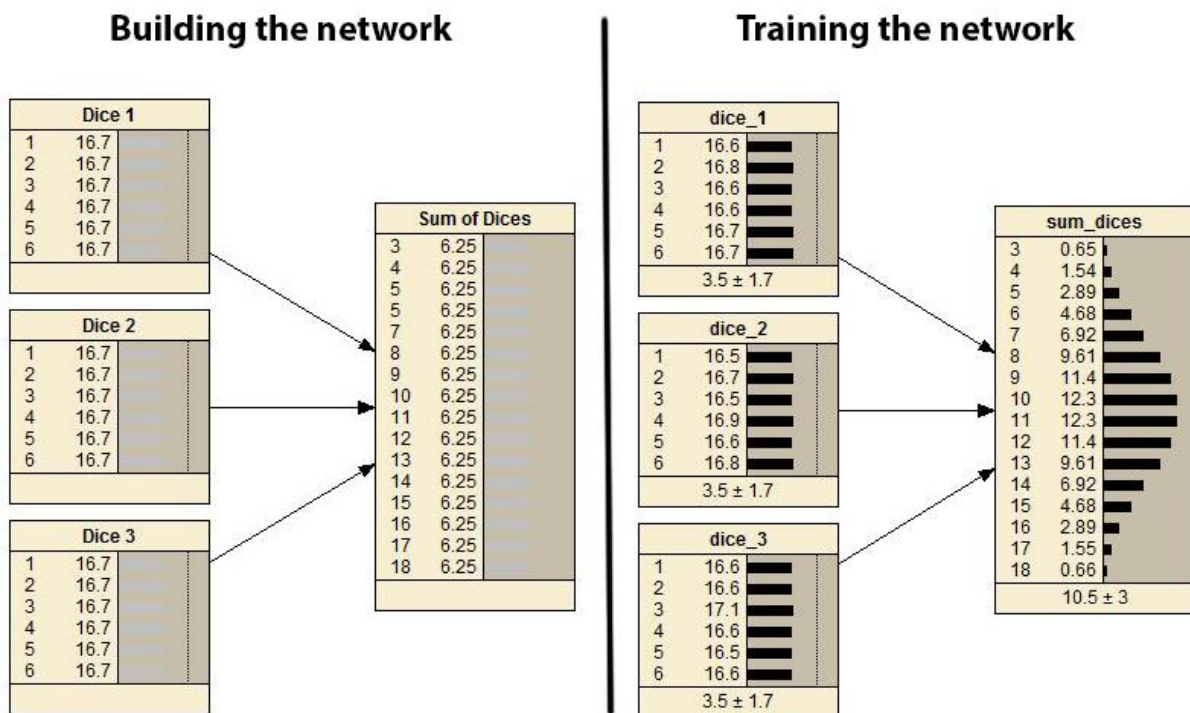


Figure 3-10 - Left: non-trained net of the dice example; right: trained net

The arrows are all directed from the dice (parent nodes) to the variable ‘sum of dices’ (child node), since the sum depends on the number of eyes that have been thrown with the three dice. This example has discrete states, which Netica is capable of handling well. Continuous nodes on the contrary, Netica is not capable to cope with, but discretized continuous variables (in bins) does the trick³⁴. This is amongst others important for the continuous local storm conditions like inundation depth ranging from 0 to several meters and can be discretised by using a bin size of for instance 1m. Since Netica only allows using discrete nodes, the conditional probability functions have become CPT’s.

The training phase consists of ‘feeding’ the network with training data. These data contain observations, either obtained from surveys or model simulations. When trained well, every node in the network has an unconditioned marginal PMF (possible values/states and corresponding probabilities). For the example of the three dice the trained situation is shown in Figure 3-10 on the right side; trained on a set of 10,000 observations³⁵ created with Matlab’s random function.

Since variables can be mutually dependent, the distribution of a certain variable will change when the value/state of a related variable is known, e.g. the number of eyes on dice 1 is 6; see the result in Figure 3-11. On the right side of Figure 3-11 the opposite of the left side has been done. Now the outcome (sum of the eyes on the dice) is known. The CPT’s of the dice show what Bayes things (has learned) the number of eyes on the dice would probably have been given the fact that the result (sum of the dice) was 10. This means that Netica is also capable of giving predictions upstream (in the opposite direction of the arrows).

³⁴ Other software packages are developed that can handle continuous variables. One of these packages is Uninet (TU Delft 2008). Unfortunately, Uninet is not capable of working with non-numerical nodes with states like ‘affected’, ‘minor’, ‘major’ and ‘destroyed’, which is a great disadvantage for present study.

³⁵ Note: due to a lack of anything better, the results of (physics-based) model simulations, which are used as training data for the statistical model, are called ‘observations’ as well, where they have of course not been observed in reality.

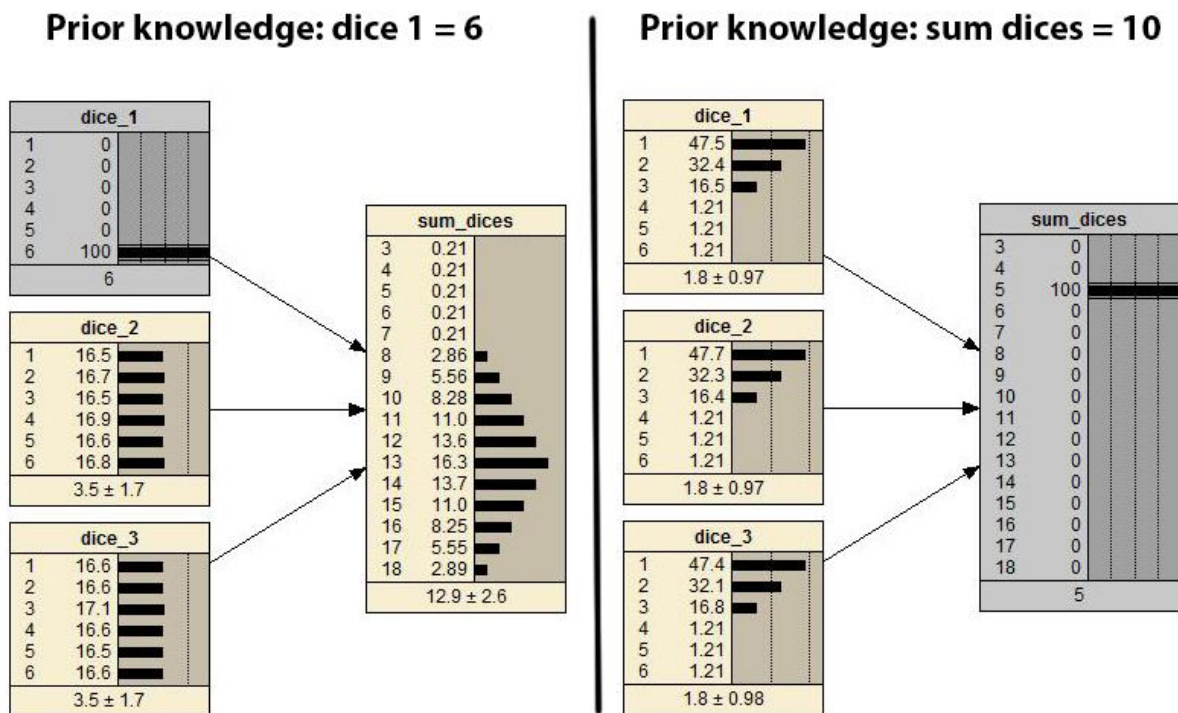


Figure 3-11 - Example of the three dice; left: conditioned on one of the dice and right: conditioned on the sum of the dice.

It should be noted that in the left part of Figure 3-11 Netica still gives a chance of occurrence for the sum of dice being 1, which is of course not possible. Moreover, the marginal PMF's in Netica of Figure 1-11 are not 100% the same as the PMF's of the data. This is because the PMF's are not directly extracted from a database, but calculated with use of the established joint distributions (Joint PMF's) (Norsys Software Corp. 1997). This makes the BBN much faster, but the outcome is not one on one with reality anymore; Netica is a model and thus the outcome is an approximation. This is also the reason for the little differences between the dice, considering the probability of the predictions, together with the fact that there are small differences within the training data as well. Nonetheless, it can be seen that Bayesian Nets work great for dice.

Now we want to know how well it works for predicting damage. Finding a starting point for the overall structure of the BBN is not difficult. As a matter of fact, it should look pretty much the same as the flow chart in Figure 3-8. On the contrary, optimizing the structure is a difficult and time consuming job. Some structure characteristics are not always easy to determine where they can make a large difference. From reference studies on the prediction of dune erosion impact (Den Heijer et al. 2011) and the prediction and assimilation of surf-zone processes (Plant and Holland 2011), which are elaborated in more detail in Appendix H, some valuable insights can be gained:

- For picking the right indicators and establishing the right relations, a lot of process and system knowledge is required (or life becomes not so easy);
- Bayesian networks do not perform well outside the ranges of the training data;
- The more nodes and the more states (bins) per node are added, the more training data are required; see section 1.2.1 as well.
- The more arrows or links are added, the more training data are required;
- Which nodes should be coupled by an arrow is not always clear, which can make optimization a time consuming job.

Besides insight in the limitations these papers also show that usage of BBNs can lead to powerful tools and are

very well applicable in the field of coastal engineering. In both studies the statistical BBN model appeared to be well capable of reproducing the physical patterns with prediction skills in the order of 0.7 to 0.9. Moreover, the uncertainty is incorporated really well in the prediction and the models run relatively fast.

3.2. Implementation

The concepts of section 3 have been applied to the Rockaway study site described in chapter 2. This section will elaborate on the implementation of all steps and briefly describe all elements.

3.2.1. Overall model structure

As has been concluded in section 3.1 the final structure will probably differ from site to site, since it highly depends on what kind of information is available. For the propagation of the storm four different models are used: Delft3D (twice), D-Flow FM and XBeach. For the largest spatial scale level the open source model software package Delft3D (including SWAN)³⁶ is used, which embodies larger parts of the East Coast and includes the physical processes wind, wave and surge. One spatial scale level lower, the New York Bight is modelled in Delft3D again for the propagation of waves (but also including the processes surge and wind again) and D-Flow Flexible Mesh (D-Flow FM)³⁷ for the surge (also including wind). For the last spatial scale step the XBeach software package is used for the Rockaway peninsula, in which the process wind has been turned off and morphology turned on next to the processes wave and tide.

The Delft3D and D-Flow FM models were already set up for this area and calibrated for Sandy beforehand. The D-flow FM model gives better storm surge results in the Jamaica Bay, but has not yet been coupled to SWAN. This is why for the wave propagation the Delft3D model is used on that same scale level. An overall flow chart of the different elements is given in Figure 3-12.

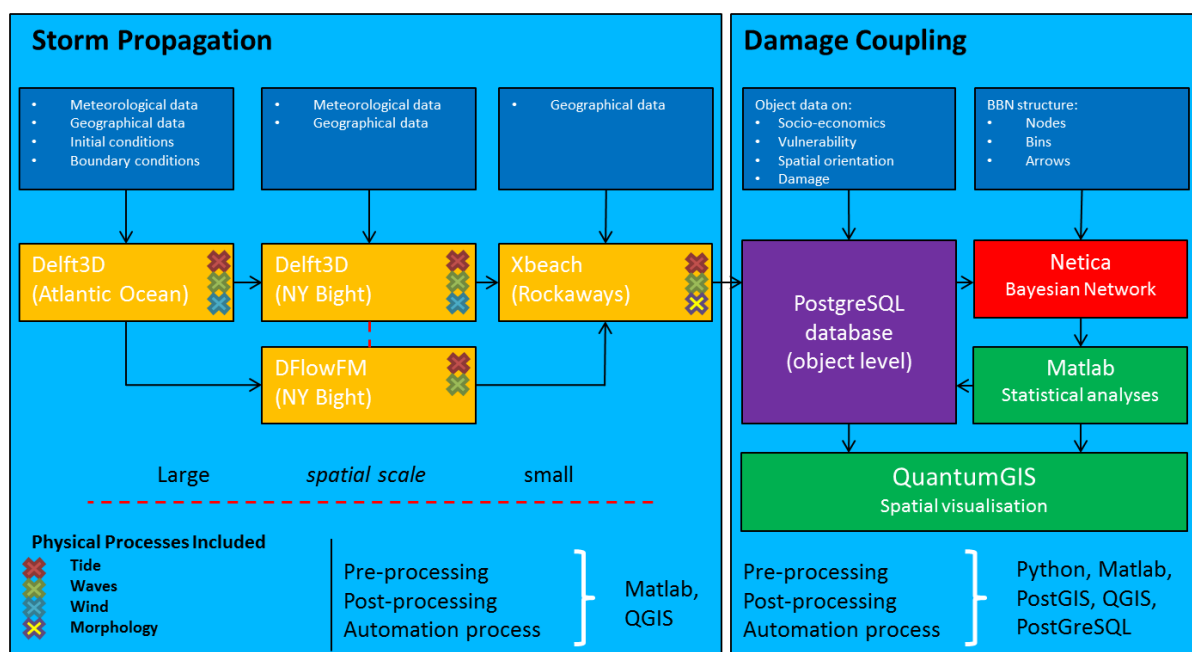


Figure 3-12 – Flow Chart: model structure and flow of information

Since coupling of all information is quite data extensive an SQL database is created with use of PostgreSQL³⁸. Next to all the local storm conditions, simulated from XBeach, also other types of data are stored in the

³⁶ <http://oss.deltares.nl/web/delft3d/>

³⁷ <http://oss.deltares.nl/web/delft3d/d-flow-flexible-mesh>

³⁸ <http://www.postgresql.org/>

database, knowing building polygons, building height, damage observations, information on household income, etc. With the use of the PostgreSQL's extension PostGIS³⁹ it becomes easy to join all different datasets based on geospatial querying; see Appendix A for the coupling of data based on geospatial information. Moreover, PostGIS gives the possibility to make a direct connection between the SQL database and QuantumGIS (short: QGIS)⁴⁰ which is an open source alternative for the ArcGIS software packages. QGIS makes it easy to spatially visualize predictions, of which Figure 2-4 is an example.

With the use of Netica's Java and Python APIs in combination with Python and Matlab a connection between Netica and the SQL database has been established which makes it possible to train the BBN fairly easily. And in the opposite direction: storing predictions extracted from Netica into the database again, which then can be visualized spatially again with the use of QGIS. By storing all information in one directory overview is guaranteed.

3.2.1.1. Area of Application

The area that has been described in Chapter 2 embodies the whole Rockaway Peninsula. However, for the implementation the western part of the Rockaway Peninsula has not been included within the area of application. The following reasoning lies at the root of this decision:

- 1) PLUTO data are not available on the object level for this area;
- 2) A huge amount of buildings was destroyed by the electrical fire, of which the physics have not been taken into account in present study⁴¹;
- 3) Computational time for the XBeach runs would double where there wouldn't be twice as much damage observations. This is because the western part of the Rockaway Peninsula is mostly rural.

In Figure 3-13 the boundaries of the area of application are shown. Within this area almost 7800 buildings can be found of which 24% are garages. Of the other 76%, 5300 buildings contain at least one residential unit. These statistics are based on the PLUTO data.



Figure 3-13 - Area of Application

³⁹ <http://postgis.net/>

⁴⁰ <http://www.qgis.org/en/site/>

⁴¹ Electrical fires seem to be significant for the total amount of damage. It is therefore recommended to study the driving forces for these phenomena in more detail.

3.2.2. Describing the elements

3.2.2.1. Netica

The most important element (considering the purpose of present thesis) is the Netica part, which includes the Bayesian Belief Networks. More than one BBN structure has been tested, of which the different structures are elaborated in section 3.3. The result of the performed analyses can be found in chapter 0. The structure of Figure 3-14 forms a starting point for more comprehensive Bayesian nets.

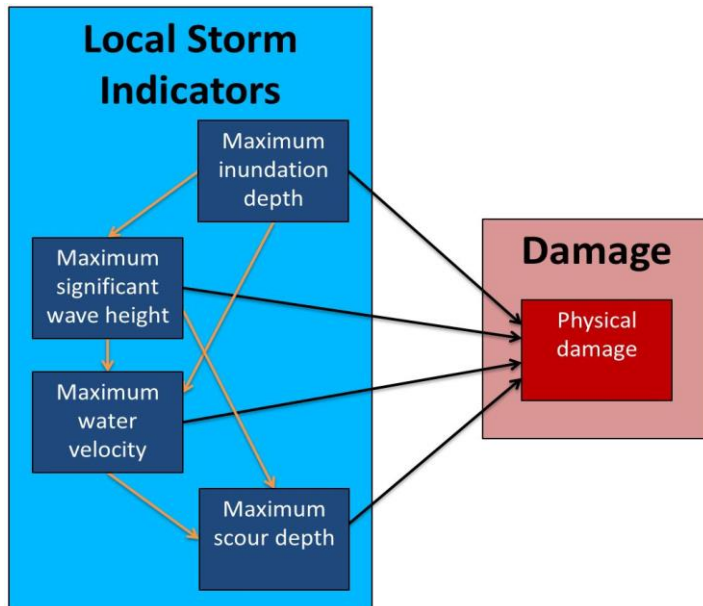


Figure 3-14 - Local hazard indicator nodes coupled to the damage node. The yellow arrows can be added to include the mutual dependencies between the local hazard indicators

Storm characteristics indicating the hazards on the building level are coupled with black arrows to the results of the ImageCat damage survey with the four categories: “Affected”, “Minor damage”, “major Damage” and “destroyed”. The local storm conditions are not mutually independent and therefore orange arrows are added between these nodes. These connections are based on knowledge about the underlying physical processes. First of all, wave height is bounded by water depth and therefore inundation depth. Secondly, both inundation depth and wave height influence the flow velocity, which is a combination of stream velocity and orbital motions. Third, bed erosion (which is called scour around obstacles like buildings) is influenced by flow velocity and wave action stirring up the sediment. One possible arrow is absent, between inundation depth and scour depth, since it is assumed that the corresponding dependency is only indirect via significant wave height and flow velocity. The way these indicators have been determined from the XBeach simulations is discussed in the next subsection.

The number of bins is also a variable. More bins per node will yield more detail, but increases the required amount of observations. This has been elaborated in previous chapters as well. The effects of the number of bins on the validation error and calibration error are analysed as well and the results can be found in paragraph 4.3.1.3 of the results.

To the simple structure of Figure 3-14 more variables are added indicating the type of the building, which can be seen in the schematization of Figure 3-15. The added value of these variables is discussed in the results in Subsection 4.3.2. It should be noted that the damage node is specifically named “physical”. Monetary damage could have been included as well if that data was available, but that would probably ask for another configuration as for instance can be seen in Figure 3-8.

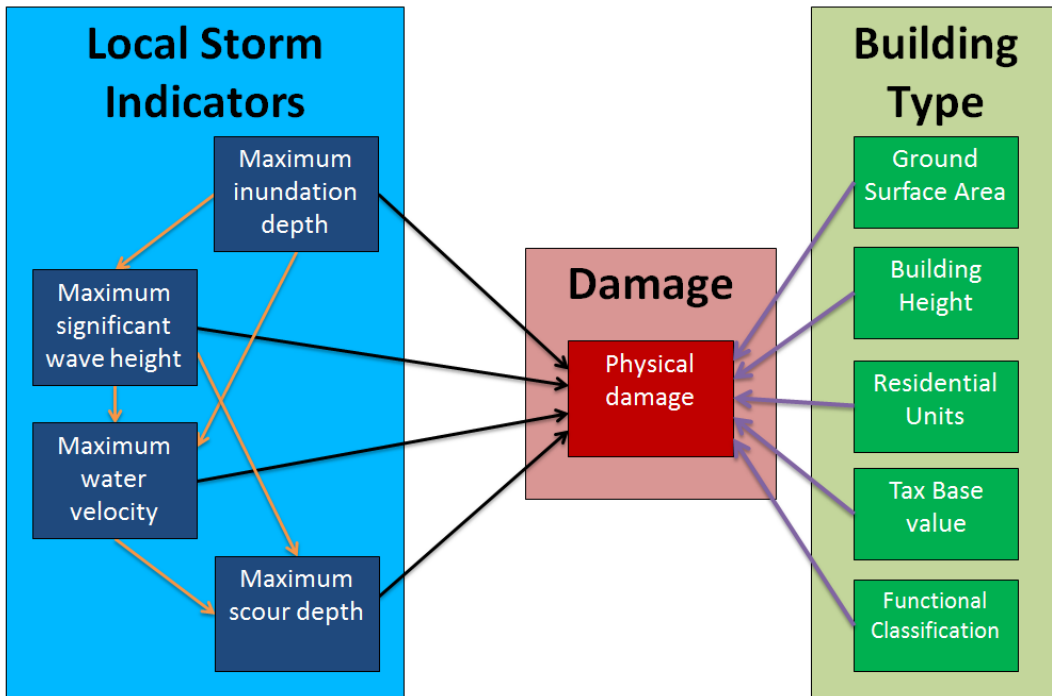


Figure 3-15 - Local hazard indicator nodes coupled to the damage node. The yellow arrows can be added to include the mutual dependencies between the local hazard indicators. Additionally, the building type indicators are shown on the right side, connected to the damage node with blue arrows.

3.2.2.2.XBeach

To determine the local storm conditions an XBeach model has been set up for the area of application. The set up and all model inputs are extensively elaborated in Appendix C. An overall view and the most important assumptions are given here.

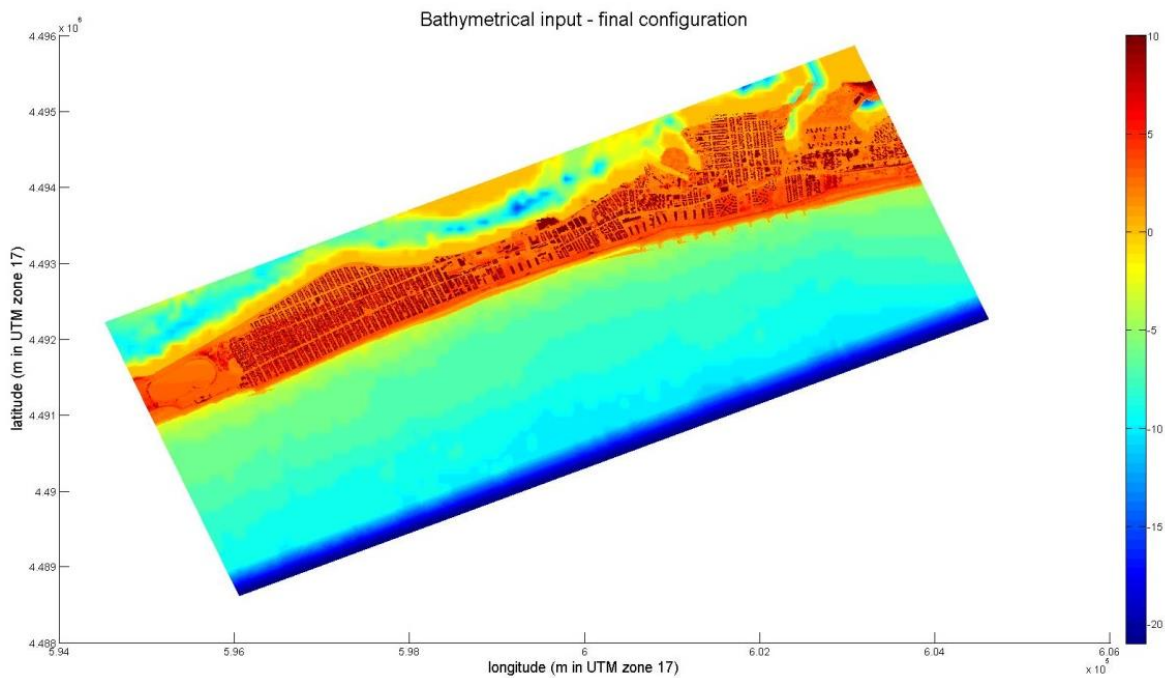


Figure 3-16 - Bathymetry input for the XBeach Model (elevation in m ref. to NAVD88)

In Figure 3-16 the final topo-bathymetry input is plotted, which is composed of LIDAR data from three different surveys performed by USACE and bathymetrical data from the Coastal Relief Model (CRM)⁴². The model domain is almost 9 by 4 km² large and the grid size varies between 25 by 25 m² at the offshore boundary and at minimum 3 by 3 m² in the area of interest near buildings. This implies 711 by 2403 grid cells in total, which can be considered as a very large XBeach model. Running one Linux simulation with 32 cpu's takes about three days. Multiple things have been done to decrease the simulation time, which includes the usage of a morphological factor of 10 and fairly large wave bins of 20 degrees; see Appendix C.

The grid size onshore of 3 by 3 m² is the result of computational limitations: a smaller grid size would be unfeasible due to a corresponding increase of the computational time. A larger grid size is assumed to have negative effects on the amount of detail captured. The latter is studied by comparing the result to results of similar runs with 5 by 5 m² and 9 by 9 m² grid cell sizes onshore. More detail is given in section 3.3 and the results are discussed in chapter 0. A zoomed view of the bathymetry is shown in Figure 3-17.

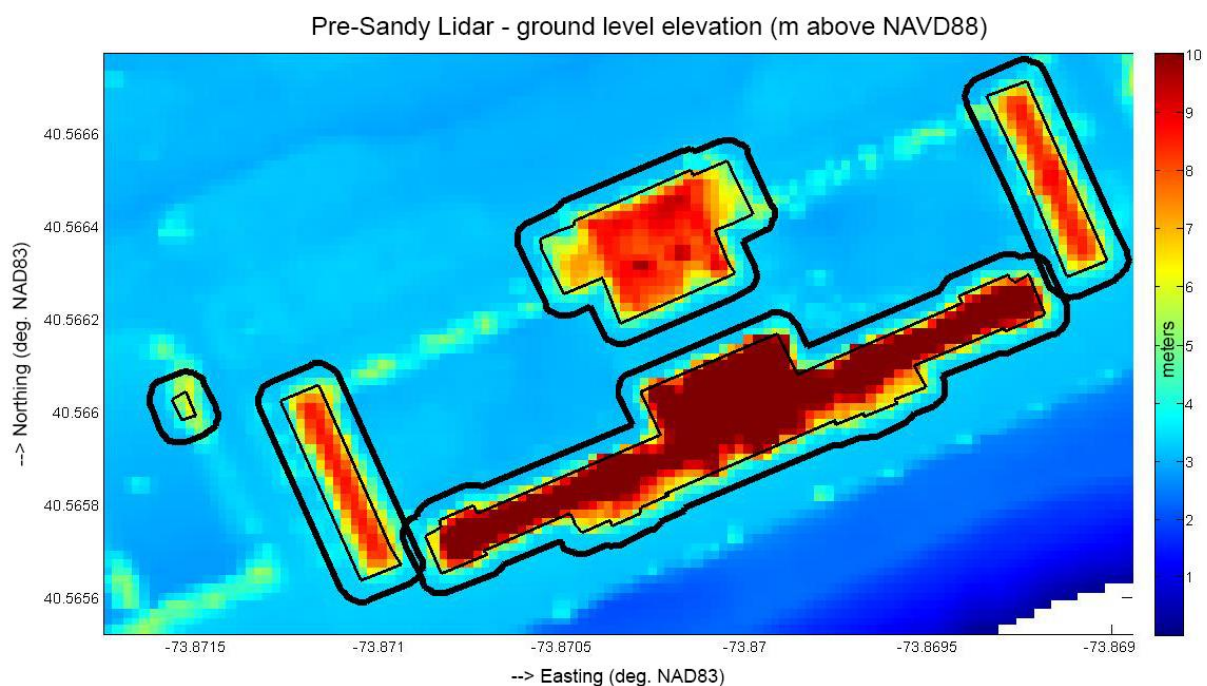


Figure 3-17 - Zoomed view of the topo-bathymetry input file with building polygons (thin black lines) and an 10m-offset of these polygons (thick black line)

On top of the bathymetry the building polygons are plotted, which are used to make a seamless transitions between the different data layers and to determine which cells lay within a building and therefore have to be non-erodible during the simulation. By offsetting the building polygons with 10 m a buffer zone is created. The indices of the cells lying within that buffer zone are assigned to that specific building. These cells are used to determine the local hazard indicators after the simulation has finished. Results from chapter 0 show that there is scope for improvement on this part. The four hazards “inundation depth”, “wave attack”, “flow velocity” and “scour depth” are represented in the BBN’s by indicators. For the determination of the four hazard indicators, extraction formulations have been used. Inundation Depth is assumed to be the most important one and for that indicator more than one formulation has been tried of which the results in relation to the damage is compared. These formulations are given in paragraph 3.3.2; here formulations of the other three indicators are given.

⁴² <http://www.ngdc.noaa.gov/mgg/coastal/coastal.html>

To end up with one indicator value per building per storm event, aggregation in time and space (over the cells) is necessary. The following formulations for wave attack, scour depth and flow velocity have been used, where cursive text corresponds to spatial aggregation operations and underlined to temporal aggregation operations:

- **Wave attack:** $\max(\max(H_s))$, the absolute maximum of the local significant wave height during the storm. The cell for which this is maximal is taken.
- **Scour depth:** $\max(\max(h_{b0} - h_b))$, the absolute maximum of the difference between initial bed level and bed level during the storm. The cell for which this is maximal is taken.
- **Flow velocity:** $\max(\max(\sqrt{(u_{\text{mean},30\text{min}})^2 + (v_{\text{mean},30\text{min}})^2})^{0.5})$, the maximum of the half hourly mean velocity vector. The cell for which this is maximal is taken.

With: h_{b0} = initial bed level (from the LIDAR data)
 h_b = updated bed level
 H_s = significant wave height
 $u_{\text{mean},30\text{min}}$ = the 30min mean flow velocity in x-direction
 $v_{\text{mean},30\text{min}}$ = the 30min mean flow velocity in y-direction

The flow velocity is based on means instead of maxima, because it is not said that during the maximum of the velocity in y-direction (v_{max}) the velocity in x-direction (u_{max}) is maximum as well. It should be noted that other formulations of these variables might work as well, maybe even better. However, for delivering a proof of concept it is assumed to be of minor importance here. Scour depth can be considered as a strange indicator, since 1) in the post-Sandy data hardly any scour has been observed in the urban areas (pavements and vegetation prevent this from happening); 2) sedimentation (overwash deposits) was dominant over erosion onshore. However, bed level changes are caused by a combination of inundation, waves and velocity, which are considered the most important indicators. Therefore, scour depth (or bed level change) might be an indicator with potential. Moreover, for other case studies scour can play a role in the stability of buildings, which makes it interesting to research its added value.

Within the area of application (area of interest in Figure 3-18) more than 7800 buildings are situated of which a bit more than 5300 are residential and overlap with the other datasets, knowing PLUTO and ImageCat. The two areas on the side of the domain are shadow zones. Since the normative wave direction is West-northwest (see Figure 2-17), the shadow zone at the east side is a bit larger.

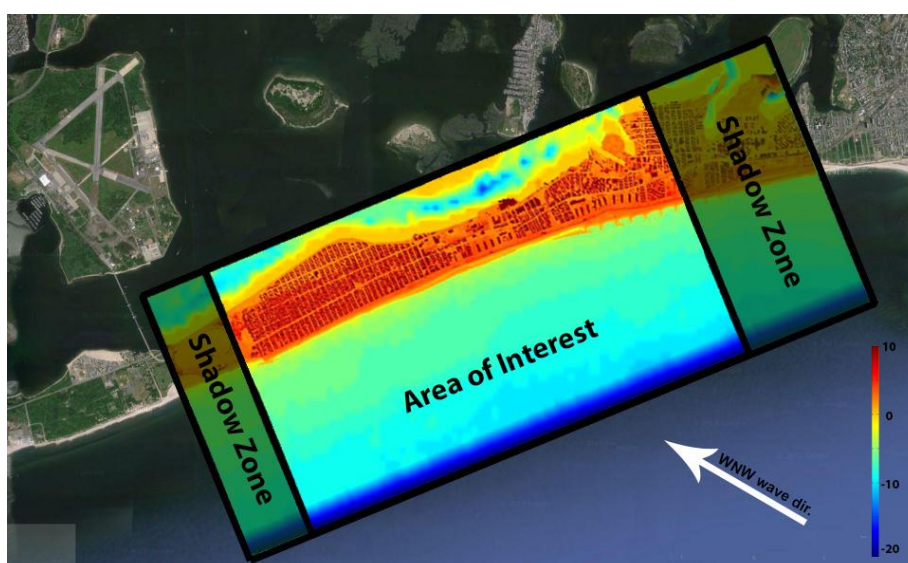


Figure 3-18 - The area of interest (or area of application) and shadow zones within the XBeach model domain.

The boundary conditions, both wave and surge are extracted from Delft3D and D-Flow FM respectively. Both models are briefly elaborated in the next subsection. At the bay side wave conditions are neglected, because the bay is sheltered by the Rockaway Peninsula. In Figure 3-19 the water levels, significant wave height and significant wave period are graphed in time for Hurricane Sandy.

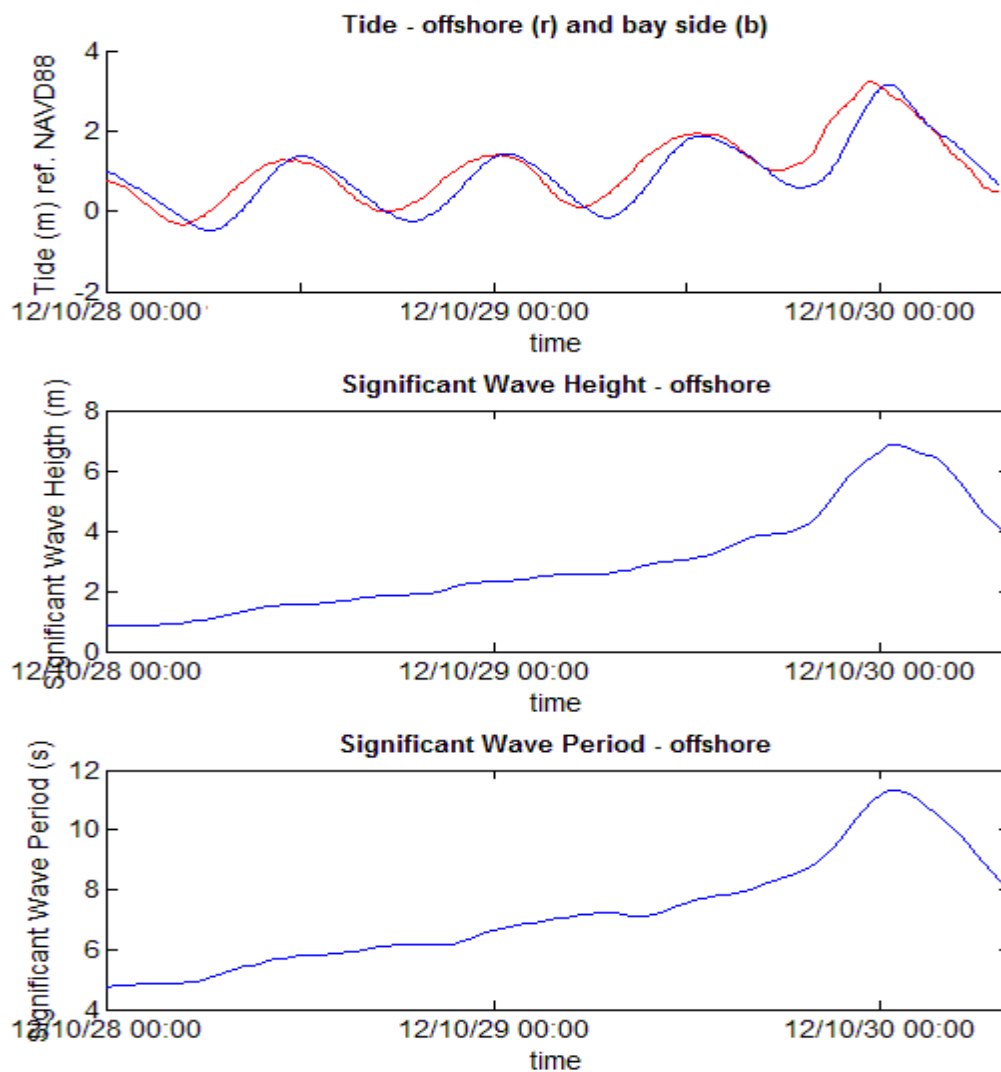


Figure 3-19 - XBeach boundary conditions: tide, wave height and wave period; red for bay side and blue for the ocean side.

The water levels have been predicted fairly well compared to temporarily installed water level gauges and records of offshore buoys. These gauges predicted slightly lower water levels during the peak (order of 10-30 cm) than D-Flow-FM does at the offshore boundary. The significant wave height and wave period have both been corrected with scaling factors obtained from a comparison between observations of Buoy 44065 (see section 2.2), which is located several kilometres out of the coast, and observations of the Delft3D simulation. This is also discussed in Appendix D.

3.2.2.3. Delft3D and D-Flow Flexible Mesh

Delft3D – US East Coast

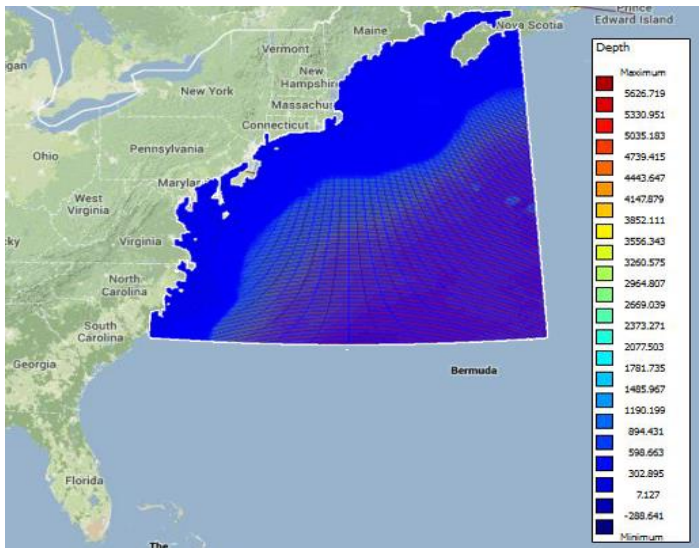


Figure 3-20 - Bathymetry input of Delft3D - US East Coast model

The Delft3D US East Coast model is set up by Maarten van Ormondt (Deltares) and no documentation is yet published. It ranges from Nova Scotia (Canada) to South Carolina and it has a minimum grid size of approximately 5.5 by 5.5 km². The SWAN wave grid is a factor two coarser. The bathymetry is coming from the Coastal Relief Model and the boundary conditions for Hurricane Sandy are:

- Tidal information: amplitudes and phases of 13 tidal components from TPX07.2 dataset⁴³ for 26 boundary locations;
- Wave conditions: No wave boundaries, so all waves are internally created;
- Wind: NOAA's North American Meso-scale Forecast System (NAM).

Results of model simulations have been compared to observations of multiple buoys located within the model domain and it can be concluded that the model performs fairly well. See Appendix E for more detail.

Delft3D – New York Bight

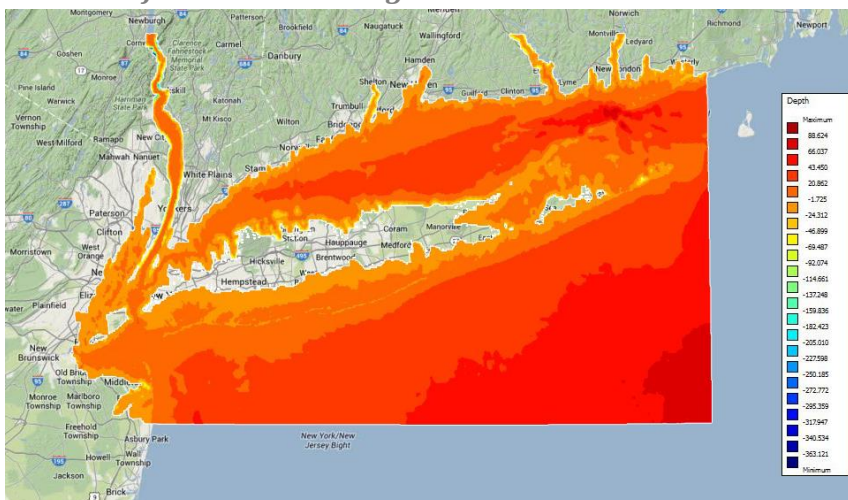


Figure 3-21 - Bathymetry input of Delft3D – New York Bight model

⁴³ https://www.esr.org/polar_tide_models/Model_TPX071.html

The Delft3D New York Bight model is developed by Deltares and Royal HaskoningDHV and is not documented either. It ranges from Long Branch, NJ to the state of Rhode Island and has a minimum grid size of 500 by 500 m², which is thus 10 times finer than the US East Coast model. The SWAN wave grid is a factor two coarser again. The bathymetry is coming from the NGDC Coastal Relief Model in combination with Shuttle Radar Topography Mission (SRTM)⁴⁴ data and the boundary conditions for Hurricane Sandy are:

- Tidal information: nested in the Delft3D – US East Coast model;
- Wave conditions: nested in the Delft3D – US East Coast model;
- Wind: NOAA’s North American Meso-scale Forecast System (NAM).

Model simulations have been compared to observations of buoys located within the model domain and it can be concluded that the model underestimates the wave conditions quite significantly; see Appendix E. Unfortunately, there have no particular reasons been found yet for this underestimation. Measures to compensate for this have been preferred over model optimization, since the latter has potential of being very time consuming. See Appendix D.5 for more detail.

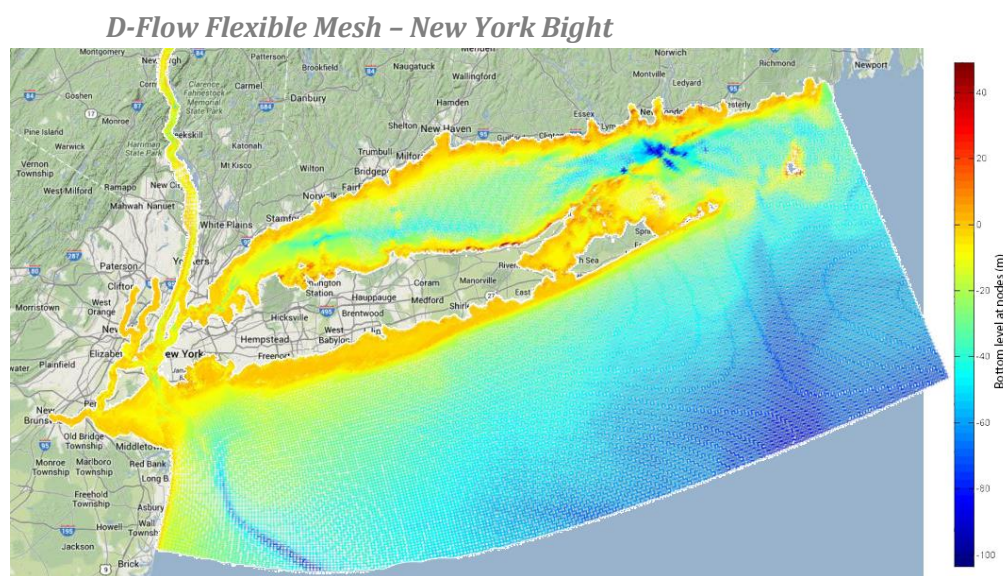


Figure 3-22 - Bathymetry input of D-Flow FM – New York Bight model.

The D-Flow FM - New York Bight model is developed in 2013 by Deltares and Royal HaskoningDHV as a better alternative for the Delft3D –New York Bight model (Tuinhof 2013). It ranges from Long Branch, NJ to the state of Rhode Island as well, but the southern and eastern boundaries are curved and angled. Since D-Flow FM works with a flexible mesh grid, size and form depend on water depth and hydraulic configurations. A zoomed view of the grid in the Jamaica Bay is shown in Figure 3-23. The bathymetry is coming from the NGDC Coastal Relief Model in combination with Shuttle Radar Topography Mission (SRTM).

⁴⁴ <http://srtm.csi.cgiar.org/>



Figure 3-23 - Grid configuration in the Jamaica Bay and around the Rockaway Peninsula.

The boundary conditions for Hurricane Sandy are based on:

- Tidal information: nested in the Delft3D – US East Coast model;
- Wave conditions: nested in the Delft3D – US East Coast model;
- Wind: NOAA’s North American Meso-scale Forecast System (NAM).

Model simulations have been compared to observations of multiple buoys located within the model domain and it can be concluded that the model performs adequately. For more detail see the report ‘Modeling New York in D-Flow FM’ by Taco Tuinhof⁴⁵ and Appendix F. Moreover, the master input files of the two Delft3D and D-Flow FM model can be found in Appendix E.

3.3. Scenarios

3.3.1. XBeach Runs

As is stated in section 3.2 three XBeach runs have been executed with three different grid resolutions and corresponding cell sizes of 3x3, 5x5 and 9x9 m². This is in order to study the sensitivity of the damage predictions to model resolution. These resolutions have been chosen, because of the following reasons:

- 1) 3x3 m² is considered the smallest grid cell size, since a smaller grid size would be infeasible due to a corresponding increase of the computational time.
- 2) In Figure 3-24 the Cumulative Distribution Function (CDF) is given for a length indicator (square root of the ground floor area) of all residential buildings within the domain. The grid cell size should be at least smaller than the majority of the buildings in order to extract information with detail on the object level. 9x9 m² is considered the largest grid cell size for which this is still true.
- 3) 5x5 m² is used for the third run, where the length scale ratios 3/5 and 5/9 are pretty much equal.

⁴⁵ <http://kennisonline.deltares.nl/3/m/search/products.html?qtype=1&q=tuinhof>

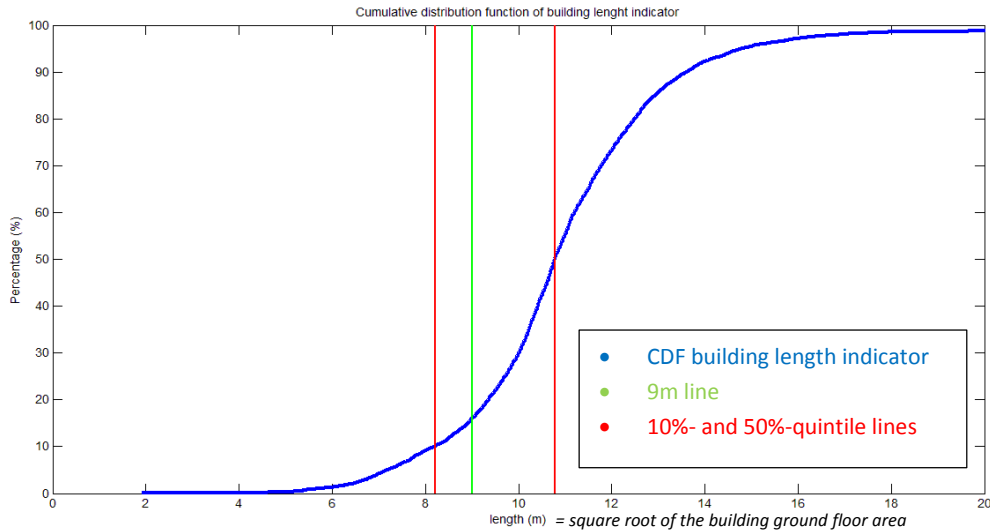


Figure 3-24 - Cumulative distribution function of the building length indicator (blue), which is the square root of the ground floor area; 9m is marked in green and the 10%- and 50%-quintiles in red.

The runs are compared to observations on hydro- and morphodynamics and on how well the extracted local storm characteristics can be used as indicators for damage predictions with use of the Bayesian Belief Network.

3.3.2. Local Hazard indicators-Damage Relations

Depth-Damage

Since the depth-damage relation is assumed to be the most important one, these are analysed more extensively in this thesis. Inundation depth is said to be the difference between the water level and the ground elevation. Again, to end up with one value per building per storm aggregation in time and space (nearby cells) is necessary. The formulations for the extraction of the other hazard indicators all take the maximum in time and space, except for flow velocity. For inundation depth more options are considered, like (half-hourly) mean or minima. Three axis of freedom can be distinguished:

1. Temporal aggregation: absolute maximum or maximum of 30minute-means;
2. Spatial aggregation: minimum, mean or maximum of surrounding cells;
3. Order: subtracting (bed level from water level) before aggregating (in space and time) or the other way around.

Not all possible combinations are assumed to have potential. The following eight formulations are compared, where cursive text corresponds to spatial (over the cells) operations and underlined to temporal (over time) operations:

Table 3-1 - Eight different extraction formulations for the inundation depth indicator

#	Order (first)	Temporal aggr.	Spatial aggr.	Formulation
1.	Aggregate	Max	Max	$Max(\underline{\max}(h_s)) - Min(h_{b0})$
2.	Aggregate	Max	Mean	$Mean(\underline{\max}(h_s)) - Min(h_{b0})$
3.	Aggregate	Max	Min	$Min(\underline{\max}(h_s)) - Min(h_{b0})$
4.	Subtract	Max	Max	$Max(\underline{\max}(h_s - h_{b0}))$
5.	Aggregate	Max of 30minute-mean	Max	$Max(\underline{\max}(h_{s,mean,30min})) - Min(h_{b0})$
6.	Aggregate	Max of 30minute-mean	Mean	$Mean(\underline{\max}(h_{s,mean,30min})) - Min(h_{b0})$
7.	Aggregate	Max of 30minute-mean	Min	$Min(\underline{\max}(h_{s,mean,30min})) - Min(h_{b0})$
8.	Subtract	Max of 30minute-mean	Max	$Max(\underline{\max}(h_{s,mean,30min} - h_{b0}))$

In addition to this, the inundation depths gained from the XBeach simulations are compared to inundation depth establishment based on the bathtub concept, which assumes one single water level for the whole area. Both are compared in relation to the damages as well. In analogy with the water level variations, also the ground elevation levels can be chosen differently. According to the concept the ground elevation levels are taken from the bathymetrical file and thus from the LIDAR data, but it is also possible to use the ground elevation levels from the Buildings dataset; see section 2.3. In combination with the water level options, four alternatives to determine inundation depth are compared in relation to damage:

- 1) Water levels from XBeach and ground elevation levels based on LIDAR;
- 2) Water levels from bathtub concept and ground elevation levels based on LIDAR;
- 3) Water levels from XBeach and ground elevation levels based on Building dataset;
- 4) Water levels from bathtub concept and ground elevation levels based on Building dataset.

Wave Attack, Flow Velocity and Scour Depth

Next to the depth-damage relations also the wave-damage, velocity-damage and scour-damage relations have been studied. The correlations with damage are given in section 4.2 and the corresponding added value to the prediction of damage is discussed in 'Coupling Storm Conditions to Damage' (section 4.3.1). Moreover, the differences of Bayesian nets with and without mutual connections between the local hazard indicators are elaborated. This means with and without the orange arrows from Figure 3-8.

3.3.3. Indicators for building type and value at risk

The sensitivity of the damage observations and predictions to the following indicators is studied:

- Building height;
- Surface area of the ground floor;
- Tax base value (which is also based on the size of the building and lot area);
- Number of residential units in building;
- Building class.

Most of these indicators speak for themselves; "building class" needs some additional explanation. The classification is based on functional aspects. More than 150 different classification groups (in the PLUTO dataset) are brought back to 5:

- A: One family dwellings;
- B: Two family dwellings;
- C: Walk-up apartments;
- D: Elevator apartments;
- Other.

In the case of multiple functionalities per building the one is used which has the largest share of surface area. Detailed descriptions of the building type indicators and classes are given in appendix J.

4. Results

4.1. XBeach

In this section the skill of XBeach and the extraction of local hazard indicators are elaborated. The hydrodynamics and morphodynamics are compared to the observations and the differences are discussed partly here but also in chapter 0. In this section some results are given for the 3x3m² run, as has been described in section about implementation.

It must be said that the model is poorly calibrated and not validated at all. The 3x3m² run with scaled wave boundary conditions gives far from best results. Considering the morphodynamics (see subsection 4.1.2) the 5x5m² run with non-scaled waves appeared to give better results when comparing to the observed erosion and sedimentation. However, this conclusion has been drawn too late in the process and with a limited amount of time the best shot had to be taken, which is presented here. A comparison on grid resolution in the urban areas (3x3m², 5x5m² and 9x9m²) is made in relation to the damage, which is elaborated in section 0.

4.1.1. Hydrodynamics

Surge

In Figure 4-1 the water levels are plotted together with the updated bathymetry, both in a top view and in cross section. The three regimes collision, overwash and inundation can be distinguished. Approximately 2.5 hours before the tide peak (offshore) the beaches and berm have already been eroded heavily, as can be seen in the cross section of the upper left panel. One hour later (10pm), the berm gets overtopped at multiple places and the berm starts breaching. A little later after midnight, during the peak of the tide, larger part of the area is flooded by the sea water. First the water comes from the ocean side and after the peak a gradient in the opposite direction lets the water flow from the Jamaica Bay side into the domain. This can be explained by the phase lag in surge between the offshore and bay side boundary; see Figure 3-19.

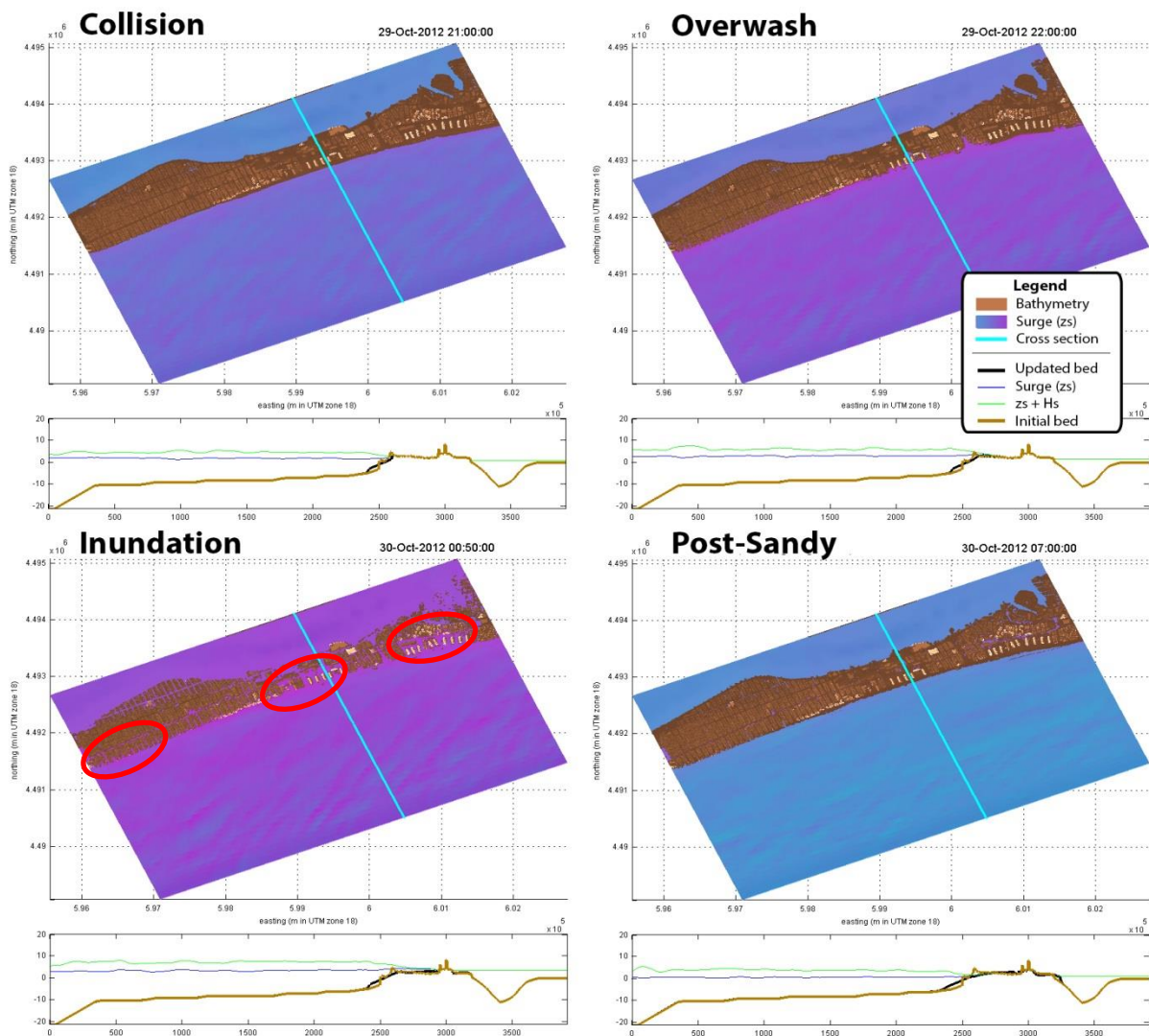


Figure 4-1 - Snapshots of the simulated hazard propagation: Upper left panel: collision regime with heavy beach erosion; upper right panel: overwash regime with high long waves penetrating into the urban area; lower left panel: inundation regime where almost the whole peninsula is flooded; lower right panel: post-Sandy situation (note updated bed)

It should be noted that the inundation regime has only been reached at some locations, where at other locations the beach and berm prevented this from happening. The cross-sectional plot in the lower right panel shows the change in bed level for a location where the inundation regime was reached. According to the XBeach run, three areas can be assigned as hotspots, where the inundation regime was reached and severe flooding was at stake. These areas are encircled with red. If we compare this to the observations discussed in paragraph 2.2.1.1 it can be concluded that the model predicts two of these hotspot locations well, knowing the area in the middle and the western part of the domain. On the contrary, the eastern part did not show full inundation in reality, where there was still a relative wide stretch of beach observed after the storm. Moreover, hardly any sediment deposits were found inland at these spots and the boardwalk survived.

In Figure 4-2 the absolute maximum surge level for each grid cell is graphed, which includes tide and long waves. The non-flooded areas are white. In the same figure, in the three lower panels, the surge levels are given for the locations of the three high water marks within the domain. Comparing the peaks with the high water marks an underestimation is found for locations 5, where for location 6 and 7 overestimation is at stake, both in the order of 20-50cm. Thereby, it is assumed that the high water marks correspond to the highest water levels excluding short waves, which are negligible at these locations. The latter holds according to Figure

4-3 as well.

The underestimation of the storm tide at location 5 can be explained by the large white gap south of it corresponding to a non-flooded area, which shelters that location from the ocean side. However, the area corresponding to the white gap did flood in reality, which can be learned from the ImageCat damage dataset. Comparing the ground elevation levels from the buildings dataset and LIDAR (see Figure 2-4 and Figure 3-16) it can be concluded that this problem can be assigned to obstructing objects in the LIDAR data. The non-flooded area contains a lot of vegetation (mainly trees), which seems to be problematic for the water flowing into that area.

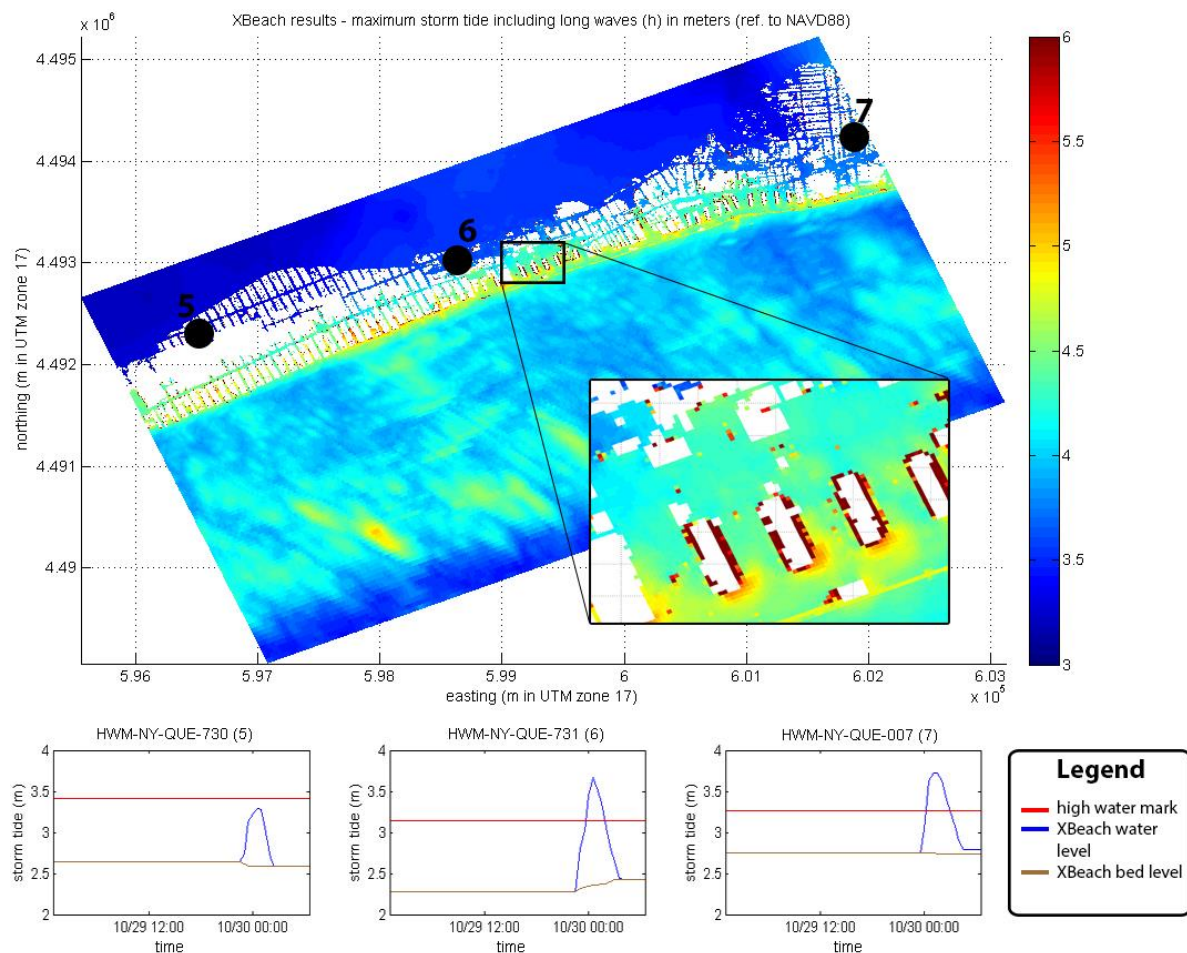


Figure 4-2 - upper panel: Maximum simulated storm tide including long waves; lower panels: observed and simulated water levels at location 4, 5 and 6

The overestimation of the other two locations seems to be more in line with the rest of the domain. Although ~ 3.8 m water levels are high compared to the observed high water marks, they are still low compared to water levels in larger part of the domain. Especially at the ocean side of the peninsula maximum surge levels of 4.5 to 5 m are no exception. Moreover, in the zoomed view of Figure 4-2 it can be seen that around buildings, especially the higher ones, the maximum water levels rise to 6 m and even higher. These local peaks are assumed to be caused by local instabilities due to steep bed level gradients.

Comparing the results with the observations, a structural overestimation of the water levels is likely. However, it is hard to underpin this since 1) at the ocean side no high water marks are documented for verification and 2) the assumption that the absolute maximum water level gives a good approximation for the high water marks can be wrong. Nonetheless, a structural overestimation is not necessarily a big problem for delivering a proof

of concept for present study. As long as all observations are overestimated to the same extent, Bayes might be forgivable. On the contrary, the local peaks due to instabilities do form a problem, which is discussed in more detail in subsection 4.1.3.

Waves

In Figure 4-3 the absolute maximum significant wave height for each grid cell is graphed. It can be concluded that the height of the waves decreases when they approach the coast. This is in line with expectation, since wave height is limited by depth. The maximum significant wave heights are in the order of 2-3 m near the first buildings, which is considered pretty severe. The waves rapidly decay between the buildings and wave height becomes negligible even within the first block from the beach.

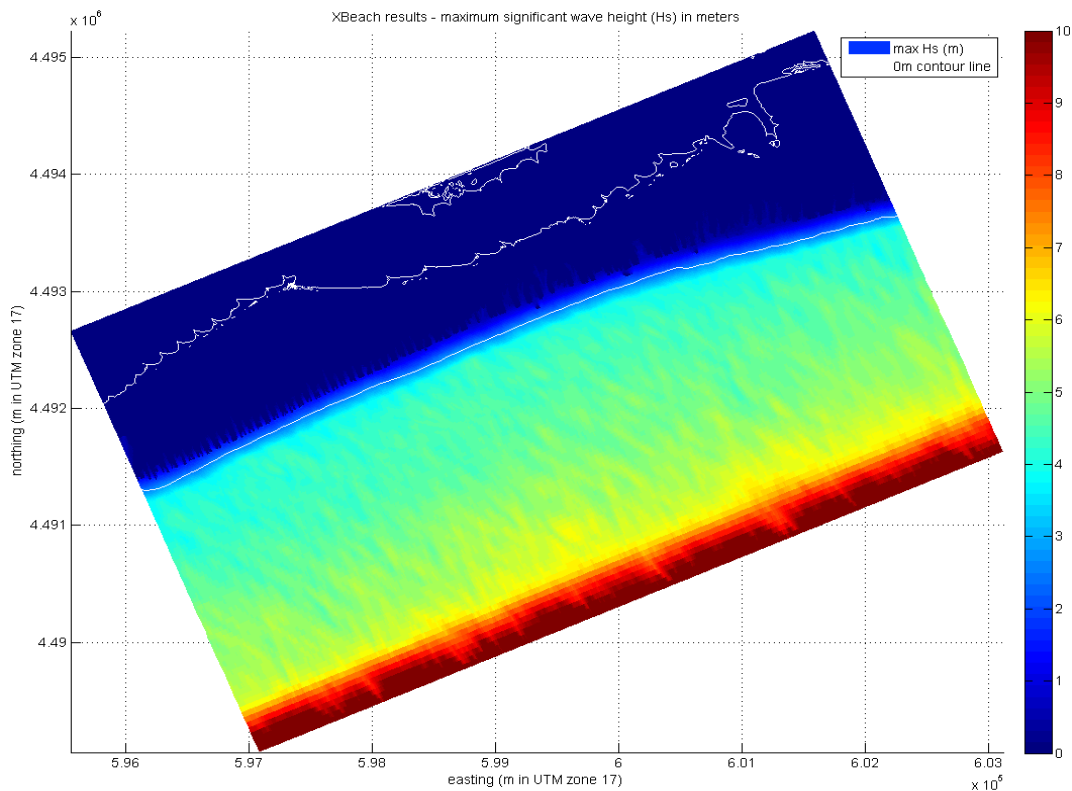


Figure 4-3 – Maximum simulated significant wave height (Hs)

Since the maximum water levels are assumed to be overestimated by XBeach, the question can be asked whether this can be explained by too high infragravity waves (long waves). The long wave heights are a direct result of the offshore wave boundary conditions, which have been scaled to an offshore buoy; see paragraph 3.2.2.2. The scaling implies an increase of the significant wave height gained from the Delft3D/SWAN model by a factor of 1.5, which is quite a lot. This might have been wrong, implying an overestimation. From the scatter plots in Figure 4-4 it can be concluded that a 5x5m run with non-scaled wave conditions gives onshore lower maximum storm tide levels and wave conditions than with scaled conditions. However, the differences are minimal and the 5x5 m² non-scaled wave run still shows an overestimation compared to the observed (see Appendix G). The onshore hydraulic sensitivity to offshore variability in significant wave height is thus not so high. Moreover, it can be concluded that other reasons must be there as well for the overestimations of onshore hydraulic storm characteristics, other than uncertainty in wave boundary conditions.

Scatter plots : 5x5m2 Scaled Waves run vs 5x5m2 NON-Scaled Waves run

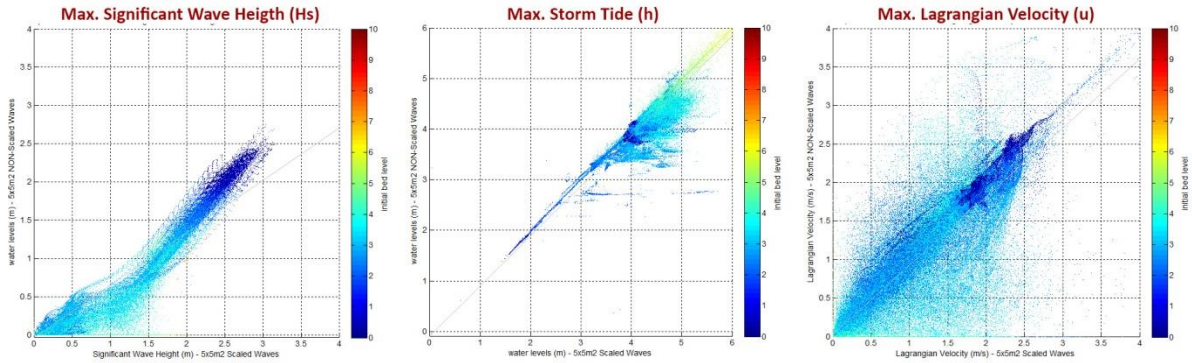


Figure 4-4 - Scatter plots: 5x5m2 Scaled Waves run vs 5x5m2 NON-Scaled Waves run

Velocity

The magnitude of the absolute maximal occurred Lagrangian flow velocities during Hurricane Sandy have been plotted in Figure 4-5. The lighter band in front of the coast corresponds to the surf zone and the high velocities in that area can be assigned to alongshore water flow induced by the refracting waves. A lot of the wave energy transforms into kinetic energy, which in the overwash and inundation regime results in flooding of the streets. The street pattern is clearly visible and the wider the street, the higher the maximal velocities. In the middle of the model domain maximal velocities of 4 m/s can be seen, which is quite high for urban areas. In the western part of the domain in the non-flooded area (white gap in Figure 4-2) the water is blocked, which limits the flow velocities around this area. It is therefore assumed that the velocities are underestimated at these locations. On the bay site this is in analogy with the water levels, but on the ocean side the kinetic energy of the waves has to go somewhere and transforms in potential energy again, piling up the water in the streets. The blockage of the non-flooded area might therefore, locally, be an explanation for the assumed overestimation of the water levels. In the other areas no such large blockage can be found, but local objects like trees are the visible cause of smaller obstacles in the LIDAR data.

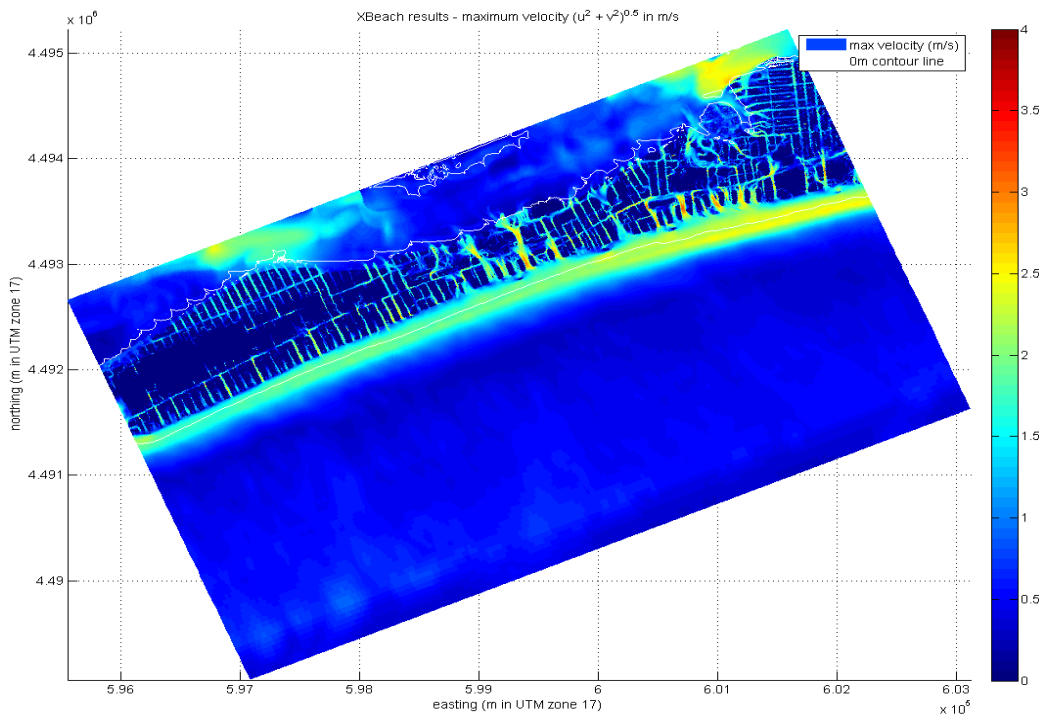


Figure 4-5 - Maximum simulated absolute flow velocity (m/s) (Lagrangian flow)

The direction of the maximal velocities during the time of occurrence varies, but is mainly offshore directed. This can be explained by Figure 4-6 in which the time of occurrence is spatially shown. The darker orange colors correspond to a time of occurrence after the offshore tide peak. At that time the berm has already completely eroded away near breaches and forms no obstacle to the water anymore. After the offshore tide peak the water gradient becomes negative and water flows from high (bay side) to low (ocean side), mainly channelling through the streets. In the zoomed view of Figure 4-6 the lighter orange colors correspond to a time of occurrence before the storm tide peak. This can be explained by the fact that these areas are sheltered from bay side flooding mostly by buildings. The local (lower) maximal flow velocities are therefore caused by incoming water from the ocean side in combination with wave celerity.

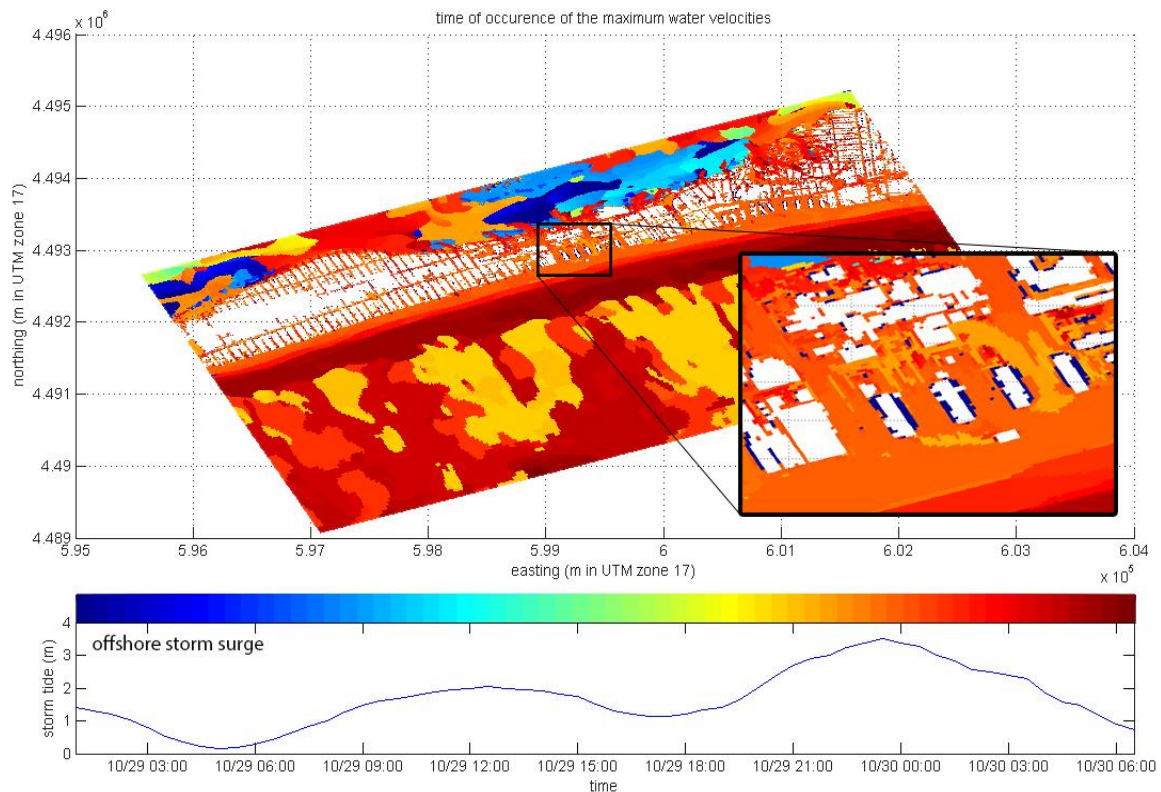


Figure 4-6 - Time of occurrence of the maximum simulated flow velocity; The colors correspond to the timeline graphed below the map and the offshore storm surge levels have been plotted as well to give a reference.

Last, it should be noted that the comparison between the 5x5m² runs with and without scaled wave boundary conditions did give some differences in flow velocities; see Figure 4-4. This shows that a substantial part of the additional wave energy in the scaled run is transformed into kinetic energy. Unfortunately, no flow velocity observations have been documented which can support the calibration and validation process.

4.1.2. Morphodynamics

The purpose of including morphodynamics is first of all to better predict the hazard propagation in time. Therefore, it is most important that the erosion and erosion rates of natural and manmade barriers (beach and berm which reduce the hazard intensity behind it) are predicted in harmony with reality. If these barriers erode too fast, the hazard intensity in the hinterland will be overestimated and vice versa. Secondly, scour depth and sediment deposits in urban areas are of interest.

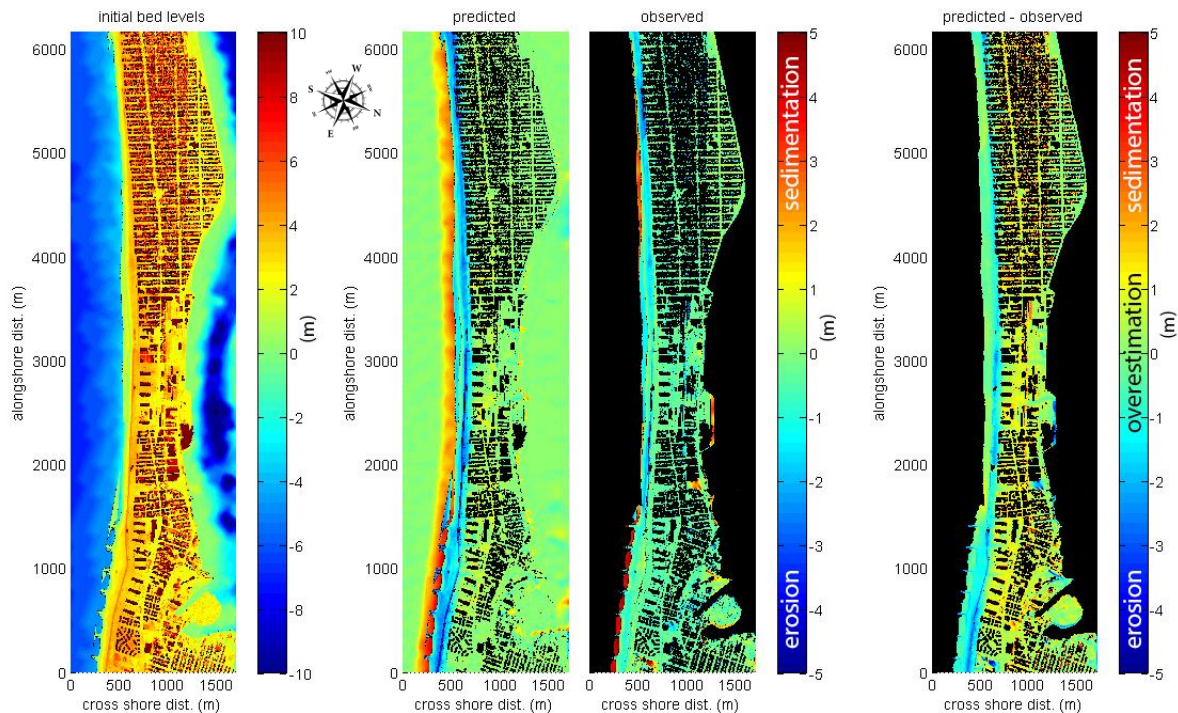


Figure 4-7 - Morphological change. From left to right: initial bed levels, predicted post-Sandy bed levels, observed post-Sandy bed levels and the difference between these two.

In Figure 4-7 maps of the post-Sandy bed level changes are given for the observations (second panel) and the XBeach results (third panel) of the 3x3m run with scaled waves. In the first panel one can see the initial bed levels and in the last panel the difference between predicted and observed bed level changes. The following things can be concluded:

- At the beach and berm much more predicted erosion can be found than observed; see the large long stretched blue band;
- The littoral zone shows a large sedimentation/erosion gradient at the place where LIDAR data overlaps the CRM data;
- In general larger inland sediment deposits are predicted than observed.

In Figure 4-8 three areas have been zoomed into, which tell the story in more detail. At location one (western part of the domain), the erosion at the beach is predicted fairly well. However, the erosion doesn't stop near the first buildings but continues into the streets of the first block. This is not in line with the observations. More inland, in the middle of the peninsula, the influence of LIDAR differences is clearly visible: the pre-Sandy LIDAR (XBeach input) still contains all the trees and other vegetation in this area and thus the XBeach output as well, whereas in the Post-Sandy LIDAR these obstacles have been filtered out. The difference of these two indicates therefore intense sedimentation, which is of course not true.

At location two, in the middle of the domain, XBeach overestimates the erosion at the beach and berm, whereas inland sedimentation is overestimated. It is assumed that the latter is a direct result of the first, because the erosion of the berm enables the inundation regime from happening. For location three similar overestimation can be seen. However, here the differences between predicted and observed are even larger. The beach in this area is at its widest and together with the larger grains less erosion is observed. Moreover, the boardwalk here is mainly intact. On the contrary, XBeach doesn't show less erosion than in the other parts, which is hard to explain.

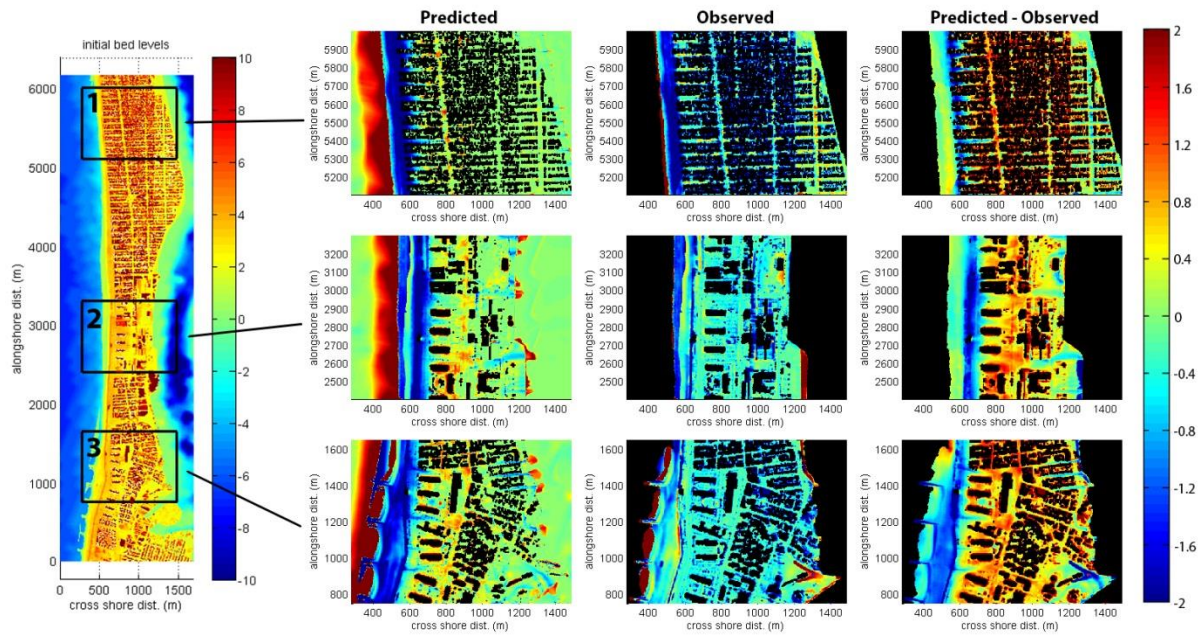


Figure 4-8 - The same as Figure 4-7 but now zoomed views of three representative locations.

The overestimation of the beach erosion, especially in the eastern part, cannot only be explained by too severe offshore storm conditions. Results of the 5x5 non-scaled wave run, which are graphed in Appendix G, show much better agreement between predicted and observed beach and berm erosion. However, the overestimation in the eastern part of the domain stays the same. The sudden transition of LIDAR to CRM data in the littoral zone, which is at these specific areas visible, might give some explanations for this; see Figure 4-9.

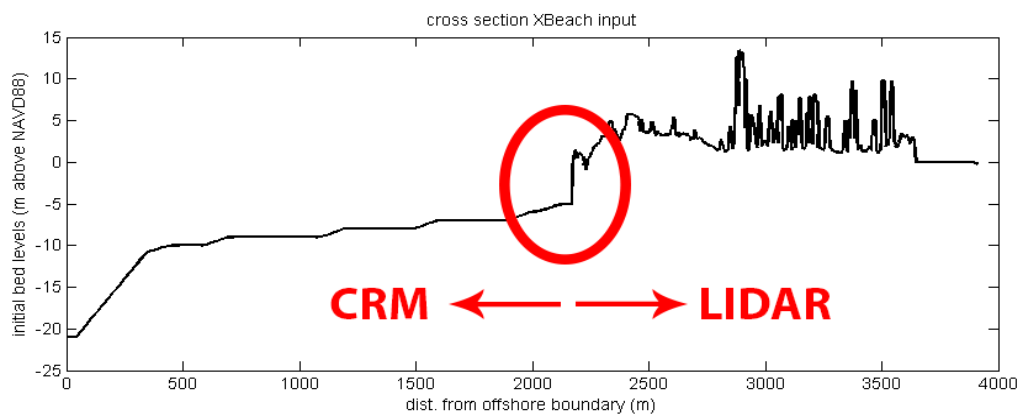


Figure 4-9 - Cross sectional plot of the initial bed level profile. The sudden jump in bed level due to CRM-LIDAR differences is encircled in red.

The drop in bed level, encircled in red, is not natural for sandy beaches and is caused by the inaccuracy of the CRM data. Therefore it is probable that the littoral zone in XBeach has less sand than in reality and more sediment from the beaches is transported offshore to compensate for this, which implies an increase of the erosion rate onshore. Hereby it should be said that even if the bathymetry is more veracious than it is right now, than it would still be difficult to predict morphological changes correctly for this particular case study. Sandy was a critical storm, breaching the berm at some places and at other places not. A small change in offshore boundary conditions can therefore have a large effect on the morphological changes and the accompanying consequences for the urban areas. This is in analogy with a threshold problem.

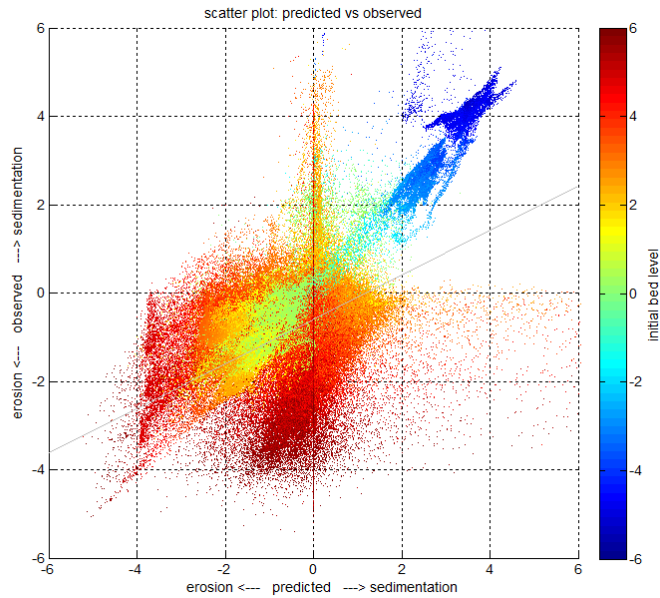


Figure 4-10 - Scatter plot: predicted (vertical) versus observed (horizontal) bed levels. The colors correspond to the initial bed levels (in meters ref. to NAVD88)

Figure 4-10 holds a scatter plot of the predicted and observed bed level changes. The colors correspond to the initial bed levels. It can be concluded that the nearshore parts (-6m to 0m) and the beaches (0m to 2m) are predicted fairly well and thus XBeach shows skill. The predictions onshore are insufficient and in general one could say that the higher the initial bed level is, the worse the prediction becomes. One explanation for this can be found in the earlier mentioned differences

between pre- and post-Sandy LIDAR. Trees for instance will end up in the dark red zone, showing observed erosion and negligible predicted erosion. Another explanation can be found in the fact that the cells just outside the building polygons are not assigned as non-erodible cells. Building walls are not straight but a bit blurred in the LIDAR data and therefore these erodible cells have higher initial bed levels. In XBeach heavy erosion can be seen around especially higher buildings and the sediment is deposited in neighbouring cells. This is shown in Figure 4-11.

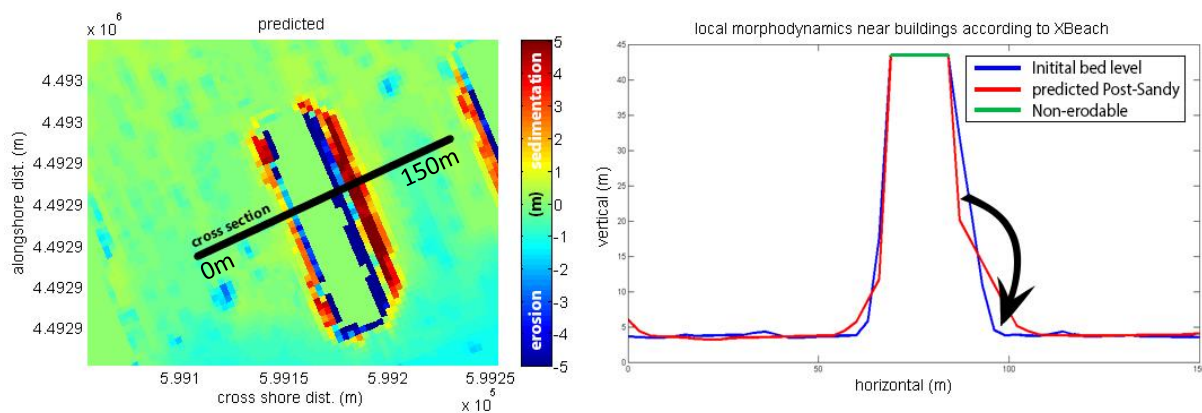


Figure 4-11 - Predicted bed level changes around a relative high building with corresponding cross section in which the initial bed level and predicted post-Sandy bed level are plotted.

4.1.3. Local hazard indicators

The local hazard indicators “inundation depth”, “wave attack”, “flow velocity” and “scour depth” are extracted from the XBeach results according to chapter 0. It is to be expected that overestimations of the onshore storm characteristics also have their impact on the local hazard indicators. Nonetheless, as long as the over- or underestimation is structural, buildings with major observed damage will probably still correspond to higher indicator values than buildings with minor or no damage. To what extend this is the case is studied and is elaborated in the next two sections. Here the spatial distributions and associated marginal probability mass functions are given for the 3x3 m² run. Comparisons between different runs have been made, but only in relation to the observed damage, which is discussed in section 4.2.

Inundation Depth

Inundation depth indicators extracted from the XBeach results according to formulation 1 from Table 3-1 in subsection 3.3.2 can be graphed spatially. An example is given in Figure 4-12.



Figure 4-12 - Impression of the spatial distribution of the inundation depth indicator

Next to the above used formulation, seven other ways to determine the local inundation depth have been defined and posited. To compare for the whole domain, the spatial distribution can be best illustrated by interpolating the local conditions (one record per building) to the rest of the urban area of the domain. The result is shown in Figure 4-13. Note that buildings surrounded with more free space will attribute to a larger area of the colored map. The PMF's are given in Figure 4-14.

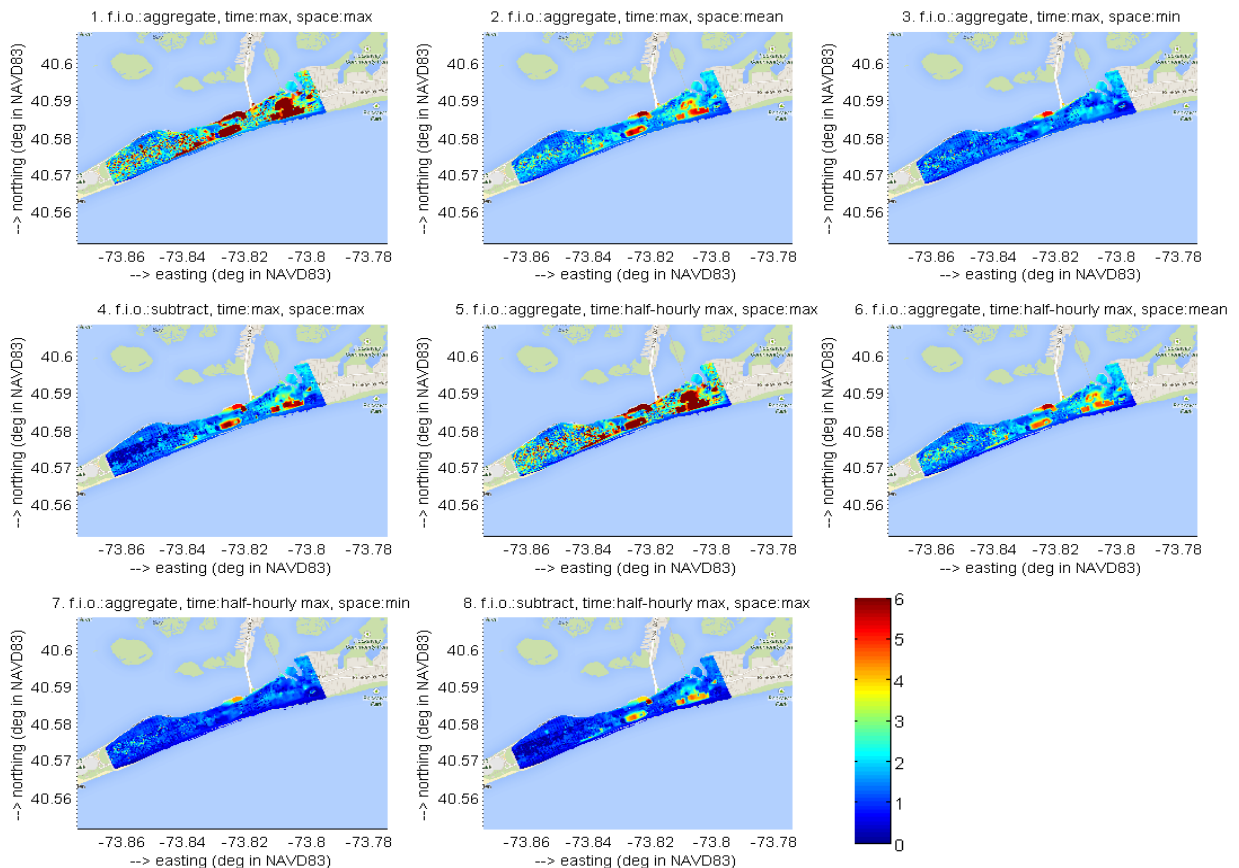


Figure 4-13 - Inundation depth indicators according to the 9 different extraction formulations

One general problem that can be observed is that the erosion around high buildings in XBeach (see subsection 4.1.2), which does not exist in reality, is taken normative for the inundation indicator; the dark red areas in the

graphs correspond to buildings for which this is the case. By taking the spatial minimum of the water level (of the surrounding cells) the results seem to be less sensitive to this problem than by taking the mean or maximum. Moreover, starting with subtracting the ground elevation from the water level gives more realistic results than starting with spatial and temporal aggregating. The latter can give unrealistic high inundation depths (> 20 m for formulation 1 and 5). However, where differences are small it is hard to pick one based on the above information. The depth damage relations, discussed in section 4.2, give more insight in the functionality of the different formulations.

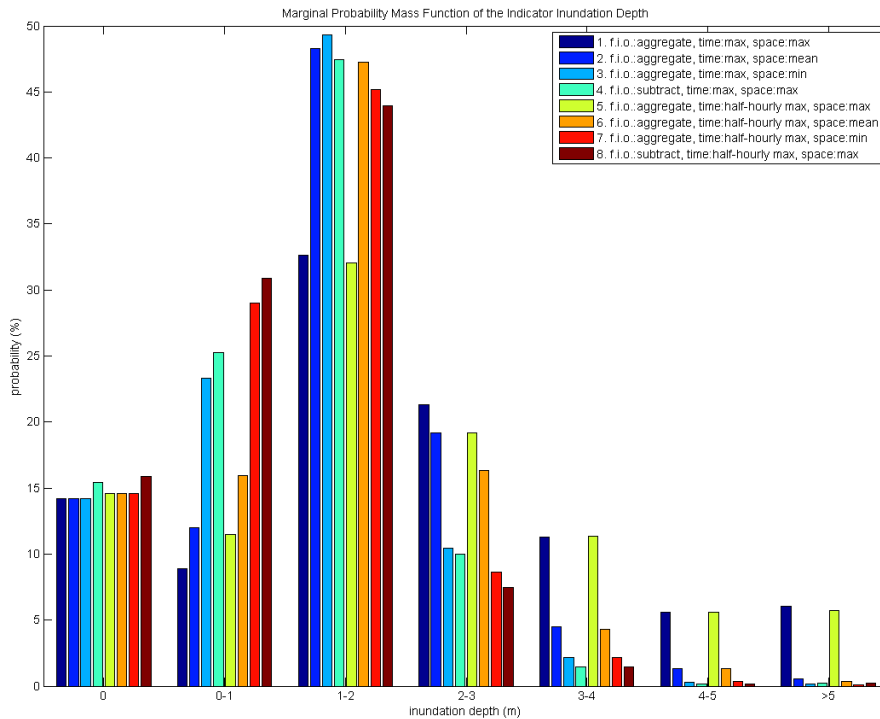


Figure 4-14 - Marginal Probability Mass Functions of the inundation depth indicator according to the 9 different extraction formulations

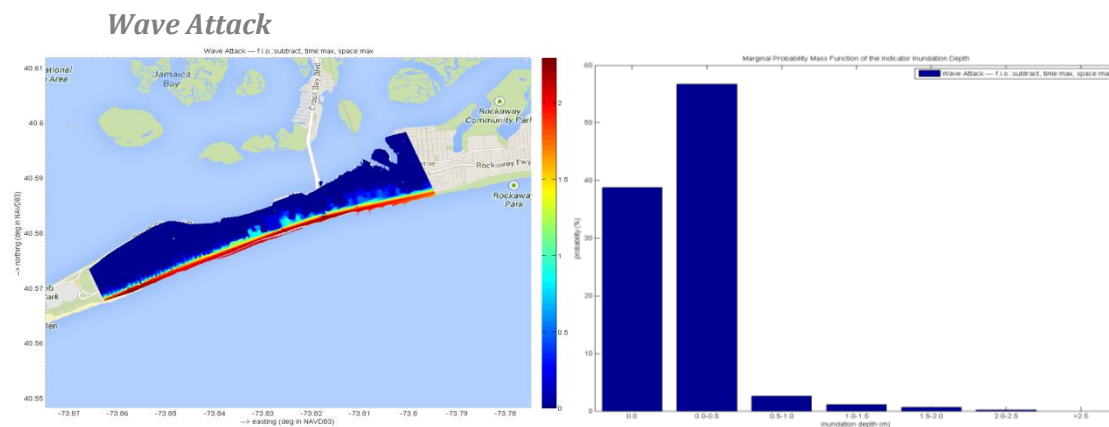


Figure 4-15 - Left: Spatial distribution of the wave attack indicator; right: marginal Probability Mass Function of the wave attack indicator

The indicator “wave attack” is defined as the maximum occurred significant wave height in space and time. The spatial distribution of maximum wave height appeared to be straightforward in subsection 4.1.3: the waves are relatively high on the beach and quickly decay land inwards. Exactly the same can be observed for the wave attack indicator; see Figure 4-15 for a similar spatial distribution as for the inundation depth.

In Figure 4-16 three zoomed views of the spatial distribution of the wave attack indicator are plotted. Where inundation depth showed an unrealistic positive correlation with building height, this does not seem to be the case for significant wave height, which is good.



Figure 4-16 - three Impressions of the spatial distribution of the wave attack indicator

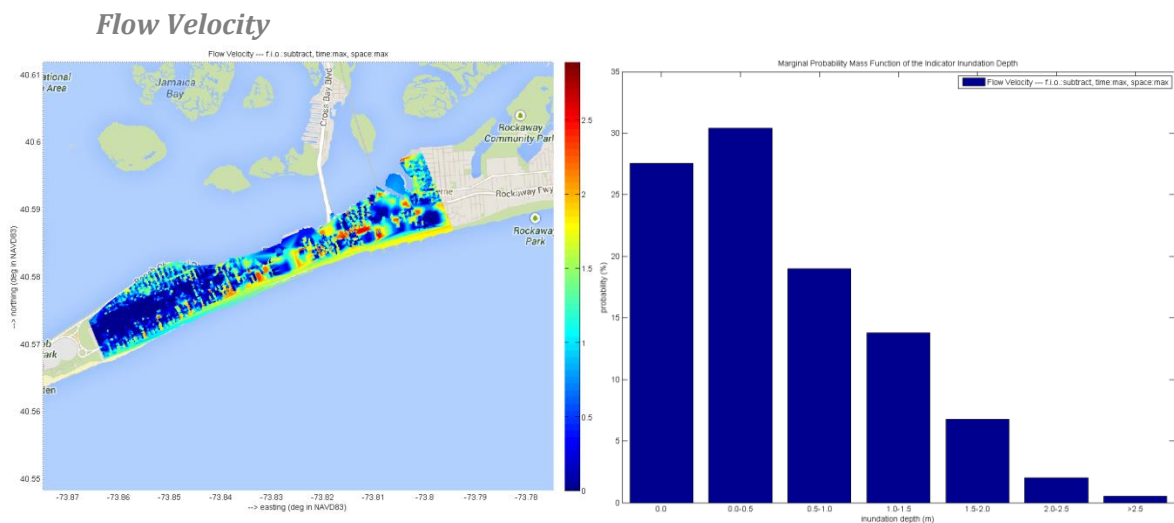


Figure 4-17 - Left: Spatial distribution of the flow velocity indicator; right: marginal Probability Mass Function of the flow velocity indicator

In analogy with wave attack, the spatial distribution of the flow velocity indicator shows a fairly similar picture as can be seen in Figure 4-17. Some streets are definitely subject to higher flow velocities than others. If this is a correct representation of reality, is hard to say. There is definitely a lot of inaccuracy due to objects obstructing the flow; see subsection 4.1.1. Velocity-damage relationships in section 4.2 give more insights on this matter.



Figure 4-18 - three Impressions of the spatial distribution of the flow velocity indicator

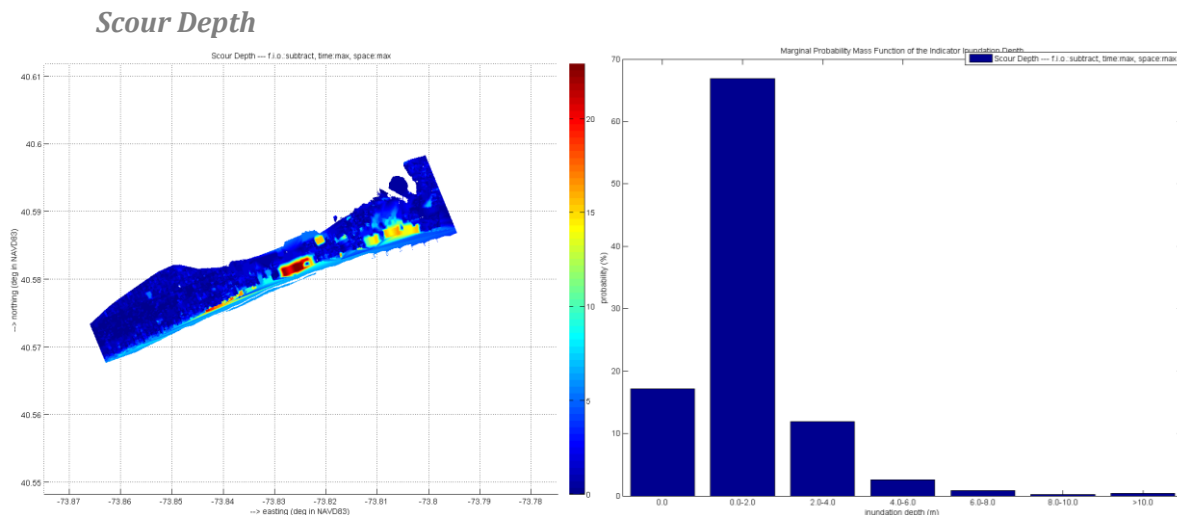


Figure 4-19 - Left: Spatial distribution of the scour depth indicator; right: marginal Probability Mass Function of the scour depth indicator

As is elaborated in subsection 4.1.2 observed scour depths around buildings are negligible, where sedimentation was dominant and pavements or vegetation prevented scour from happening. Although streets and gardens are not set to non-erodible in XBeach, sedimentation was still the main XBeach output on land; see Figure 4-7. Nonetheless, over 15% of the buildings show a maximum occurred scour depth of at least 2 meter, which can be seen in Figure 4-19. This is again caused by the erosion around especially high buildings, in analogy with the overestimations of the inundation depth. Therefore scour depth shows a high correlation with building height; see Figure 4-20 and the Pearson correlations in the next section. This correlation has of course no physical explanation but finds its origin in the way XBeach is set up and the extraction method/formulation.



Figure 4-20 - three Impressions of the spatial distribution of the scour depth indicator

4.1.4. Grid resolution

The other subsections in this section only consider the results of the run with a grid cell size of $3 \times 3 \text{m}^2$ in the urban areas. This subsection compares these results with hazard indicator values extracted from runs with cell sizes of $5 \times 5 \text{m}^2$ and $9 \times 9 \text{m}^2$. In Appendix G, visualisations of the XBeach output for these runs are given for water levels, bed level changes, waves and flow velocity. In general it can be concluded that the big picture is pretty much the same. More important are the effects on the final hazard indicators, which are elaborated here.

Except for the grid resolution, all other model properties were exactly the same during the XBeach runs. Considering the extraction method for the local storm conditions, keeping all parameters the same gave the following problem: more than 60% of the buildings were assigned as 'non-flooded' for the $9 \times 9 \text{m}^2$ run. In comparison to the $3 \times 3 \text{m}^2$ run with only 14% non-flooded buildings, 60% is quite significant. The following can give explanation: in the case of the $9 \times 9 \text{m}^2$ in combination with a 10m-buffer zone only one or no cell at all falls within the buffer for the majority of the buildings. Moreover, a lot of these 'lonely' cells appear to be non-

flooded due to a high ground elevation level (influenced by noise of the building). To a lesser extent this is also the case for the 5x5m² run. The 10m-buffer zone is thus too small, but what happens when a larger buffer zone is taken? To find out, three comparisons are made between:

- 1) Local hazard indicators of the 3x3m², 5x5m² and 9x9m² runs extracted with use of the same 10m buffer;
- 2) Local hazard indicators of the 3x3m², 5x5m² and 9x9m² runs extracted with the use of three different buffers, knowing 10, 18 and 30 meter respectively.
- 3) Local hazard indicators of the 3x3m² run for the earlier mentioned different buffer zone sizes in order to say something about the effect of using a larger buffer size.

In Figure 4-21 the PMF's of the four indicators are graphed for the three different runs with a 10m buffer for the extraction. Remark the peaks at zero for the 9x9m² run, which reflects the large amount of 'non-flooded' buildings (over 60%).

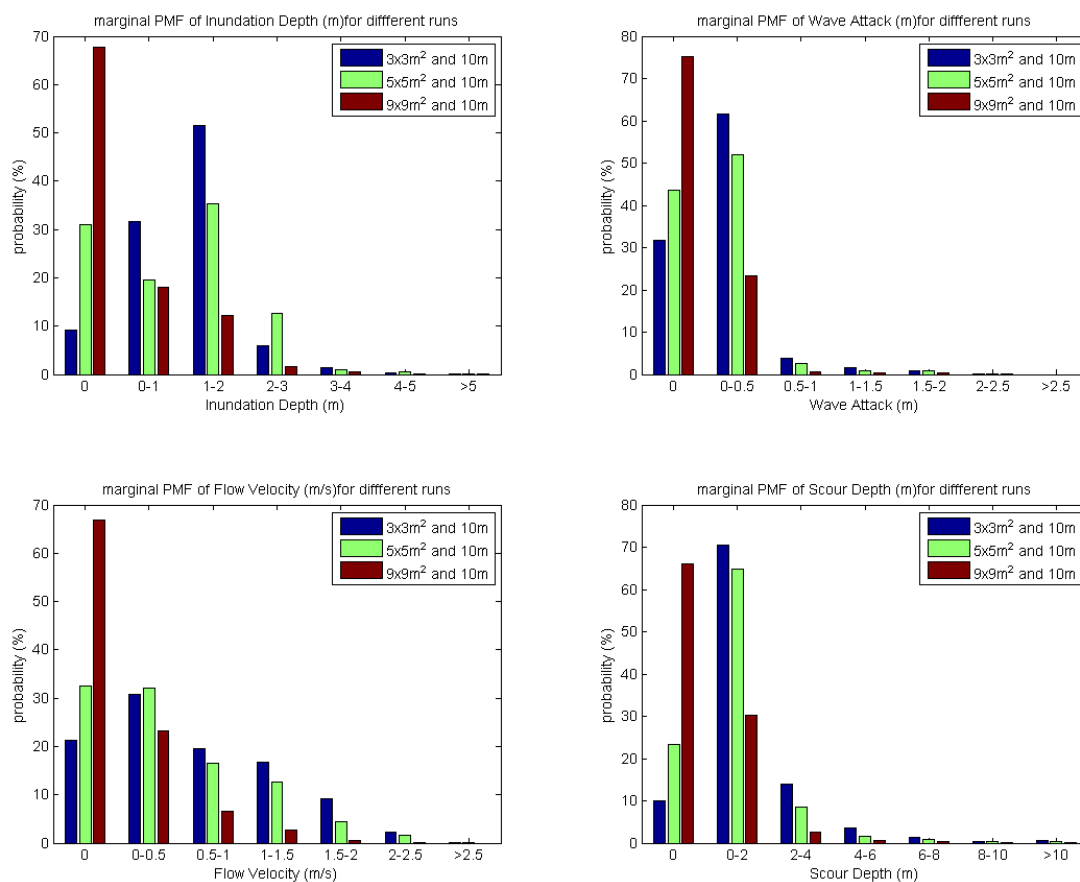


Figure 4-21 - Marginal PMF's of the four local hazard indicators for runs with grid cell sizes of 3x3, 5x5 and 9x9 m² and equal extraction buffer areas

In the following graphs the buffer size is adjusted to the grid resolution. The corresponding non-flooded percentages are given in Table 4-1, which are now almost all mutually equal. Still, the 3x3m² run shows less non-flooded buildings, which is assumed to be caused by the fact that water will easier flow to sheltered areas with finer grid resolutions.

Table 4-1 - Percentage non non-flooded per run and buffer size related to the minimum grid cell size

Run	Buffer Size (m)	Percentage Non-Flooded (%)
3x3m ² run	10	14
5x5m ² run	18	18
9x9m ² run	30	18

The impact on the hazard indicators of larger buffers for courser grids can be seen in Figure 4-22, where mutual differences between the runs are now smaller for inundation depth, wave attack and scour depth. Flow velocity on the contrary (lower left panel) shows a significant shift to higher velocities for a courser grid and related larger buffer zone. Whether this phenomenon can be assigned to the variability in grid resolution or variability in size of the extraction buffer zone can be answered by comparing the results of Figure 4-22 and Figure 4-23. In the latter the PMF's are given of local hazard indicators for the 3x3m² run extracted with different buffer zone sizes. The same shift can be observed and therefore it is concluded that an increased buffer zone causes an increase in flow velocities. A logical explanation can be found in the fact that in the middle of the street higher flow velocities are more likely to occur. This is in analogy with higher flow velocities in the main channel of a river. The middle of the street falls easily within the buffer zone when the buffer expands 30m from the building perimeter outlines and less easy with an expansion length of 10m.

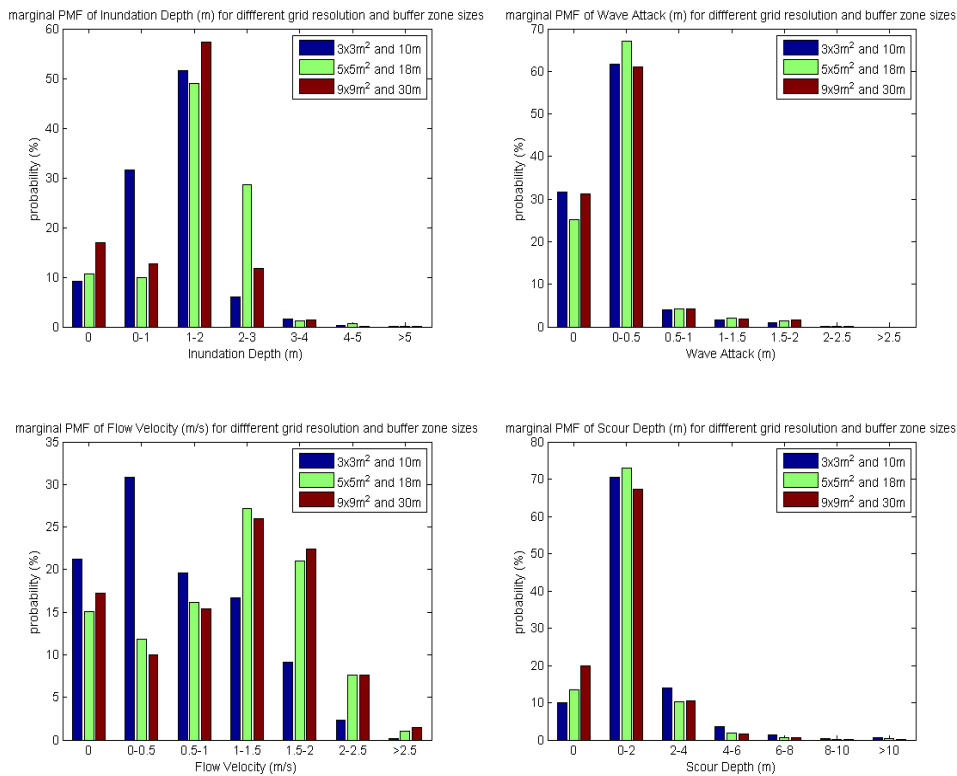


Figure 4-22 - Marginal PMF's of the four local hazard indicators for runs with grid cell sizes of 3x3, 5x5 and 9x9 m2 extracted with different buffer sizes

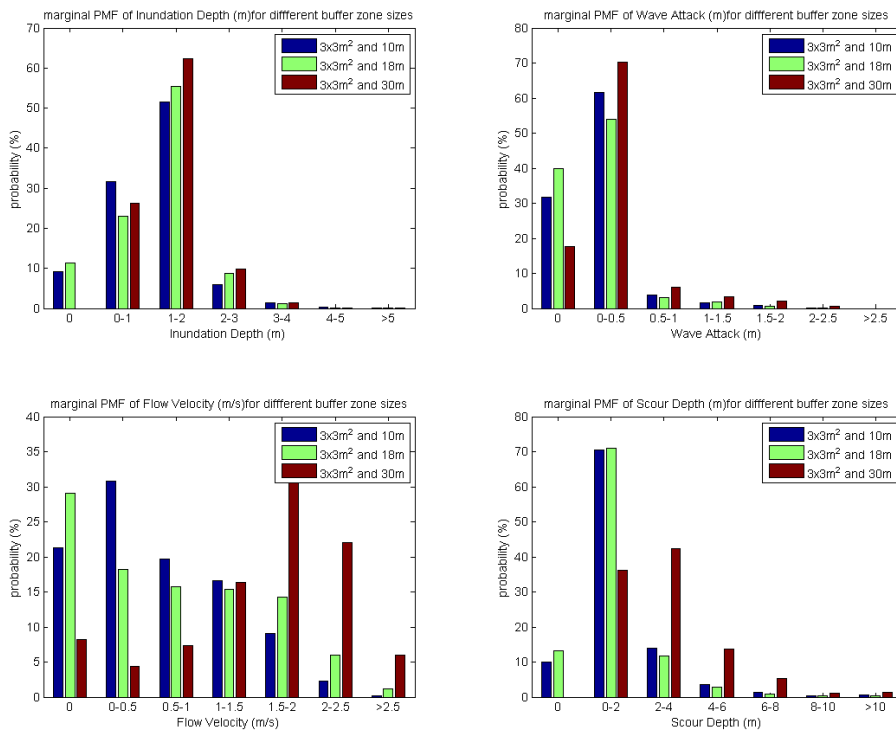


Figure 4-23 - Marginal PMF's of the four local hazard indicators extracted from the run with a grid cell size of 3x3 m2 for different extraction buffer areas

Another thing that can be observed from Figure 4-23 is that the PMF's seem to be fairly sensitive to the buffer zone size. Whether this sensitivity also holds for the quality of damage predictions is elaborated in the next section. Here it is concluded that the choice of extraction method and/or formulations can be very determinative for the obtained distributions.

4.2. Damage Dependencies

In this section the local hazard indicators and other potential indicators are discussed in relation to the physical damage from the ImageCat dataset. These relations are one-on-one, which means that simple correlation, sensitivity formulations and BBN's with only two nodes are sufficient enough to demonstrate the mutual dependencies. In the next section (section 0) the real potential of Bayesian nets is elaborated by adding more variables.

In analogy with the Muti-variate flood damage assessment (Merz, Kreibich, and Lall 2013) the Pearson correlation have been determined between different indicators; see also chapter 0. The same thing has been done for the present study as well, of which the results are shown in Figure 4-24.

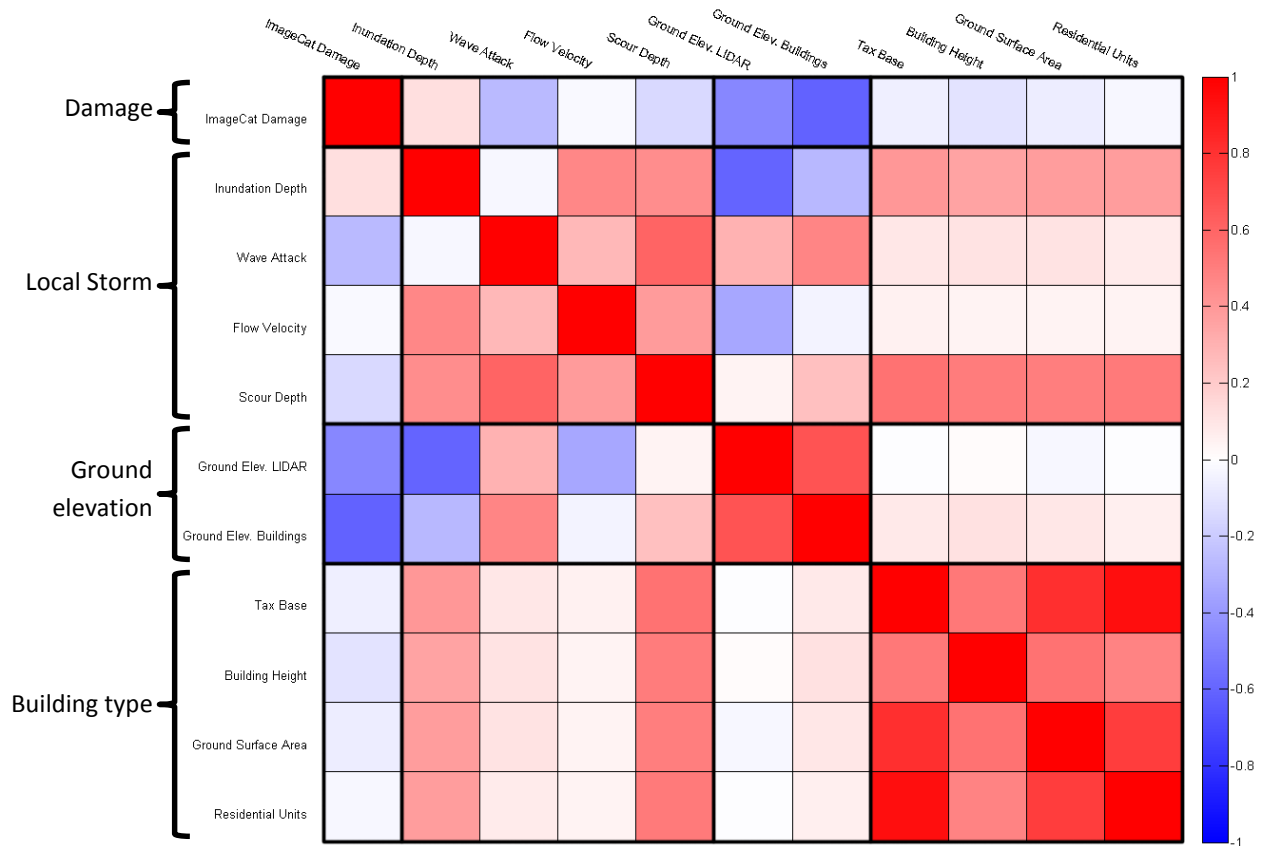


Figure 4-24 - Pearson correlations between potential indicators. Inundation Depth is according to formulation 8, which is $\max(\max(hs, \text{mean}, 30\text{min} - hb0))$

The Pearson correlation is expressed in the Pearson product-moment correlation coefficient, which is formulated as:

$$\rho_{X,Y} = \frac{\text{cov}(X, Y)}{\sigma_X \sigma_Y} = \frac{E[(X - \mu_X)(Y - \mu_Y)]}{\sigma_X \sigma_Y}$$

In the figure dark red stands for a strong positive correlation ($\rightarrow +1.0$) and dark blue for a strong negative correlation ($\rightarrow -1.0$). A coefficient of 0 means no correlation at all. Some mutual dependencies are straightforward; for instance building height is positively correlated with the ground surface area of a building. In general, it can be seen that the building type indicators are strongly correlated with each other and the local hazard indicators mutually as well. This is in line with expectations. On the contrary, the found correlation between local hazard indicators and the observed ImageCat damages⁴⁶ are, to put it lightly, counterintuitive. The positive depth-damage correlation is weak and a negative damage correlation for wave attack and scour depth are not to be expected. An explanation for this can be found in the fact that Pearson's formulation assumes a linear relationship between the indicators, which is not necessarily true for all combinations.

To give a more realistic picture of the damage relations, Figure 4-25 gives the probability of the damage conditioned on A) the 10% lowest values of the specific variable and B) the 10% highest⁴⁷. The variables are the same as in Figure 4-24. The marginal probability distribution is plotted as well in green in the upper left panel.

⁴⁶ To calculate the Pearson correlation coefficients for the damages the qualitative description of the ImageCat dataset (affected, minor, major and destroyed) have been substituted by quantitative values, knowing 1, 2, 3 and 4 respectively. One should be careful with drawing conclusions on the results, but whether a correlation is positive or negative can be concluded with sufficient confidence.

⁴⁷ Note: the PMF's are not based on output of a BBN, but directly established from all data.

Additionally, Figure 4-26 shows the change of probability between the lower and higher conditions for the different damage classes.

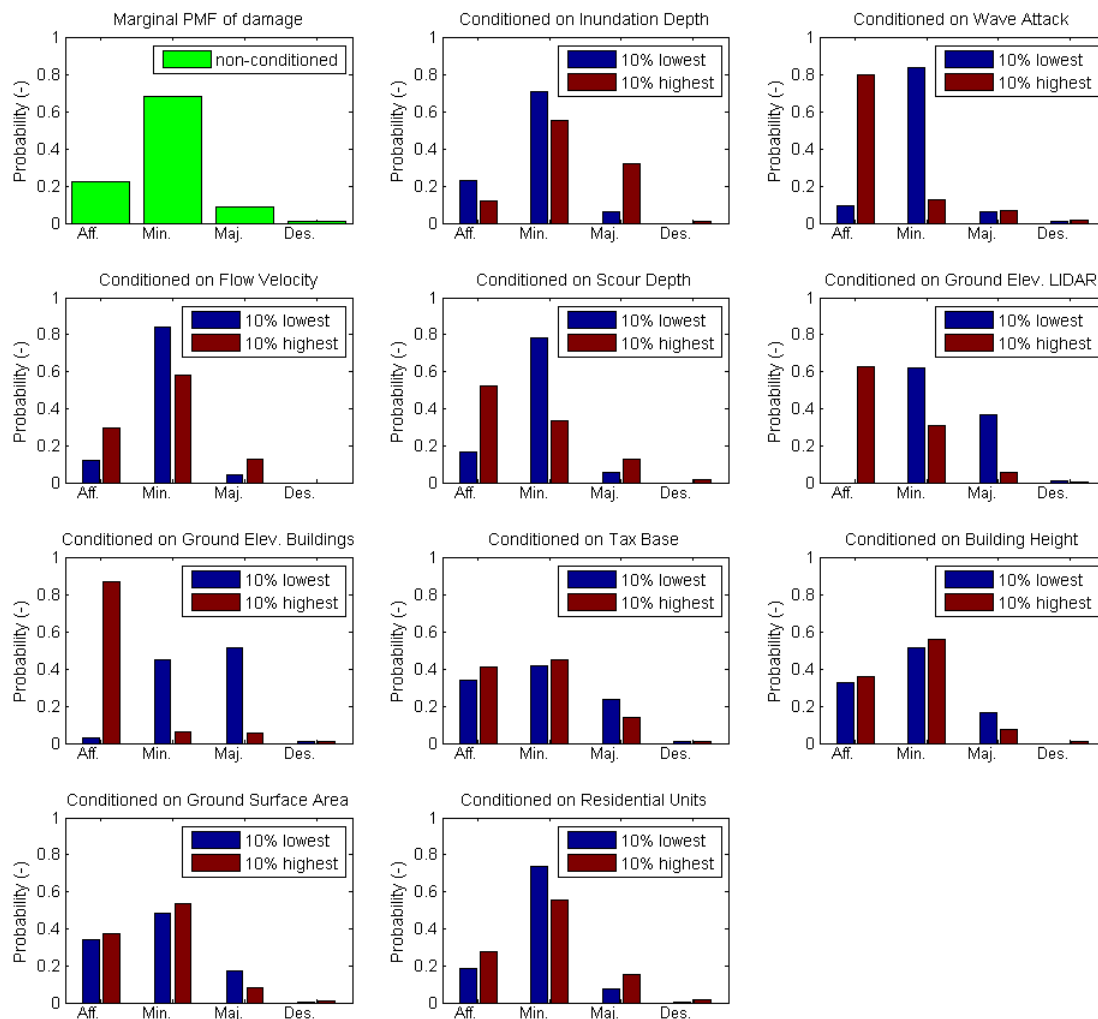


Figure 4-25 - PMF's of Damage conditioned on different indicators with 1) the lowest 10% (blue); 2) the highest 10% (red). Left upper panel: marginal PMF of damage.

One of the remarkable things that can be concluded from these figures is that for higher significant wave height the chance of a building being “affected” increases significantly and the chance of “minor damage” decreases. This indicates a decrease of risk, where one would expect the opposite. This can be explained by geographical features of the peninsula. It can be seen in Figure 4-3 that waves are rapidly decaying between the buildings and therefore the buildings with the highest wave attack are all found in the block closest to the beach. In Figure 2-4 in subsection 2.1.1 it can be seen that these houses have been built on higher grounds. Therefore, the inundation depth during Sandy was lower, which can also be seen in Figure 4-13. Studying the relation to damage of one hydraulic variable without considering the influence of other properties can thus give a distorted picture of reality. This is a direct result of spatial correlations within the domain.

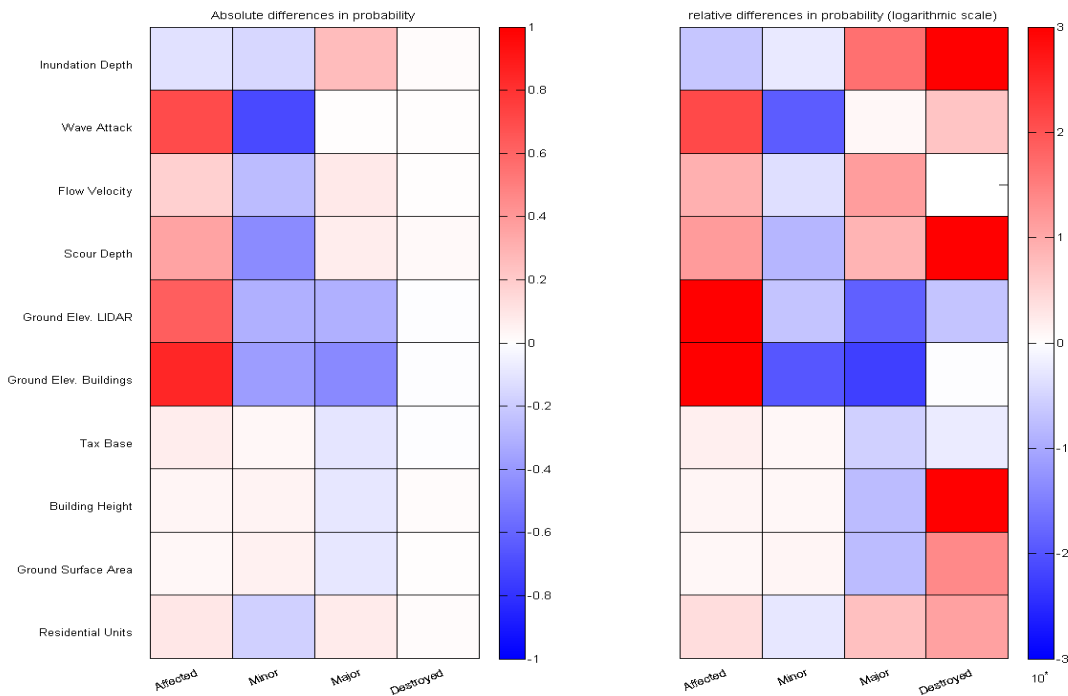


Figure 4-26 - Difference of probability between PMF's conditioned on either the 10% lowest values or 10% highest. Left: absolute difference; right: relative difference on a logarithmic scale. Red means that the probability of the PMF conditioned on the 10% highest values is higher and blue vice versa.

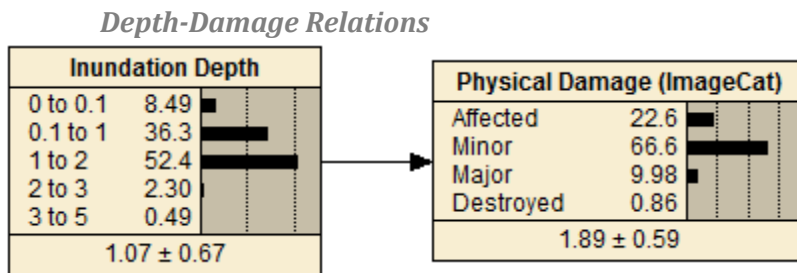


Figure 4-27 - Simple Bayesian net with the inundation depth indicator as predictor for damage

For inundation depth the correlation with damage is positive, where the chance on 'major damage' and 'destroyed' increases when higher inundation depths are found within the XBeach results. The eight different formulations for the inundation depth indicator are now considered in relation to the damage. Both the Pearson correlation coefficient and the Log-Likelihood Ratio (LLR) test scores for the simple Bayesian net of Figure 4-27 are given in Table 4-2, together with the mean and standard deviation of all candidate indicator values. The LLR test is very much suitable to relatively compare predictions of competing models or model configuration. In the test the log-likelihood of the prediction (in this case the CPT after conditioning on "inundation depth") is compared to the log-likelihood of the marginal probability, according to:

$$LLR_j = \log \{p(F_i|\tilde{O}_j)_{F_i=O_j}\} - \log \{p(F_i)_{F_i=O_j}\}$$

Here F is the forecast and O is the observed on which is conditioned. If the log-likelihood ratio is positive, the model has predictive skill, but if the ratio is negative the prediction is worse than guessing based on the marginal probability. By summing the LLR's of all hindcast events the LLR test score can be determined. The larger the score, the better the model performs. See Appendix 1.2 for a more extensive elaboration of the LLR ratio test concept.

Table 4-2 - Pearson correlation and log-likelihood ratio test scores for the indicator 'Inundation Depth' extracted from the XBeach results according to eight different formulations

#	First	Time	Space	Mean water level (m ref. NAVD88)	Mean depth	Std	Pearson correlation	LLR test score	Relative to perfect check
1.	Aggregate	Max	Max	5.25	2.38	1.94	-0.01	71.03	0.05
2.	Aggregate	Max	Mean	4.37	1.59	0.88	0.08	73.97	0.05
3.	Aggregate	Max	Min	3.99	1.23	0.73	0.14	90.48	0.06
4.	Subtract	Max	Max	-	1.21	0.75	0.06	76.63	0.05
5.	Aggregate	Max of 30min-mean	Max	5.13	2.28	1.72	0.02	79.22	0.05
6.	Aggregate	Max of 30min-mean	Mean	4.25	1.48	0.87	0.12	84.92	0.06
7.	Aggregate	Max of 30min-mean	Min	3.87	1.13	0.71	0.21	98.74	0.07
8.	Subtract	Max of 30min-mean	Max	-	1.09	0.73	0.12	84.97	0.06

From Table 4-2 it can be concluded that formulation 7 scores best, which subtracts the minimum initial bed level from the normative water level derived by taking the minimum in space and maximum of the half-hourly mean in time. Moreover, the LLR-test scores are positive, which means that the Bayesian net shows some prediction skill. However, the scores are only a bit larger than zero compared to the perfect check⁴⁸, which has a score of 1480. This means that it performs barely better than randomly guessing from the marginal damage PMF.

In subsection 4.1.3 it is stated that the more conservative formulations are better capable of filtering out the inaccuracies due to the non-realistic erosion around buildings. In addition to this insight, it can be concluded from Table 4-2 that the indicators based on these formulations also have a higher predictive capacity. The inaccuracies are thus of influence. Moreover, the predicted mean water levels are relatively high compared to the high water marks. This raises the question if the bathtub concept, having none of these inaccuracies at all, would do better. By taking the mean of the high water marks (3.27m above NAVD88) as the bath tub water level and subtracting the minimum bed levels extracted from XBeach the following results are found:

Table 4-3 - Pearson correlation and log-likelihood ratio test scores for the indicator 'Inundation Depth' based on the bath tub concept with a constant water level of 3.27m above NAVD88

#	method	formulation	Mean water level (m ref. NAVD88)	Mean depth	Std depth	Pearson correlation	LLR-test score	Relative to perfect check
1.	Bathtub	$h_{s,bt} - \text{Min}(h_{b0})$	3.27	0.69	0.62	0.46	299.62	0.20

The conclusion is that using one single water level for the whole domain works better than using water levels extracted from the XBeach results. But is this because XBeach overestimates the water levels structurally or because of a wrong prediction of the spatial variability? In the maximum water levels. In Figure 4-28 the Pearson correlation coefficient is plotted for different bathtub water levels, together with the LLR-test score relative to the perfect check.

⁴⁸ The Perfect check is explained in more detail in Appendix 1.2. In a nutshell: it is the LLR-test score for a certain node (in this case 'Damage') conditioned on itself; it gives therefore the highest possible score and forms an upper limit for the skill of prediction.

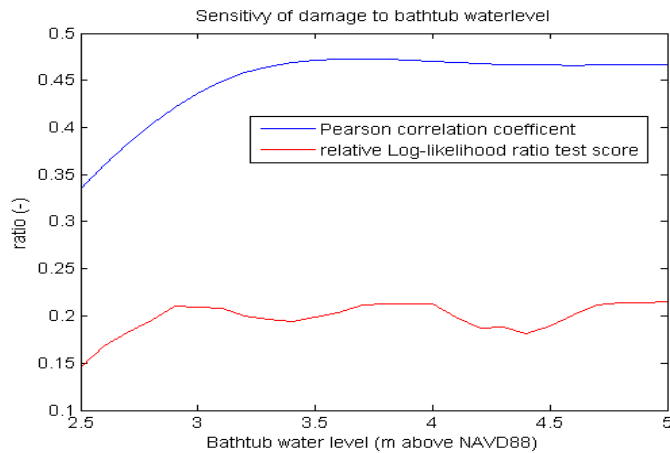


Figure 4-28 - The log-likelihood ratio test scores for the bathtub concept with varying water levels, divided by the perfect check score (red) and the Pearson correlation coefficient.

The Pearson correlation peaks for a bathtub water level of 3.65 m (above NAVD88). For higher water levels the correlation does not change much, which strengthens the theory that for present study an overestimation of the hazard indicators is not a big problem as long as it is structural (see section 4.1.3). Based on this graph it can be concluded that it is not the overestimation of the water level that decreases the prediction skill, but it must be the incapability of this specific XBeach model to represent the spatial variability of the water level realistically.

It is noticed that the graph of the relative LLR-test score shows two saddle points with local minima. An explanation for this might be found in the fact that Netica uses bins to discretize the nodes, implying that the classification of the bins also has its influence on the quality of prediction. This is not further studied in this thesis, but it is recommended to look at in more detail in future research.

Next to the water surface elevation levels, the inundation depth depends on the ground elevation level. For the formulations 1to 3 and 5 to 7 these are extracted from the LIDAR by determining the minimal bed level of the surrounding cells. However, ground elevation per building is available in the Buildings dataset as well. In Figure 4-24 and Figure 4-26 it can be seen that these ground elevation levels are more strongly correlated to the damage than the ground elevation levels from the LIDAR data. Therefore, the LLR-test scores for the inundation depth based on the ground elevation levels from the Buildings dataset have been determined as well. The scores are given in Table 4-4 and from these results it can be concluded that the inundation depth indicator based on the buildings data scores better when using the bathtub concept, but worse when using the XBeach results. It is assumed that this is because the Buildings data ground elevation levels are more accurate than the levels based on the LIDAR. However, inaccuracy of the XBeach bathymetrical input will subsequently influence the output and thus the water levels.

Table 4-4 - Log-likelihood ratio test scores for the inundation depth indicator based on a combination of A) XBeach results or the bathtub concept and B) ground elevations from the LIDAR data or Buildings data.

Ground elevation\Water Level	XBeach – formulation 7	Bathtub concept: 3.27m ref. to NAVD83
LIDAR data	↓	↓
Buildings data	44.73	437.38

It should be noted that having both options is a luxurious position; for other sites the buildings data might not be available and then LIDAR does work. Moreover, it is likely that the extraction method can still be optimized, but that goes beyond the scope of present study.

4.3. Bayesian Belief Network

The chance of two nearby lying houses showing similar damage predictions is larger than for two distant houses. This is assumedly mainly because of geographical features, which show variations on a larger scale than the building level. This phenomenon is in present thesis understood as spatial correlation. Reason for the spatial correlation of the damage is that some (but not all) physical processes that cause the damage are correlated in space; e.g. inundation depth and wave attack. Considering only one physical process as damage indicator and neglecting other spatially correlated indicators, can give a distorted picture of the actual indicator-damage relations, as can be learned from the findings in subsection 4.1.3. It must be said that this is inescapable when you only use data from one storm at one study site.

As an extreme hypothesis, if one would be able to correctly determine all physical processes on the building level that influence the damage (both for the establishing of the statistical relations and the conditioning for the prediction), these negative effects of spatial correlation wouldn't exist. Therefore, another way to minimize the negative effects of spatial correlation, besides using data from a wide range of study sites and storms, is to condition on more indicators (or on more important ones). Bayesian Nets are extremely useful for doing so, as is demonstrated in this section.

4.3.1. Coupling Storm Conditions to Damage

The local storm conditions are separately studied in relation to the damage in the previous section; here they are combined. Two net configurations are considered: 1) one with only connections between the local storm nodes and damage (left panel of Figure 4-29); 2) and one where Connections are added between the local storm characteristics according to the configuration of Figure 3-8; see the right panel⁴⁹.

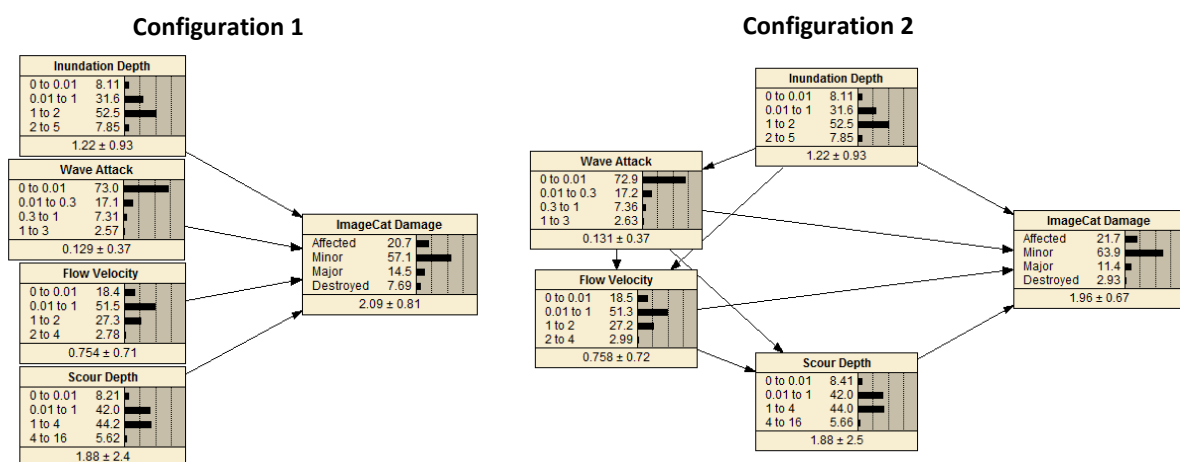


Figure 4-29 - Local storm conditions coupled to damage in a Bayesian Belief Network. Left: no arrows between local hazard indicators; right: mutually coupled local hazard indicators

For both configurations some hindcasting scenarios have been carried out. The resulting LLR-test scores are given in Table 4-5. It can be concluded that conditioning on more indicators raises the quality of prediction. This means that when more is known, the prediction becomes better, which is in line with the theory discussed in chapter 3.

⁴⁹ Note that the marginal distributions of the 'ImageCat Damage' are not the same as each other and differ from the marginal distribution in reality as well. This is because Netica does not use the real data for the distributions of child nodes but established CPT's instead. The (conditional) distributions are therefore only a reflection of reality.

Table 4-5 – Log-likelihood ratio test scores for different hindcasting scenarios

Hindcast scenarios	Conditioning on:					LLR-test score:			
	Inundation Depth	Wave Attack	Flow Velocity	Scour Depth	Physical Damage	Configuration 1		Configuration 2	
						Absolute	Relative	Absolute	Relative
1	1	0	0	0	0	13	0.01	63	0.04
2	0	1	0	0	0	241	0.15	278	0.19
3	0	0	1	0	0	19	0.01	32	0.02
4	0	0	0	1	0	2	0.00	60	0.04
5	1	1	0	0	0	263	0.16	331	0.22
6	1	1	1	0	0	415	0.26	376	0.25
7	1	1	1	1	0	515	0.32	405	0.27
Perfect Check	0	0	0	0	1	1607	1.00	⁵⁰ 1496	1.00

“Wave attack” is the most skilful indicator, followed by “flow velocity”, “inundation depth” and “scour depth”. This was to be expected based on the results of previous sections. Netica’s sensitivity analysis can confirm this; see Table 4-6 showing the results for configuration 2. Another interesting thing that can be observed is that the sum of the individual LLR-test scores (scenario 1 to 4) is less than the combined score of hindcast scenario 7, which implies that the individual components work like a team. Together they are better able to tell what is actually happening.

Table 4-6 - Netica's sensitivity analysis of configuration 2: variance reduction of Beliefs.

Node	Mutual Info	Percent	Variance of Beliefs
ImageCat Damage	13.566	100.000	0.320
Wave Attack	0.186	13.700	0.037
Inundation Depth	0.054	3.980	0.007
Flow Velocity	0.027	1.990	0.005
Scour Depth	0.048	3.560	0.009

If we now compare both configurations, two things can be concluded. First, configuration 2 scores better when conditioned on only one indicator. This makes sense since the other indicators are now better known as well (their mutual dependency is used). Hereby it should be noted that in the case of Rockaway Peninsula the bigger waves are found on relative higher grounds and thus lower inundation depths. Adding this inverse proportionality as a relation in the network (with configuration 2 as a result) may work fine for the Rockaways where it will decrease the negative effects of spatial correlation when conditioning on one indicator. However, this can be totally wrong when using these relations for predictions to other sites. In that case configuration 2 will probably not perform better than configuration 1. The second conclusion that can be drawn is that for conditioning on all indicators (hindcast scenario 7) configuration 1 seems to do better.

Hereby, it is important to note that the Bayesian nets have been trained on 100% of the data and the hindcasting has been performed for exactly the same observations (also 100% of the data). This means that Netica is always familiar with every event the nets are conditioned on during the hindcasting, since that same event is also used for training purposes. When the BBN is used for predicting a new situation, this will be different, since the hindcasting dataset differs from the training dataset. How well the BBN is capable of

⁵⁰ It can be seen that the Perfect Check differs for the two configurations. This is because CPT's of both models are different. The fact that the score for configuration 1 is higher does not necessarily mean that it is better capable of representing reality, only that the hindcast data better fits to what Netica thinks is reality.

predicting this new situation depends amongst others on the quality of the CPT's. Too many nodes or bins will have a negative influence on the quality. This can be best explained by an example; see the illustration of Figure 4-30. The white dots are random picked observations for two variables. With two bins all possible conditioning combinations are covered by observations (white dots); the CPT's can thus be well substantiated. Four bins give some extra detail, which makes the prediction better, but now some (red) cells and thus some corresponding poorly substantiated CPT's can be find as well. With eight bins the number of empty (red) cells increases further, which on a certain moment makes the model worse instead of better. The same problem occurs when more nodes are added, which also results in more conditioning combinations.

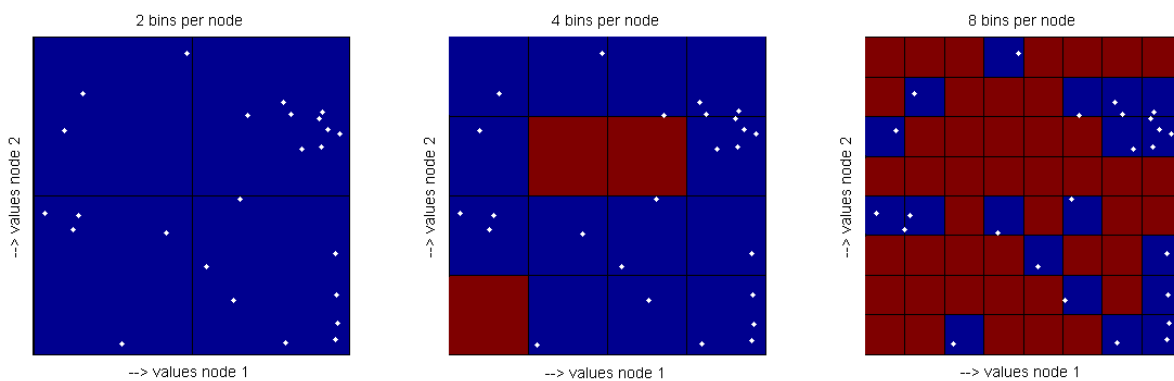


Figure 4-30 - Example (no results); More bins give more detail, but at a certain point also less validation for the CPT's.

Within the 5333 available data points 144 of the 256 (= 4⁴) possible conditioning combinations are not found for configuration 1 and 2. For the corresponding blind spots, Netica assumes all possible outcomes to be equally probable (Affected: 25%, Minor: 25%, Major: 25%, Destroyed: 25%). This default will become dominant when the number of nodes or bins increases. Hereby it must be noted that from the 144 poorly substantiated combinations, some are not likely to happen (e.g. 0-0.1 m inundation and 1-3 m high waves).

Instead of 100% usage of the data for both training and hindcast purposes, it is also possible to train the BBN's with a randomly picked 90% of the observations and performing hindcast scenario 7 on the other 10%. This has been done 10 times (changing the spatial distribution of the 90% training data and thus 10% hindcasting data) and the results can be found in Table 4-7.

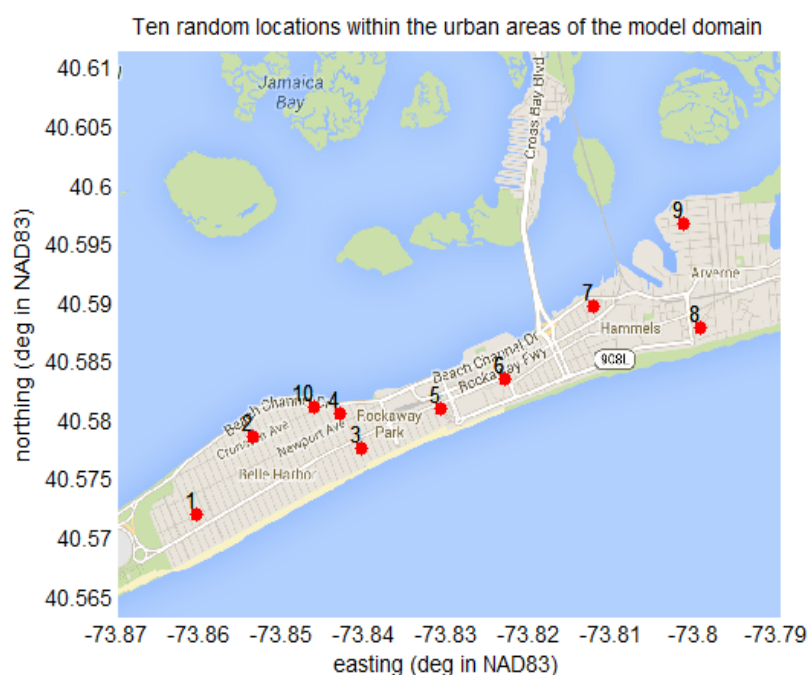
Table 4-7 - Log-likelihood ratio test scores for 10 runs; trained with randomly picked 90% of the observations and hindcasting with the remaining 10%

LLR test score – Configuration 1			LLR test score – Configuration 2			
Scenario 7	Perfect Check	ratio	Scenario 7	Perfect Check	ratio	
46	161	0.29	36	151	0.24	
51	163	0.31	39	151	0.26	
41	158	0.26	27	145	0.19	
43	159	0.27	30	146	0.2	
43	169	0.25	32	159	0.2	
52	163	0.32	40	150	0.26	
45	152	0.29	33	141	0.24	
42	155	0.27	31	143	0.22	
53	165	0.32	42	154	0.27	
49	158	0.31	40	149	0.27	
Sum	465	1603	0.29	350	1489	0.24
Std.	4.4	5.0	0.03	5.1	5.4	0.03

The average of the ratio for both configurations can now be compared with the results from Table 4-5. The ratio drops from 0.32 to 0.29 and 0.27 to 0.24 for configuration 1 and 2 respectively. This is in line with expectations. Moreover, in 34 of the 5330 (0.6%) hindcast cases the BBN was not familiar with the given conditions, resulting in a practically flat conditional PMF. It is assumed that if this percentage gets much higher, the predictions will become worse. This is elaborated in more detail in the bin analysis of paragraph 4.3.1.3.

4.3.1.1. Spatial Correlation

The negative effects of spatial correlation have been mentioned already a few times. Where the damage predictions are spatially correlated, also the bias (difference between predicted and actually observed) is spatially correlated. If for instance the hazard indicators within the training data are structurally overestimated (or underestimated) and the hazard indicators used for the prediction are not (and vice versa), the quality of prediction becomes worse. It is hard to say how disadvantageous this is for making predictions for other sites, since no other site is studied in present thesis. However, the negative effects can already be seen within this



study site area. In theory, the perfect model would give qualitatively similar good results for different sub areas within the domain. In practice, this will not be the case, since the average bias of a sub areas will differ from place to place as well due to this spatial correlation. In Figure 4-31 ten randomly chosen locations within the domain are shown. For these locations the 10% nearest buildings are used for the hindcast and the other 90% for training purposes. The results for all ten locations are given in Table 4-8, together with the sum and standard deviation.

Figure 4-31 - Ten randomly picked locations within the urban areas of the model domain.

Table 4-8 - Log-likelihood ratio test scores for 10 runs; hindcasting on the observations of the 10% closest buildings and trained with the remaining 90%.

location	LLR test score – Configuration 1			LLR test score – Configuration 2		
	Scenario 7	Perfect Check	ratio	Scenario 7	Perfect Check	ratio
1	62	178	0.35	43	160	0.27
2	54	149	0.36	35	130	0.27
3	32	174	0.18	12	154	0.08
4	49	154	0.32	26	131	0.2
5	-31	200	-0.15	-34	197	-0.17
6	32	185	0.17	29	181	0.16
7	12	126	0.09	10	124	0.08
8	19	76	0.24	21	79	0.27
9	13	96	0.13	27	110	0.25
10	62	152	0.41	40	130	0.3
Sum	304	1490	0.21	209	1396	0.17
Std.	28.8	39.5	0.17	22.1	34.6	0.14

Again, the average of the ratios for both configurations can now be compared with the results from Table 4-7 and Table 4-8. The ratios drop even more from 0.32 to 0.21 and 0.27 to 0.17 on average for configuration 1 and 2 respectively.

It wouldn't be fair to assign this drop in score only to the negative effects of spatial correlation when only considering one study site. In 51 of the 5330 (1.0%) hindcast cases Netica was not familiar with the given conditions, which is an increase compared to the 0.6% for the evenly distributed 90-10 experiment. When the Bayesian net is less familiar with the given conditions of the hindcast, uncertainty will increase and the LLR decrease, resulting in a lower score. This phenomenon is certainly at stake as well.

Moreover, it can be concluded that the standard deviation of the scores increased significantly, implying a larger spatial variance in the quality of prediction. For location 5 the LLR test score is negative, which means that the statistical model does worse than guessing based on the marginal PMF, where on the contrary the results for location 10 are on average better.

4.3.1.2. Grid Resolution

As is discussed in section 4.1.4 a buffer size of 10m is small for a minimum grid cell size of 9x9m². The effects on the log-likelihood-ratio test score of the BBN according to configuration 2 are clear: scores get worse for a larger grid cell size; see Table 4-9. By adjusting the buffer size to the grid resolution, the non-beneficial effects of too much 'non-flooded' buildings can be minimized, which results in better scores for the 5x5m² and 9x9m² runs. But now the opposite seems to be true: higher scores for higher grid resolutions. This raises the question if a courser grid is actually better than a grid with very high resolution or the increase in score is caused by a larger buffer size. This is hard to say based on the scores, since differences are small, but it is a fact that the scores for the 3x3m² run increase too when the buffer size is taken larger.

Table 4-9 - Log-likelihood ratio test scores for configuration 2 and extraction formulations 7; the results for different runs and varying extraction buffer sizes are given.

Run \ buffer size	10m	18m	30m
3x3 m ²	405	451	501
5x5 m ²	354	477	
9x9 m ²	178		496

4.3.1.3. Number of bins

The number of bins per node in this section is set to four. This number is not picked randomly but based on an analysis, of which the results are graphed in Figure 4-32. The BBN's with the structures of configuration 1 and 2 have been tested with 2 until 10 bins per node. Calibration corresponds in this context to a set of observation used for the training of the BBN and validation corresponds to a set of observations that is used for the hindcasting. One can fit any data set better and better by increasing the bins (calibration). However, if one only fits noise in the calibration set, the validation becomes worse. In that case better calibration also means overfitting the data in the model causing a decrease in the robustness of prediction.

The error rate grades how often the most likely prediction matched the observations. The error rate for both validation and calibration are pretty much similar and unchanging until 4 or 5 bins, then calibration gets better and validation worse. This is logical, since more bins means more resolution, but the quality of the joint and conditional distributions become worse where the establishing is based on less data; this has also been explained in section 4.3.1. The data are divided into three sets and the shading shows the standard deviation of the three estimates around the mean (central blue or red line) of the estimates.

The lower the error rate value is the better, which would suggest 3 or 4 bins, but 5 bins seem to be justified as well. With more than 5 bins the calibration improves but the validation increases rapidly. By this measure the chosen number of 4 bins (bins = 0 in the graph) is fine with a fairly low error rate of 25%.

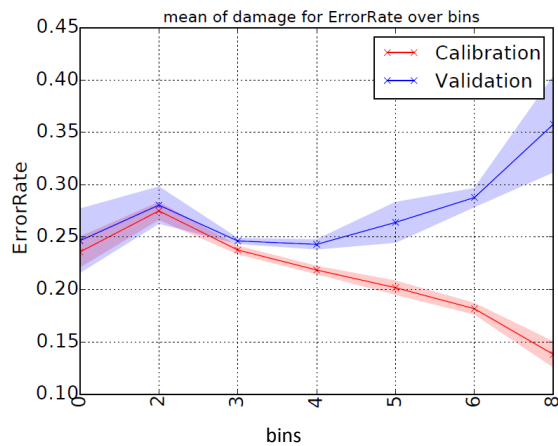


Figure 4-32 - Mean of damage for ErrorRate over bins

It should be noted that more similar analysis could be executed in order to find the optimal number of bins per node. However, this is of minor importance for delivering a proof of concept. Moreover, the outcome would be different if one decides to use less local hazard indicators, other additional nodes and more or less observations.

4.3.1.4. Most Probable and Risk

Table 4-10 - Most probable damage versus observed; total counts per combination


Observed - Most Probable (Number of Counts)		Predicted				Percentage correct
		Affected	Minor	Major	Destroyed	
observed	Affected	549	350	1	1	60.9%
	Minor	136	2571	21	1	94.2%
	Major	30	284	41	0	11.5%
	Destroyed	5	19	1	2	7.4%

In Table 4-10 the observations are coupled to the most probable outcome of the prediction, which is the outcome within the prediction with the highest probability. Based on the column ‘percentage correct’ it can be concluded that the model is very good at predicting minor damage and less good at predicting affected, major damage and destroyed respectively. This makes sense because wherever you look in the domain, also in the severest damaged areas, minor damaged buildings can be found in large numbers. Therefore minor damage will in most of the predictions predominate.

This does not mean that the Bayesian net is not capable of predicting higher risks for more severely damaged buildings. One of the problems with the ImageCat damage dataset for analysing the skill of prediction is that observations are not quantitative. By assigning the values 1, 2, 3, 4 to “affected”, “minor damage”, “major damage” and “destroyed” respectively, it becomes easier to take for instance the mean of the conditional PMF’s. The latter has been done per combination of Table 4-10 and the results are given in Table 4-11. The mean of a conditional PMF is a measure for the expected average damage, where a higher mean means more risk. Based on these results it can be concluded that if the most probable outcome is the same for two buildings, the risk can still differ.

Table 4-11 - Mean of the conditional damage PMF's; categorized on the combinations of observed and most probable predicted.

Mean of conditional PMF's (categorized on Observed - Most Probable)		Predicted			
		Affected	Minor	Major	Destroyed
observed	Affected	1.44	1.92	2.38	2.50
	Minor	1.45	2.02	2.59	2.68
	Major	1.73	2.08	2.63	-
	Destroyed	1.83	2.08	2.74	2.59



Another way to check if the model shows skill is looking at the mean predicted probabilities given the observed. In Table 4-12 the mean chances are given with in green the mean predicted probability of what actually has been observed. As an example: for all buildings that are observed as being destroyed, the mean predicted chance of being destroyed is 5.8%. This is not a big chance, but it is at least higher than the mean predicted chance of buildings being destroyed while that in reality didn't happen. The fact that the values in green cells are all maximal in their column implies that the Bayesian net not only has some skill for affected and minor damage, but also for major damage and destroyed. However, this is marginal.

Table 4-12 - Average of the predicted probabilities given the observed

Predicted Mean probabilities given the observed		Predicted				Total
		Affected	Minor	Major	Destroyed	
observed	Affected	50.1%	39.8%	6.9%	3.2%	100%
	Minor	13.4%	75.3%	9.5%	1.7%	100%
	Major	12.4%	66.5%	18.3%	2.9%	100%
	Destroyed	17.4%	60.7%	16.1%	5.8%	100%
Marginal PMF		21.3%	65.5%	10.6%	2.6%	100%

4.3.1.1. Uncertainty

The good part of working with Bayesian Belief Networks is that it is easy to find out how confident the prediction is. In Table 4-13 the average of standard deviations are given for the configuration 1 and 2 per hindcasting scenario (see also Table 4-5). Again, this is only possible by assigning quantitative values to the qualitative descriptions of the damage (1, 2, 3 and 4). In absolute sense the standard deviations do not say much, but mutual comparisons are now possible to make. From the table it can be concluded that the uncertainty of prediction decreases by conditioning on more indicators. The quality of prediction thus grows. Another conclusion is that for conditioning on only one indicator the predictions of the BBN with configuration 2 are more confident. This is to be expected since the mutual dependencies between the local storm conditions provide extra information.

Table 4-13 - Mean standard deviation of hindcasted PMF's for configuration 1 and 2 and different hindcast scenarios.

Hindcast scenarios	Number of nodes	Mean Standard Deviation	
		Configuration 1	Configuration 2
1	1	0.788	0.631
2	1	0.787	0.601
3	1	0.804	0.640
4	1	0.797	0.636
5	2	0.769	0.585
6	3	0.676	0.570
7	4	0.543	0.543
Perfect Check	4	0	0

If we now look at hindcast scenario 7 in more detail and condition on the observed the results of Table 4-14 can be gained. Differences between configuration 1 and 2 are negligible as can be seen. Another conclusion that can be drawn is that the BBN is more certain in predicting the “minor” and “major” damage than “Affected” and “Destroyed”. This makes sense, since both contain a lot of noise. Moreover, it has already been mentioned that destroyed appears to be hard to predict since it is an extreme.

Table 4-14 - Mean standard deviation of the hindcasted PMF's given the observed for configuration 1 and 2 and hindcast scenario 7.

Mean Standard deviation of prediction given the observed		Configuration 1	Configuration 2
observed	Affected	0.658	0.657
	Minor	0.501	0.501
	Major	0.563	0.563
	Destroyed	0.659	0.659
	Unconditioned	0.543	0.543

4.3.1.2.Spatial variability

Now we know that it is hard to use the model for predicting which buildings will be destroyed (the extremes). However, a higher risk for these buildings has been predicted (see paragraph 4.3.1.4). Here we look at the spatial variability of the prediction.

In Figure 4-33 the spatial variability of the mean of the CPT of the predicted damage for both configuration 1 and 2 is shown⁵¹. The spatial pattern of the observed -the beach fronting houses severely damaged, the rows behind barely and the lower lying areas in the rest of the domain showing minor or major damage- can be found in the spatial distribution of the predictions as well, which is good. The observed spatial pattern of the damage can thus be regained fairly well by the predictions. Configuration 1 and 2 both do a good job and the mutual differences are very small.

⁵¹ Trained and hindcasted with 100% of the data

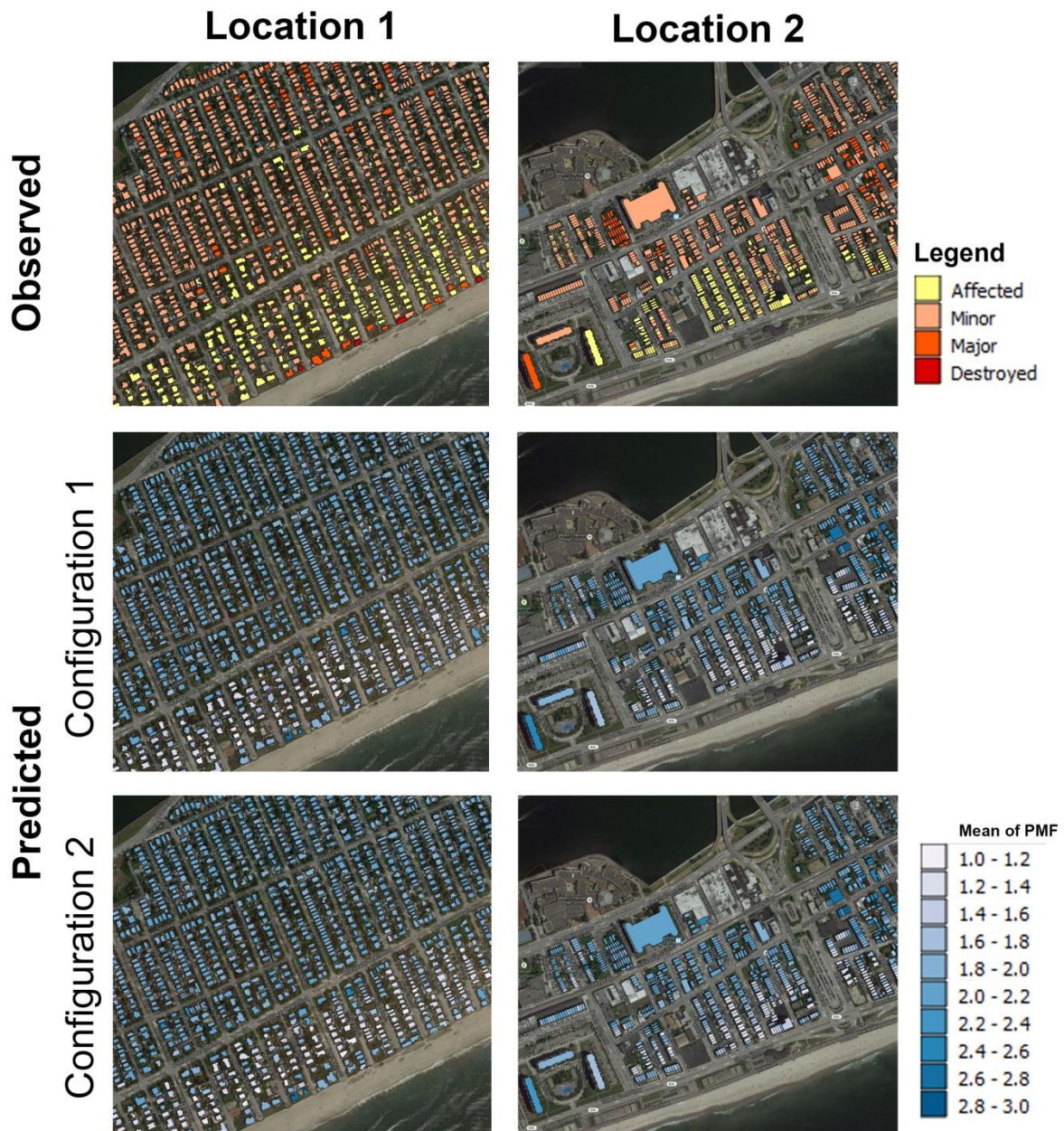
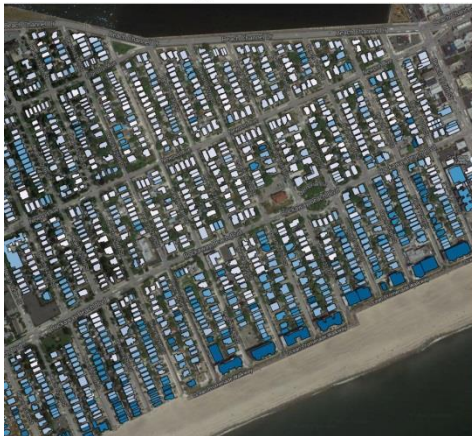


Figure 4-33 - Spatial representation of the mean of predicted PMF's for configuration 1 and 2. The two upper panels show the observed.

For the standard deviation of the predictions one can do the same. This has been done and is shown in Figure 4-34. It can be seen that the BBN is quite confident about the predictions in the sheltered areas on the bay side and the closer you come to the beach the higher the standard deviation becomes. Although the differences are small, configuration 1 seems to be a little bit more confident in the areas close to the beach (with the exception of the first row), which explains the higher LLR-test score ratio with the Perfect Check.

Configuration 1



Configuration 2



Legend

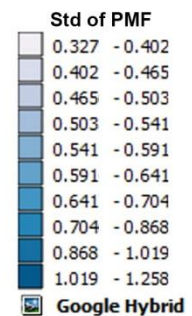


Figure 4-34 - Spatial representation of the standard deviation of predicted PMF's for configuration 1 and 2.

4.3.2. Building Type Indicators

The Bayesian net of section 4.3.1 with configuration 1 is here expanded with either one of the indicators “roof height”, “ground floor surface area”, “residential units”, “tax base”, “building class” or a combination of these. In Figure 4-24 it can be seen that these indicators show strong mutual positive correlations, which makes sense (e.g. it is more likely that larger buildings are higher, have a larger surface area, contain more residential units, have a higher tax base and fall in another building class than small buildings). Adding all five indicators might therefore be unnecessary and even unwanted considering the negative effects of adding too much nodes. However, to show these effects this has been done and described in this section as well.

For the hindcasting three configurations are used, which are here called configuration 3, 4 and 5 in order to avoid confusion; see the figures below.

Configuration 3

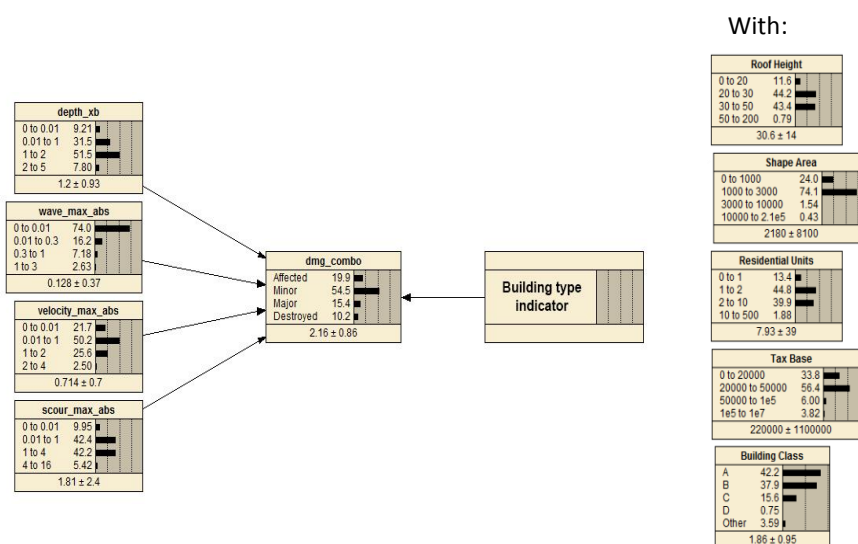


Figure 4-35 - Trained Bayesian Belief Net with one building type indicator; the five different building type indicator nodes that have been used are shown on the right side.

Table 4-15 - Absolute and relative log-likelihood ratio test scores for configuration 3 with different building type indicator nodes.

Building type indicator	LLR-test scores				
	Perfect check	Conditioned on building type		Conditioned on all	
		Absolute	Relative	Absolute	Relative
Roof Height	1653	20	0.012	605	0.366
Shape Area	1651	17	0.010	585	0.354
Residential Units	1656	8	0.005	584	0.353
Tax Base	1667	39	0.023	628	0.377
Building Class	1675	25	0.015	618	0.369

Configuration 3 is based on configuration 1 with one additional building type indicator. The hindcasting results of configuration 3 are given in Table 4-15. It can be concluded that “tax base” is the best indicator, both alone and in combination with the local storm conditions, followed by “building class”, “roof height”, “shape area” and “residential areas” respectively.

By adding all building type indicators, configuration 4 can be obtained; see Figure 4-36. In the same figure also configuration 5 is shown, which also contains arrows between the local storm conditions. This is in analogy with configuration 2. Again, some hindcasting scenarios have been carried out, of which the results are given in Table 4-16. It should be noted that in the two configurations the building indicators are not mutually connected, while there are strong dependencies; see Figure 4-24. This is because the relations can differ significantly from site to site, which is in contrast with the mutual relations between the forcing indicators (the underlying assumed physical principles are everywhere the same⁵²). Still, it would be worth trying connecting them in future research.

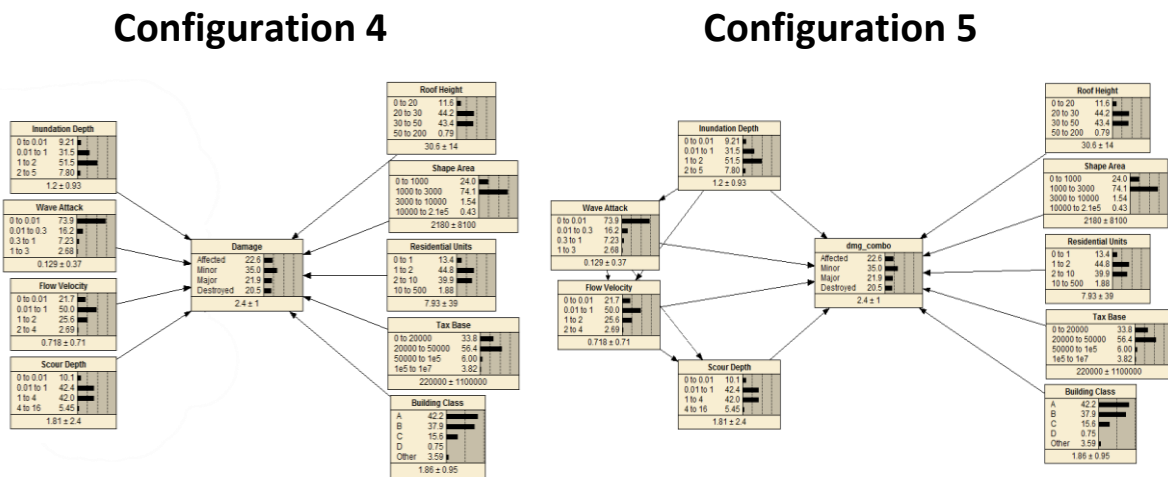


Figure 4-36 - Trained Bayesian Belief Nets with all building type indicators. Left: No arrows between the local hazard indicator nodes; right: arrows between them.

⁵² This is only the case when the training data is composed out of a wide range of case studies. Else, spatial correlation and the corresponding problems earlier discussed will be at stake.

Table 4-16 - Absolute and relative log-likelihood ratio test scores for configuration 4 and 5 and different hindcast scenarios.

Hindcast scenarios	Conditioning on:						LLR-test score:			
	Local Hazard indicators	Roof Height	Shape Area	Residential Units	Tax Base	Building Class	Configuration 4		Configuration 5	
							Absolute	Relative	Absolute	Relative
8	1	0	0	0	0	0	213	0.10	133	0.06
9	1	0	0	0	1	0	255	0.12	175	0.08
10	1	0	0	0	1	1	316	0.15	236	0.11
11	1	1	0	0	1	1	405	0.19	324	0.16
12	1	1	1	0	1	1	515	0.24	435	0.21
13	1	1	1	1	1	1	1018	0.47	937	0.45
Perfect Check								1		1

The first conclusion that can be drawn from the results of Table 4-16 is that the LLR-test scores for hindcast scenario 8 (only conditioned on the local hazard indicators) are worse than for hindcast scenario 7 of Table 4-5. This implies that adding more nodes without conditioning on them has a bad influence on the quality of prediction.

Secondly, it can be concluded that scores are increasing when more indicators are added. This looks promising, because this often means that the BBN gets more skilful. However, the fact that the hindcasting is performed based on the same observations as for the training is somehow misleading. With configuration 4 and 5, 327680 (= 4⁸ x 5) combinations of conditions can be made. Again, a share of these combinations is extremely unlikely or impossible to happen (e.g. 10-500 residential units in a one-family house). Still, only 1549 of these 327680 combinations are found within the dataset and the majority (99.5 %) of the covered combinations is thus not represented by any observation in the training dataset. In contrast with the BBN's from subsection 4.3.1 (with only local hazard indicators), most of the CPT's in Netica are now very poorly substantiated⁵³. This negatively affects the quality of prediction and quantification of uncertainty.

Table 4-17 - Log-likelihood ratio test scores for 10 runs with configuration 4 and 5; hindcasting on the observations of the 10% closest buildings and trained with the remaining 90%.

location	LLR test score – Configuration 4			LLR test score – Configuration 5		
	Scenario 13	Perfect Check	ratio	Scenario 13	Perfect Check	ratio
1	77	268	0.29	66	257	0.26
2	117	256	0.46	103	243	0.42
3	40	243	0.17	30	233	0.13
4	85	256	0.33	71	242	0.29
5	13	223	0.06	9	219	0.04
6	26	198	0.13	24	196	0.12
7	-2	162	-0.01	-8	156	-0.05
8	15	77	0.19	14	76	0.19
9	8	86	0.09	7	86	0.09
10	106	259	0.41	92	244	0.38
Sum	485	2028	0.21	408	1951	0.19
Std.	43.8	71.7	0.16	39.0	66.8	0.15

The negative effect on the quality of prediction can be best demonstrated by predicting something 'new'. Hindcast scenario 13 of Table 4-16 has also been executed on 10% of the observations corresponding to the

⁵³ This is logical, since the number of bins is adjusted to the amount of data and the configuration with four indicator nodes. With more nodes the bin analysis would suggest fewer bins, for instance 3 per node. The number of conditioning combinations would in that case already drop from more than 300,000 to less than 20,000.

buildings closest to the ten locations of Figure 4-31. The other 90% is used again for training purposes; see the results in Table 4-17.

Compared to the relative LLR test scores for hindcasting on 100% of the data (0.47 for configuration 4 and 0.45 for configuration 5) scores of 0.21 and 0.19 respectively are very low. However, they are still positive and pretty much the same as the scores of configuration 1 and 2 with the 10%-90%-hindcasting scenarios (0.21 for configuration 1 and 0.17 for configuration 2; see Table 4-8). Where we thus see an increase in prediction skill when adding more indicators (and thus more resolution) for the 100%-hindcasting scenarios, this increase cannot be seen when considering the 10%-90%-hindcasting scenarios. The added value of extra indicators is thus negatively compensated by the fact that the extra resolution decreases the range of applicability of the network due to a lack of training data. It is assumed that this negative effect on the quality of prediction can only become larger when using the Bayesian net for predictions on a completely new case study, where the conditions (for the hindcasting) differ more significantly from the training data than in the above given example.

The negative effect on the quantification of uncertainty can be seen by looking at the mean standard deviations of the conditional PMF's. Note that the mean standard deviation of the predictions decreased when more local hazard indicators were added to the BBN in subsection 4.3.1; see Table 4-13. In Table 4-18 we see the opposite happening, namely an increase of the standard deviation. An explanation for this can be found in the large number of poorly substantiated CPT's. When this is the case (no or very few observations within the training data for specific conditioning combinations) the standard deviation of the prediction (with Affected =1, Minor = 2, Major = 3 and Destroyed =4) will go to 1.11, since Netica assumes that if nothing is known all outcomes are equally probable. The result is that the quantification of uncertainty gets distorted and with more of these poorly substantiated CPT's the average standard deviation of the prediction (damage in this case) will continue to increase. This is exactly what is happening by adding the building type indicators.

Table 4-18 - Mean standard deviation of hindcasted PMF's for configuration 4 and 5 and different hindcast scenarios.

Hindcast Scenarios	Nr of nodes	Mean Standard Deviation
Config. 1	4	0.54
+ Tax Base	5	0.59
+ Building Class	6	0.66
+ Roof Height	7	0.74
+ Shape Area	8	0.78
+ Residential units = Config. 4	9	0.82

These negative effects can also be seen in space. In Figure 4-37 the observed, most probably outcome, mean of the predicted PMF and standard deviation are shown. It can be seen that the most probable outcome is almost a one-on-one copy of the observed. This is not because of the good prediction skill of the BBN but because of the fact that the hindcasting has been performed based on the same data as the training. With 9 indicator nodes and more than 300,000 corresponding conditioning combinations the 5300 observations get technically isolated within the net and during the hindcasting one will find a slightly higher predicted chance for the actual observed outcome than for the others. The mean and standard deviation of the conditional PMF's confirm that this is happening, where the means are all much closer to 2.5 (which is the mean of 1, 2, 3 and 4) and the standard deviations much higher than in Figure 4-34.

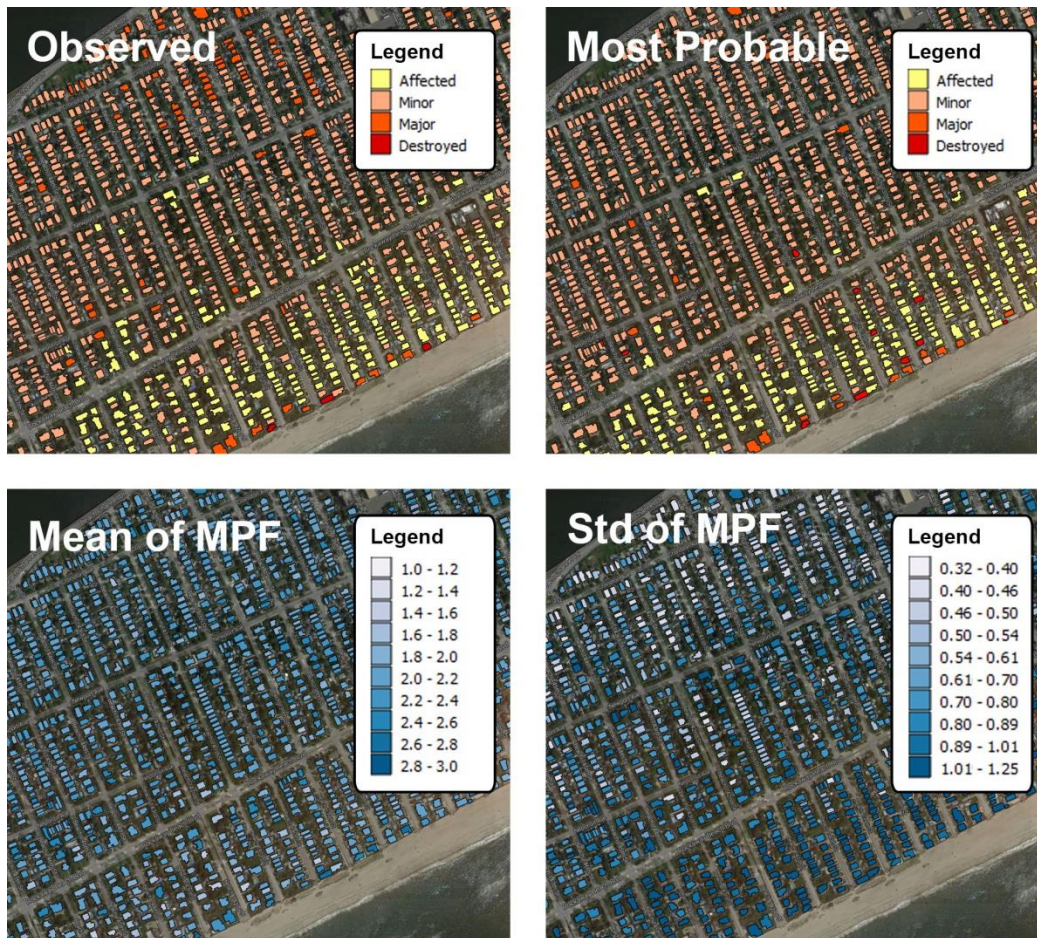


Figure 4-37 - Upper left panel: Spatial representation of observed damage; others: Spatial representation of most probable, mean and mean standard deviation of the hindcasted MPF's for configuration 4 and hindcast scenario 13 (conditioned on all indicators).

5. Discussion and Recommendations

In chapter 0 most of the results have already been discussed and some conclusions been drawn. Here they are elaborated in a broader context.

5.1. Achievements

5.1.1. Overall Model Structure

Considering the overall model structure (including all components of Figure 3-12), it can be concluded that most of the elements work well. The three used physics-based models in the model train, knowing Delft3D, D-Flow FM and XBeach have been successfully coupled, which made a propagation of storm hazard from large to very small scale possible. The use of an SQL database and related tools (e.g. PostGIS) appeared to be very useful in joining all data on the same scale level of analysis, which is the building level. This also enabled an easy coupling of the data to the Bayesian Belief Networks. Moreover, coupling of the database to QGIS made spatial visualisation of the BBN input and output easy as well.

5.1.2. Physical Processes and Hazard Propagation

The implementation of XBeach for the hazard propagation from the nearshore to the buildings (scale of analysis) entailed some difficulties. First of all, it is very time consuming to set up a fairly large XBeach model which has the amount of detail as in present study. Secondly, although high resolution (topo-bathymetrical) data was available, the input leaves a lot to be desired. The LIDAR dataset includes buildings, which is a must to simulate flow around buildings, but also other obstacles such as trees and cars obstructing or even blocking the flow completely. Bare earth LIDAR was not available to compromise for this problem. Moreover, in the surf zone only low-resolution CRM data was available. For a critical storm like Sandy that data appeared to be unsatisfactory, resulting in too much beach and berm erosion with all associated negative consequences. Also the boundary conditions were subject to large uncertainty (especially the wave conditions) of which the negative effects probably could have been reduced by a thorough calibration process. It must be said that with a model in a stage like this all of these aspects have to be improved to ensure better result. With a limited amount of time for present study this was simply not possible.

The results of the XBeach runs are therefore moderate showing a structural overestimation of the local storm conditions; see section 4. However, this does not mean that the decision of using XBeach was a bad one. The indicators “wave attack” and “flow velocities”, both based on XBeach approximations are considered very beneficial; this is for instance not possible when using the bathtub concept. Even with the moderate results of the used XBeach model runs the Bayesian nets are capable of delivering fairly good damage predictions. Combining the information of multiple hazard indicators (representing different hazards) appears to give much better results than only using one indicator. XBeach fits perfectly in this multi-hazard approach.

5.1.2.1. Morphodynamic Processes

Considering the inclusion of morphodynamic processes, other studies have pointed out that XBeach is really good capable of predicting the morphodynamics due to storms like hurricane Sandy realistically. In order to answer the question if inclusion of morphodynamic processes really improves the quality of prediction, it is necessary to make a comparison on runs with and without morphodynamics. The answer will differ from case to case, but it is for sure that inclusion pays off in some cases; for others the significant decrease of computational expenses by excluding them can be more beneficial. Making these kind of comparison only makes sense when the model is fully calibrated, which is not the case in present study. Therefore, firm conclusion on this matter can't be made based on present results. However, it can be concluded that in the Rockaway-Sandy study case morphodynamics (e.g. breaching of the berm) formed a key element in the hazard propagation and associated damages. It is assumed that an improved XBeach model will give much better

predictions on morphodynamics and the thereon depending local storm conditions than it does right now; also better than the results of the bathtub concept.

It must be said that simulation of the morphodynamics realistically is hard for other reasons as well in the case of the Rockaways and Hurricane Sandy. Sandy is said to be a critical storm for the Rockaway peninsula since the protective functioning of the beaches and berm were for a lot of places only slightly sufficient or slightly insufficient. With the present model a structural overestimation of local storm conditions is at stake due to too much erosion of the protective elements (beach and berm). The opposite can easily be the case as well: when the morphodynamics are slightly underestimated, not enough beach and berm erosion can lead to large underestimation of the local storm conditions in the hinterland if the beaches and berm manage to withstand all forces. The accompanying uncertainty of this strong sensitivity can't be found back in the damage predictions when only one run is considered for the training of the BBN's. A solution for this would be executing multiple XBeach runs, varying the input within the range of uncertainty. This has not been done in present study due to time limitations.

5.1.2.2. Model Resolution

Considering the model resolution, some problems with using XBeach appeared which cannot be addressed to the inadequacies of the present model. One of these problems was that the 3x3m² run has larger bed level gradients than the runs with courser grids, which causes unrealistic surging of the water around buildings. On the contrary, the low-resolution run needs bigger extraction buffer zones in order to compensate for the problem of buildings being assigned as 'non-flooded' where this was in reality not the case. Moreover, the flow is easier obstructed by obstacles in the LIDAR for runs with courser grids.

In relation to the damage, the results of Table 4-9 show better LLR-test scores for the high resolution 3x3m² run, but it is hard to draw conclusions from it, since differences are small. It seems that the added value of grid cells smaller than 9x9m² is marginal, where the computational time was almost a factor 25 higher for the 3x3m² run (2300 versus 90 CPU hours). Based on this a courser grid is preferred, but it definitely depends on the site (e.g. a lot of small alleys and small buildings will ask for more detail). Note: it is not excluded that the differences will be larger (or smaller) with an improved model.

As is explained above, inclusion of the morphodynamic processes is most of all interesting for better prediction of the hazard propagations; the added value of the morphological indicator "scour depth" is considered to be marginal. For the Rockaway Peninsula, but also for other sites, the normative erosion and sedimentation that significantly changes this propagation can be found predominantly in the shore facing areas where (hardly) no residential buildings are found. On the contrary, the desire for high grid resolution only exists for the urban areas and not for the areas with beaches and dunes. Since high grid resolution and the inclusion of morphodynamic processes are both competing due to scarcity of computational means, this raises the question if bed level changes can be calculated by an XBeach model with a much courser grid, which then can be coupled to a model with a much finer grid but with the morphodynamic processes turned off. This might significantly reduce computational expenses and, as a pleasant side effect, encounter the erosion/sedimentation problems around buildings.

5.1.3. Determining local hazard indicators

For the determination of the local hazard indicators one value per indicator per building needs to be extracted from the XBeach output. The extraction method, including spatial and temporal aggregation, seems to work well; by using the building perimeter outline polygons the extraction buffer zones can be determined fairly easily. Subsequently the corresponding grid cells can be assigned to the specific building. Results, regarding the inundation depth indicator, are given for different extraction formulations, showing that they can help encountering the problems around buildings.

As is mentioned above, unrealistic high water levels and bed level changes around buildings (especially the higher ones) are approximated by the model, which appears to be unbeneficial for the damage predictions; see section 4 and Table 4-4. This problem cannot be seen separately from grid resolution, the reach of the non-erodible layer, the extraction method and formulations for the local hazard indicators. The high water levels are assumedly caused by numerical instabilities due to high bed level gradients; something that is inescapable with a high resolution grid in combination with (high) buildings. Figure 4-21 shows that the low-resolution run (grid cell size of $9 \times 9 \text{m}^2$) does have fewer problems with the high water levels around buildings. This strengthens the assumption that this phenomenon is caused by high bed level gradients, which are smaller for larger grid cells.

The high bed level changes around buildings, both erosion and sedimentation (see Figure 4-11), can be addressed to the fact that the representation of buildings in the LIDAR data and building polygons (and thus non-erodible layer within XBeach) do not match perfectly in the horizontal. Next to picking the right extraction formulations, one could also think of other solutions to encounter this problem. Expanding the non-erodible areas around buildings is one of them.

In general it can be concluded that all of these aspects appear to have a large impact on the final local hazard indicators with corresponding influences on the quality of prediction. It is therefore recommended to study this in more detail.

5.1.4. Predicting Damage

Even though XBeach results were moderate, combining the potential of multiple indicators in a BBN resulted in a prediction tool that shows skill. With a model domain of only a few kilometres wide observations of about 5300 residential buildings can be used for training and hindcasting purposes. This number appeared to be enough to demonstrate the possibilities of a BBN with four local hazard indicators. Both quantitative and qualitative nodes can be used; Netica does not make a difference. However, the fact that the variable to predict was non-numerical makes analysing the quality of prediction more difficult. Adding another node to the BBN is easy and the added value can be quantitatively compared to alternatives; a bunch of analysis tools is available to do so.

The limitations of the BBN's are clear: adding more nodes will rapidly lower the quality of prediction and uncertainty quantification since the number of data is not sufficient enough to substantiate all the relations within the net. Compromises have to be made to encounter this problem, such as decreasing the number of bins or increasing the scale of application.

The potential of building type indicators is analysed. It is demonstrated that by adding these indicators the quality of prediction increases. The tax base indicator performs best, followed by the building class indicator. For the building classification only functional differences are considered. Other ways of classification, such as on building material stating something about the resistance of the building, was not possible with the available data, but this is assumed to have potential as well. It must be said that tons of other indicators and combinations can be tried too; the accompanying choices that have to be made depend on the number of data available and (expected) mutual dependencies. The latter can be easily tested by applying correlation formulations, such as Pearson's correlation coefficient. This has been done in section 4.2. It is expected that monetary damage instead of or in combination with physical/structural damage will give better results as well. Supporting variables indicating the amount of value at risk, such as household income, are expected to be only relevant in combination with monetary damage. It must be said that these types of data are not easy to get due to privacy issues. Working together with (re)insurers or in closer collaboration with parties like FEMA might give opportunities.

In present study the BBN is trained on observations of one storm and one study site only. From a mathematical

(theoretical) point of view this is not strong; observations should be independent, where in this case observations are clearly spatially correlated. In practice, these correlations limit the applicability of the BBN for predicting damage for other sites and storms. To which degree this is the case, cannot be concluded from the results presented. Validation of the model is required on other sites and storms. However, that the spatial correlations negatively influence the quality of prediction can already be seen within the limits of this study. First of all, it has proven to be very dangerous to draw conclusions on one-on-one relations; see 'Depth-Damage Relations' in section 4.2. Secondly, hindcasting on specific areas of which the observations are not used for training purposes shows a significant drop in LLR-test scores; see Table 4-8.

It must be said that the market standard damage curves are subject to the same problems concerning spatial correlation. There are two ways to minimize these effects within this concept: 1) train the Bayesian nets on data from more storms and sites (this is how market standard damage curves are improved as well); 2) or include as much processes (in the form of indicators) as possible in the statistical model. With the existence of option 2 for BBN's they have a huge advantage over the current damage prediction methods.

5.1.5. Quantifying Uncertainty

The quantification of uncertainty is fairly easy with BBN's. The standard deviations of individual predictions (per building) can be determined and together they can be spatially visualized. In this way it is possible to determine where and when predictions are or aren't confident. The limitations of the Bayesian Belief Network, considering the quality of uncertainty qualifications, are clear as well: the number of nodes, bins and relations are limited by the number of training data. Iteratively these three aspects have to be balanced in order to optimize the Bayesian Nets. Too much nodes, bins or mutual relations (arrows) result in a large share of poorly substantiated CPT's. The consequence is that the uncertainty of prediction increases due to Netica's default assuming all outcomes equally probable when the training data is insufficient for the amount of demanded detail. Moreover, if the event to be predicted qua conditions falls outside the range of events on which the BBN is trained, the uncertainties will be extremely large resulting in a low or negative LLR-test score; BBN's do not lie.

It is questionable what kinds of uncertainty are actually incorporated within Netica's CPT's (the predictions). The answer lies in the training data. The inaccuracy within the predictive part of the input data is a source that is included, which is mostly epistemic uncertainty. The inaccuracies in the LIDAR data (in some cases a bit higher ground elevation levels than in reality, in others a bit lower) can be seen as examples. This is the main reason why predictions can be better (more confident) when the XBeach model is improved; a better representation of the spatial variability in the local storm conditions can then make a difference. Moreover, the aleatoric uncertainty is incorporated as well. This comprises the uncertainty that cannot be explained by adding more complexity. No building is for instance completely the same as another one. Even if they are categorized the same for a million building type indicators and are subject to the same (discretized) forcing conditions, the amount of damage can still differ in the end.

Uncertainties that are not incorporated are structural over- or underestimations within the input data. Training the net based on local storm conditions that are structurally overestimated won't cause any problem if the local storm conditions for the prediction are structurally overestimated (in the same order) as well. This is the case if you hindcast on the exact same observations, which has been done for this study. However, this is not the case if you want to predict a new situation. Then a relative structural under- or overestimation in the local hazard indicators between training data and prior data (used for the predictions) will give structural higher or lower predictions. To incorporate the accompanying uncertainty one can think of the following solution: run multiple scenarios per event with the physics-based models. One can for instance run a

conservative, expected and optimistic scenario and train (and predict) on all⁵⁴. This will only solve the problem to a certain extent.

Finding solutions for structural over- or underestimation of other types of data is more difficult. One could for instance think of structural variations in surveying technics (e.g. different damage formulations for different sites) or variations in the surveyed quantity (e.g. a wooden one-family house in New York might be more resilient than in other states). The only way to incorporate these uncertainties is to train the BBN's with observations from multiple other sites and storms.

5.1.6. Spatial Aggregation

In order to determine total expected damage for a block, neighbourhood or complete city, spatial aggregation of predictions is necessary. The best guess for the expected total damage (or risk given the event) can be determined by summing the means of the PMF's of all predictions (here called the grand mean or GM). For predictions of qualitative damage (qualitative description instead of numbers as is the case in present study) this is not possible⁵⁵, but in the case of monetary damage it is.

Aggregating the uncertainty to a higher scale level is unfortunately not straightforward, since (the bias of) the individual predictions on the building level are spatially correlated; if the expected total amount of damage for a certain house is overestimated in a prediction, it is to a certain extent likely that this is also the case for the neighbouring houses. This correlation has been explained in subsections 0 and 4.3.1. Therefore damage predictions for a certain area cannot be seen as independent stochastic events and are thus mutually correlated with unknown joint probability distributions. This makes it very difficult to say what the uncertainty of the aggregated prediction is.

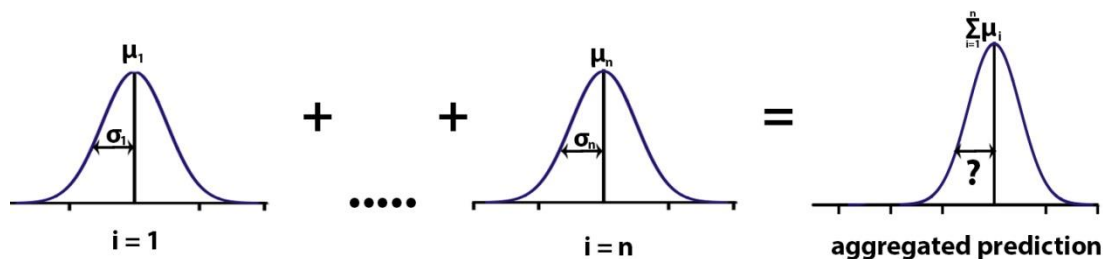


Figure 5-1 - The problem with aggregating predictions to higher spatial scale levels

Upper and lower limits for the uncertainty might give some solution. The theoretical case of totally independent predictions provide a lower limit. The square root of the standard deviation of the individual predictions can then be summed to get the grand variance and subsequently the grand standard deviation. In formula form this comes down to⁵⁶:

$$GS = \sqrt{GV} = \sqrt{\sum_{i=1}^N S_i^2}$$

With: GS = Grand Standard Deviation
 GV = Grand Variance

⁵⁴ It should be noted that if the presented BBN's in this thesis would be part of (or coupled to) a much larger BBN that incorporates more information levels, the uncertainty due to structural over- or underestimation of the local storm conditions, this would not be necessary since these uncertainties would then be included within the net.

⁵⁵ One could of course use a numerical scale as substitution for the qualitative descriptions, but this is not always as straightforward. Moreover, one has to be careful on attaching too much importance to the results.

⁵⁶ http://www.burtonsys.com/climate/composite_standard_deviations.html

S	=	Standard Deviation
N	=	Total number of observations

The (grand) standard deviation of the grand mean is relatively much smaller than the standard deviation of individual predictions. As an example: take 1000 comparable buildings with on average \$ 50,000,- damage and a standard deviation of \$ 20,000,-, which is assumed to be realistic. The expected total amount of damage is 50 M dollar; the grand standard deviation now becomes 0.63 M dollar, which is a little bit more than 1% of the expected total amount of damage. Where predictions of the total damage in the past showed errors in the order of 50% or even more⁵⁷, a relative error of 1% seems most questionable. Moreover, this ratio keeps decreasing for an increasing amount of buildings until the uncertainty becomes negligible. This lower limit is thus not very practical.

Assuming fully mutually correlated predictions and all possible uncertainties incorporated in the corresponding conditional PMF's might have the potential of an upper limit. However, this is not easy and can be best investigated when more storm scenarios and study sites are incorporated in the research. In that way all uncertainties, including uncertainties regarding the input parameters of the model, can be incorporated on the building level. Something like the weighted Std/mean ratio of the individual predictions might be useful as a first guess for the GS/GM ratio. With the current concept, though, where the uncertainties of structural over- or underestimations are not incorporated in the PMF's, it is certainly not possible to determine this upper limit.

Considering all this together, the uncertainty of prediction on the aggregated level cannot be determined within the present concept; other ways need to be developed in order to do so. However, comparing averaged standard deviations for different areas within a site might still be useful, since it says something about the confidence of prediction on the object level.

5.2. Applicability of the Concept

Based on the results and considerations of sections 0 and 5, it can be concluded that using BBN's as substitute for the market standard damage curves is proven to be feasible. However, it must be said that the method is extremely data extensive. If one wants to use more than 4 indicator nodes with four bins each (which is assumed to be reasonable) much more than 5000 observations are necessary. Setting up multiple XBeach models for different case studies would be a solution, but that is a time consuming job. For the American situations where quite a lot of destructive hurricanes have caused damage, and subsequently the damage observations have been documented fairly well, the concept offers opportunities. In the European situation, for instance in the Netherlands, real wind induced sea flood with disastrous consequences are scarce. In that case data has to be used from other countries, which entails additional uncertainty due to for instance differences in building standards and surveying technics.

Moreover, data for other types of assets might be scarcer or harder to get than for residential buildings. This is for instance the case for roads, of which damage observations are rare. About the damaging physical processes also very little is documented. On the other hand, BBN's have proven to be ideal tools for finding out which aspects are important and which are not. In that sense Bayesian nets might offer some opportunities for these types of assets if a critical number of data can be gathered.

Another benefit of the presented concept is that additional training data can be added fairly easy. Every time a new event occurs, the model train can be setup, local hazard indicators can be generated and the Bayesian nets can be updated. By automating this process a constant improvement of the quality of prediction can be ensured. For an updated version of the BBN's not much has to be done.

⁵⁷ This can especially be concluded on the findings of "Comparative flood damage assessment towards an European approach" (Jongman et al. 2012).

5.3. Recommendations

It must be said that with all these axis of freedom a lot of optimizations can be carried out in order to improve the results and further expand the findings of present study. This thesis comprises an exploratory research only and to end up with a fully operational model much more research needs to be done.

The first and most important recommendation for future research is testing the concept with observations from multiple study cases. The fact that present study was limited to data from only one event made validation impossible. By considering more events, the uncertainties on aggregated level and the problems with spatial correlations can be studied in more detail. It must be said that only one additional site or storm might not be enough. At least several storms and sites are necessary to properly research these aspects. If so, one can play with the datasets and vary with the distribution over hindcast and training purposes. In that way a better understanding can be gained of how well the model approach works for predicting the impacts of new situations and how much training data is necessary to obtain satisfactory results.

Secondly, it is recommended to further study the inclusion of morphodynamic processes. In order to do so, a fully calibrated and optimized XBeach model is a must. Where in this study a lot of time was spend on high resolution modelling, this appeared to be not so important. A grid cell size of $9 \times 9 \text{ m}^2$ in the urban areas is probably enough when obstacles in the bathymetrical data (e.g. trees, cars) are removed. The computational expenses are then much lower, which makes running more simulations (varying input in the range of uncertainty) better feasible. In that same way also the uncertainty of other XBeach input parameters can be included in the predictions by training the BBN based on data from more conservative and more progressive runs as well.

Third, the BBN's can be further optimized. More configurations can be tested and compared, including different indicator nodes, varying the number of bins and relations between nodes. Moreover, it would be very interesting to study monetary damage predictions. It is therefore recommended to work in close relation with either a governmental organisation, like FEMA, or (re)insurers to get the required data. To which extend the BBN's of present concept can be build out or coupled to other nets in order to cover more information levels is a question that needs to be answered as well.

Furthermore it should be noted that other software packages can be tried as substitutes for some elements. As a substitute for XBeach other models can be thought of; especially in areas where the morphodynamics are not so important it is definitely recommended to use another type of model, which at least has to be capable of approximating water levels, waves and flow velocity. Other hazard indicators can be considered too. Netica has its limitations as well and an alternative can for instance be found in Uninet. Comparisons need to point out which option is the best for what situation.

6. Conclusions

In general it can be concluded that the presented model approach succeeded. The hazards, predominantly coming from sea in the case of Hurricane Sandy, had to be propagated from large scale (100-1000 km) to the building level (1-10 m). In order to do so, a nested routine is assumed to be most suitable. As part of the nested structure the morphodynamic storm impact model XBeach is implemented to propagate the hazard from the nearshore to the assets at risk (scale of analysis), which are limited to residential buildings only in present study. With the use of extraction methods local hazard indicators are generated for every single residential building. Together with building type indicators (e.g. building class, size parameters) these hazard indicators have been used as damage predictors in the predicting element of the model structure: the Bayesian Belief Network (BBN). In this statistical model observations of a qualitative damage assessment have been coupled successfully to corresponding local hazard and building type indicators. 5300 damaged residential buildings at the Rockaways, NY, were enough to train BBN's capable of reproducing the spatial pattern of the damage fairly well; see Figure 4-33 and Figure 4-34. Multiple analysis tools, like a bin-analysis and log-likelihood ratio test, are available to analyse the quality of prediction and uncertainty quantification and it is easy to visualize that in space with the use of an SQL database coupled to GIS software.

XBeach is capable of providing multiple local hazard indicators on the building level, which proved to having predictive capacity. The indicators "inundation depth", "wave attack" and "flow velocity" and (to a lesser extend) "scour depth" give together much better predictions than they do alone; see Table 4-5. The implementation of XBeach therefore fits perfectly in the multi-hazard approach that Bayesian Belief Networks make possible. On the contrary, it must be said that setting up an XBeach model for high resolution simulations (grid cell sizes of in the range of meters) with a relatively large model domain (8 km wide, see Figure 3-16) requires high detailed input data and is a time consuming job. The results of the XBeach model used for present study show a structural overestimation of storm conditions, which can be addressed to a poor calibration process, uncertainties in the boundary conditions and problems with shortcomings in the bathymetrical data. This assumedly limits the predictive skill of the statistical BBN model (e.g. hardly any predictive capacity is found for inundation depth, which can be assigned to the bad representation of the spatial variability in maximum simulated water levels). There is certainly a large scope for improvement, which means that the results can only become better. However, for proof of concept the presented results are sufficient enough.

Grid resolution of the XBeach model appears to be not as important as expected; indicator values based on model runs with grid cell sizes of $3 \times 3 \text{ m}^2$ in the urban areas give hardly better predictions than runs with grid cell sizes of $9 \times 9 \text{ m}^2$; see Table 4-9. Computational expenses are 25 times higher though. Moreover, the added value of including morphodynamic processes can't be quantified based on the results of present study. However, it can be concluded that morphodynamics are important for the hazard propagation in the treated case study. XBeach has proven to be capable of coping with these morphodynamics in other studies.

Next to these aspects, the extraction method, in which hazard indicators are generated out of the XBeach output, appeared to be very important for the predictive capacity of these indicators. It can be concluded that the used method, in which the building perimeter outlines play a very important role, performs well; see Figure 3-17. Extraction formulations and the size of extraction buffer zones around the buildings can make a substantial difference; see Figure 4-23. From Table 4-4 it can be concluded that courser XBeach grids ask for larger extraction buffer zones, which is to be expected.

Considering the statistical model part, the Bayesian Belief Networks give the opportunity to relate the damage to multiple aspects instead of only one, which has great advantages over the market standard damage curves. This is because together, the indicators give much better predictions, and the consequences of relations based on special correlated training data are minimized. The established BBN's are good in capturing the spatial

variability in risk (given the event) per building, comparing the spatial distribution of the means of the conditional PMF's to the observed damages (Figure 4-33). The predicted chance of extreme damage for buildings that had been extremely damaged in reality is higher than for buildings that suffered less damage. However, for these extremely damaged buildings the predicted chance of being extremely damaged was often still lower than the chance of being subject to minor damage. Therefore the BBN's perform not so well in predicting extremes; see the predicted most probable outcomes in Table 4-10. Considering the added value of integrating vulnerability and socio-economic data, adding nodes indicating differences between buildings increases the hindcasted Log-likelihood ratio test scores. The "tax base" indicator appears to be most skilful. It is said that one has to be really careful with adding too much nodes. The consequences of the latter are demonstrated in subsection 4.3.2: the predictions become worse if too much complexity is added to the BBN, since in that case the limited amount of data gets overfitted. Adding nodes indicating the value of a property at risk (e.g. household income, Tax Base Parameters) is assumed to have great potential as well, but only if monetary damage is considered. The latter is recommended for future research.

Also the quantification of uncertainty depends strongly on the number of nodes, bins and relations added within the BBN. More complexity in the network needs to be compensated by more training data in order to retain the same quality of the PMF's of the predictions. Indicators for uncertainty, such as standard deviation of these conditional PMF's, can be easily visualized in space (Figure 4-34) and used to say something about the confidence of predictions. However, quantitatively the PMF's do not cover all sources of uncertainty in the approach as it is proposed right now. This is a direct cause of the limited training of the BBN's, which is based on the results of only one XBeach run and not multiple, more conservative and progressive, runs. Therefore, uncertainties concerning structural over- or underestimations (for instance due to input parameter uncertainty of the XBeach model) are not represented in the distributions of predictions.

Aggregation of the damage predictions to higher spatial scale levels, such as a neighbourhood or a complete city, is not straightforward within the present approach. Aggregation of risk given the event (mean of the PMF's) is a matter of summation. On the contrary, predictions for buildings in a certain area cannot be seen as independent, since (spatial) correlation between the predictions is at stake. This, in combination with the fact that not all uncertainty is incorporated in the PMF's, makes aggregation of uncertainty difficult. Future research is necessary in order to find ways to overcome those aggregation issues.

Appendices

A. Merging Data based on Geospatial Information

To use all information on the same scale of application, which is the building level for this study, data from different datasets have been coupled. This is done based on geospatial information with the use of PostGIS SQL querying tools. The building polygons from the Buildings dataset have been used as a base and properties from the ImageCat and PLUTO datasets have been assigned to the building polygons based on geospatial relations.

The ImageCat data are assigned to buildings as follows:

- 1) The majority of the points fall within a polygon. These were coupled first;
- 2) The rest of the damage observations have been attached to the closest polygon, which had not been coupled yet;
- 3) The remaining building polygons, of which the majority corresponds to garages and pavilions, are not coupled to damage observations.

It is noted that garages and other non-residential buildings are not included in the Bayesian Networks. Of the 9800 buildings within the XBeach domain 7800 buildings fall within the area of application (the rest is situated within the shadow zones). Of these 7800 buildings a bit more than 5300 are residential buildings and to almost all of them a damage observation has been assigned.

The PLUTO data are assigned to buildings as follows:

- 1) All buildings falling completely within a tax lot, get the properties of that tax lot;
- 2) All buildings that fall in two or more tax lots get the properties of the closest tax lot center.

No buildings fall completely outside the tax lots, which makes the coupling less complicated. Some tax lots contain more houses. Properties like the tax base values and residential units are then divided by the number of buildings (excluding garages and pavilions again). This implies the assumption that in these cases all buildings are considered comparable.

B. Multi-variate flood damage assessment – abbreviation description

In addition to Figure 3-9 on page 56.

Table 1. Description of the 28 candidate predictors (*C*: continuous, *O*: ordinal, *N*: nominal).

	#	Predictors	Type and range	Amount of data*
hydrologic, hydraulic aspects	1	wst Water depth	C: 248 cm below ground to 670 cm above ground	2108
	2	d Inundation duration	C: 1 to 1440 h	2094
	3	v Flow velocity indicator	O: 0 = still to 3 = high velocity	2120
	4	con Contamination indicator	O: 0 = no contamination to 6 = heavy contamination	2122
	5	rp Return period	C: 1 to 848 yr	2158
early warning and emergency measures	6	wt Early warning lead time	C: 0 to 336 h	1364
	7	wq Quality of warning	O: 1 = receiver of warning knew exactly what to do to 6 = receiver of warning had no idea what to do	955
	8	ws Indicator of flood warning source	O: 0 = no warning to 4 = official warning through authorities	1675
	9	wi Indicator of flood warning information	O: 0 = no helpful information to 11 = many helpful information	1631
	10	wte Lead time period elapsed without using it for emergency measures	C: 0 to 335 h	842
precaution, experience	11	em Emergency measures indicator	O: 1 = no measures undertaken to 17 = many measures undertaken	2158
	12	pre Precautionary measures indicator	O: 0 = no measures undertaken to 38 = many, efficient measures undertaken	2158
	13	epre Perception of efficiency of private precaution	O: 1 = very efficient to 6 = not efficient at all	2043
	14	fe Flood experience indicator	O: 0 = no experience to 9 = recent flood experience	619
	15	kh Knowledge of flood hazard	N (yes/no)	1472
building characteristics	16	bt Building type	N (1 = multifamily house, 2 = semi-detached house, 3 = one-family house)	1816
	17	nfb Number of flats in building	C: 1 to 45 flats	1726
	18	fsb Floor space of building	C: 45 to 18 000 m ²	1496
	19	bq Building quality	O: 1 = very good to 6 = very bad	1758
	20	bv Building value	C: 92 244 to 3 718 677 €	1419
socio-economic status	21	age Age of the interviewed person	C: 16 to 95 yr	2097
	22	hs Household size, i.e. number of persons	C: 1 to 20 people	2125
	23	chi Number of children (< 14-yr) in household	C: 0 to 6	1877
	24	eld Number of elderly persons (> 65 yr) in household	C: 0 to 4	1983
	25	own Ownership structure	N (1 = tenant; 2 = owner of flat; 3 = owner of building)	2158
	26	inc Monthly net income in classes	O: 11 = below 500 € to 16 = 3000 € and more	1666
	27	socp Socioeconomic status according to Plapp (2003)	O: 3 = very low socioeconomic status to 13 = very high socioeconomic status	1469
	28	socs Socioeconomic status according to Schnell et al. (1999)	O: 9 = very low socioeconomic status to 60 = very high socioeconomic status	1308

*Since not all people were willing to answer all questions, not all information is available for each interview.

C. XBeach model formulations

The formulations and descriptions in this appendix form a brief summary of the XBeach manual (Deltares 2010).

The physics-based model XBeach can use both a local and global coordinate system, but the configuration is always the same: the x-axis is oriented towards the coast, approximately perpendicular to the shoreline, see Fig XI. A staggered grid is used, in which fluxes (velocities, sediment transport, radiation stress gradients, etc.) are calculated on the interfaces of cells and conservative quantities (water level, bed level, etc.) are calculated in cell centres.

C.1. Short wave equations

Different from most other physics-based models, XBeach solves short wave equations (order of 10s per cycle) on the time scale of the long wave groups and thus long waves. Wave input data is reduced to a 2D-spectrum in which the directional distribution is taken into account (in bins, of which the size has to be predefined). The frequency distribution, however, is reduced to one single peak frequency. Time-varying wave action belongs to the possibility and is used for present study. The wave action balance reads:

$$\frac{\partial A}{\partial t} + \frac{\partial c_{g,x} \cdot A}{\partial x} + \frac{\partial c_{g,y} \cdot A}{\partial y} + \frac{\partial c_{\theta} \cdot A}{\partial \theta} = - \frac{D_{waves}}{\sigma}$$

With:	A	=	wave action, which is defined as E/σ
	E	=	wave energy
	σ	=	intrinsic wave frequency
	c _g	=	wave group velocity
	c _θ	=	Velocity in directional space
	D _{waves}	=	the energy dissipation due to breaking waves

The fourth term on the left side represents energy exchange between the bins due to refraction, which is on its turn caused by bottom friction and currents. In the newest versions of XBeach it is also possible to include a source term for wind-generation, which has not been used in present study; diffraction is not included. Wave breaking (ride side dissipation term) is modeled according to the Roelvink's formulations (1993a).

C.2. Roller energy balance

XBeach uses a roller energy balance in order to model the energy redistribution of breaking waves. Short wave energy is transformed in kinetic energy and is used as a source term in the roller energy balance, which reads:

$$\frac{\partial E_r}{\partial t} + \frac{\partial c_x E_r}{\partial x} + \frac{\partial c_y E_r}{\partial y} + \frac{\partial c_{\theta} E_r}{\partial \theta} = -D_r + D_{waves}$$

With:	E _r	=	roller energy
	c	=	roller celerity (assuming that waves and rollers propagate in the same direction)
	D _r	=	the roller energy dissipation

Again, the velocity in directional space takes refraction into account. Furthermore, the roller energy dissipation

Is given by Reniers et al. (2004a) combining the concepts of Deigaard (1993) and Svendsen (1984):

$$D_r(x, y, t, \theta) = \frac{S_r(x, y, t, \theta)}{E(x, y, t)} \cdot \frac{2g\beta_r E_r}{c}$$

In which S_r represents the radiation stresses, which can be directly determined from the spatial distribution of wave energy. Moreover, also roller induced shear stresses are calculated from these spatial wave energy distributions.

C.3. Shallow water equations

In order to solve the long infragravity waves, XBeach uses shallow water equations, both depth integrated momentum and mass balance. However, only considering the long waves would not give a satisfying answer, where the short waves cause mass fluxes and return currents in the littoral zone. Therefore, XBeach uses the Generalized Lagrangian Mean (GLM) formulations (Andrew and McIntyre, 1978, Walstra et al., 2000), in which the Lagrangian velocity is defined as the distance a water particle travels in one wave period, divided by that period. The Lagrangian velocity relates to the Eulerian velocity and Stokes drift by:

$$u^L = u^E + u^S \quad \text{and} \quad v^L = v^E + v^S$$

With:

$$u^S = (E_{waves} + 2 \cdot E_{roller}) \cdot \cos(\theta) \quad \text{and} \quad v^S = (E_{waves} + 2 \cdot E_{roller}) \cdot \sin(\theta)$$

The Stokes velocities are thus calculated from the wave and roller energy. The GLM equations, which are based on the non-conservative dimensional form of the Saint Venant equations, are given as follows:

$$\text{x-direction :} \quad \frac{\partial u^L}{\partial t} + u^L \frac{\partial u^L}{\partial x} + v^L \frac{\partial u^L}{\partial y} - f v^L - \eta_h \left(\frac{\partial^2 u^L}{\partial x^2} + \frac{\partial^2 u^L}{\partial y^2} \right) = \frac{\tau_{sx}}{\rho h} - \frac{\tau_{bx}^E}{\rho h} - g \frac{\partial \eta}{\partial x} + \frac{F_x}{\rho h}$$

$$\text{y-direction :} \quad \frac{\partial v^L}{\partial t} + v^L \frac{\partial v^L}{\partial x} + u^L \frac{\partial v^L}{\partial y} - f u^L - \eta_h \left(\frac{\partial^2 v^L}{\partial x^2} + \frac{\partial^2 v^L}{\partial y^2} \right) = \frac{\tau_{sy}}{\rho h} - \frac{\tau_{by}^E}{\rho h} - g \frac{\partial \eta}{\partial y} + \frac{F_y}{\rho h}$$

$$\text{z-direction :} \quad \frac{\partial \eta}{\partial t} = - \frac{\partial u^L h}{\partial x} - \frac{\partial v^L h}{\partial y}$$

The horizontal eddy viscosity η_h is in XBeach related to the roller energy dissipation D_{roller} according to Reniers et al. (2004). Moreover, the bed friction τ_b is calculated with use of Eulerian velocities. The formulations are solved in Xbeach in general. At the boundary multiple options are available (e.g. open or closed, Neumann boundaries) for which divergent formulations are used. These formulations can be found in the XBeach manual.

C.4. Sediment transport

The depth averaged advection-diffusion equation according to Gallappatti and Vreugdenhil (1985) is used in order to calculate the transports of sediment. Where the depth integrated Lagrangian velocity in the surf zone is assumed to be zero on average (balance principle considering a closed system), the mass flux related to the Stokes drift (and thus Stokes velocities) must be compensated by an equally large but opposite flux, which can be related to the undertow (and thus the Eulerian Velocities). The undertow and thus the Eulerian velocities are normative, resulting in:

$$\frac{\partial hC}{\partial t} + \frac{\partial hC U^E}{\partial x} + \frac{\partial hC v^E}{\partial y} + \frac{\partial}{\partial x} \left[D_h h \frac{\partial C}{\partial x} \right] + \frac{\partial}{\partial y} \left[D_h h \frac{\partial C}{\partial y} \right] = \frac{hC_{eq} - hC}{T_s}$$

With:	C	=	depth-averaged sediment concentration
	D_h	=	sediment diffusion coefficient
	h	=	depth
	C_{eq}	=	Equilibrium sediment concentration (depth-average)
	T_s	=	Adaptation time scale

The adaptation time T_s , which depends amongst others on the water depth and fall velocity of the particles, is a measure for the response time of a specific situation going to the equilibrium situation with C_{eq} . For C_{eq} different sediment transport formulations do exist where in XBeach the formulation of Soulsby-van Rijn (1997) has been implemented; see the manual for the basic formulation and variations.

C.5. Bed updating

Bed updating due to sediment transport is calculated with the following formulation⁵⁸:

$$\frac{\partial z_b}{\partial t} + \frac{f_{mor}}{1-p} \left(\frac{\partial q_x}{\partial x} + \frac{\partial q_y}{\partial y} \right) = 0$$

With:	p	=	porosity
	f_{mor}	=	Morphological acceleration factor; see Appendix C.7
	z_b	=	Bottom level
	q	=	Sediment transport rate in x- or y-direction

The sediment transport rates q_x and q_y are depth integrated and are within XBeach determined with the following formulations, which do not include the optional bed-slope correction factors here:

$$q_x(x, y, t) = \left[\frac{\partial hcU^E}{\partial x} \right] + \left[\frac{\partial}{\partial x} \left[D_h h \frac{\partial C}{\partial x} \right] \right] \quad \text{and} \quad q_y(x, y, t) = \left[\frac{\partial hcU^E}{\partial y} \right] + \left[\frac{\partial}{\partial y} \left[D_h h \frac{\partial C}{\partial y} \right] \right]$$

C.6. Avalanching module

The avalanching approach, as has been introduced in paragraph 3.1.1.1, accounts for the slumping of sandy material when dune erosion is at stake. When a user-defined critical level is exceeded avalanching takes place in the model:

$$\left| \frac{\partial z_b}{\partial x} \right| > m_{cr}$$

When this critical level is reached, the bed-change within one time step is the determined as follows:

$$\Delta z_b = \min \left(\left(\left| \frac{\partial z_b}{\partial x} \right| - m_{cr} \right) \Delta x, 0.05 \Delta t \right), \quad \text{when } \frac{\partial z_b}{\partial x} > 0$$

$$\Delta z_b = \max \left(- \left(\left| \frac{\partial z_b}{\partial x} \right| - m_{cr} \right) \Delta x, -0.05 \Delta t \right), \quad \text{when } \frac{\partial z_b}{\partial x} < 0$$

Both conditions are always at stake at the same time in neighbouring cells. When the critical slope between two adjacent grid cells is exceeded, sediment is exchanged between these two cells to the amount that is needed to bring the slope gradient back to the critical situation.

⁵⁸ Coastal Dynamics I – lecture notes (J. Bosboom & M. Stive, 2012)

C.7. Morphological acceleration factor

Important for this thesis, since it is used to speed up the computations, is the morphological factor (or short: morfac). Calculating the bed level changes and updating the bed to its new state takes a lot of time and this is why the morphological factor is used. As an example, if one uses a morfac of 10, the model runs effectively only 6 minutes of every hydrodynamic hour including the morphodynamics. The morphological changes are then multiplied everything with a factor 10, which then save a factor 10 in computation time. The assumption that the result would be pretty much the same as without the morphological factor holds until a certain extend; in practice a morfac of 10 normally works fine, but a higher factor is not recommended⁵⁹.

⁵⁹ According experts within Deltares.

D. XBeach model set-up

D.1. Bathymetrical/topographical data

This paragraph elaborates on the bathymetrical and topographical data used for the Rockaway Peninsula case study. To obtain high resolution storm characteristics on land with the use of XBeach modelling it is very important to have topographical and bathymetrical input that is at least as detailed as the desired output.

The US Army Corps of Engineers (USACE) has done multiple LIDAR surveys in order to obtain high-resolution topo-bathy datasets covering most parts of the Long Island coastline, including Rockaway Peninsula. Although the density of elevation data seems to be sufficient for the aim of this study, some remarks should be made:

- Some buildings have been deleted and at these locations you find data gaps.
- For some layers, at some urban areas data are completely absent.
- In the other urban areas buildings, trees, cars and other objects caused trouble in capturing the right elevations (noise), which has negative effects on the accuracy of the LIDAR data. The datasets are corrected for this as good as possible, but the topographical profile will always be a bit blurry.
- Geographical positioning is not as good as one would expect. The location (in the horizontal) of an object can differ in the order of 100m for different layers.

All this has its effects on the accuracy and therefore outcome of the XBeach modelling. In order to reduce these negative effects, datasets are combined and corrected where possible. Data gaps are filled in with use of interpolation routines and information on building height. Next section gives a short elaboration on the final topo-bathy file and the process of getting there.

The remaining of this section will give specific details on the used datasets and corresponding sources.

2005 USACE – Pre-Sandy

The 2005 topo-bathymetry of the United States Army Corps of Engineers (USACE) is part of a larger survey campaign. For coastline of Delaware, Maryland, New Jersey, New York, North Carolina and Virginia bed elevation levels have been measured by the department of Joint Airborne LIDAR Bathymetry Technical Center of Expertise. This is part of the National Coastal Mapping Program and it is performed on a 5 to 7 year update schedule⁶⁰. According to NOAA, the program uses the CHARTS system, which integrates topographic and bathymetric LIDAR sensors, a digital camera, and a hyperspectral scanner on a single remote sensing platform. The data can be downloaded on NOAA's Digital Coast webpage, either gridded or in xyz. A visualisation of the coverage in the model domain is given in Fig I, both an overview and zoomed in view. The resolution of the dataset is 0.25 observations/meter and corresponds to a grid cell size of 2 x 2 m.

⁶⁰ <http://www.csc.noaa.gov/digitalcoast/data/chartstopobathy>

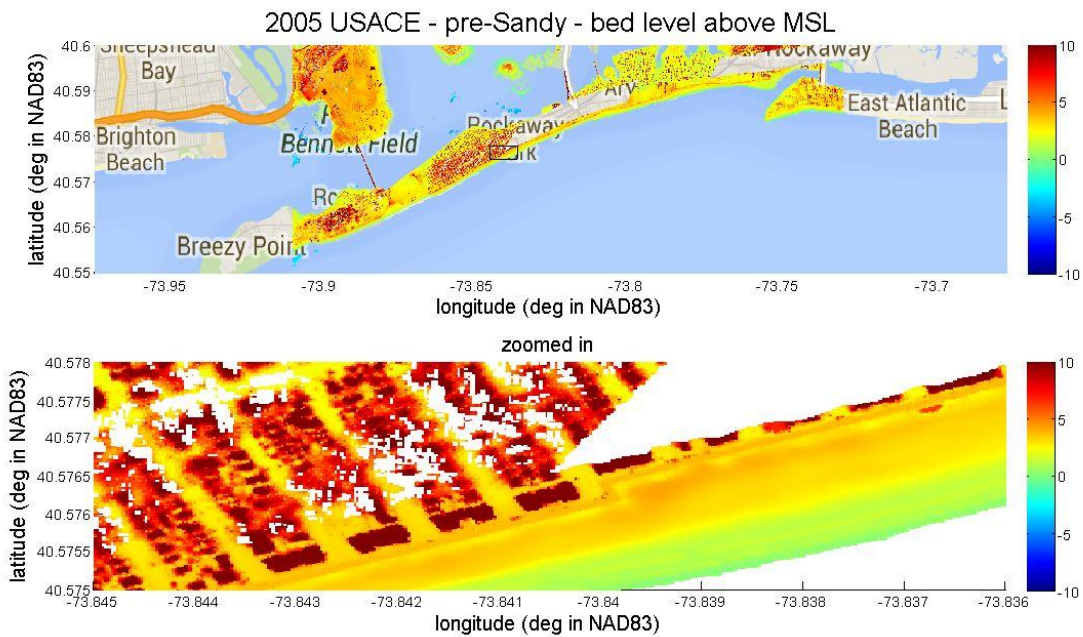


Fig 1 - Bed levels of the 2005 USACE survey. Upper panel: overview; lower panel: zoomed view of the squared box in the upper panel

It is noticed that where data are available, the dataset is pretty good: high resolution and not too much noise. However, large and some smaller gaps can be found within the area of interest.

2010 USACE - Pre-Sandy

As part of the same program the '2005 USACE – Pre-Sandy' LIDAR is part of, the 2010 survey looks fairly similar. One important difference: within the area of interest no data gaps are found. Together with the fact that the 2010 survey has been the last survey carried out before Sandy, it is considered to be the most important topographical dataset for present study. A visualisation of the coverage in the model domain is given in Fig II, both an overview and zoomed view. The resolution of the dataset is 0.25 observations/meter and corresponds to a grid cell size of 2 x 2 m.

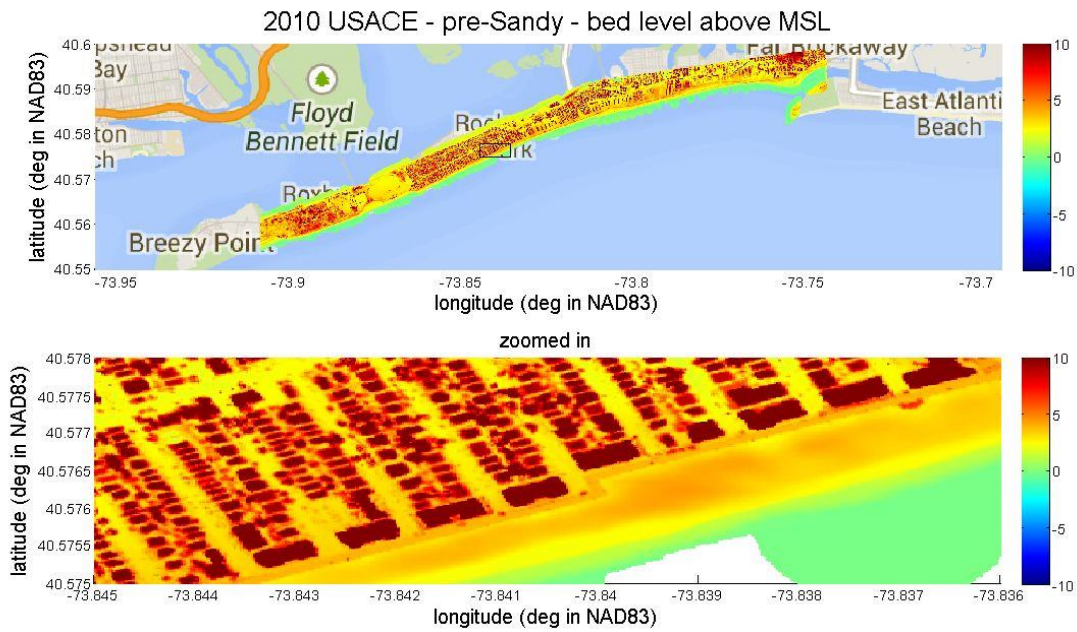


Fig II - Bed levels of the 2010 USACE survey. Upper panel: overview; lower panel: zoomed view of the squared box in the upper panel

2012 USACE - Post-Sandy

The 2010 USACE survey is not part of the National Coastal Mapping Program and a different system than CHARTS is used for the measurements, knowing the Coastal Zone Mapping and Imaging LIDAR (CZMIL) system. The data were collected as a part of the Post Sandy effort to determine the morphological changes due to Sandy above and below the mean water level in the NY coastal zone. In that perspective, buildings and other terrain objects are of no interest and have therefore been filtered out as can be seen in Fig III. The larger buildings have been completely removed resulting in data gaps, which correspond to the white spots in the figure. The resolution of the dataset is 0.25 observations/meter and corresponds to a grid cell size of 2 x 2 m.

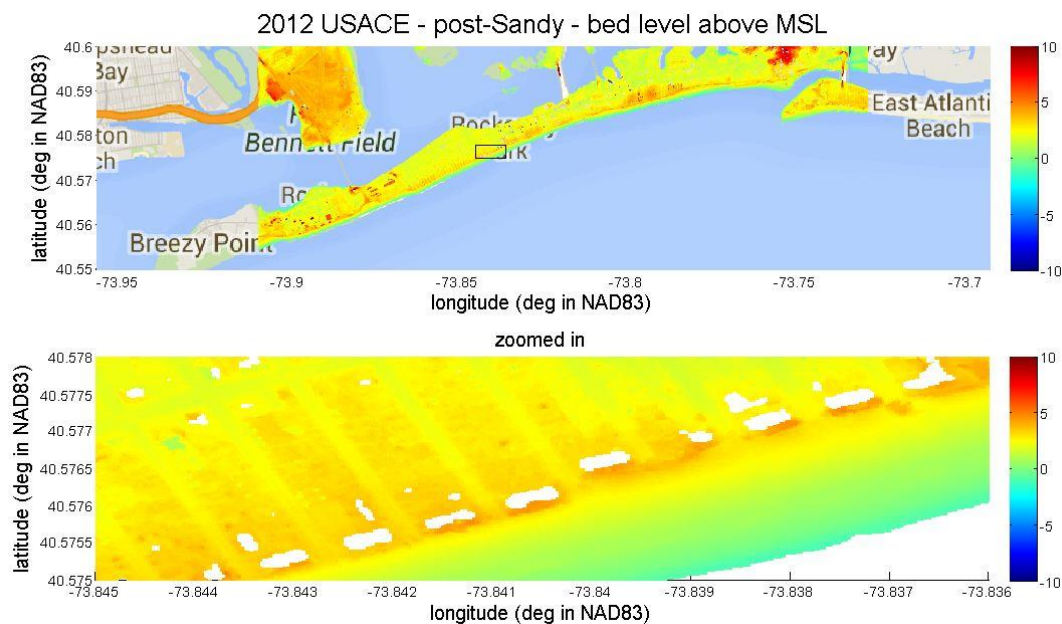


Fig III - Bed levels of the additional post-Sandy 2012 USACE survey. Upper panel: overview; lower panel: zoomed view of the squared box in the upper panel

Coastal Relief Model

Where the LIDAR data are mainly concentrated onshore, the Coastal Relief Model (CRM) bathymetrical dataset is used for the offshore bed levels. It covers almost the complete US coast; east, west and the Gulf. According to NOAA⁶¹, the CRM is composed of bathymetrical and topographical sources of U.S. National Ocean Service Hydrographic Database, the U.S. Geological Survey (USGS), the Monterey Bay Aquarium Research Institute, the U.S. Army Corps of Engineers, Shuttle Radar Topography Mission (SRTM), and various other academic institutions. The resolution of the gridded dataset is one observation every 3 arc-second and corresponds to a grid cell size of about 90 x 90 m, which is considered relatively coarse compared to the LIDAR data. However, as could have been expected, no buildings are located in the offshore areas, thus a high resolution is less important. Moreover, the littoral zone, where most of the morphological impact can be observed, is included in the LIDAR data as well. This implies that the resistant parts of the coastline, consisting of dunes and beach fronts, are mostly captured in the previous mentioned datasets.

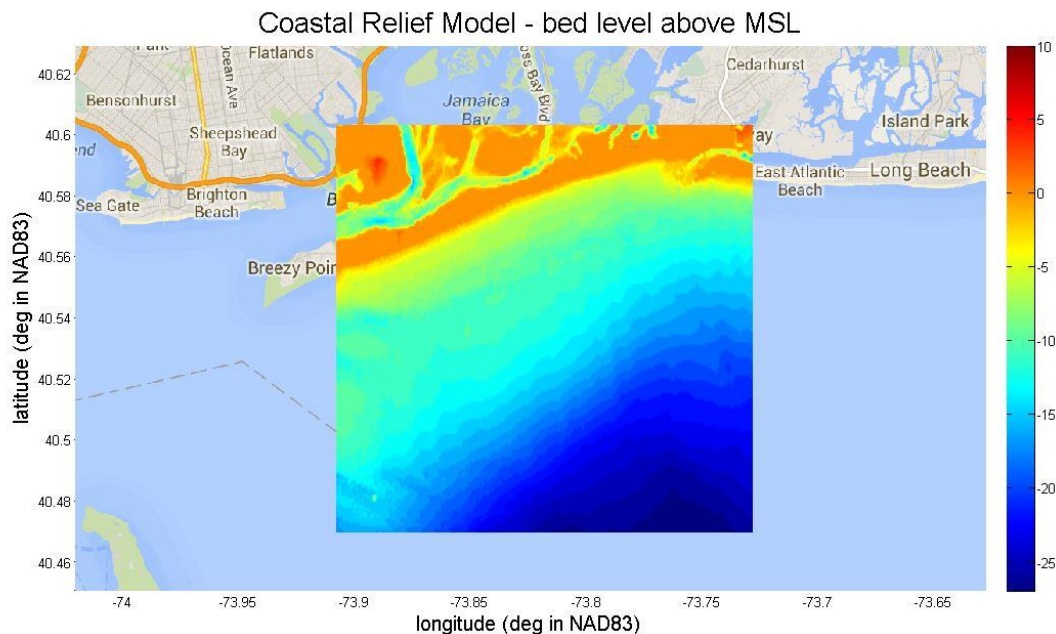


Fig IV - Bed levels of the used CRM data.

D.2. Final bathymetrical input

The final bathymetrical input file for XBeach has been established by combining the available datasets, which are elaborated in Appendix D.1, and some repair and interpolation routines.

To get the best result for every location within the domain a specific dataset should be used based on general requirements. The following requirements are used to sequence the datasets for the interpolation process:

- Where buildings are located (practically almost everywhere above Mean Sea level) a grid resolution of at least 3x3m is required, which gives a preference for datasets with that same resolution or higher.
- Minimal noise and no deletion of buildings and other objects are both preferred.
- Although large onshore morphological changes are not expected in the 10 years before Hurricane Sandy struck the area, observations which have been recorded closer to Sandy's lifetime are preferred.

⁶¹ <http://www.ngdc.noaa.gov/mgg/coastal/crm.html>

Based on the above mentioned requirements the '2010 USACE' is used for the areas above Mean Sea Level. Data gaps are filled up with '2005 USACE'. The bathymetrical data from the CRM dataset is used for the areas below Mean Sea Level (MSL), both in the littoral zone (Bay side and Ocean side) as in the deeper parts. The result is shown in Fig V.

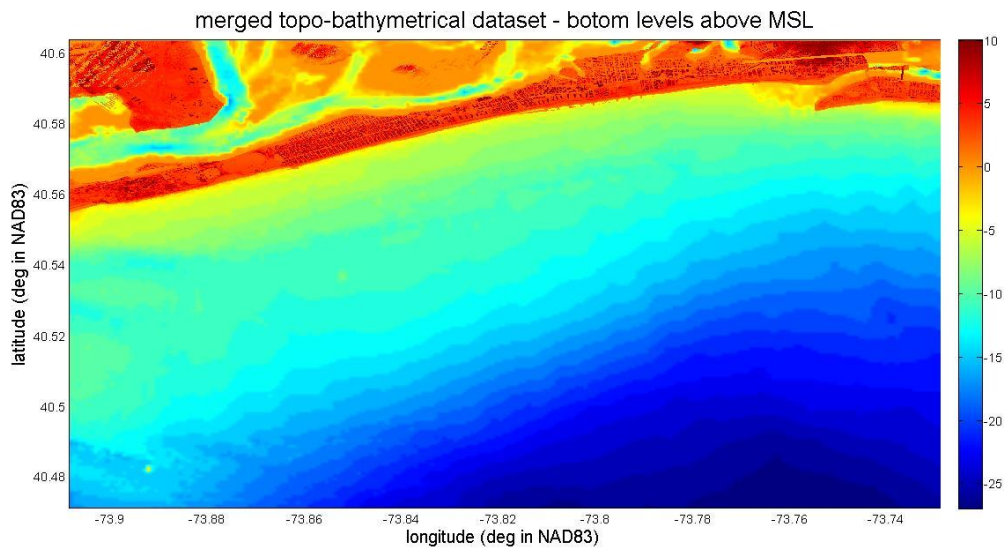


Fig V - Spatial visualization of the merged topo-bathymetrical dataset

To be sure that the water flows in the XBeach runs where it flowed in reality some obstacles are removed. Three bridges and corresponding ramps within the model domain have been lowered to surrounding elevations, knowing Marine Parkway Bridge, the Cross Bay Bridge and the railway bridge in the northeast. Moreover, the railway viaduct, which is constructed along the coastline and spans almost half of the model domain, is removed as well. Fig VI illustrates the locations (left) and a zoomed view of one of the repairs (right, Viaduct removal).

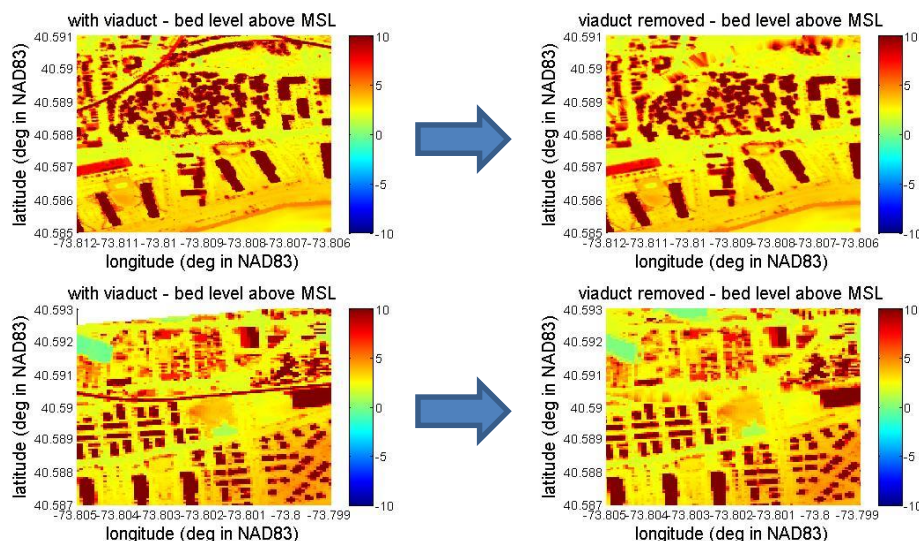


Fig VI - Two visualisation (up and below) of the removing of the railway viaduct

Seamless transitions between the layers are very important for the sake of present study. Moreover, to extract

local storm characteristics for every individual building after running the model, it is extremely important to know where the buildings are located within the grid. This is because if you know which grid cells correspond to a building, you can determine which grid cells are located directly next to the buildings which is useful for post processing purposes. The more accurate this spatial distribution is known, the more accurate local storm conditions can be determined. For a few buildings this can easily be done by looking to the depth file and expert judgement, but how to do this for thousands of buildings?

D.2.1. Building Perimeter Outlines

To answer the above posed question: a polygon dataset is used which contains the perimeter outlines of every building within the model domain. This polygon dataset has been obtained from FEMA, but is constructed by the Department of Buildings of New York City (DOB). It consists of building polygons from every single building in Queens, including the buildings within the model domain. In Fig VII the perimeter outlines of the buildings are plotted on top of a Google Maps hybrid map.

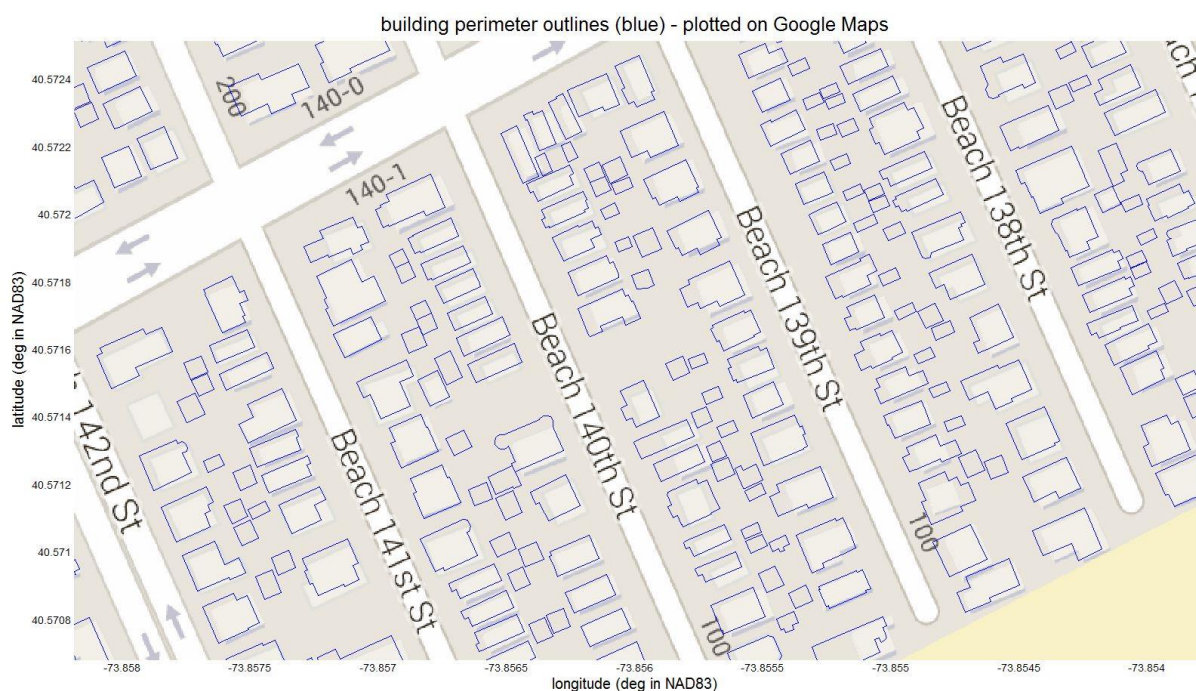


Fig VII - Building perimeter outlines of the DOB polygon dataset on top of a Google Maps layer

The polygons are very useful for post processing purposes, which are discussed in Chapter 0. However, geographical positioning of the buildings seems to match poorly with the topo-bathymetrical layers, which can be seen in Fig VIII (left). To overcome these spatial irregularities, all four LIDAR datasets are individually shifted, rotated and skewed in such a way that all buildings in the LIDAR data (recognized by peaks in the elevation) fall within their corresponding building polygons. The result is fairly good and can also be seen in Fig VIII (right) as well.

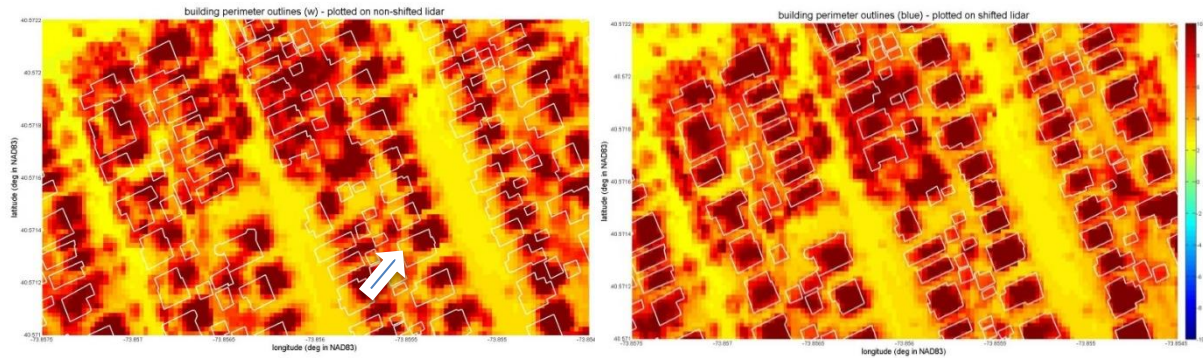


Fig VIII - Visualization of the building polygons on top of the merged topo-bathymetrical data. Left: original configuration matches poorly; right: After shifting of the topographical data a good match is obtained.

In some parts of the model domain, buildings have been removed by the post processing LIDAR routines from the surveyors or the building height is just lower than it is in reality due to blurriness. Therefore, the building perimeter outlines are used once again to raise the grid cells that fall within the polygon to a minimum building height of 7 meters above MSL, way above the maximum surge levels. The result can be seen in Fig IX.

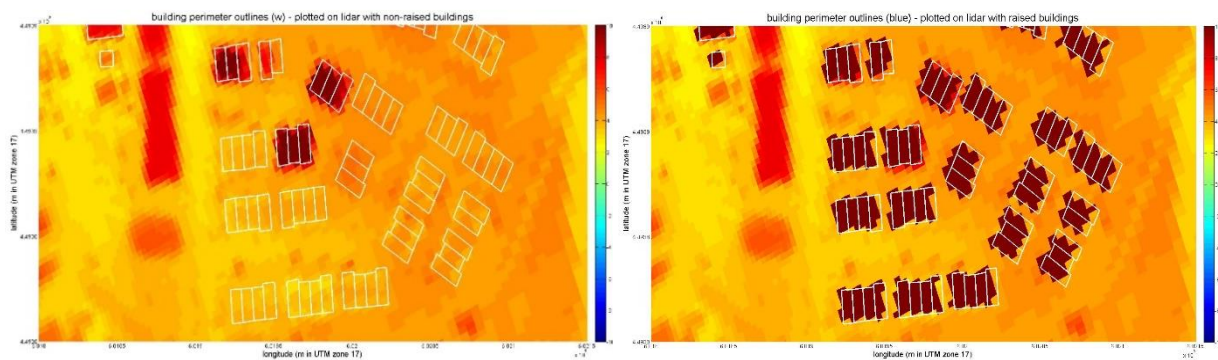


Fig IX – Visualization of the building polygons on top of the merged topo-bathymetrical data. Left: original file does not contain all buildings; right: the bathymetrical file has been raised to a minimum height of 7m above MSL.

D.2.2. Non-Erodible Layer

XBeach is designed particularly for sandy coastal systems, capable of calculating morphological impacts due to storm events to beaches, sand bars, dunes and (barrier) islands. As a default, every (vertical) obstacle in the bathymetry will be taken as a large pile of sand, subject to erosion during floods. This is also the case for buildings, while this is certainly not true in reality where (most of) the buildings will not change shape. Neglecting this will locally cause an overestimation of the erosion and therefore an unrealistic change of hydraulic properties (feedback loop in time) and will imply a change in sediment/erosion rates in the whole system.

A solution for this unwanted effect can be found in the non-erodible layer possibility within XBeach. For every grid cell one has to determine how many meters soil can be eroded away of the initial bed. Putting the erodible depth values of grid cells within building polygons to zero, these cells practically become non-erodible (sedimentation is still possible though). The erodible depth values of the other grid cells are set to 100, which is far more than the expected maximum erosion, which is in the order of a couple of meters. A visualization of the non-erodible layer is given in Fig IX.

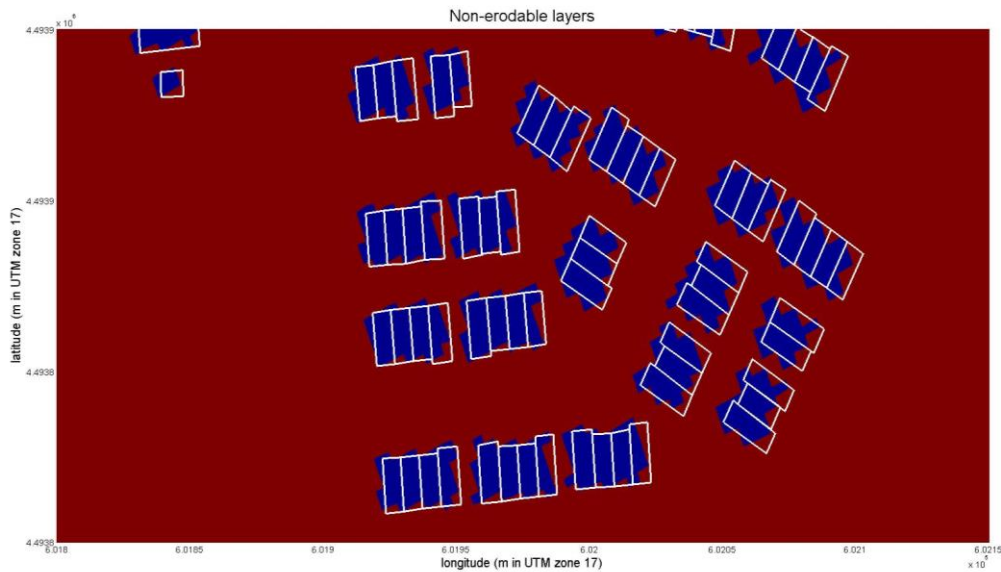


Fig X - Non-erodible layer plotted with the building perimeter outlines (white) on top of it. Blue is non-erodible, red is erodible.

It should be noted that some obstacles in the bathymetry, other than buildings, could be considered non-erodible as well. This is for instance true for strong trees. However, since trees and other but similar objects seem to be scarce within the model domain, these effects are neglected for the sake of simplicity. Moreover, one could argue that paved streets and other kinds of land usage/coverage should be non-erodible as well or at least interact differently with water flow than sand. Although the total surface of these areas is certainly not negligible, the negative effects of omitting differentiation are assumed to be small. This is true because these (urban) areas, located directly behind the beaches and dunes, mostly showed sedimentation and not erosion for the case of Hurricane Sandy.

D.3. Grid properties

Grid properties depend on multiple factors. The final grid configuration is established based on four main requirements:

- Near buildings in the area of interest the grid resolution should be dense enough to locally compute hydraulic and morphologic properties in order to sufficiently indicate local storm conditions.
- Overall the grid resolution should be dense enough to propagate long waves from the boundaries into the model domain.
- The domain should be laterally wide enough to prevent significant shadow zone effects within the area of interest.
- The offshore boundary locations should be located so deep that the assumption of deep water holds.
- The total amount of grid cells should be minimized to decrease run time and expenses.

The latter contradicts the other three requirements, which makes the process subjective to expert judgement. The following paragraphs elaborate on the choices made and with which expenses they come.

D.3.1. Domain

The configuration of XBeach models knows few degrees of freedom. In the XBeach manual (Deltares 2010) a figure of the required configuration can be seen, which is also used for present study; see Fig XI.

The coordinate reference system (CRS) is chosen to be global and has to be metric. Conversions from the locally used systems NAD83 and WGS84 have been made to the Universal Transverse Mercator (UTM) reference system. For New York City and surroundings the UTM zone corresponds to '18 T'. Moreover, the grid should be rotated with angle α to have a coastline alignment perpendicular to the Y-axis. This is fairly true with an α of 113 degrees.

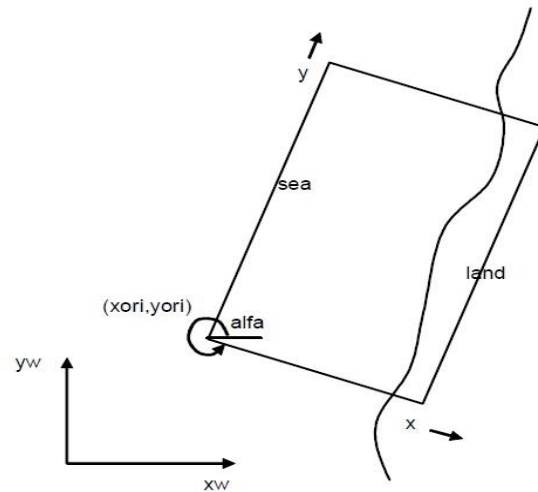


Fig XI - Normal XBeach model configuration (source: XBeach manual)

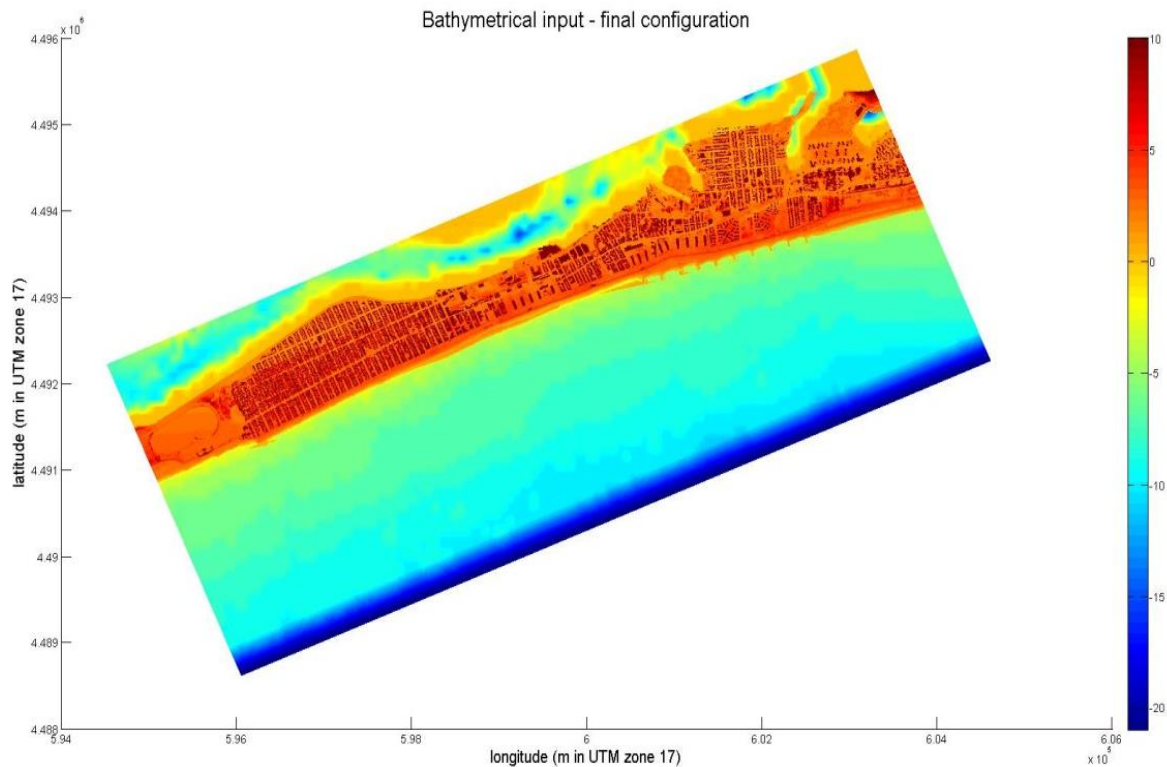


Fig XII - Visualization of the final Bathymetrical file for the XBeach model

The total model domain consists of multiple elements. First of all, the area of interest, which consists by itself of the Rockaway Peninsula, as has been discussed in chapter 2, and the associated littoral zone. This is also the impacted area by Hurricane Sandy. Secondly, a shadow zone on both sides is determined, of which the size depends on wave direction during the storm event. During Sandy the waves were mainly coming from the Southeast, which demands for a slightly larger shadow zone on the Far Rockaway side (East).

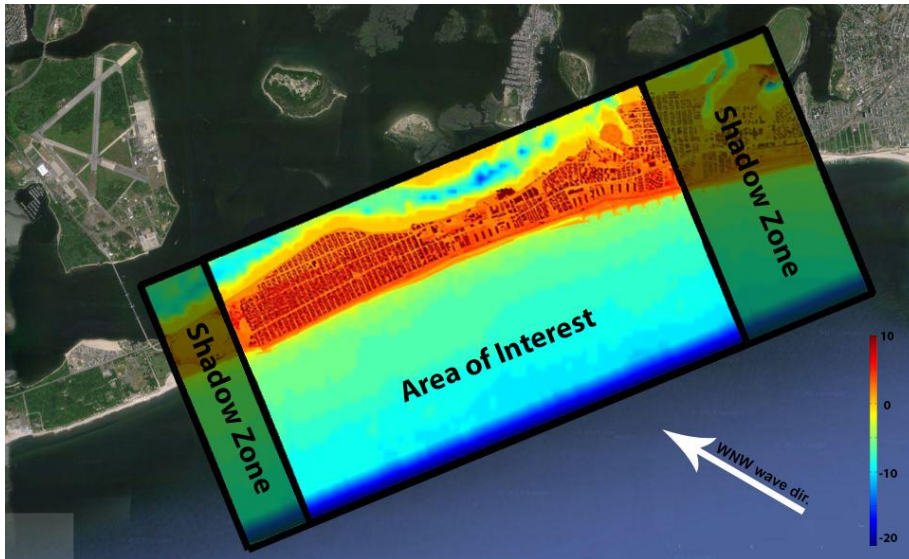


Fig XIII - The area of interest (or area of application) and shadow zones within the XBeach model domain.

Where the littoral zone ends in seaward direction is arbitrary, but it depends on the wave conditions and depth profile. With the rule of thumb $h = H_s/\gamma_b$ ⁶² with significant wave height $H_s = 10\text{m}$ and breaker index $\gamma_b = 0.6$ the depth where the littoral zone ends is estimated to be about 16m. A breaker index γ_b of 0.6 is on the safe side compared to the theoretically based value of McCowan (1894) but less conservative compared to the findings of Dally in 1985 (Nelson 1991). Moreover the domain should be extended in seaward direction to a minimum depth. As a rule of thumb⁶³ this depth is reached when

$$\frac{C_g}{C_p} = \frac{1}{2} \cdot \left(1 + \tanh^{-1}(k \cdot h) \cdot \frac{1 - (k \cdot h)^2}{k \cdot h} \right) \geq 0.8$$

With: C_g = group speed of the waves
 C_p = phase speed of the waves
 h = water depth
 k = wave number

With use of the linear wave dispersion relation, a normative wave period of 10.5 m, and some iteration, a depth of 22 meters appears to be on the save side and is therefore used. The Seaward extension is carried out with a slope of 1/50.

D.3.2. Grid density

Also the grid density is subject to the requirements posited in the beginning of this section. A higher grid density gives a higher output resolution, but everything comes with a price: computational time and expenses will increase. This has been discussed in detail in section 1.2.4.

Multiple measures have been used of in order to decrease computational expenses: smaller area of interest; smaller computational runtime; less wave bins; and (most effectively) a larger grid cell size. This was necessary, since else a minimum grid resolution of 3 x 3 m in the urban areas of interest would not be computationally feasible. In the other areas (near shore, offshore and in the shadow zones) the minimum grid size is based on the propagation of long waves, which implies a dependency on depth and normative wave periods. As a result the grid densities in X and Y direction are shown in Fig XIV.

⁶² From the book Coastal Dynamics I (Bosboom and Stive 2012)

⁶³ Based on expert judgement within Deltares

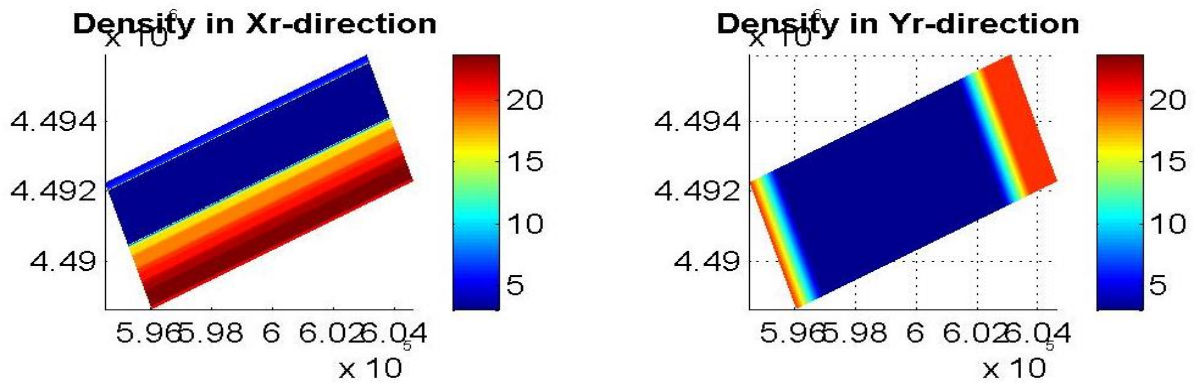


Fig XIV - Grid density. Left: in x-direction (cross-normal); right: in y-direction (along shore)

D.4. Surge

As has been discussed in the implementation section 3.2 surge levels during superstorm Sandy are extracted from the D-FlowFM model, of which some results can be found in Appendix E. The reason for using the D-FlowFM model is because it's high resolution and good prediction skills in the Jamaica Bay compared to the Delft3D - NYB model. It can be concluded that water levels are predicted fairly well with a relatively small overestimation at the storm peak; 3.2m above MSL for the predicted water level (on the offshore boundary) in comparison to the gauged water level of 3.2m above MSL (onshore), see Figure 3-19.

The predicted water levels offshore and observed onshore are thus the same, where one would expect higher onshore water levels due to wind and wave setup. The surge levels are caused by wind, piling up the water against the coast. It should be noted that wind is taken into account in the D-flowFM and Delft3D models, but is neglected within the XBeach model. The assumption implies a small underestimation during the peak in the order of 20-30cm with a fetch length of 2km, an average depth of 8m and maximum wind speeds of about 300km/h. Therefore this might imply a difference in predicted (offshore) and observed (onshore) water levels.

For both the offshore and bay side boundaries one time series of surge levels is used. It should be noted that XBeach gives the opportunity of working with two series per boundary (on every corner one, so four in total), which is in general preferable with relatively large domains. The boundary conditions are then interpolated for every grid cell on the boundary (y-direction). However, when using this option, water levels exploded within the domain after a few hours computational time for no particular reason. This is why I chose for only one boundary per side, since that appeared to be stable on the contrary. This simplification has no further disadvantages for present study, since water levels at both corners were pretty much the same for the case of Sandy, see Fig XV.

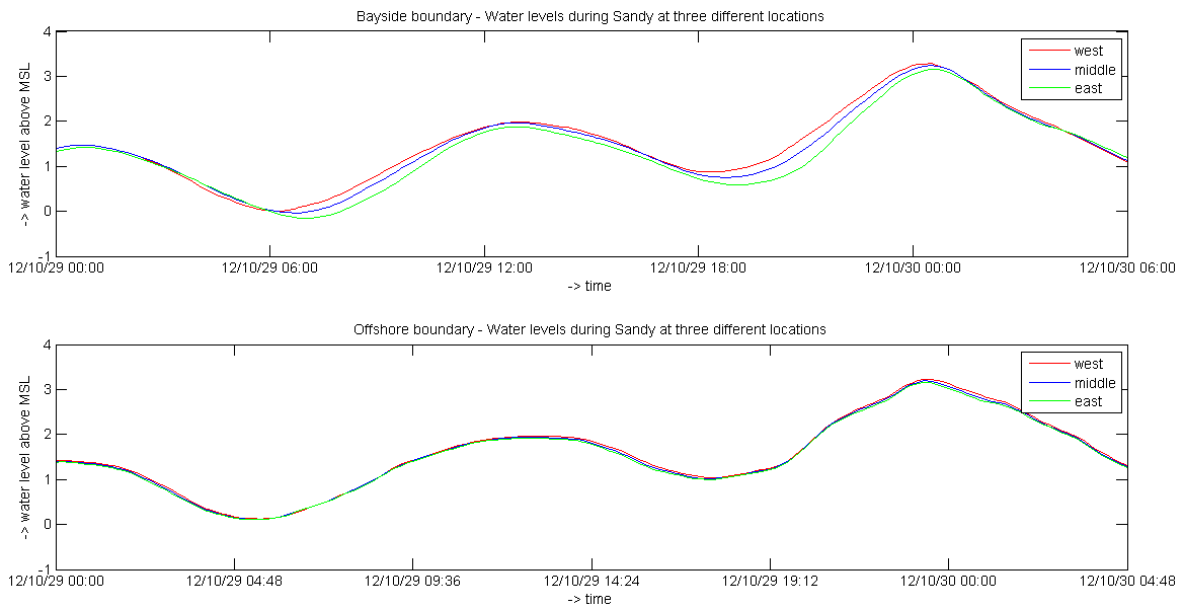


Fig XV - Alongshore variation in water level at the boundary locations. Upper panel: Bay side; lower panel: offshore

D.5. Waves

Comparable to the water level boundary conditions, wave boundary conditions have been extracted from another model in which Xbeach is nested. The wave conditions are coming from the Delft3D - NYB model as has been discussed in subsection 3.2.1. The Delft3D runs were executed parallel with SWAN and every half hour 2D energy wave spectra have been produced for the offshore boundary. Xbeach is capable of handling the associated '.sp2' files as input. A visualization of such a wave spectrum is given in Fig XVI.

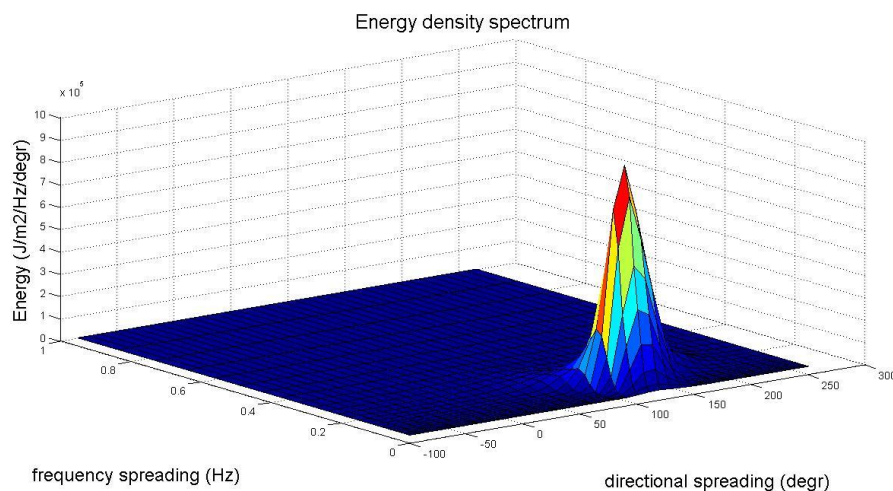


Fig XVI - Energy density spectrum produced by SWAN during the peak of the storm

Wave conditions are imposed only at the offshore boundary and not on the bay side boundary. It is assumed that waves are relatively small in the bay, due to the shallowness of the bay (bottom friction absorbs wave energy) and the fact that it is sheltered by the Rockaway Peninsula.

Comparison predictions and buoy – Based on the 2D spectra, significant wave height H_s and significant wave period T_{m01} can be determined. Both have been done for hurricane Sandy at the exact same location as

NOAA's buoy 44065. A comparison can be found in Fig XVII.

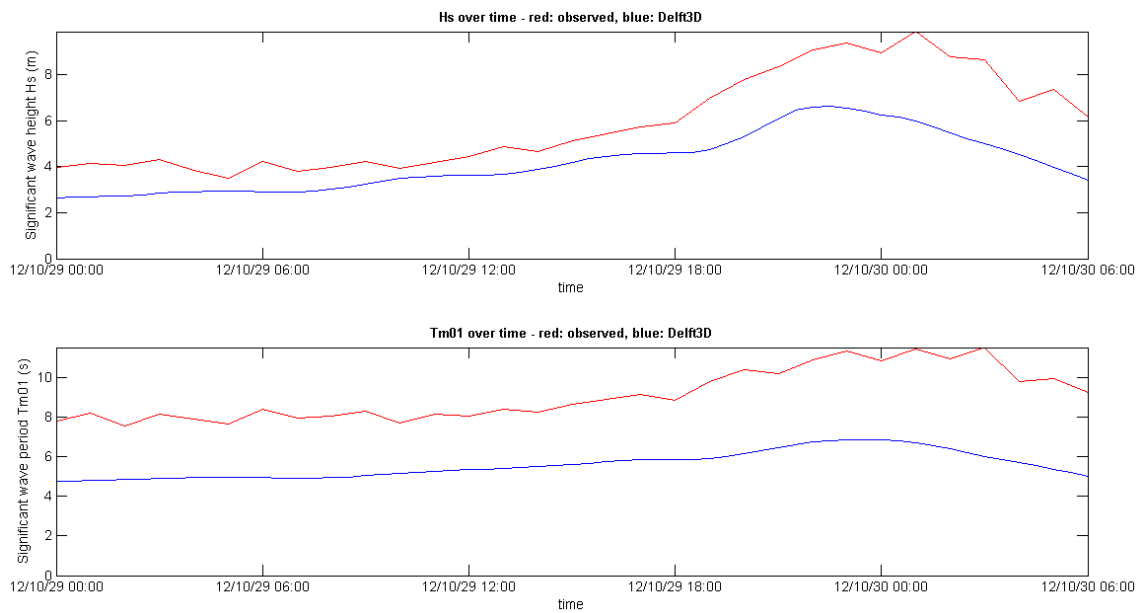


Fig XVII - Wave properties significant wave height (upper) and significant wave period (lower panel) during the storm at the offshore boundary. Red: observed; blue: modelled with Delft3D

It can be seen that Delft3D/SWAN underestimates the significant wave height with a factor 1.6 during the storm peak and a factor 1.4 for the significant wave period. This is a significant underestimation and no particular reason has been found yet. However, it is certainly not negligible and two solutions have been proposed:

1. Improve: this implies a change in whitecapping formulations and coefficients. Larger wind speeds are not preferred, since water level predictions have been proved to be fairly good.
2. Compensate: increasing of the energy in the 2D wave spectra so that H_s and T_{m01} are linearly scaled with a factor 1.6 and 1.4 respectively.

Three different whitecapping formulations within SWAN, knowing van der Westhuysen, Komen and Rogers (see also the XBeach manual), have been tried and all gave comparably results. This is why option two has been chosen, of which the result can be seen in Fig XVIII.

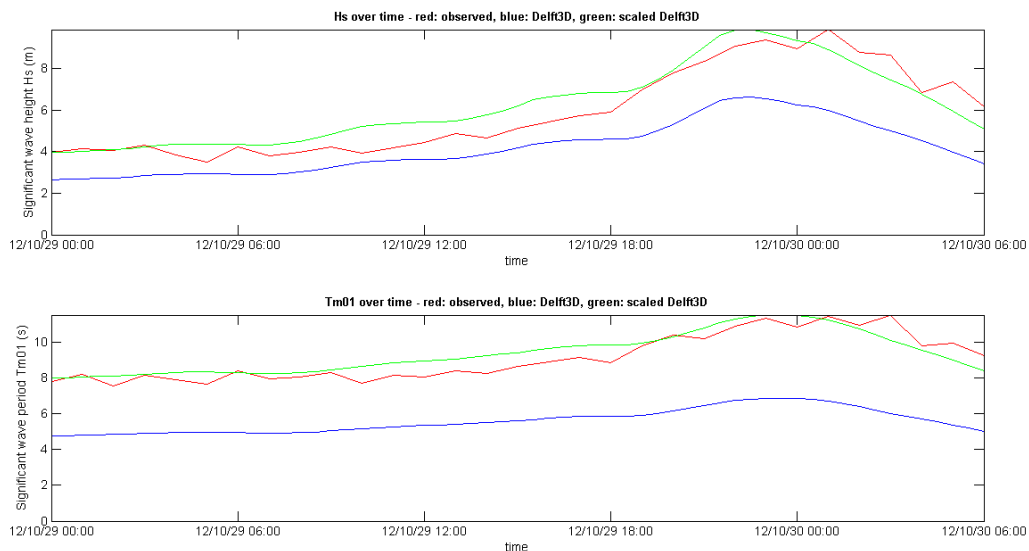


Fig XVIII- Wave properties significant wave height (upper) and significant wave period (lower panel) during the storm at the offshore boundary. Red: observed; blue: non-scaled simulation with Delft3D; green: scaled simulation

Next to the scaled prediction and observation of the significant wave heights and periods at Buoy 44605, another graph is added, which presents the scaled prediction at the boundary location. It should be noted that due to the linearity of the scaling process storm conditions are probably slightly overestimated at the tails of the storm. The effects to total damage and morphological changes of this overestimation are assumed to be small, since most of the damage will be caused by the peak. Therefore these effects are neglected.

In Fig XIX significant wave height and period are graphed for both offshore corners. No large alongshore variations in wave conditions are observed and this is why only one time series of sp2 files is used. This is in analogy with the imposed water level boundaries (appendix D.4).

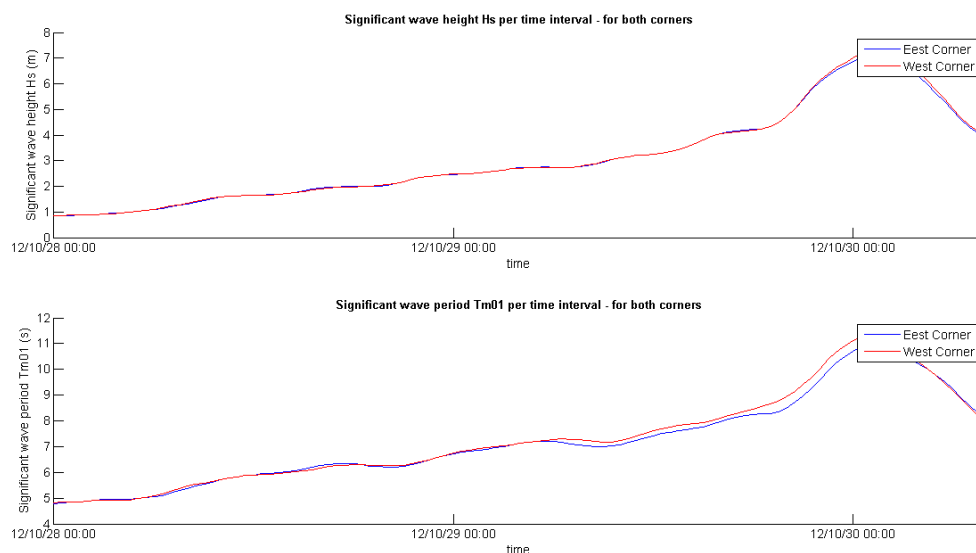


Fig XIX - Wave properties significant wave height (upper) and significant wave period (lower panel) during the storm at the two offshore model domain corners

During the scaling of the '.sp2' files the shape of the wave spectra has not been changed. This is very important, because the directional spreading is assumed to be modeled correctly. In Fig XX the energy density spectrum over time and wave direction during the storm is displayed. Directions are in degrees and nautical oriented. An

upper and lower bound is given (red) between which 90% of the energy is situated, together with the dominant wave direction.

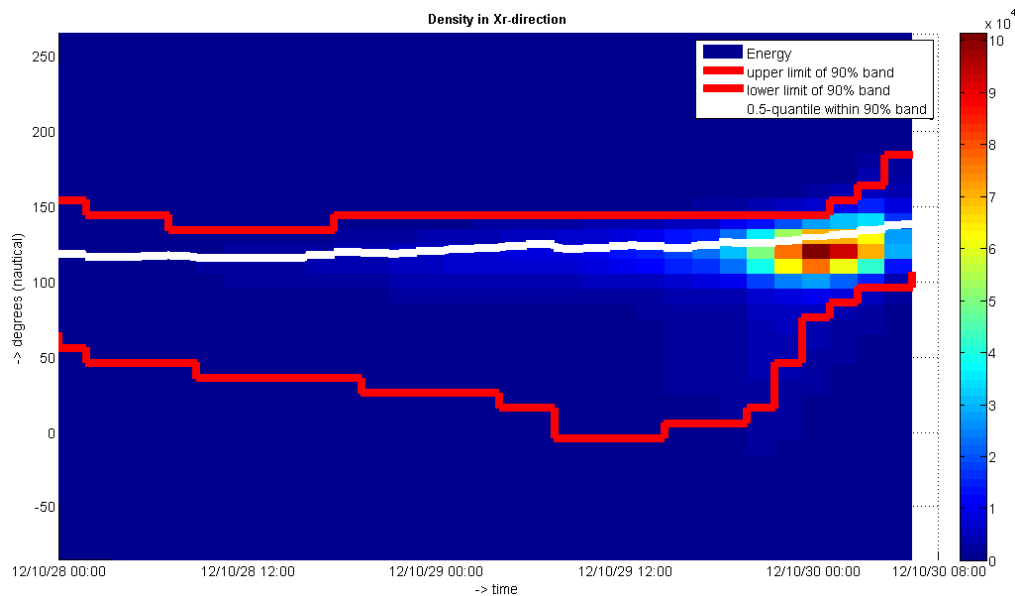


Fig XX - Energy per wave direction bin (10 degrees per bin) during hurricane Sandy. Between the red lines 90% of the energy is situated.

During Sandy the dominant wave direction slightly changed from 120 to 140 nautical degrees, which correspond both more or less to winds coming from the South-East. The two 90% energy-limits provide bounds for the XBeach simulation. At any time during the whole simulation more than 90% of the wave energy is found between -10 and 190 nautical degrees.

Moreover, it should be noted that all energy above 250 and below 70 degrees is oriented offshore and will never reach a normal straight coast, which is the case for present study. This gives two limits, between which most of the effective energy lays, knowing 70 and 190 degrees; see Fig XXI. Xbeach solves numerical computations for every predefined wave bin and with wave bin of 20 degrees (based on expert judgment) six wave bins are used, instead of nine (180/2). This implies a saving of computational expenses in the order of 33%.

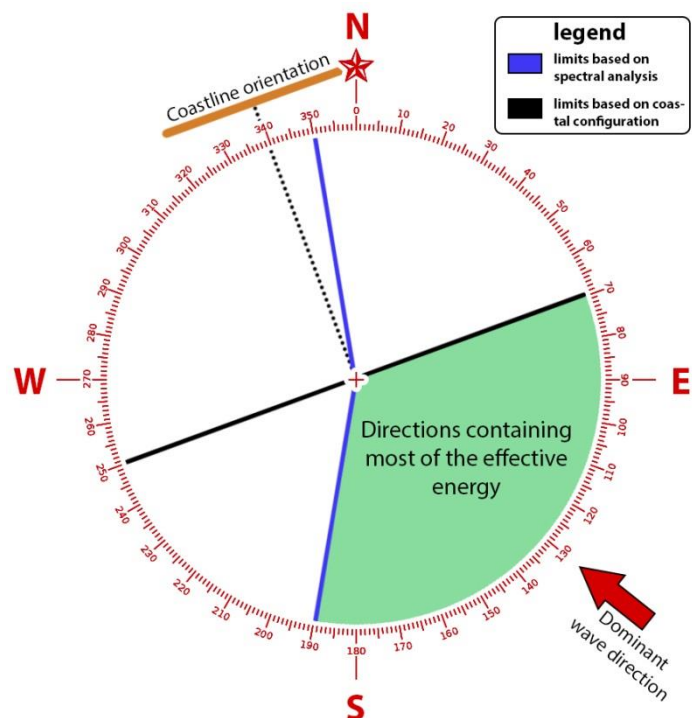


Fig XXI - Determining effective wave directions

D.6. Input parameters

Additional model input, different from everything discussed above, is given in this paragraph. Morphological

parameters and sediment roughness coefficients are chosen XBeach default. This implies a Chezy roughness coefficient of 0.17, based on a flow friction coefficient (cf) of 0.003 and $C = \sqrt{g/cf}$. Comparable values have been used in the Delft3D and D-flowFM models. A morphological factor ‘Morfac’ of 10 is used to speed up the process, which means that bed level changes are once in 10 time steps computed. This is another way to reduce computations expenses (Deltares 2010). In Fig XXII a scatter plot of the morphological change is given between two identical runs except for the morphological factor. One has a factor of 10, the other one of 1. There are definitely differences in bed level change; especially on the horizontal and vertical axes of the scatter plot strange results can be found (see red arrows). These differences can be explained by unnatural sedimentation/erosion spots offshore and in the shadow zone (see red circles). However, for the majority of the onshore cells (with colors corresponding to 0 or higher in the scatter plot) the results are pretty much equal. Therefore, a morphological factor of ten seems to be justifiable⁶⁴.

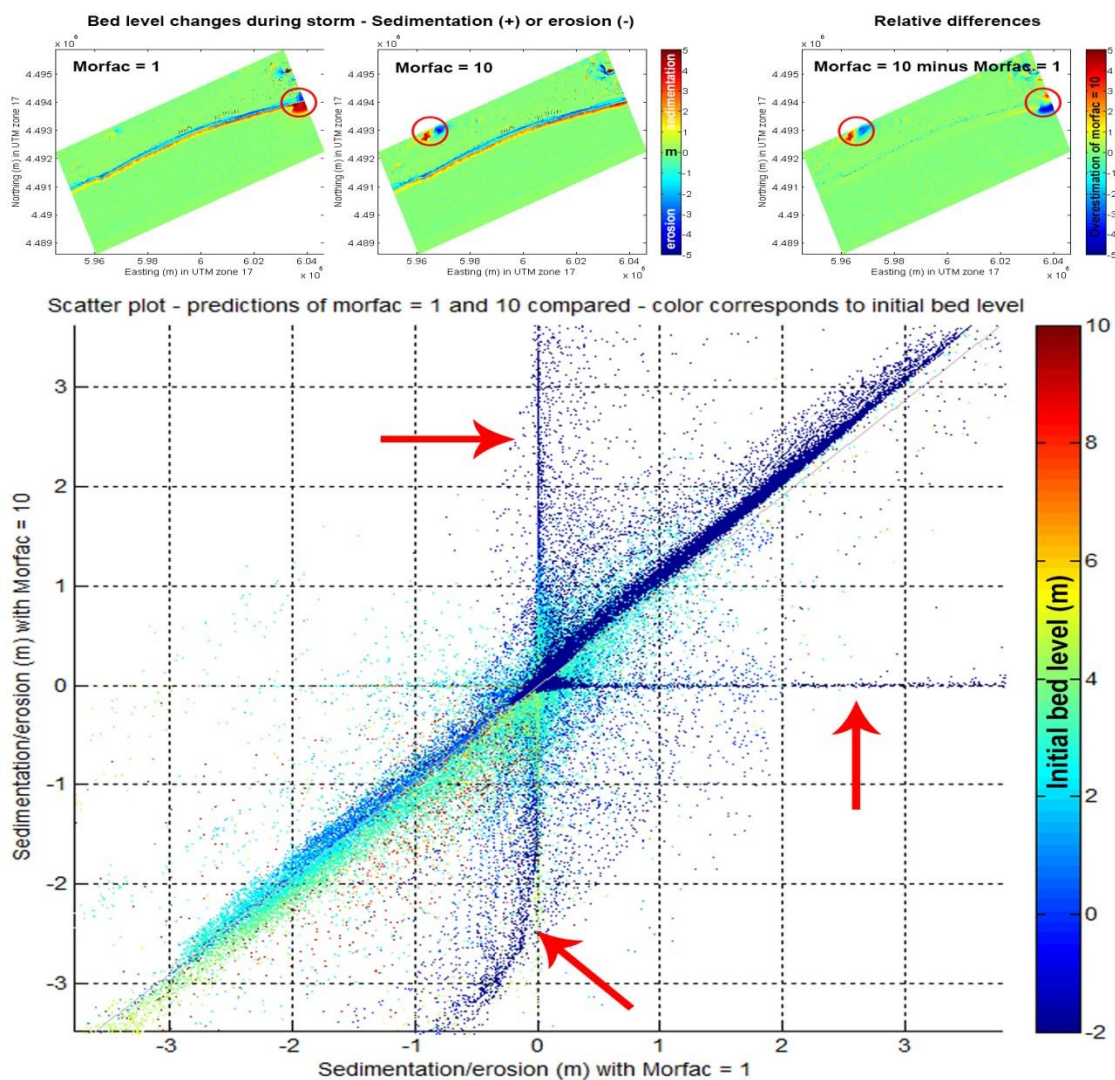


Fig XXII - upper panels: absolute and relative bed level changes; lower panel: scatter plot - morfac 1 vs morfac = 10

Since XBeach’s numerical schemes are explicit, the time step depends on the Courant–Friedrichs–Lewy (CFL) condition, knowing:

$$C = \frac{u \cdot \Delta t}{\Delta x} \leq C_{max}$$

⁶⁴ It is not excluded that with other grid cell properties the differences will be larger (or smaller).

With:

C	=	Courant number
u	=	Velocity
Δt	=	Time step
Δx	=	One-dimensional grid dimension
C_{\max}	=	Maximum Courant Number

The default in Xbeach for the maximum courant number is chosen to be 0.7 instead of the absolute max of 1 as criterion for stability. Output however is not derived for every time step, but every 10min for global variables and every 30min for mean variables. The desired output variables depend on their use for the Bayesian Network and are therefore elaborated in the implementation section 3.2.

E. Delft3D and D-Flow FM model set-up

E.1. Delft3D - US East Coast model

MDW file

```
[WaveFileInformation]
FileVersion = 02.00

[General]
OnlyInputVerify = false
SimMode = non-stationary
TimeStep = 30-
DirConvention = nautical
ReferenceDate = 2012-01-01
TimePoint = 0.000000e+00
WaterLevel = 0.000000e+00
XVeloc = 0.000000e+00
YVeloc = 0.000000e+00
WindSpeed = 0.000000e+00
WindDir = 0.000000e+00

[Constants]
Gravity = 9.810000e+00
WaterDensity = 1.000000e+03
NorthDir = 9.000000e+01
MinimumDepth = 5.000000e-02

[Processes]
GenModePhys = 3
WaveSetup = false
Breaking = true
BreakAlpha = 1.000000e+00
BreakGamma = 8.000000e-01
Triads = false
TriadsAlpha = 1.000000e-01
TriadsBeta = 2.200000e+00
BedFriction = jonswap
BedFricCoef = 6.700000e-02
Diffraction = false
WindGrowth = true
WhiteCapping = Komen
Quadruplets = true
Refraction = true
FreqShift = true
WaveForces = radiation stresses

[Numerics]
DirSpaceCDD = 5.000000e-01
FreqSpaceCSS = 5.000000e-01
RChHS_Tm01 = 2.000000e-02
RChMeanHS = 2.000000e-02
RChMeanTm01 = 2.000000e-02
PercWet = 9.000000e+01
MaxIter = 5

[Output]
TestOutputLevel = 0
TraceCalls = false
UseHotFile = true
MapWriteInterval = 6.000000e+01
WriteCOM = true
COMWriteInterval = 3.000000e+01
Int2KeepHotfile = 7.200000e+02
AppendCOM = false
LocationFile = nyc.loc
WriteTable = false
WriteSpec1D = false
WriteSpec2D = true

[Domain]
Grid = usn_swn.grd
BedLevelGrid = usn_swn.grd
BedLevel = usn_swn.dep
DirSpace = circle
NDir = 36
StartDir = 0.000000e+00
EndDir = 3.600000e+02
NFreq = 24
FreqMin = 5.000000e-02
FreqMax = 1.000000e+00
FlowBedLevel = 1
FlowWaterLevel = 1
FlowVelocity = 1
FlowWind = 1
Output = 1
```

MDF file

```
Ident = #Delft3D-FLOW .03.02 3.39.26#
Filcco = #usn.grd#
Fmccco = #FR#
Grdang = 0.000000e+00
Filgrd = #usn.enc#
Fmtgrd = #FR#
MNKmax = 300 232 1
Thick = 1.000000e+02
Fildep = #usn.dep#
Fmtdep = #FR#
ltdate = #2012-01-01#
Tunit = #M#
Tstart = 4.248000e+05
Tstop = 4.367700e+05
Dt = 5.000000e+00
Tzone = 0
Sub1 = # W #
Sub2 = # W#
Wnsvwp = #Y#
Wndint = #Y#
Filwu = #ncep_nam_sandy.amu#
Filwv = #ncep_nam_sandy.amv#
Filwp = #ncep_nam_sandy.amp#
Zeta0 = 0.000000e+00
U0 = []
V0 = []
Filbnd = #usn_wl.bnd#
Fmbnd = #FR#
Filana = #usn_wl.bca#
Fmтана = #FR#
Ag = 9.810000e+00
Rhow = 1.000000e+03
Alph0 = []
Tempw = 1.500000e+01
Salw = 3.100000e+01
Rouwav = # #
Wstres = 1.000000e-03 0.000000e+00 3.000000e-03
Rhoa = 3.000000e+01 1.500000e-03 5.000000e+01
Betac = 1.000000e+00
Equill = 5.000000e-01
Tkernod = #Y#
Ktemp = # #
Fciou = 0
Sarea = 0.000000e+00
Temint = 0.000000e+00
Roumet = #Y#
Ccofu = #M#
Ccofv = 2.000000e-02
Xlo = 2.000000e-02
Vicouv = 0.000000e+00
Dicouv = 1.000000e+00
Htur2d = #N#
Irov = 0
Iter = 2
Dryflp = #YES#
Dpsopt = #MEAN#
Dpuopt = #MEAN#
Dryflc = 1.000000e-01
Dco = -9.990000e+02
Tlsmo = 6.000000e+01
TheqH = 0.000000e+00
Forfuv = #N#
Forfw = #N#
Sigcor = #N#
Trasol = #Cyclic-method#
Momsol = #Cyclic#
Filsta = #usn.obs#
Fmsta = #FR#
SMhydr = #YYYYY#
SMderv = #YYYYY#
SMproc = #YYYYYYYYY#
PMhydr = #YYYYY#
PMderv = #YYYYY#
PMproc = #YYYYYYYYY#
SHhydr = #YYYYY#
SHderv = #YYYYY#
SHproc = #YYYYYYYYY#
SHflux = #YYYYY#
PHhydr = #YYYYY#
PHderv = #YYY#
PHproc = #YYYYYYYYY#
PHflux = #YYYYY#
Online = #N#
Waqmod = #N#
WaveOL = #Y#
Prhis = 0.000000e+00 0.000000e+00 0.000000e+00
Filmap = 4.248000e+05 3.000000e+01 4.367700e+05
Flhis = 4.248000e+05 1.000000e+01 4.367700e+05
Flgp = 4.248000e+05 3.000000e+01 4.367700e+05
First = 0.000000e+00
AirOut = #Y#
Pavbnd = 1.020000e+05
WaveOL = #Y#
```

E.2. Delft3D – New York Bight model

MDW file

```
[WaveFileInformation]
FileVersion = 02.00

[General]
OnlyInputVerify = simulation run
SimMode = non-stationary
TimeStep = 30-
DirConvention = nautical
ReferenceDate = 2012-01-01
TimePoint = 0.0000000e+00
WaterLevel = 0.0000000e+00
XVeloc = 0.0000000e+00
YVeloc = 0.0000000e+00
WindSpeed = 0.0000000e+00
WindDir = 0.0000000e+00

[Constants]
Gravity = 9.8100000e+00
WaterDensity = 1.0000000e+03
NorthDir = 9.0000000e+01
MinimumDepth = 5.0000000e-02

[Processes]
GenModePhys = 3
WaveSetup = false
Breaking = true
BreakAlpha = 1.0000000e+00
BreakGamma = 8.0000000e-01
Triads = false
TriadsAlpha = 1.0000000e-01
TriadsBeta = 2.2000000e+00
BedFriction = jonswap
BedFricCoef = 6.7000000e-02
Diffraction = false
WindGrowth = true
WhiteCapping = Komen
Quadruplets = true
Refraction = true
FreqShift = true
WaveForces = dissipation

[Numerics]
DirSpaceCDD = 5.0000000e-01
FreqSpaceCSS = 5.0000000e-01
RCHsTm01 = 2.0000000e-02
RCHMeanHs = 2.0000000e-02
RCHMeanTm01 = 2.0000000e-02
PercWet = 9.0000000e+01
MaxIter = 5

[Output]
TestOutputLevel = 0
TraceCalls = false
UseHotFile = true
MapWriteInterval = 3.0000000e+01
WriteCOM = true
COMWriteInterval = 3.0000000e+01
Int2KeepHotfile = 7.2000000e+02
AppendCOM = false
LocationFile = list.loc
WriteTable = false
WriteSpec1D = false
WriteSpec2D = true

[Domain]
Grid = nyc_swn.grd
BedLevelGrid = nyc_swn.grd
BedLevel = nyc_swn.dep
DirSpace = circle
NDir = 36
StartDir = 0.0000000e+00
EndDir = 3.6000000e+02
NFreq = 24
FreqMin = 5.0000000e-02
FreqMax = 1.0000000e+00
FlowBedLevel = 1
FlowWaterLevel = 1
FlowVelocity = 1
FlowWind = 1
Output = 1

[Boundary]
Name = nyc.sp2
Definition = fromsp2file
OverallSpecFile = nyc.sp2
```


E.3. D-Flow FM – New York Bight model

MDU file

```

# Generated on 15:35:20, 10-10-2013
# Deltares, D-Flow FM Version 1.1.54.24756, Nov 08 2012, 02:02:12

[model]
Program           =          D-Flow FM
Version           =          1.1.90.31666
AutoStart        =          0                # Autostart simulation after loading MDU or not (0=no, 1=autostart, 2=autostartstop).

[geometry]
NetFile          =          newyork_net.nc    # *.net.nc
BathymetryFile  =          # *.xyb
WaterLevIniFile =          # Initial water levels sample file *.xyz
LandBoundaryFile =          # Only for plotting
ThinDamFile     =          # *.thd.pli, Polyline(s) for tracing thin dams.
ThindykeFile   =          # *.tdk.pli, Polyline(s) x,y,z, z = thin dyke top levels
ProflocFile    =          # *.proflocation.xyz x,y,z, z = profile refnumber
ProfdefFile    =          # *.profdefinition.def definition for all profile nrs
ManholeFile    =          # ...
WaterLevIni    =          0                # Initial water level
BotLevIni      =          -5.              # Uniform bottom level, (only if Botlevtype>=3, used at missing z values in netfile
BotLevType     =          3                # 1 : Bottom levels at waterlevel cells (=flow nodes), like tiles xz, yz, bl, bob = max(bl left, bl right)
                                           # 2 : Bottom levels at velocity points (=flow links), xu, yu, blu, bob = blu, bl = lowest connected link
                                           # 3 : Bottom levels at velocity points (=flow links), using mean network levels xk, yk, zk bl = lowest connected link
                                           # 4 : Bottom levels at velocity points (=flow links), using min network levels xk, yk, zk bl = lowest connected link
                                           # 5 : Bottom levels at velocity points (=flow links), using max network levels xk, yk, zk bl = lowest connected link
PartitionFile  =          # *.part.pol, polyline(s) x,y
AngleLat       =          30.              # Angle of latitude (deg), 0=no Coriolis
Conveyance2D  =          3                # -1:R=HU,0:R=H, 1:R=A/P, 2:K=analytic-1D conv, 3:K=analytic-2D conv

[numerics]
CFLMax         =          0.7              # Max. Courant nr.
CFLWaveFrac   =          0.1              # Wave velocity fraction, total courant vel = u + cflw*wavevelocity
AdvectType     =          3                # Adv type, 0=no, 1= Wenneker, qu-udzt, 2=1, q(uiu-u), 3=Perot q(uiu-u), 4=Perot q(ui-u) without itself
Limtyprom     =          4                # Limiter type for cell center advection velocity, 0=no, 1=minmod,2=vanLeer,3=Kooren,4=Monotone Central
Limtypsa      =          4                # Limiter type for salinity transport, 0=no, 1=minmod,2=vanLeer,3=Kooren,4=Monotone Central
Icgsolver     =          1                # Solver type , 1 = sobekGS_OMP, 2 = sobekGS_OMPthreadsafe, 3 = sobekGS, 4 = sobekGS + Saadilud
Hdam          =          0                # Threshold for minimum bottomlevel step at which to apply energy conservation factor i.c. flow contraction

[physics]
UnifFricCoef  =          65.              # Uniform friction coefficient, 0=no friction
UnifFricType  =          0                # 0=Chezy, 1=Manning, 2=White Colebrook, 3=z0 etc
Vicuov       =          1.                # Uniform horizontal eddy viscosity
Smagorinsky  =          0.                # Add Smagorinsky horizontal turbulence : vicu = vicu + ((Smagorinsky*dx)**2)*S, e.g. 0.1
Elder        =          0.                # Add Elder contribution : vicu = vicu + Elder*kappa*ustar*H/6), e.g. 1.0
irov         =          0.                # 0=free slip, 1 = partial slip using wall_ks
wall_ks     =          0.                # Nikuradse roughness for side walls, wall_z0=wall_ks/30
Vicuov      =          0.                # Uniform vertical eddy viscosity
TidalForcing =          1                # Tidal forcing (0=no, 1=yes) (only for jsferic == 1)
Salinity     =          0                # Include salinity, (0=no, 1=yes)

[wind]
ICdtyp       =          3                # ( ), Cd = const, 2=S&B 2 breakpoints, 3= S&B 3 breakpoints
Cdbreakpoints =          1.0000000e-02 3.0000000e-03 1.5000000e-03
Windspeedbreakpoints =          0.0000000e+00 2.5000000e+01 5.0000000e+01
                                           # (m/s), e.g. 0.0 100.0

[time]
RefDate      =          20120101          # Reference date (yyyymmdd)
Tunit       =          #M#               # Time units in MDU (H, M or S)
DtUser     =          300.               # User timestep in seconds (interval for external forcing update & his/map output)
DtMax      =          30.                # Max timestep in seconds
DtInit     =          1.                 # Initial timestep in seconds
AutoTimestep =          0                # Use CFL timestep limit or not (1/0)
TStart    =          4.2912000e+05       # Start time w.r.t. RefDate (in TUnit)
TStop     =          4.3677000e+05       # Stop time w.r.t. RefDate (in TUnit)

[restart]
RestartFile =          # Restart file, only map, hence: *.map.nc
RestartTime =          20020101000000    # Restart time (yyyymmddhhmmss)

[external forcing]
ExtForceFile =          boundaries.ext    # *.ext

[output]
ObsFile     =          newyork.xyn       # *.xyn Coords+name of observation stations.
CrsFile     =          # *.crs.pli Polyline(s) defining cross section(s).
HisFile     =          # *.his.nc History file in NetCDF format.
HisInterval =          600.              # Interval (s) between history outputs
XLSInterval =          0.                # Interval (s) between XLS history
FlowGeomFile =          1200.            # *.flowgeom.nc Flow geometry file in NetCDF format.
MapFile     =          # *.map.nc Map file in NetCDF format.
MapInterval =          3600.             # Interval (s) between map file outputs
RstInterval =          0.                # Interval (s) between map file outputs
WaqFileBase =          run               # Basename (without extension) for all Delwaq files to be written.
WaqInterval =          0.                # Interval (in s) between Delwaq file outputs
StatsInterval =          0.              # Interval (in s) between simulation statistics output.
SnapshotDir =          # Directory where snapshots/screendumps are saved.

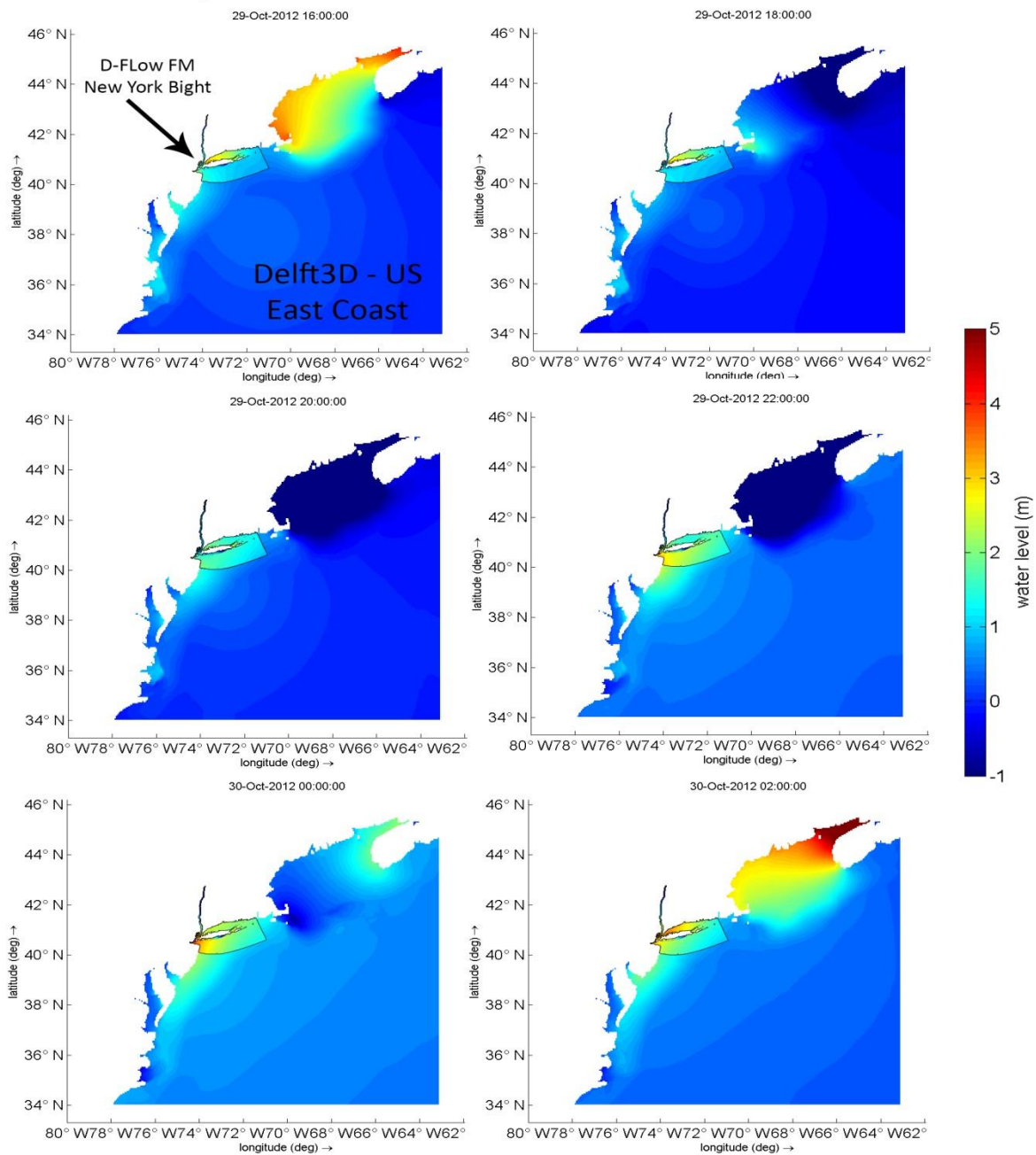
```

F. Delft3D and D-Flow FM model results

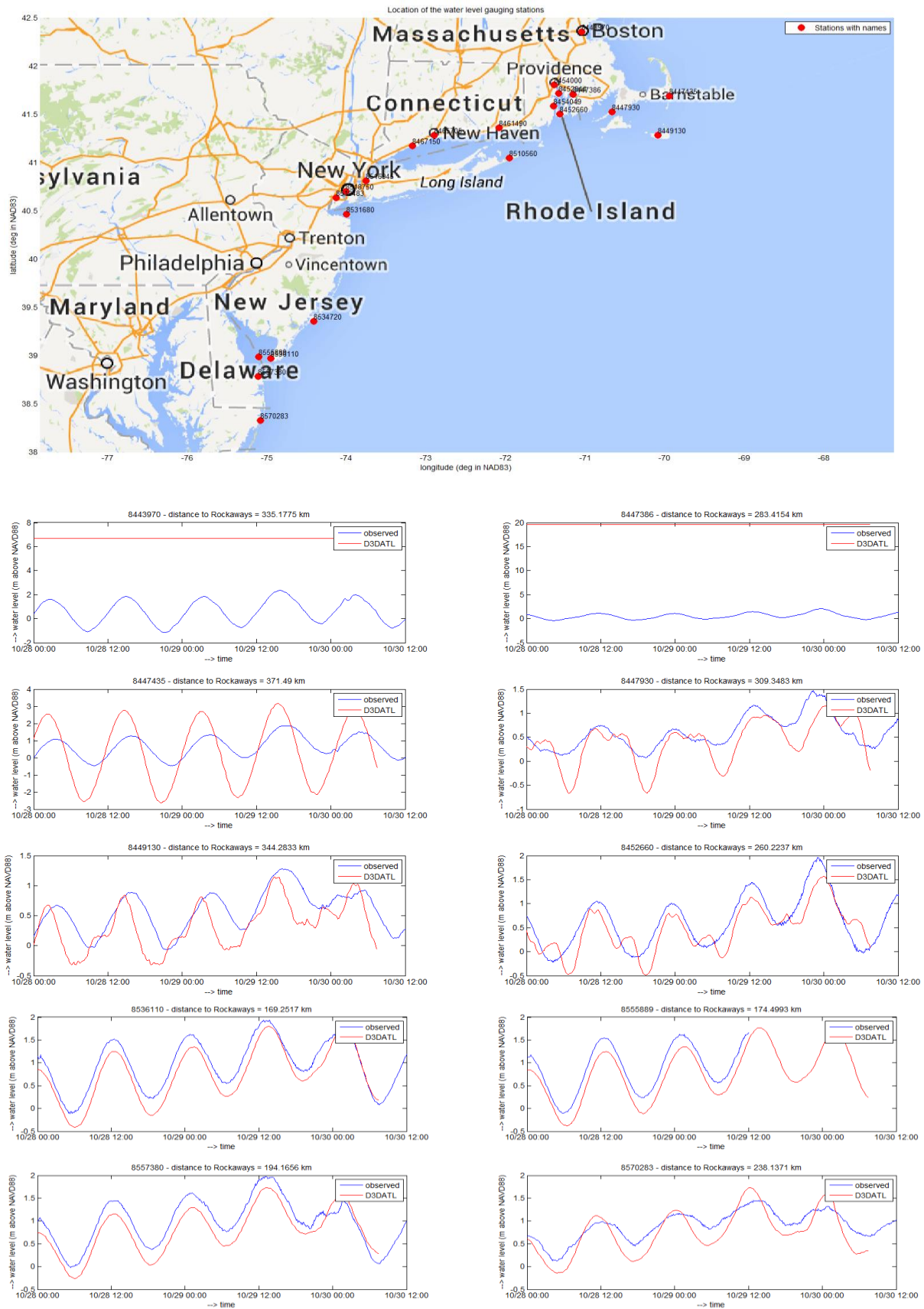
In this appendix some results of the Delft3D and D-Flow FM models are given, considering the propagation of wave information and surge. This is in addition to the brief descriptions of the models in paragraph 0. First the propagation of storm tide (surge + astronomical tide) is graphed in space by using a few snapshots. This is followed by a comparison of the simulated storm tide to the observations of water level gauging stations. Subsequently the same is done for waves by considering the significant wave height and peak wave period. It must be said that no conclusions about the results are drawn here.

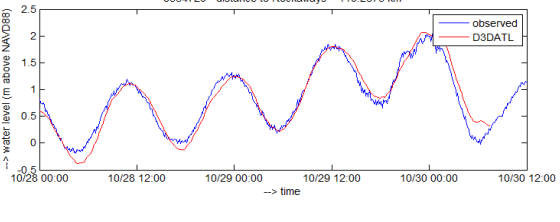
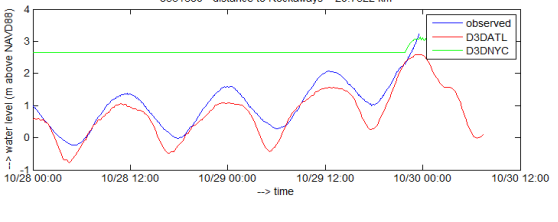
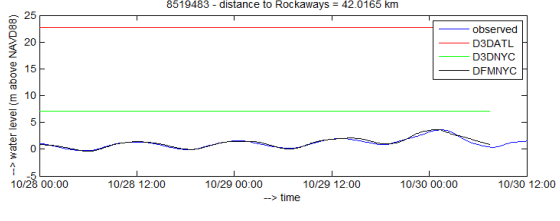
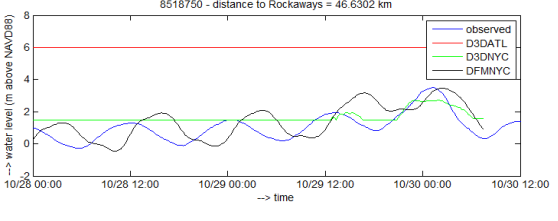
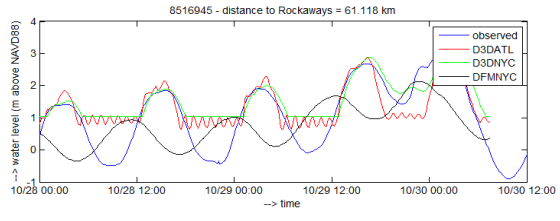
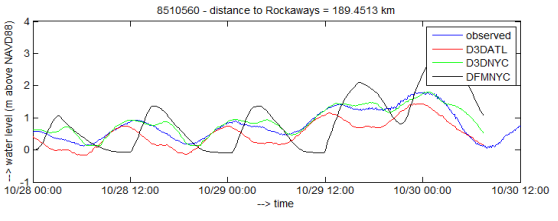
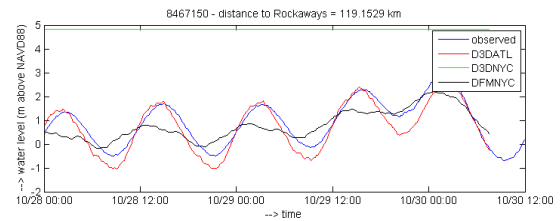
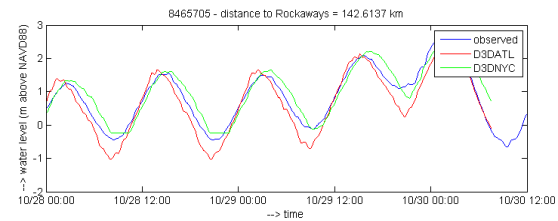
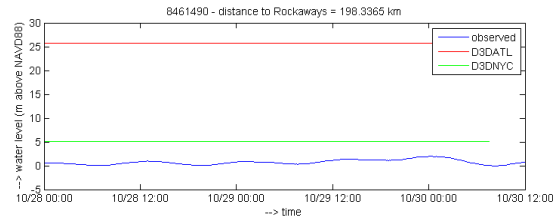
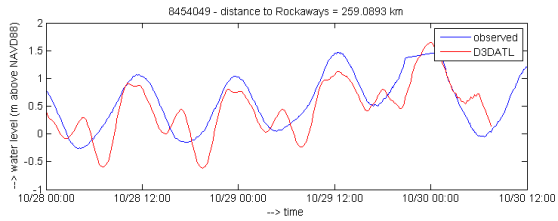
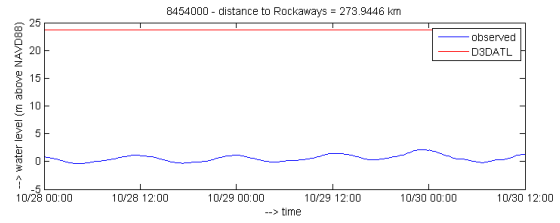
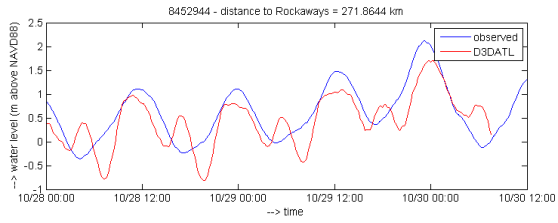
F.1. Storm Tide Propagation

Spatial Visualization of the Simulated Storm Tides



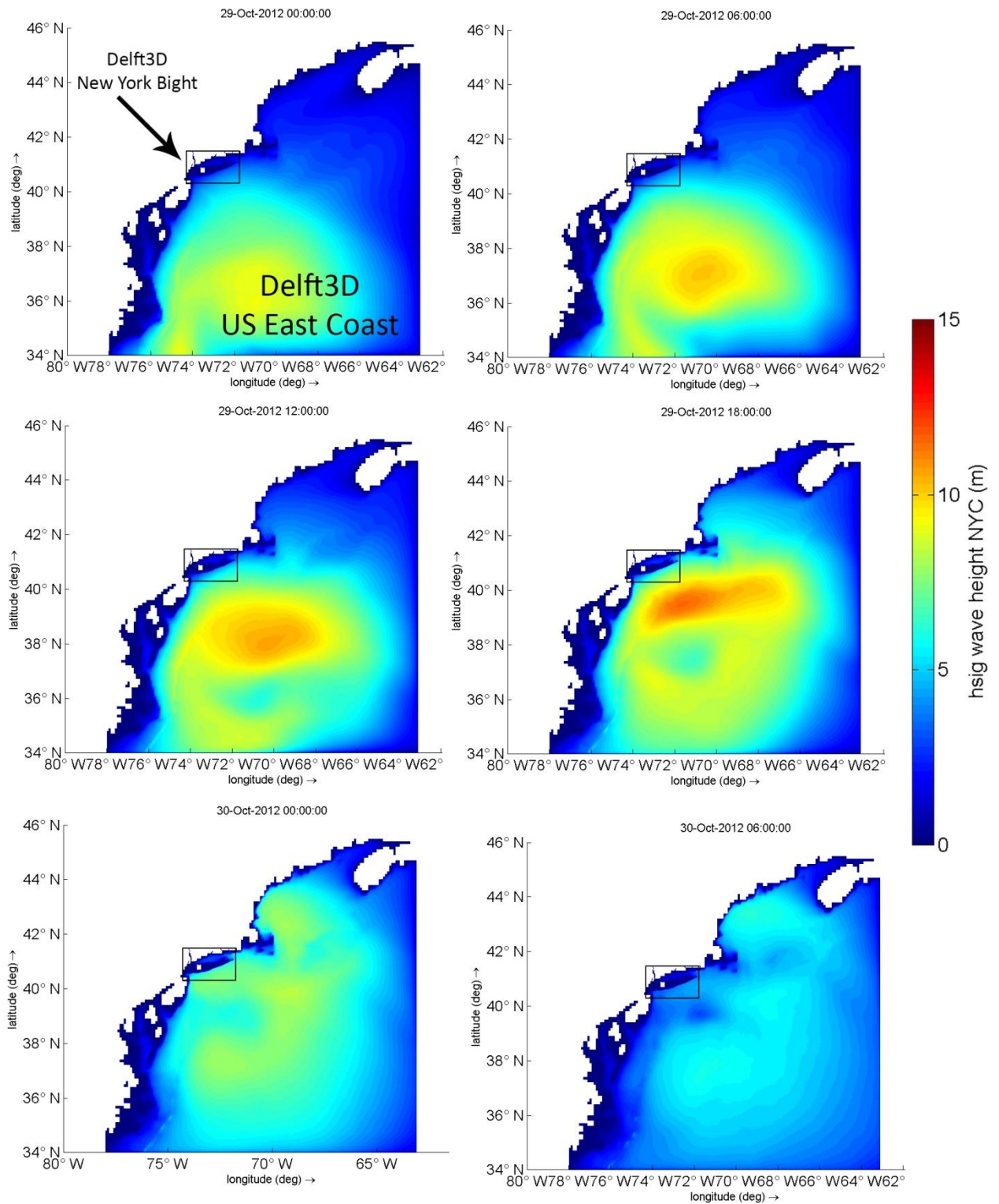
F.2. Storm Tide- Observed versus Simulated



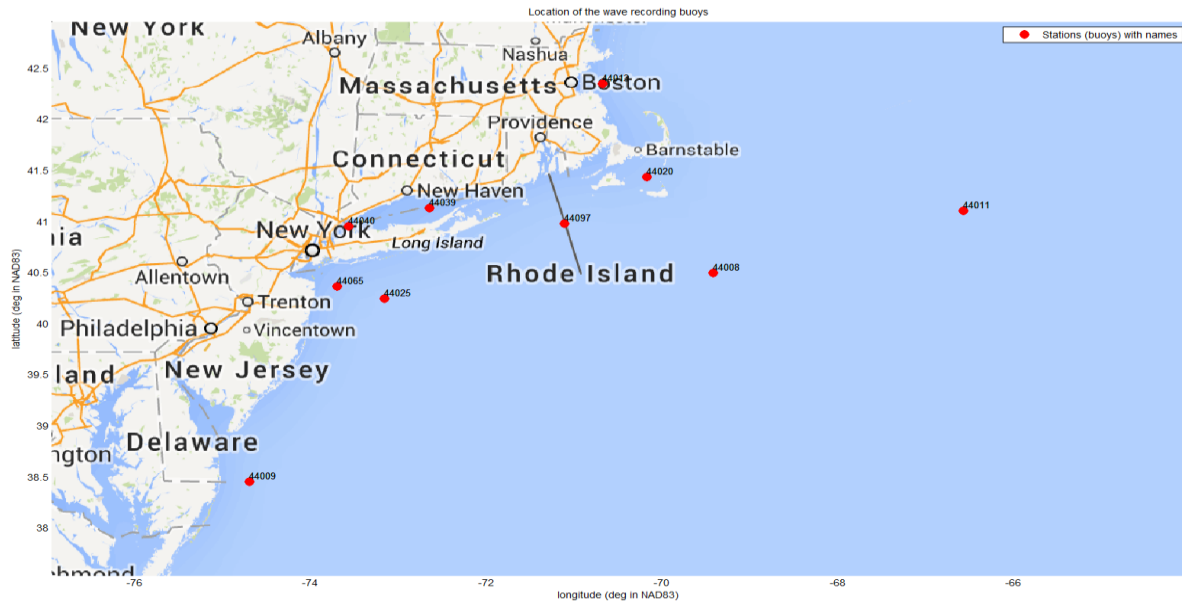


F.3. Wave Propagation

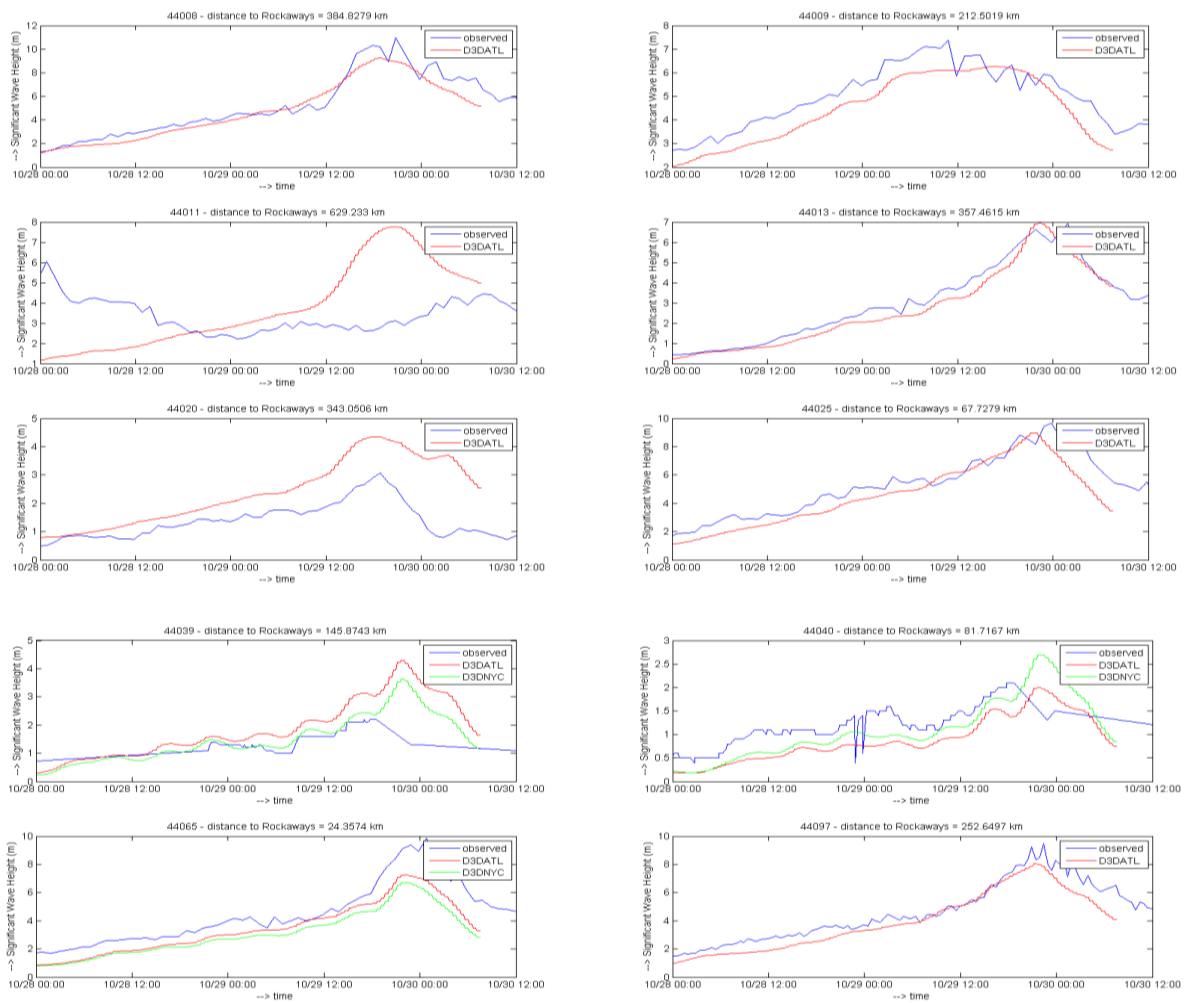
Spatial Visualization of the Simulated Waves



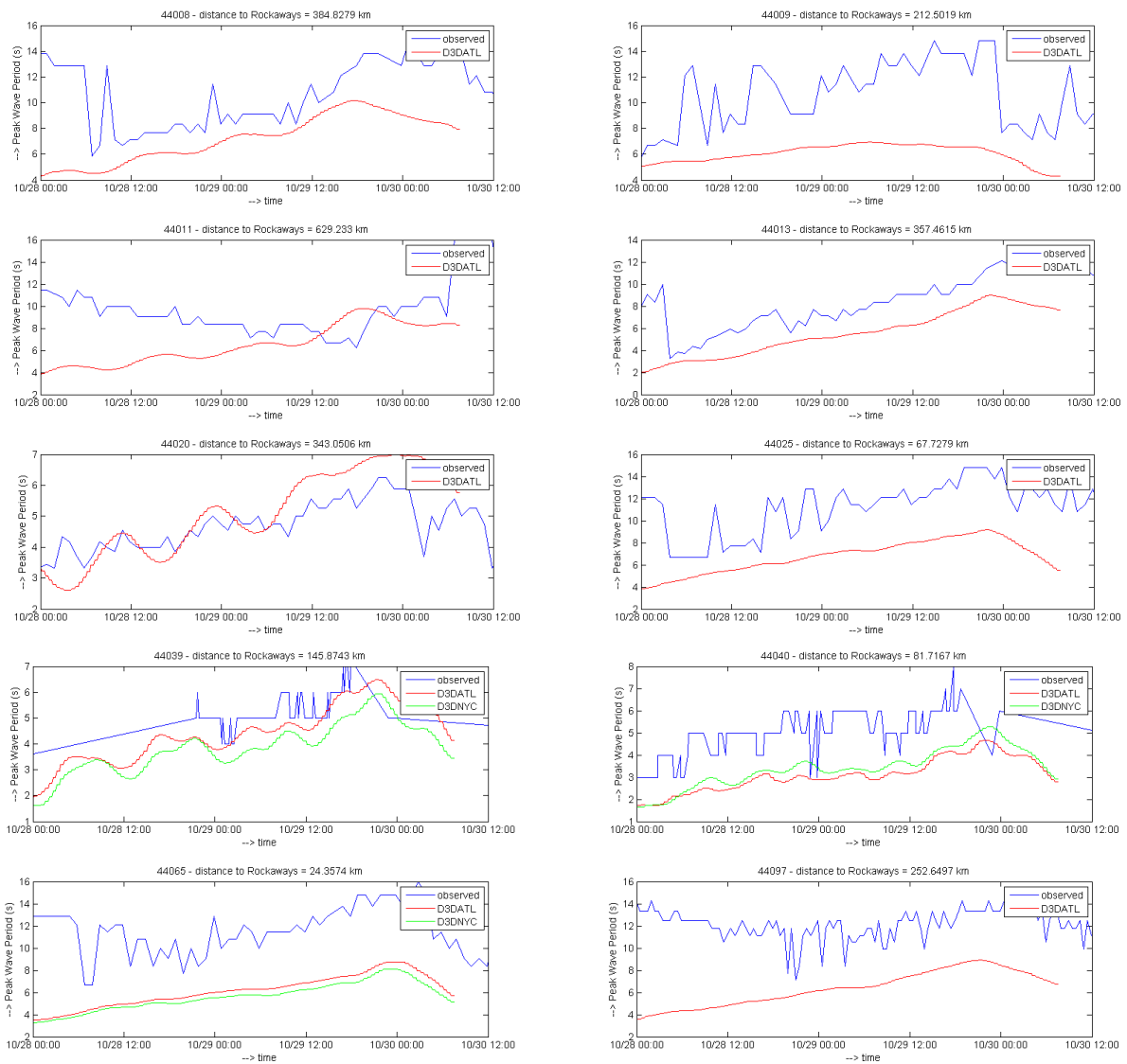
F.4. Waves– Observed versus Simulated



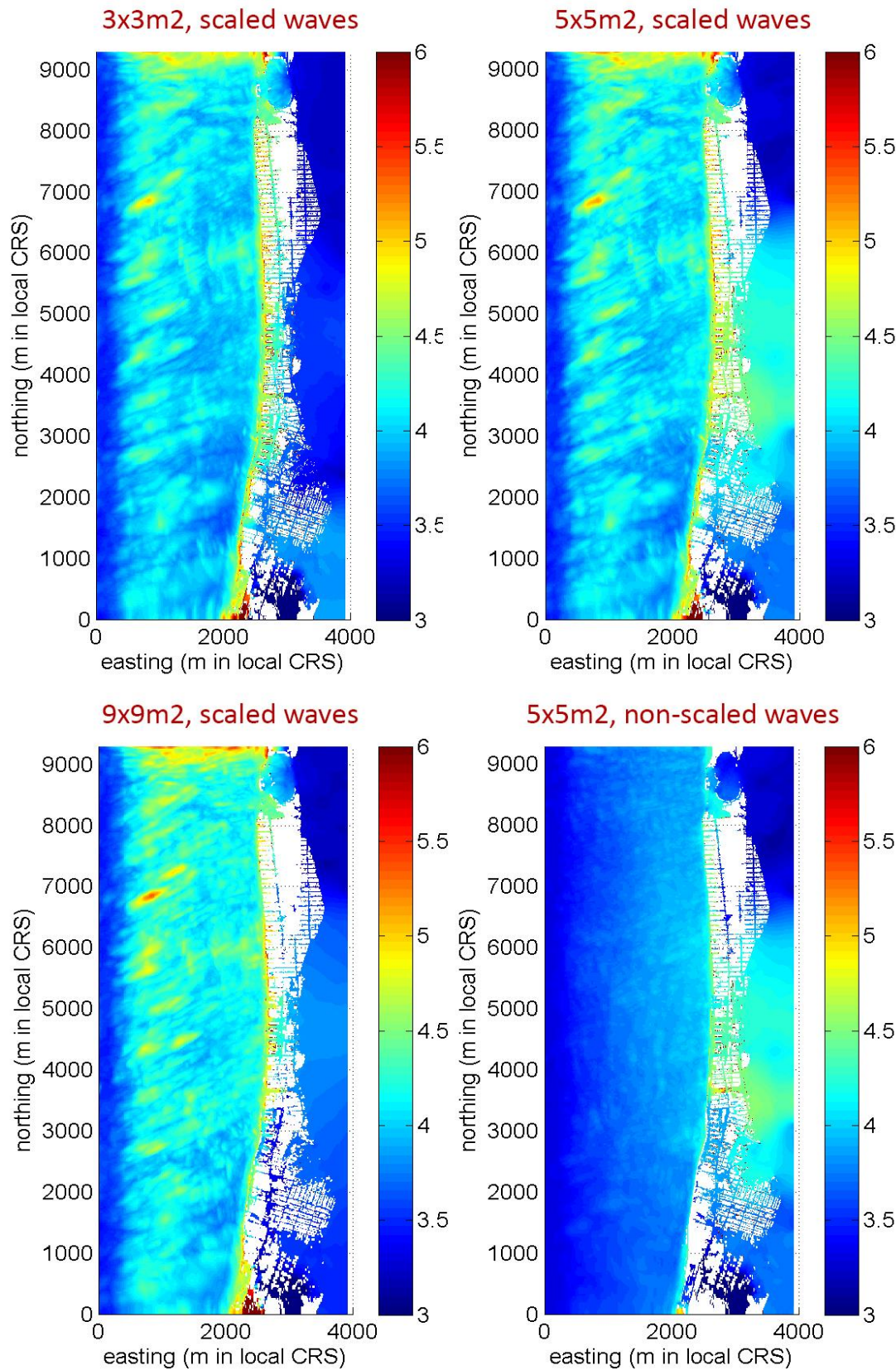
F.4.1. Significant Wave Height



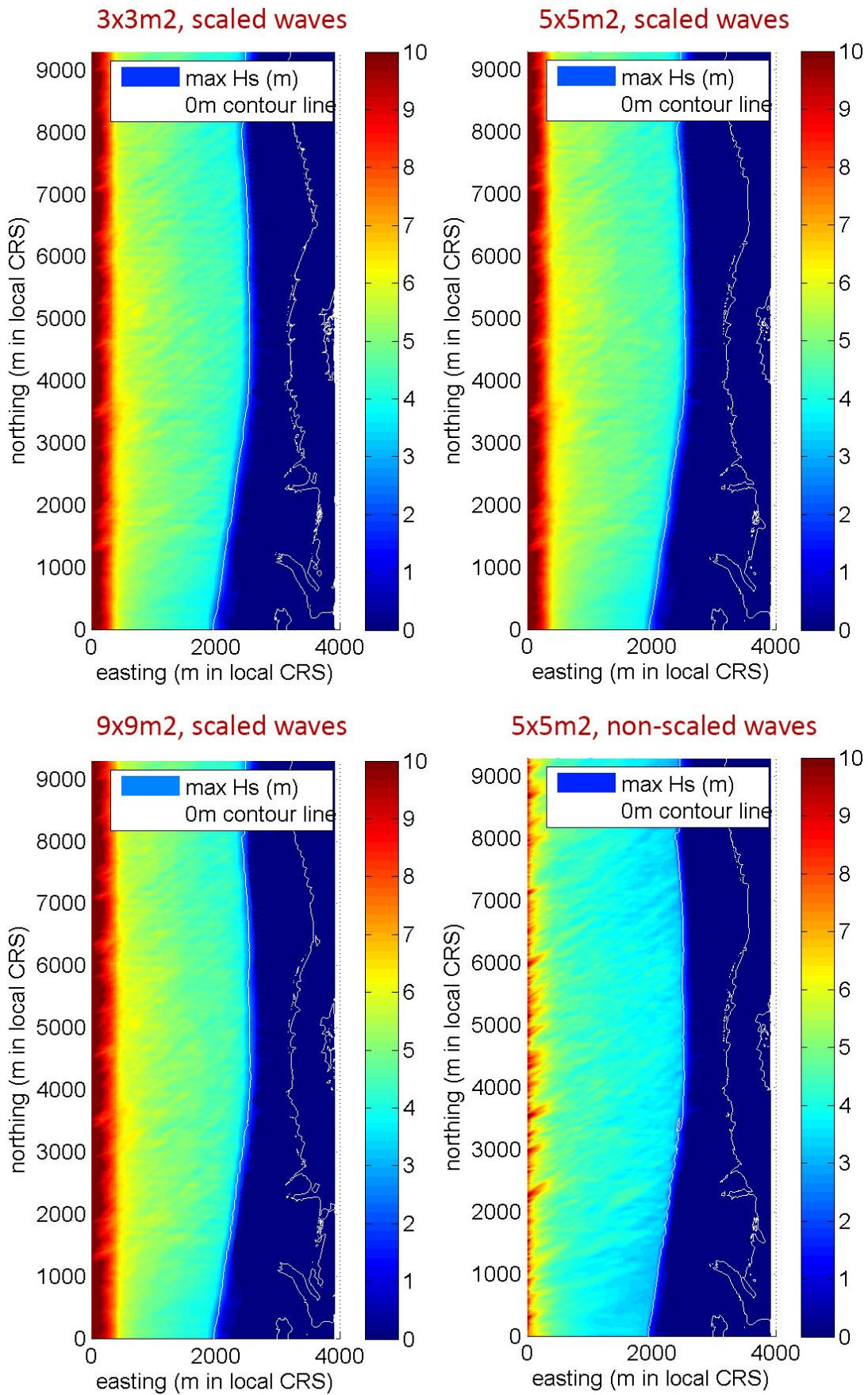
F.4.2. Peak Wave Period



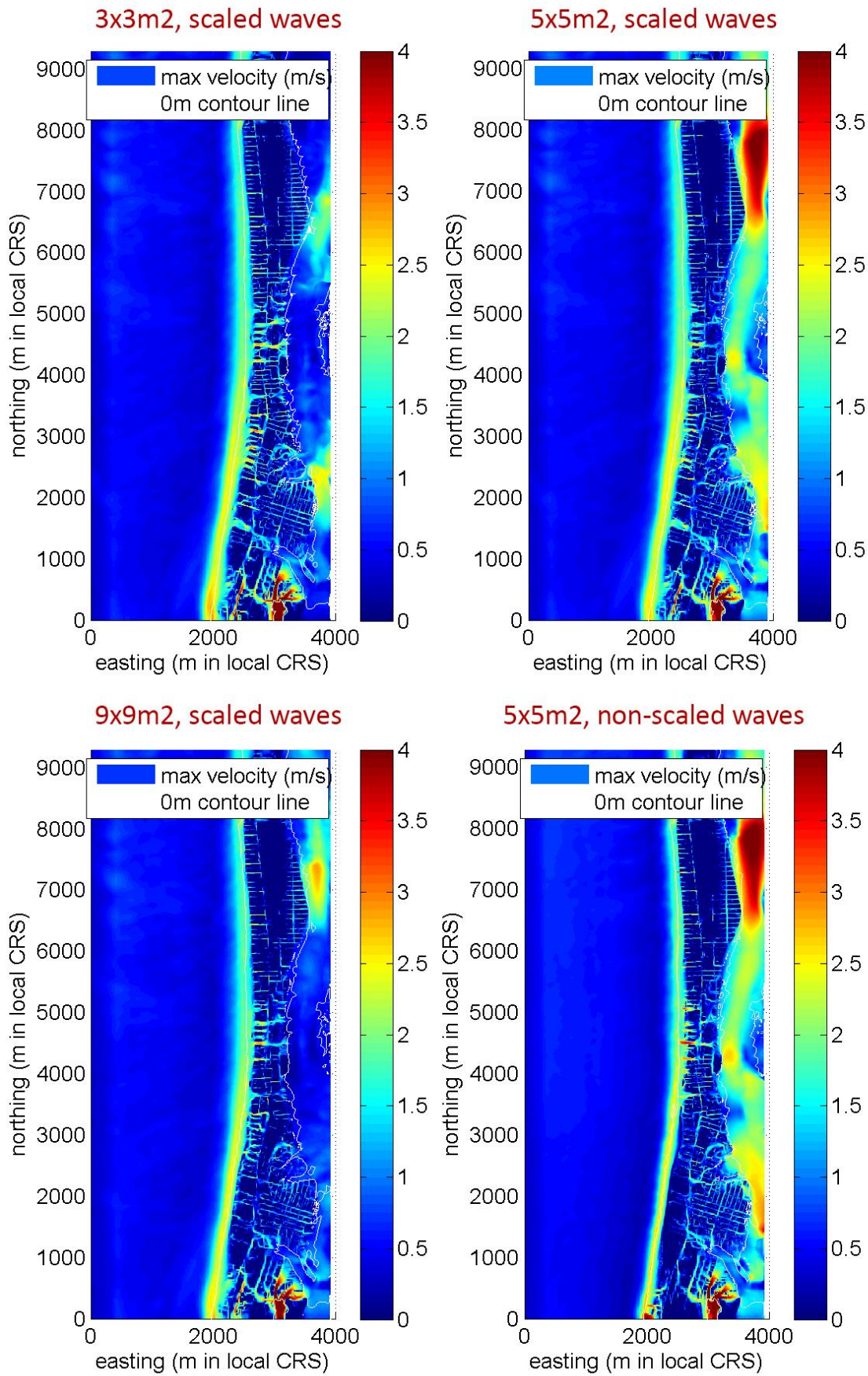
G.XBeach model results – multiple runs



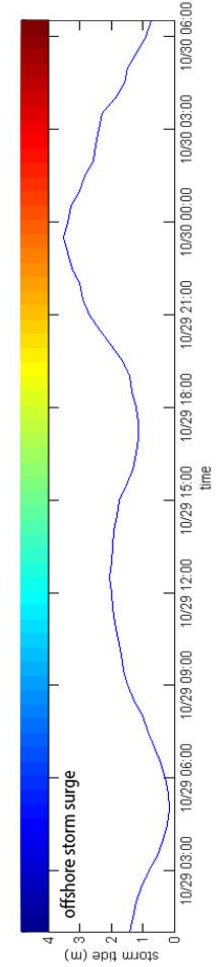
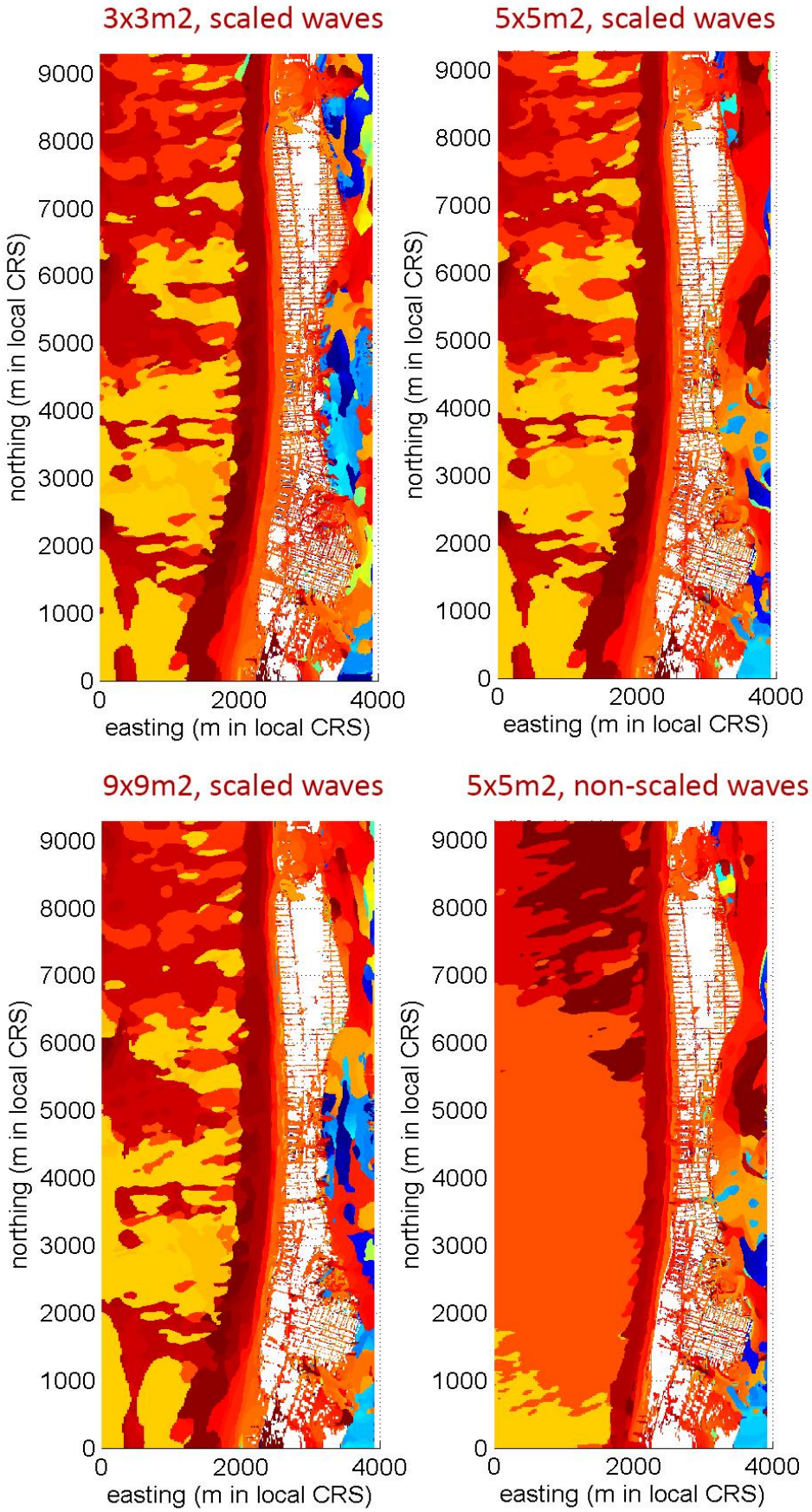
XBeach Results - Maximum storm tide including long waves (m ref. to NAVD88)



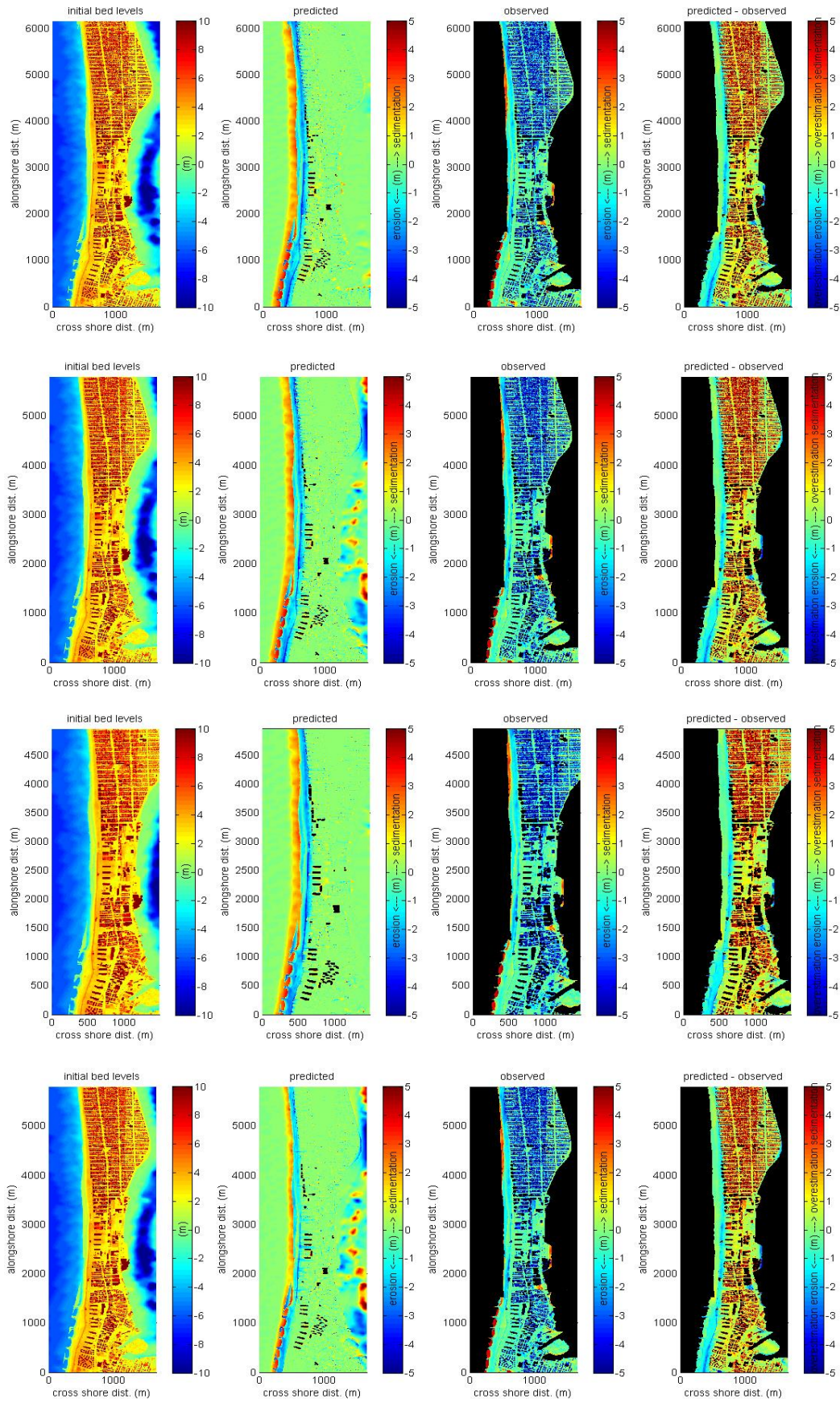
XBeach Results - Maximum significant wave height in m.



XBeach Results - Maximum velocity $(u^2+v^2)^{.5}$ in m/s



XBeach Results - time of occurrence
of the maximum water velocity
(colors correspond to time --->)



3x3m2, scaled waves

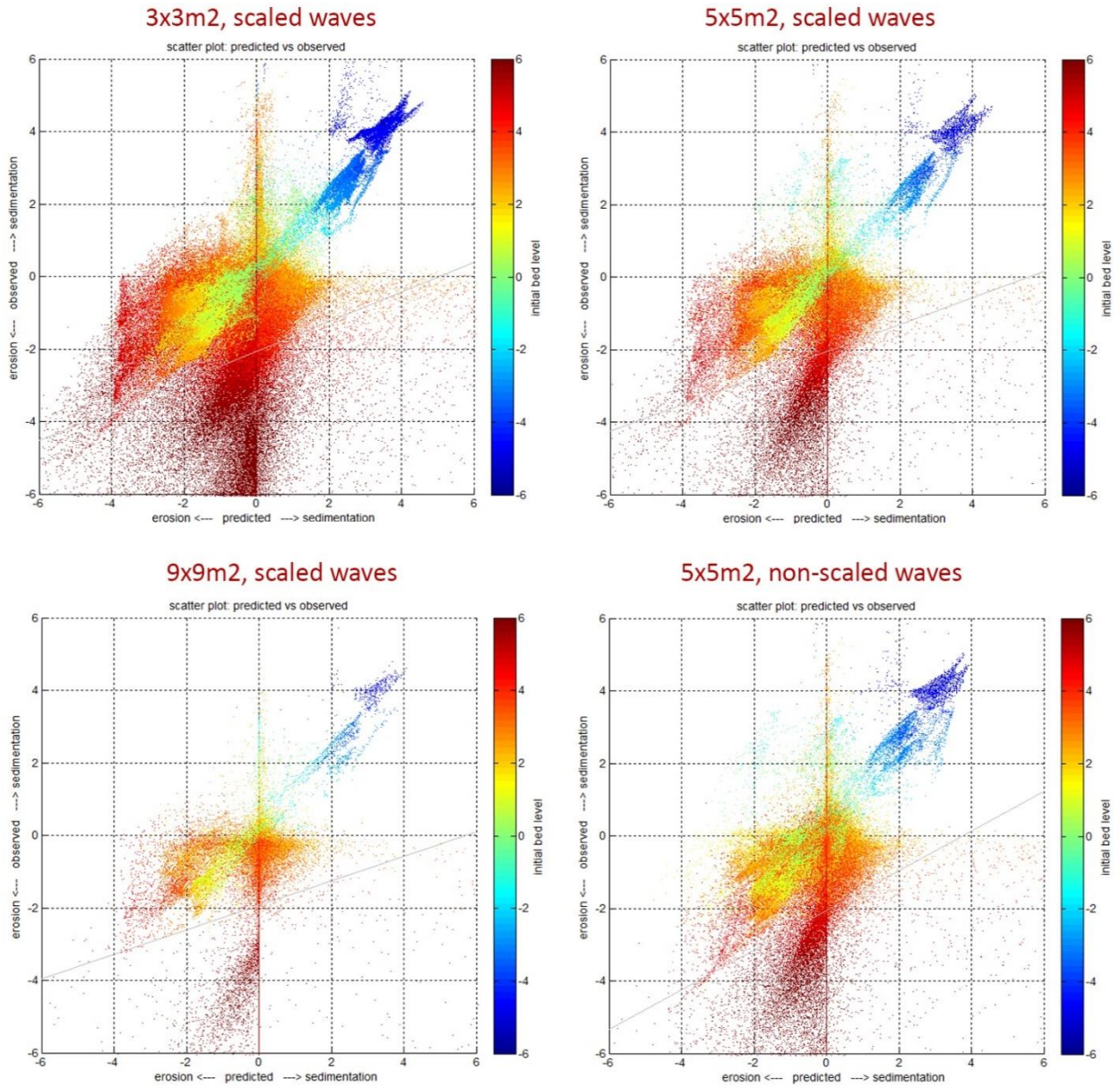
5x5m2, scaled waves

9x9m2, scaled waves

5x5m2, non-scaled waves

XBeach Results - Scatter plot: Predicted vs Observed

XBeach Results - Scatter plot: Predicted vs Observed



H. Reference studies - Bayesian Belief Networks

In the field of Coastal Engineering some papers have been written about the application of BBNs, for instance for the prediction of dune erosion impact (Heijer, 2013) and the prediction and assimilation of surf-zone processes (Plant & Holland, 2011).

Den Heijer investigated the usefulness of BBN's in assessments for the safety of dune coasts. The BBN model, constructed within the software package Netica, predicts dune erosion impact based on hydraulic boundary conditions and a number of cross-shore profile indicators like crest height and beach slope. The configuration of the network can be seen in Fig XXIII.

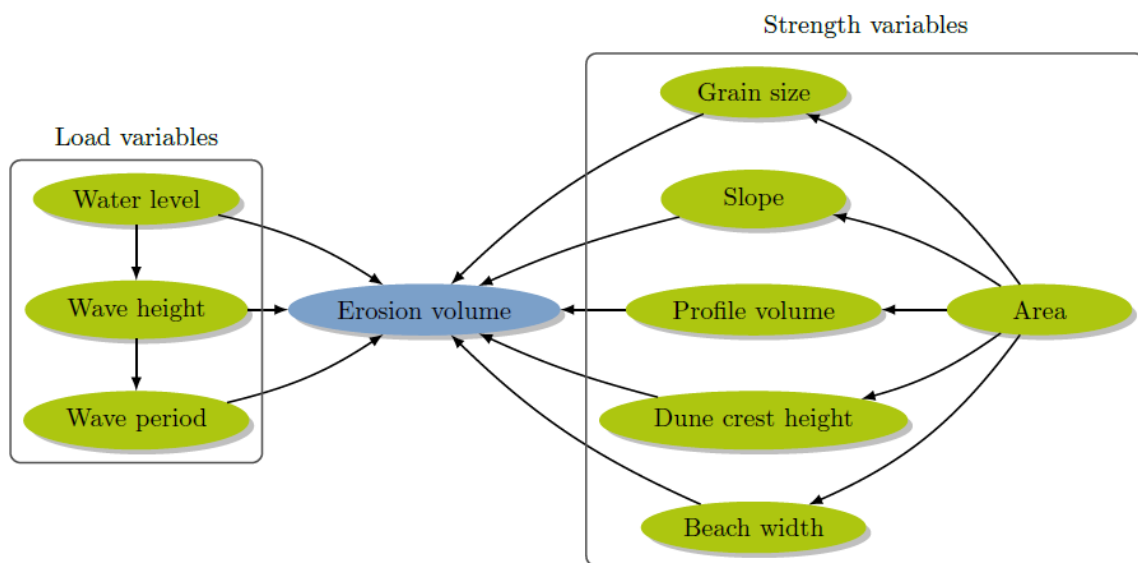


Fig XXIII - Overview of the Bayesian Network (source: Den Heijer, 2013)

In both left and right side of the figure the variables (green boxes) and dependency relations (arrows) are shown. The Network is strained with data obtained from empirical dune erosion simulations with the model Duros+. Comparing the results of the BBN predictions and the Duros+ predictions a skill up 0.88 is found. In this way the BBN can be used as a substitute for the Duros+ model, which has the advantage that not only process knowledge can be integrated in impact assessments but also the accompanying uncertainties. Another advantage can be found in the fact that predictions can be performed really fast, which is beneficial in emergency forecasting. Den Heijer also found limitations for the usage of BBNs: "the model cannot be used out of the range of the training data. A BBN is only capable of interpolating and extrapolating its training data".

Plant and Holland demonstrated how a Bayesian Belief Network can be used to provide predictions of the evolution of wave-height in the surf-zone given with sparse boundary condition-data from two buoys. They show that predictions of a detailed geophysical model of the wave evolution are reproduced accurately using a Bayesian approach, resulting in a forward prediction skill of 0.83. Moreover, uncertainties in the model inputs were accurately transferred to uncertainty in output variables. Observed and simulated data at three places in the surf-zone (at a depth of ~5m, ~4m and ~1.5m) were coupled in the Bayesian net; see Fig XXIV and Fig XXV.

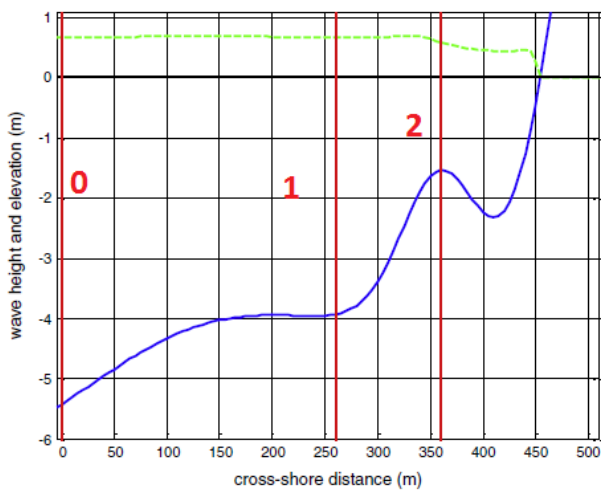


Fig XXV - Cross-shore profile (blue), wave height (green) and locations of observations (source: Plant and Holland, 2011)

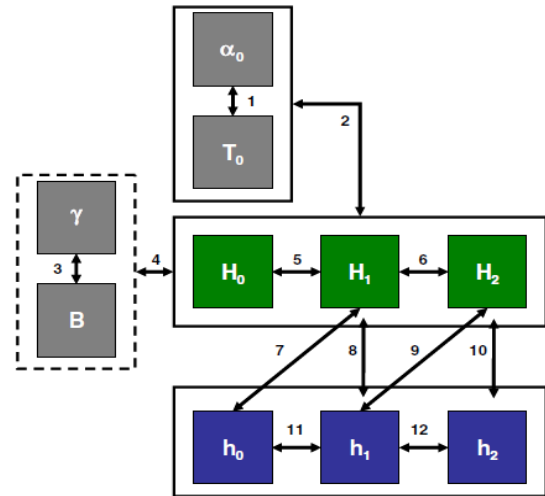


Fig XXIV - overview BBN. H = wave height; h = depth; alpha = wave angle; T = wave period; gamma and beta are model parameters in TG83 (source: Plant and Holland, 2011)

In this way a BBN has been created which was able to reproduce the detailed results obtained from a forward model of surf-zone wave evolution. The cross-shore profile of Fig XXV also showed depth variations in along shore direction, which was included as uncertainty in the input parameters in a second test. This caused an increase of uncertainty in the output data which was in better agreement with reality than without including that uncertainty. Plant and Holland state that the usage of BBN's has several advantages: "It significantly reduces the dimensionality of the problem, compared to detailed models; uncertainty estimates are made for all predictions, and it is possible to estimate model parameters simultaneously with making the wave-height prediction."

More examples can be found in other fields, for instance the master thesis 'Using Dynamic Nonparametric Bayesian Belief Nets (BBNs) to Model Human Influences on Safety' (Jäger, 2013). These papers show that usage of Bayesian Belief Networks can lead to powerful tools, as well as insight into their limitations.

I. Tools of Analysis

I.1. Sensitivity Analysis

Sensitivity analysis is the study of appointing the uncertainty of a prediction or outcome to the different source. The larger the sensitivity of an indicator is, the larger the dependency and more important the variable is for the damage prediction.

Quantifying sensitivity between variables is straight forward for numerical variables, but not for non-numerical variables like damage based on the ImageCat dataset (Affected, Minor, Major and Destroyed). In order to say something about the sensitivity, extremes are studied and compared. For instance the conditional PMF's of the variable damage conditioned on the 10% lowest and 10% highest inundation depth observations are compared; see Fig XXVI.

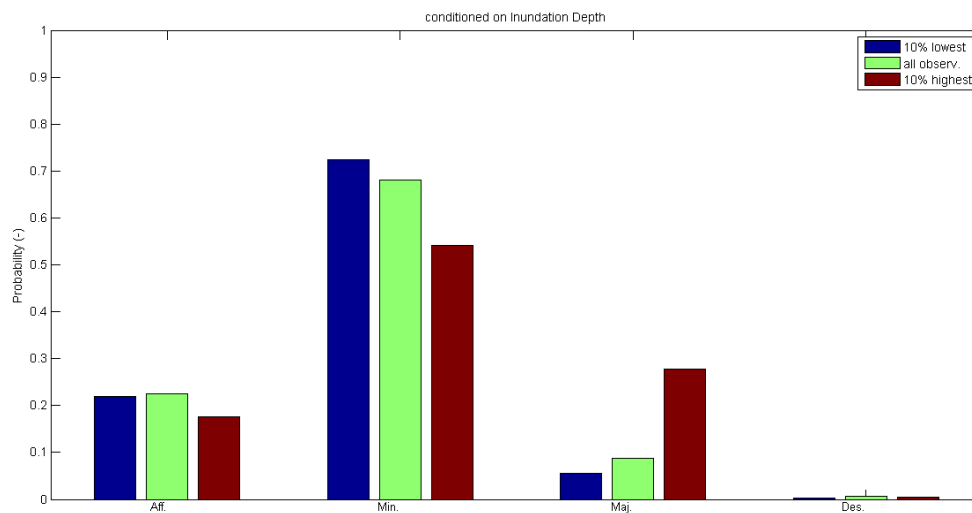


Fig XXVI - Marginal (green) and conditional PMF's of damage; conditioned on either the 10% highest or 10% lowest inundation depths

I.2. (Log-)Likelihood Ratio Test

An approach to testing the Bayesian-network prediction is to compare it to a competing model. One such competing model is for instance taking the marginal CPT (based on all the trainings data) as the prediction. In the test the log-likelihood of the prediction is compared to the log-likelihood of the marginal probability, according to:

$$LLR_j = \log \left\{ \frac{p(F_i | \tilde{O}_j)_{F_i=O_j}}{p(F_i)_{F_i=O_j}} \right\}$$

$$LLR_j = \log \left\{ p(F_i | \tilde{O}_j)_{F_i=O_j} \right\} - \log \left\{ p(F_i)_{F_i=O_j} \right\}$$

Here F is the forecast and O is the observed on which is conditioned. If the log-likelihood ratio is positive, the model shows predictive skill since the prediction is better than guessing randomly based on the marginal distribution; if the ratio is negative the prediction is worse. In the Fig XXVII an example is given for a damage prediction. Marginal and conditional PMF both give a competing prediction for the observed (which is "Major

damage” in this case). The corresponding Log-likelihood ratio $LLR = \log_{10}\{0.28\} - \log_{10}\{0.05\} = 2.4429$ is positive, since the conditioned model gives a better prediction than the marginal distribution.

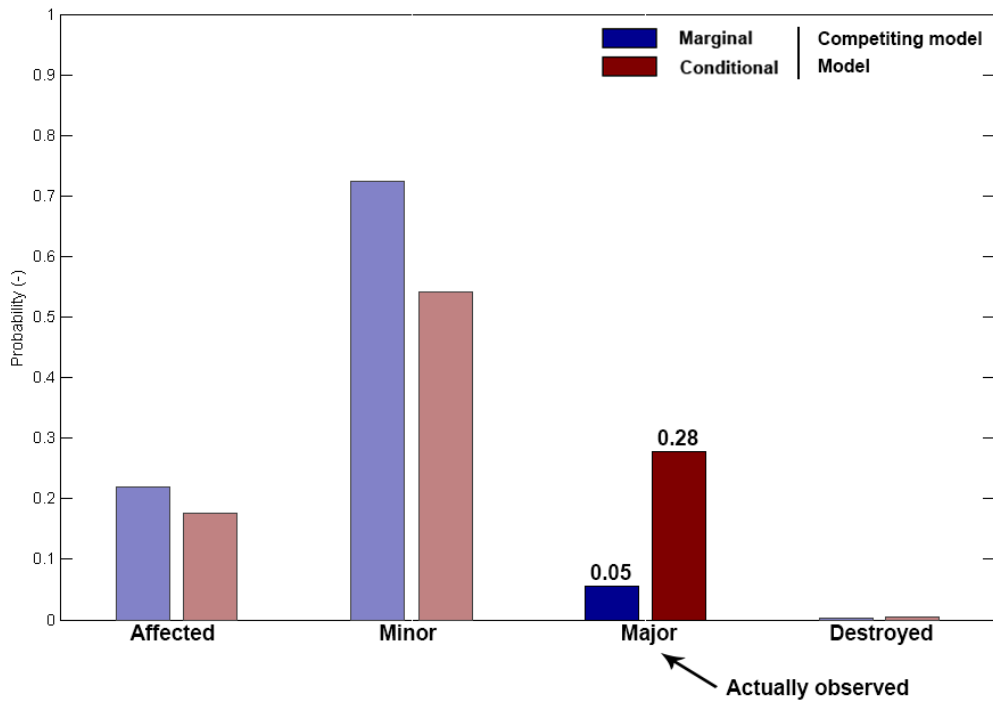


Fig XXVII – Example - determining input for the Log-Likelihood ratio

By summing the LLR’s of all hindcast events the LLR test score can be determined. Therefore, if you consider more hindcast events, the score will increase (or decrease in case of a negative score). So what is this score worth? A way to answer that question is by looking at the perfect check. The perfect check is the score of the LLR test in which the conditional PMF has a 100% probability for the actual observed. The log-likelihood ratio for the example of above then becomes $LLR = \log_{10}\{1.00\} - \log_{10}\{0.05\} = 2.9957$. Again, the sum of the LLR’s of all hindcast events results in the LLR test score. Relative to this LLR test score of the perfect check different configurations can be compared.

J. FEMA Damage Classification description

Table 6-1 - Description of the Damage Classification which is used for the ImageCat Impact Analysis (source: FEMA)

FEMA DAMAGE CLASSIFICATION		VISIBLE IMAGERY BASED CLASSIFICATION				INUNDATION ASSESSMENTS
DAMAGE LEVEL	OBSERVED DAMAGE	Roof Covering	Roof Diaphragm	Collapsed Walls	Other Considerations	
Affected	Generally superficial damage to solid structures (loss of tiles or roof shingles); some mobile homes and light structures damaged or displaced.	Up to 20%	None	None	Gutters and/or awning; loss of vinyl or metal siding	Field Verified Flood Depth (or Storm Surge): >0 to 2 feet relative to the ground surface at structure. Depth damage relationships may vary based on building or foundation type, as well as duration or velocity of flood event.
Minor	Solid structures sustain exterior damage (e.g., missing roofs or roof segments); some mobile homes and light structures are destroyed, many are damaged or displaced.	>20%	Up to 20%	None	Collapse of chimney; garage doors collapse inward; failure of porch or carport Mobile homes could be partially off foundation	Field Verified Flood Depth (or Storm Surge): 2 to 5 feet relative to the ground surface at structure. Depth damage relationships may vary based on building or foundation type, as well as duration or velocity of flood event.
Major	Wind: Some solid structures are destroyed; most sustain exterior and interior damage (roofs missing, interior walls exposed); most mobile homes and light structures are destroyed.	-	>20%	Some exterior walls are collapsed.	Mobile home could be completely off foundation – if appears to be repairable.	Field Verified Flood Depth: Greater than 5 feet, modeling observed, relative to the ground surface at structure, and not high rise construction. Depth damage relationships may vary based on building or foundation type, as well as duration or velocity of flood event.
	Storm Surge: Extensive structural damage and/or partial collapse due to surge effects. Partial collapse of exterior bearing walls.			Some exterior walls are collapsed		Major is the general category where the onset of Substantial Damage (>50% of building value) as defined by the National Flood Insurance Program (NFIP) may occur.
Destroyed	Wind: Most solid and all light or mobile home structures destroyed.	-	-	Majority of the exterior walls are collapsed.	-	
	Storm Surge: The structure has been completely destroyed or washed away by surge effects.	-	-	Majority of the exterior walls are collapsed		

K. PLUTO - Data Description⁶⁵

K.1. Tax Base Value

Field Name: ASSESSED VALUE, TOTAL (AssessTot)
Format: Numeric - 11 digits (99999999999)
Data Source: Department of Finance - RPAD Master File
Description: The assessed total value for Fiscal Year 2014.
The Department of Finance calculates the tentative assessed value by multiplying the tax lot's estimated full market value by a uniform percentage for the property's tax class.

Fig XXVIII – Total Assessed Value description from 'PLUTO data Dictionary' (Source: DOB NYC)

K.2. Residential Units per Building

The indicator 'residential units per building' is determined by the ratio of residential units per lot and buildings per lot.

Field Name: UNITS, RESIDENTIAL (UnitsRes)	Field Name: BUILDINGS, NUMBER OF (NumBldgs)
Format: Numeric - 5 digits (99999)	Format: Numeric - 5 digits (99999)
Data Source: Department of Finance - RPAD Master File	Data Source: Department of City Planning - based on data from: Department of City Planning - Geosupport System Department of Finance - RPAD Master File
Description: The sum of residential units in all buildings on the tax lot. If there are no residential units in the tax lot, this field will be zero. NOTE: Hotels/motels, nursing homes and SROs do not have residential units, while boarding houses do have residential units.	Description: The number of buildings on the tax lot. With few exceptions, buildings are permanent structures. If an assessor values a semi-permanent structure, such as a parking attendants building, then it is considered a building. NUMBER OF BUILDINGS does not include extensions.

Fig XXIX – Residential Units and Number of Buildings description from 'PLUTO data Dictionary' (Source: DOB NYC)

K.3. Building Class

Field Name: BUILDING CLASS (BldgClass)
Format: Alphanumeric - 2 characters
Data Source: Department of City Planning - based on data from:
Department of Finance - RPAD Master File
Description: A code describing the major use of structures on the tax lot.
Building Classes were developed and are assigned by the Department of Finance with the exception of Q0 and the mixed use condominium building classes that were developed by the Department of City Planning (DCP). Q0 was assigned by DCP to government owned tax lots zoned as either Park or ParkNYS that are predominantly used as open space. The mixed use condominium building classes were assigned by DCP to condominiums that contain a mix of residential and commercial units or more than one type of residential or commercial unit.
If there are multiple uses or buildings on a tax lot, the building class describes the use with the greatest square footage on the tax lot. Several building classes describe mixed use buildings (combinations of residential and office or retail uses).
See Appendix C - Building Class Codes for codes and decodes.

Fig XXX - Building Class description from 'PLUTO data Dictionary' (source: DOB NYC)

⁶⁵ The descriptions are directly copied out of the PLUTO Data Dictionary (2013) http://www.nyc.gov/html/dcp/pdf/bytes/pluto_datadictionary.pdf

Figures

Figure 1-1 - Intensity and track of Hurricane Sandy (2012) from NOAA website	14
Figure 1-2 - High pressure areas (red) and Low pressure areas (blue) made Sandy turn northwest. Picture by NHC (2012)	14
Figure 1-3 - Sandy before landfall - Wind speed and schematization of track by NASA	15
Figure 1-4 - Sandy inundation map by FEMA (Source: NOAA)	15
Figure 1-5 - A breakdown of direct losses in New York State (in million US\$ and %) reported Cuomo (2012) and graphed by Kunz et al. (2013)	17
Figure 1-6 - Normalized US Hurricane Damage (source: Pielke et al.)	17
Figure 1-7 - Methodology of the Florida Hurricane Model 2013a (source: EQECAT)	20
Figure 1-8 - Overall Model Methodology with spatial scales and properties of different information levels	21
Figure 1-9 - Schematization of the HIS-SSM model methodology (source: Rijkswaterstaat)	22
Figure 1-10 – Depth – damage functions and corresponding maximum damage figures for the CORINE land use class “continuous urban fabric”. The functions of each damage model are based on a manual selection of available damage classes, except for the JRC Model. (source: Jongman et al. 2012)	23
Figure 1-11 - Probability Mass Functions of the sum of three dice	25
Figure 1-12 - Depth - Damage scatter plot with the corresponding damage curve (Merz et al. 2004)	26
Figure 1-13 - A representation of the axis of freedom	28
Figure 2-1 - Top panel: typical configurations of barrier coasts (source: Royal HaskoningDHV); lower panel: top view of the South-Western part of Long Island (source: Google Earth)	31
Figure 2-2 – Schematic evolution of the Jamaica Bay (source: Royal HaskoningDHV)	32
Figure 2-3 - Features of a Barrier Island (source: CUNY)	32
Figure 2-4 - Ground Elevations per building in meters ref. to NAVD88 (source: NYC buildings dataset)	33
Figure 2-5 - Nearshore Dynamics (source: Royal HaskoningDHV)	34
Figure 2-6 - Different regimes during a storm (source: USGS)	34
Figure 2-7 - Map showing neighbourhoods (Source: Project Jamaica Bay)	35
Figure 2-8 - Median Income in the Rockaways (source: Averne East Study)	36
Figure 2-9 - Predominant land use class per tax lot, obtained from the PLUTO dataset	36
Figure 2-10 - Gauging Stations and USGS’s temporary storm-tide sensor (based on a figure of NOAA)	37
Figure 2-11 - water level records in time by USGS’s temporary storm-tide sensor (source: USGS)	38
Figure 2-12 - Oblique aerial photographs of Neponsit, NY (source: USGS). The view is looking northwest across Rockaway Peninsula. Sand was washed from the beach into the streets, and towards the bayside of the island, and several rows of ocean-facing houses were destroyed or damaged. The yellow arrow in each image points to the same feature.	38
Figure 2-13 - Destroyed boardwalk (photographer: Nathan Kensinger)	38
Figure 2-14 - Overview of damage to the beaches and Boardwalk; based on aerial pictures taken directly after the storm.	39
Figure 2-15 - Location of the USGS high water marks	39
Figure 2-16 - buoy 44065 (source: NOAA)	40
Figure 2-17 - Wind speed and significant wave heights during Hurricane Sandy - recorded by buoy 44065	40
Figure 2-18 - Upper panels: wind directions observed (red) and simulated (black) with the North American Meso-scale Forecast System (NAM) model; lower panels: wave directions observed (blue) and simulated (white) with SWAN	41
Figure 2-19 - Bed level changes due to Sandy. Left upper panel: pre-Sandy LIDAR, right upper panel: post-Sandy LIDAR, panels below: differences between post- and pre-Sandy LIDAR	42
Figure 2-20 - The oceanfront of The Rockaways has been almost completely demolished by wave battering (photos by Nathan Kensinger)	43

<i>Figure 2-21 - Spatial representation of the ImageCat damage Analysis</i>	44
<i>Figure 2-22 - Short-circuit fires burned down complete neighbourhood at Breezy Point and some other places in the area (Photographs by USACE and Nathan Kensinger amongst others)</i>	45
<i>Figure 2-23 - impression of the available data on monetary damage. Source: FEMA’s Community Recovery Resource Mapping Tool.</i>	46
<i>Figure 2-24 - Spatial representation of the ImageCat, Buildings and PLUTO datasets</i>	46
<i>Figure 3-1 - Schematic representation of the proposed approach</i>	50
<i>Figure 3-2 - Instabilities cause episodic sliding down of land slumps. This is simulated by the avalanching-module</i>	51
<i>Figure 3-3 - Regimes during Hurricane Ivan (2004) at Beasley Park, FL (source: Dave Thompson, USGS)</i>	51
<i>Figure 3-4 - Observed and predicted bed level changes are in agreement. XBeach shows skill for predicting hurricane impacts at barrier islands.</i>	52
<i>Figure 3-5 - Schematic representation of the growing uncertainty within the model train (not based on real data)</i>	53
<i>Figure 3-6 - Information on all levels can be coupled with the use of a statistical model</i>	54
<i>Figure 3-7 - Two comparable houses are subject to different (maximal) hazard intensities during the same storm</i>	54
<i>Figure 3-8 - Schematic representation of some damage indicators with potential and how they relate to each other; Note: this is an example and can differ from site to site</i>	55
<i>Figure 3-9 - Pearson correlation of the 29 variables (28 candidate damage predictors and loss ratio); significant correlation (1% significance level) is marked by a dot (source: (Merz, Kreibich, and Lall 2013))</i>	56
<i>Figure 3-10 - Left: non-trained net of the dice example; right: trained net</i>	58
<i>Figure 3-11 - Example of the three dice; left: conditioned on one of the dice and right: conditioned on the sum of the dice.</i>	59
<i>Figure 3-12 – Flow Chart: model structure and flow of information</i>	60
<i>Figure 3-13 - Area of Application</i>	61
<i>Figure 3-14 - Local hazard indicator nodes coupled to the damage node. The yellow arrows can be added to include the mutual dependencies between the local hazard indicators</i>	62
<i>Figure 3-15 - Local hazard indicator nodes coupled to the damage node. The yellow arrows can be added to include the mutual dependencies between the local hazard indicators. Additionally, the building type indicators are shown on the right side, connected to the damage node with blue arrows.</i>	63
<i>Figure 3-16 - Bathymetry input for the XBeach Model (elevation in m ref. to NAVD88)</i>	63
<i>Figure 3-17 - Zoomed view of the topo-bathymetry input file with building polygons (thin black lines) and an 10m-offset of these polygons (thick black line)</i>	64
<i>Figure 3-18 - The area of interest (or area of application) and shadow zones within the XBeach model domain.</i>	65
<i>Figure 3-19 - XBeach boundary conditions: tide, wave height and wave period; red for bay side and blue for the ocean side.</i>	66
<i>Figure 3-20 - Bathymetry input of Delft3D - US East Coast model</i>	67
<i>Figure 3-21 - Bathymetry input of Delft3D – New York Bight model</i>	67
<i>Figure 3-22 - Bathymetry input of D-Flow FM – New York Bight model.</i>	68
<i>Figure 3-23 - Grid configuration in the Jamaica Bay and around the Rockaway Peninsula.</i>	69
<i>Figure 3-24 - Cumulative distribution function of the building length indicator (blue), which is the square root of the ground floor area; 9m is marked in green and the 10%- and 50%-quintiles in red.</i>	70
<i>Figure 4-1 - Snapshots of the simulated hazard propagation: Upper left panel: collision regime with heavy beach erosion; upper right panel: overwash regime with high long waves penetrating into the urban area; lower left panel: inundation regime where almost the whole peninsula is flooded; lower right panel: post-Sandy situation (note updated bed)</i>	74
<i>Figure 4-2 - upper panel: Maximum simulated storm tide including long waves; lower panels: observed and</i>	

<i>simulated water levels at location 4, 5 and 6</i>	75
<i>Figure 4-3 – Maximum simulated significant wave height (Hs)</i>	76
<i>Figure 4-4 - Scatter plots: 5x5m2 Scaled Waves run vs 5x5m2 NON-Scaled Waves run</i>	77
<i>Figure 4-5 - Maximum simulated absolute flow velocity (m/s) (Lagrangian flow)</i>	77
<i>Figure 4-6 - Time of occurrence of the maximum simulated flow velocity; The colors correspond to the timeline graphed below the map and the offshore storm surge levels have been plotted as well to give a reference.</i>	78
<i>Figure 4-7 - Morphological change. From left to right: initial bed levels, predicted post-Sandy bed levels, observed post-Sandy bed levels and the difference between these two.</i>	79
<i>Figure 4-8 - The same as Figure 4-7 but now zoomed views of three representative locations.</i>	80
<i>Figure 4-9 - Cross sectional plot of the initial bed level profile. The sudden jump in bed level due to CRM-LIDAR differences is encircled in red.</i>	80
<i>Figure 4-10 - Scatter plot: predicted (vertical) versus observed (horizontal) bed levels. The colors correspond to the initial bed levels (in meters ref. to NAVD88)</i>	81
<i>Figure 4-11 - Predicted bed level changes around a relative high building with corresponding cross section in which the initial bed level and predicted post-Sandy bed level are plotted.</i>	81
<i>Figure 4-12 - Impression of the spatial distribution of the inundation depth indicator</i>	82
<i>Figure 4-13 - Inundation depth indicators according to the 9 different extraction formulations</i>	82
<i>Figure 4-14 - Marginal Probability Mass Functions of the inundation depth indicator according to the 9 different extraction formulations</i>	83
<i>Figure 4-15 - Left: Spatial distribution of the wave attack indicator; right: marginal Probability Mass Function of the wave attack indicator</i>	83
<i>Figure 4-16 - three Impressions of the spatial distribution of the wave attack indicator</i>	84
<i>Figure 4-17 - Left: Spatial distribution of the flow velocity indicator; right: marginal Probability Mass Function of the flow velocity indicator</i>	84
<i>Figure 4-18 - three Impressions of the spatial distribution of the flow velocity indicator</i>	84
<i>Figure 4-19 - Left: Spatial distribution of the scour depth indicator; right: marginal Probability Mass Function of the scour depth indicator</i>	85
<i>Figure 4-20 - three Impressions of the spatial distribution of the scour depth indicator</i>	85
<i>Figure 4-21 - Marginal PMF's of the four local hazard indicators for runs with grid cell sizes of 3x3, 5x5 and 9x9 m² and equal extraction buffer areas</i>	86
<i>Figure 4-22 - Marginal PMF's of the four local hazard indicators for runs with grid cell sizes of 3x3, 5x5 and 9x9 m² extracted with different buffer sizes</i>	87
<i>Figure 4-23 - Marginal PMF's of the four local hazard indicators extracted from the run with a grid cell size of 3x3 m² for different extraction buffer areas</i>	88
<i>Figure 4-24 - Pearson correlations between potential indicators. Inundation Depth is according to formulation 8, which is $\max(\max(hs, \text{mean}, 30\text{min}) - hb0)$</i>	89
<i>Figure 4-25 - PMF's of Damage conditioned on different indicators with 1) the lowest 10% (blue); 2) the highest 10% (red). Left upper panel: marginal PMF of damage.</i>	90
<i>Figure 4-26 - Difference of probability between PMF's conditioned on either the 10% lowest values or 10% highest. Left: absolute difference; right: relative difference on a logarithmic scale. Red means that the probability of the PMF conditioned on the 10% highest values is higher and blue vice versa.</i>	91
<i>Figure 4-27 - Simple Bayesian net with the inundation depth indicator as predictor for damage</i>	91
<i>Figure 4-28 - The log-likelihood ratio test scores for the bathtub concept with varying water levels, divided by the perfect check score (red) and the Pearson correlation coefficient.</i>	93
<i>Figure 4-29 - Local storm conditions coupled to damage in a Bayesian Belief Network. Left: no arrows between local hazard indicators; right: mutually coupled local hazard indicators</i>	94
<i>Figure 4-30 - Example (no results); More bins give more detail, but at a certain point also less validation for the CPT's.</i>	96
<i>Figure 4-31 - Ten randomly picked locations within the urban areas of the model domain.</i>	97

Figure 4-32 - Mean of damage for ErrorRate over bins	99
Figure 4-33 - Spatial representation of the mean of predicted PMF's for configuration 1 and 2. The two upper panels show the observed.	102
Figure 4-34 - Spatial representation of the standard deviation of predicted PMF's for configuration 1 and 2.	103
Figure 4-35 - Trained Bayesian Belief Net with one building type indicator; the five different building type indicator nodes that have been used are shown on the right side.	103
Figure 4-36 - Trained Bayesian Belief Nets with all building type indicators. Left: No arrows between the local hazard indicator nodes; right: arrows between them.	104
Figure 4-37 - Upper left panel: Spatial representation of observed damage; others: Spatial representation of most probable, mean and mean standard deviation of the hindcasted MPF's for configuration 4 and hindcast scenario 13 (conditioned on all indicators).	107
Figure 5-1 - The problem with aggregating predictions to higher spatial scale levels	113

Fig I - Bed levels of the 2005 USACE survey. Upper panel: overview; lower panel: zoomed view of the squared box in the upper panel.....	127
Fig II - Bed levels of the 2010 USACE survey. Upper panel: overview; lower panel: zoomed view of the squared box in the upper panel.....	128
Fig III - Bed levels of the additional post-Sandy 2012 USACE survey. Upper panel: overview; lower panel: zoomed view of the squared box in the upper panel.....	128
Fig IV - Bed levels of the used CRM data.....	129
Fig V - Spatial visualization of the merged topo-bathymetrical dataset	130
Fig VI - Two visualisation (up and below) of the removing of the railway viaduct	130
Fig VII - Building perimeter outlines of the DOB polygon dataset on top of a Google Maps layer.....	131
Fig VIII - Visualization of the building polygons on top of the merged topo-bathymetrical data. Left: original configuration matches poorly; right: After shifting of the topographical data a good match is obtained.	132
Fig IX - Visualization of the building polygons on top of the merged topo-bathymetrical data. Left: original file does not contain all buildings; right: the bathymetrical file has been raised to a minimum height of 7m above MSL.	132
Fig X - Non-erodible layer plotted with the building perimeter outlines (white) on top of it. Blue is non-erodible, red is erodible.	133
Fig XI - Normal XBeach model configuration (source: XBeach manual)	134
Fig XII - Visualization of the final Bathymetrical file for the XBeach model.....	134
Fig XIII - The area of interest (or area of application) and shadow zones within the XBeach model domain.....	135
Fig XIV - Grid density. Left: in x-direction (cross-normal); right: in y-direction (along shore).....	136
Fig XV - Alongshore variation in water level at the boundary locations. Upper panel: Bay side; lower panel: offshore.....	137
Fig XVI - Energy density spectrum produced by SWAN during the peak of the storm	137
Fig XVII - Wave properties significant wave height (upper) and significant wave period (lower panel) during the storm at the offshore boundary. Red: observed; blue: modelled with Delft3D	138
Fig XVIII- Wave properties significant wave height (upper) and significant wave period (lower panel) during the storm at the offshore boundary. Red: observed; blue: non-scaled simulation with Delft3D; green: scaled simulation	139
Fig XIX - Wave properties significant wave height (upper) and significant wave period (lower panel) during the storm at the two offshore model domain corners	139
Fig XX - Energy per wave direction bin (10 degrees per bin) during hurricane Sandy. Between the red lines 90% of the energy is situated.	140
Fig XXI - Determining effective wave directions	140
Fig XXII - upper panels: absolute and relative bed level changes; lower panel: scatter plot - morfac 1 vs morfac =	

10.....	141
Fig XXIII - Overview of the Bayesian Network (source: Den Heijer, 2013)	158
Fig XXIV - overview BBN. H = wave height; h = depth; α = wave angle; T = wave period; γ and β are model parameters in TG83 (source: Plant and Holland, 2011).....	159
Fig XXV - Cross-shore profile (blue), wave height (green) and locations of observations (source: Plant and Holland, 2011)	159
Fig XXVI - Marginal (green) and conditional PMF's of damage; conditioned on either the 10% highest or 10% lowest inundation depths	160
Fig XXVII – Example - determining input for the Log-Likelihood ratio	161
Fig XXVI – Total Assessed Value description from ‘PLUTO data Dictionary’ (Source: DOB NYC)	163
Fig XXVII – Residential Units and Number of Buildings description from ‘PLUTO data Dictionary’ (Source: DOB NYC)	163
Fig XXVIII - Building Class description from ‘PLUTO data Dictionary’ (source: DOB NYC).....	163
Fig XXXI - Appendix C from ‘PLUTO data Dictionary’ (source: DOB NYC).....	164

Tables

Table 1-1 - Most lethal hurricanes for New York	16
Table 1-2 - Categorization of damage (source: Jonkman et al., 2008)	19
Table 2-1- Description of the situation and observed damaged for the locations of Figure 2-14.	39
Table 2-2- USGS High water marks for the Rockaways	40
Table 2-3 - Properties of the Buildings dataset	47
Table 2-4 - Properties of the PLUTO dataset	47
Table 3-1 - Eight different extraction formulations for the inundation depth indicator	70
Table 4-1 - Percentage non non-flooded per run and buffer size related to the minimum grid cell size	87
Table 4-2 - Pearson correlation and log-likelihood ratio test scores for the indicator 'Inundation Depth' extracted from the XBeach results according to eight different formulations	92
Table 4-3 - Pearson correlation and log-likelihood ratio test scores for the indicator 'Inundation Depth' based on the bath tub concept with a constant water level of 3.27m above NAVD88	92
Table 4-4 - Log-likelihood ratio test scores for the inundation depth indicator based on a combination of A) XBeach results or the bathtub concept and B) ground elevations from the LIDAR data or Buildings data.	93
Table 4-5 – Log-likelihood ratio test scores for different hindcasting scenarios	95
Table 4-6 - Netica's sensitivity analysis of configuration 2: variance reduction of Beliefs.	95
Table 4-7 - Log-likelihood ratio test scores for 10 runs; trained with randomly picked 90% of the observations and hindcasting with the remaining 10%	96
Table 4-8 - Log-likelihood ratio test scores for 10 runs; hindcasting on the observations of the 10% closest buildings and trained with the remaining 90%.	97
Table 4-9 - Log-likelihood ratio test scores for configuration 2 and extraction formulations 7; the results for different runs and varying extraction buffer sizes are given.	98
Table 4-10 - Most probable damage versus observed; total counts per combination	99
Table 4-11 - Mean of the conditional damage PMF's; categorized on the combinations of observed and most probable predicted.	100
Table 4-12 - Average of the predicted probabilities given the observed	100
Table 4-13 - Mean standard deviation of hindcasted PMF's for configuration 1 and 2 and different hindcast scenarios.	100
Table 4-14 - Mean standard deviation of the hindcasted PMF's given the observed for configuration 1 and 2 and hindcast scenario 7.	101
Table 4-15 - Absolute and relative log-likelihood ratio test scores for configuration 3 with different building type	

<i>indicator nodes.</i>	104
<i>Table 4-16 - Absolute and relative log-likelihood ratio test scores for configuration 4 and 5 and different hindcast scenarios.</i>	105
<i>Table 4-17 - Log-likelihood ratio test scores for 10 runs with configuration 4 and 5; hindcasting on the observations of the 10% closest buildings and trained with the remaining 90%.</i>	105
<i>Table 4-18 - Mean standard deviation of hindcasted PMF's for configuration 4 and 5 and different hindcast scenarios.</i>	106
<i>Table 6-1 - Description of the Damage Classification which is used for the ImageCat Impact Analysis (source: FEMA)</i>	162

Bibliography

- Becker, Andrea B, William M Johnstone, P Eng, Barbara J Lence, D Ph, and A M Asce. 2011. "Wood Frame Building Response to Rapid-Onset Flooding." (May): 85–95.
- Blake, Eric. 2013. "Hurricane Sandy (presentation Slides)."
<http://www.nhc.noaa.gov/outreach/presentations/Sandy2012.pdf>.
- Blake, Eric S, Todd B Kimberlain, Robert J Berg, John P Cangialosi, and John L Beven li. 2013. *Tropical Cyclone Report - Hurricane Sandy*.
https://www.google.nl/url?sa=t&rct=j&q=&esrc=s&source=web&cd=1&ved=0CCIQFjAA&url=http%3A%2F%2Fwww.nhc.noaa.gov%2Fdata%2Ftcr%2FAL182012_Sandy.pdf&ei=9nWtU7ODOKeIOAXwglGgDA&usg=AFQjCNECWIAIbJi84IMxu7P3OhM5smk3sg&sig2=uCcFE9yt9EoX7lfp83grLQ.
- Bosboom, Judith, and Marcel Stive. 2012. *Coastal Dynamics I Lecture Notes CIE4305*. VSSD.
<https://1boek.nl/artikel/9789065622860/coastal-dynamics-i-lecture-notes-cie4305>.
- Chan, Alda, Sa Liu, Jon Mcgrath, Rossana Tudo, and Kathleen Walczak. 2013. *Planning for a Resilient Rockaways : A Strategic Planning Framework for Arverne East*.
- Deltares. 2010. "XBeach Model Description and Manual."
- FEMA. 2013. "WA HAZUS User ' s Group RX GIS Update & Best Practices : Hurricane Sandy - Response & GIS Coordination / Geospatial Platform FEMA GeoPlatform Online."
http://www.usehazus.com/uploads/forum/Dewar_Sandy_04152013.pdf.
- Grossi, Patricia, and Cheryl TeHennepe. 2008. "A Guide To Catastrophe Modelling." *The Review - Worldwide Insurance*.
- GuyCarpenter. 2013. *Post-Sandy: Damage Survey*.
<http://gcportal.guycarp.com/portal/extranet/insights/reportsPDF/2013/Post-SandyReport;JSESSIONIDGCPORTALWCPORTALAPP=txGnTt4hxRwNS1Q0Yj1TJYpRLGnd126f24mB6M4DP6Rg6Pj3LyX5!-784932359?vid=1>.
- Hall, Timothy M., and Adam H. Sobel. 2013. "On the Impact Angle of Hurricane Sandy's New Jersey Landfall." *Geophysical Research Letters*.
<http://onlinelibrary.wiley.com/doi/10.1002/grl.50395/abstract>.
- Hatch, E, and A Lazaraton. 1991. *The Research Manual: Design and Statistics for Applied Linguistics*. Rowley, MA: Newbury House.
- Hazus –MH 2.1 Hurricane Model - User Manual*.
- Den Heijer, Kees, Dirk T.J.A. Knipping, Nathaniel G. Plant, Jaap S.M. Van Thiel de Vries, Fedor Baart, and Pieter H.A.J.M. Van Gelder. 2011. "IMPACT ASSESSMENT OF EXTREME STORM EVENTS USING A BAYESIAN NETWORK."
- Helm, P. 1996. "Integrated Risk Management for Natural and Technological Disasters." *Tephra* 15(1):

- Izumii, Toshichika Hirofumi Sakuma, Yokozawa, Masayuki, Jing-Jia Luo, Andrew J. Challinor, Molly E. Brown, Gen Sakurai, and Toshio Yamagata. 2012. "Prediction of Seasonal Climate-Induced Variations in Global Food Production." *Nature, Climate Change* 3. <http://www.nature.com/nclimate/journal/v3/n10/full/nclimate1945.html>.
- Jongman, B, H Kreibich, H Apel, J I Barredo, P D Bates, L Feyen, A Gericke, and J Neal. 2012. "Comparative Flood Damage Model Assessment : Towards a European Approach." *NHESS*: 3733–52.
- Klijn, F., A. Hooijer, B. Pedroli, and A. and Van Os. 2004. *Towards Sustainable Flood Risk Management in the Rhine and Meuse River Basins: Synopsis of the Findings of IRMA-SPONGE, River Research and Applications* 20.
- Kunz, M., B. Mühr, T. Kunz-Plapp, J.E. Daniell, B. Khazai, F. Wenzel, M. Vannieuwenhuysse, T. Comes, F. Elmer, K. Schröter, J. Fohringer, T. Münzberg, C. Lucas, and J. Zschau. 2013. 1 Natural Hazards and Earth System Sciences Discussions *Investigation of Superstorm Sandy 2012 in a Multi-Disciplinary Approach*. <http://www.nat-hazards-earth-syst-sci-discuss.net/1/625/2013/> (February 10, 2014).
- Lin, Ning, Kerry Emanuel, Michael Oppenheimer, and Erik Vanmarcke. 2012. "Physically Based Assessment of Hurricane Surge Threat Under Climate Change." *Nature, Climate Change* 2. <http://www.nature.com/nclimate/journal/v2/n6/full/nclimate1389.html>.
- Lloyd's. 2013. "2013: THE YEAR CAT MODELLING CHANGES?" <http://www.lloyds.com/news-and-insight/news-and-features/market-news/industry-news-2013/2013-the-year-cat-modelling-changes>.
- McCall, R.T., J.S.M. Van Thiel de Vries, N.G. Plant, a.R. Van Dongeren, J.a. Roelvink, D.M. Thompson, and a.J.H.M. Reniers. 2010. "Two-Dimensional Time Dependent Hurricane Overwash and Erosion Modeling at Santa Rosa Island." *Coastal Engineering* 57(7): 668–83. <http://linkinghub.elsevier.com/retrieve/pii/S037838391000027X> (January 28, 2014).
- McCallum, Brian E, Shaun M Wicklein, Reiser Robert G, Ronald Busciolano, Jonathan Morrison, Richard J Verdi, Jaime A Painter, Eric R Frantz, and Anthony J Gotvald. 2013. "Monitoring Storm Tide and Flooding from Hurricane Sandy Along the Atlantic Coast of the United States, October 2012." <http://pubs.usgs.gov/of/2013/1043/pdf/ofr2013-1043.pdf> (July 1, 2014).
- Merz, B, H Kreibich, A Thieken, R Schmidtke, and Section Engineering Hydrology. 2004. "Estimation Uncertainty of Direct Monetary Flood Damage to Buildings." 153–63.
- Merz, B., H. Kreibich, and U. Lall. 2013. "Multi-Variate Flood Damage Assessment: a Tree-Based Data-Mining Approach." *Natural Hazards and Earth System Science* 13(1): 53–64. <http://www.nat-hazards-earth-syst-sci.net/13/53/2013/> (June 10, 2014).
- Mühr, Bernhard, Michael Kunz, Tina Kunz-plapp, James Daniell, Marjorie Vannieuwenhuysse, Tina Comes, Florian Elmer, Adrian Leyser, Christian Lucas, Joachim Fohringer, Werner Trieselmann, Jochen Zschau, and Early Warning. 2012. *CEDIM FDA-Report on Hurricane Sandy 22-30 October*

2012. http://www.cedim.de/download/CEDIMFDAreportSandy_2012_no2.pdf.
- Nelson, Raymond C. 1991. "Random Breaking Waves: a Closed-Form Solution for Planar Beaches." http://ac.els-cdn.com/0378383991900074/1-s2.0-0378383991900074-main.pdf?_tid=714d3aa6-23ac-11e4-939d-00000aab0f27&acdnat=1408018607_0f2d182d86acda3c39f50d1e6e3f7bcb.
- NOAA. 2013. *NOAA Water Level and Meteorological Data Report - Hurricane Sandy*.
- Norsys Software Corp. 1997. *Netica - Application for Belief Networks and Influence Diagrams - User's Guide*.
- Pielke Jr, Roger A, Joel Gratz, Christopher W Landsea, Douglas Collins, Mark A Saunders, and Rade Musulin. 2008. "Normalized Hurricane Damage in the United States : 1900 – 2005." (February): 29–42.
- Pistrika, Aimilia K., and Sebastiaan N. Jonkman. 2009. "Damage to Residential Buildings Due to Flooding of New Orleans after Hurricane Katrina." *Natural Hazards* 54(2): 413–34. <http://link.springer.com/10.1007/s11069-009-9476-y> (June 1, 2014).
- Plant, Nathaniel G., and K. Todd Holland. 2011. "Prediction and Assimilation of Surf-Zone Processes Using a Bayesian Network." *Coastal Engineering* 58(1): 119–30. <http://linkinghub.elsevier.com/retrieve/pii/S0378383910001353> (January 28, 2014).
- PlaNYC. 2013. *A Stronger, More Resilient NY*. http://www.nyc.gov/html/sirr/downloads/pdf/final_report/Ch_6_Uilities_FINAL_singles.pdf.
- Rego, João Lima, and Chunyan Li. 2009. "On the Importance of the Forward Speed of Hurricanes in Storm Surge Forecasting: A Numerical Study." *Geophysical Research Letters* 36(7): n/a–n/a. <http://doi.wiley.com/10.1029/2008GL036953> (August 12, 2014).
- Roelvink, Dano, Ad Reniers, Ap van Dongeren, Jaap van Thiel de Vries, Robert McCall, and Jamie Lescinski. 2009. "Modelling Storm Impacts on Beaches, Dunes and Barrier Islands." *Coastal Engineering* 56(11-12): 1133–52. <http://linkinghub.elsevier.com/retrieve/pii/S0378383909001252> (January 28, 2014).
- Sallenger, Asbury H. 2000. "Storm Impact Scale for Barrier Island." <http://coastal.er.usgs.gov/hurricanes/publications/jcr.pdf>.
- Schott, Timothy, Chris Landsea, Gene Hafele, Jeffrey Lorens, Harvey Thurm, Bill Ward, Mark Willis, and Walt Zaleski. 2012. "Saffir-Simpson Hurricane Wind Scale." (February): 1–4. <http://www.nhc.noaa.gov/pdf/sshws.pdf>.
- Sopkin, By Kristin L, Hilary F Stockdon, Kara S Doran, Nathaniel G Plant, Karen L M Morgan, Kristy K Guy, Kathryn E L Smith, Sally Jewell, and U S Geological Survey. 2014. "Hurricane Sandy : Observations and Analysis of Coastal Change."
- TU-Delft. 2008. "UNINET Manual." 1–42.

Tuinhof, Internship. 2013. (Unpublished work) *Modeling New York in D-Flow FM (unpublished)*.

USACE. 2013. *Hurricane Sandy Coastal Projects Performance Evaluation Study, Disaster Relief Appropriations Act, 2013*.